Loughborough University
Institutional Repository

Process analytical technology based approaches for the monitoring and control of size and polymorphic form in pharmaceutical crystallisation processes

This item was submitted to Loughborough University's Institutional Repository by the/an author.

Additional Information:

Metadata Record: https://dspace.lboro.ac.uk/2134/6436

Please cite the published version.

Loughborough University

Thesis Access Form

Copy No ....Location..

Author.....Mohd Rushdi Haji Abu Bakar ....

Title......Process Analytical Technology Based Approaches for the Monitoring and Control of Size
and Polymorphic Form in Pharmaceutical Crystallisation Processes.

Status of access OPEN / ~~RESTRICTED / CONFIDENTIAL~~

Moratorium Period:.......................................years, ending............../............200.........................

Conditions of access approved by (CAPITALS):......Z K   NAGY ....

Supervisor (Signature)......*Nagy* ....

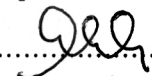Department of......**Chemical Engineering** ....

Author's Declaration: *I agree the following conditions:*

Open access work shall be made available (in the University and externally) and reproduced as necessary at the discretion of the University Librarian or Head of Department. It may also be digitised by the British Library and made freely available on the Internet to registered users of the EThOS service subject to the EThOS supply agreements.

*The statement itself shall apply to **ALL** copies including electronic copies:*

This copy has been supplied on the understanding that it is copyright material and that no quotation from the thesis may be published without proper acknowledgement.

Restricted/confidential work: All access and any photocopying shall be strictly subject to written permission from the University Head of Department and any external sponsor, if any.

Author's signature................................Date..........30th June 2010 ....

users declaration: for signature during any Moratorium period (Not Open work):			
I undertake to uphold the above conditions:			
Date	Name (CAPITALS)	Signature	Address

Loughborough University

Process Analytical Technology Based Approaches for the Monitoring and Control of Size and Polymorphic Form in Pharmaceutical Crystallisation Processes

By

Mohd Rushdi Haji Abu Bakar

A Doctoral Thesis submitted in partial fulfilment of the requirements for the award of Doctoral of Philosophy of Loughborough University

June 2010

CERTIFICATE OF ORIGINALITY

This is to certify that I am responsible for the work submitted in this thesis, that the original work is my own except as specified in acknowledgements or in footnotes, and that neither the thesis nor the original work contained therein has been submitted to this or any other institution for a degree.

………………………………….… (Signed)

30th June 2010

Abstract

Pharmaceutical crystallisation operation is often critical because it determines product properties, such as the crystal size distribution (CSD) and polymorphic form, that can influence the subsequent downstream operations and the product therapeutic performance. Driven by the United States Food and Drug Administration's (FDA) Process Analytical Technology (PAT) initiative and the Quality-by-Design (QbD) concept, the development of control approaches, which can improve the manufacturing of products with desired properties, has become of significant interest. This thesis presents the development and application of PAT-based approaches for the monitoring and control of pharmaceutical crystallisation operations that will ensure consistent production of active pharmaceutical ingredients (APIs) with the desired size and polymorphic form. The approaches utilised Lasentec focused beam reflectance measurement (FBRM) and attenuated total reflectance ultraviolet (ATR-UV) spectroscopy as the *in situ* monitoring and control tools.

Crystallisations of the APIs that posses multiple polymorphs are both critical and challenging. This was illustrated in this work by the crystallisations of sulfathiazole polymorphs using literature methods. The processes were monitored using FBRM and ATR-UV spectroscopy to define the design range of the process parameters. The defined range could be used as a recipe to reproduce the same quality of crystals. The obtained crystals were characterised using various techniques (optical microscopy, scanning electron microscopy (SEM), differential scanning calorimetry (DSC), thermogravimetry, hot-stage microscopy (HSM), Fourier Transform infrared spectroscopy and powder X-ray diffractometry) to assess the success of the crystallisation processes. The combined results of the techniques showed that all methods were able to produce the desired pure polymorphs. As a contribution to the technique of investigating polymorphism, a combined approach of DSC-HSM with image analysis, was introduced. Results show the capability of the approach to provide a unique insight into the polymorphic transformations and thermal behaviour exhibited by the model compound.

The novel direct nucleation control (DNC) approach was introduced to control the CSD. The approach utilises information on nucleation, provided by FBRM, in a feedback control strategy that adapts the process variables, so that the desired CSD of product is achieved. It also provides *in situ* fines removal through the operating policy,

rather than having additional equipment and external recycle loops. The approach does not require concentration measurement and has the advantage of being a model-free approach, requiring no information on nucleation or growth kinetics in order to design an operating curve; the system automatically and adaptively detects the boundary of the operating curve. Experimental results, using glycine in water-ethanol mixture as a model system, show the benefits of DNC to produce larger crystals with narrower CSD compared to uncontrolled operations.

The capability of seeded cooling crystallization with temperature cycling approach to control crystal size uniformity and polymorphic purity was evaluated. Using sulfathiazole in n-propanol and in water as model systems, the method was found to accelerate the growth and enhance the size uniformity of the crystals, in comparison with runs using a linear temperature profile, by promoting Ostwald ripening. Although the approach is conceptually capable of controlling polymorphic purity of a system, the effect of solvent-mediated nucleation/growth can be more dominant, as shown by the results of the experiments. The insights into this behaviour of sulfathiazole crystals were captured very well by the FBRM. The study also demonstrated the successful use of a simple non-linear function as a calibration model to relate temperature and absorbance data, obtained using the ATR-UV spectroscopy, to solute concentration during the crystallisation process.

The effect of temperature cycling, performed during seeded cooling crystallisation, on the surface features of sulfathiazole crystals was investigated using FBRM and *ex situ* optical microscopy, SEM and atomic force microscopy. It was observed during the initial stage of the process, the heating phases produced crystals with smooth surfaces, whilst the cooling phases promoted growth of features on the surfaces. These changes detected by the FBRM as an increase in the number of coarse counts during heating and a drop during cooling. Laser beam spreading caused by the surface roughness, and signal/chord splitting due to sharp edges are offered as an explanation for the FBRM results. This shows the capability of the FBRM to provide useful information about the changes on the surface of the crystalline products. The information can be used to avoid problems in the downstream operations, or in the final product property due to variations in flowability and friability, which are influenced by the surface property.

Acknowledgements

Table of Contents

List of Figures

List of Tables

CHAPTER 1: INTRODUCTION

Advantages and problems of crystallisation operation in the pharmaceutical manufacturing process are discussed. The problems encountered, which motivate this PhD work, are related to both product quality and process control performance. The aim of the work is hence the design and development of crystallisation control approaches that will ensure consistent production of the product with a desired quality. The objectives of this work cover the preliminary and necessary elements towards the achievement of the aim. The main contributions of this thesis are highlighted. This thesis is structured in the order of the progression of the objectives as outlined at the end of this chapter.

1.1 MOTIVATION

Crystallisation from solution is an important unit operation used in various industries as a technique for separating solid materials in purified forms. It is a technique of choice for solid-liquid separation due to its capability of producing high purity materials. Its importance in the pharmaceutical industries is due to a large number of active pharmaceutical ingredients (APIs) that are utilised in solid form. It is estimated that more than 80% of APIs involve at least one crystallisation step in their manufacturing process (Reutzel-Eden, 2006). The crystallisation operation is often critical because it determines the product properties, such as the crystal size distribution (CSD), morphology and polymorphic form. These properties in turn influence the efficiency of the subsequent downstream operations, as illustrated schematically in Figure 1.1, particularly filtration and drying. The properties also affect the therapeutic performance of the product, such as dissolution rate, bioavailability and stability.
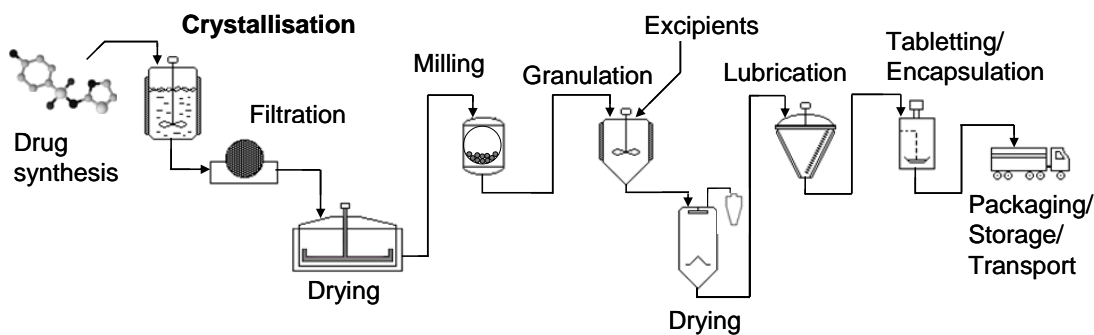
Figure 1.1 A schematic diagram of a typical flow of pharmaceutical manufacturing processes.

Statistically, about 85% of all APIs exhibit polymorphism and 50% have multiple polymorphic forms (Karpinski, 2006). Crystallisations of the APIs that possess multiple polymorphic forms are both critical and challenging. Since different polymorphs exhibit different physico-chemical properties and mechanical behaviour (Hilfiker et al., 2006), pharmaceutical manufacturers have to select a polymorph that has desirable characteristics that will assist in the efficient manufacturing and effective performance of the drug product. It is therefore pertinent to design and develop a control approach for crystallisation operations that will ensure consistent production of the desired polymorphic form of the APIs. The challenge however is great because not only every API, but every polymorph of an API has its own crystallisation characteristics that may require a unique treatment (Yu et al., 1998). An extensive solid-state characterisation of all known polymorphs of the API is therefore necessary in order to understand and differentiate them properly. It is a pre-requisite in the design and development of the polymorphic control approach and an essential part of the drug development process. There have been many cases in pharmaceutical history that signifies the important of polymorphism (Carstensen, 1993; Aldridge, 2007). One such cases occurred in 1998 where a US pharmaceutical firm, Abbott Laboratories, found that its manufacturing process was producing the wrong polymorph of its HIV drug Ritonavir since the drug was starting to fail the dissolution tests (Aldridge, 2007). The firm was forced to stop the production and to withdraw the drug from the market until it figured out how to get the original polymorph back (Aldridge, 2007). Although the properties of the different polymorphs of the API may be different, very often, they are only marginally different. One of such APIs is sulfathiazole, an antimicrobial agent with five known polymorphs. The polymorphs should therefore be differentiated using a variety of characterisation techniques to avoid making erroneous conclusions. This underscores the importance to have a reliable combined technique that can quickly differentiate between polymorphs and determine if a solid contains a pure polymorph or a mixture of polymorphs.

As shown in Figure 1.1, it is typical for the pharmaceutical manufacturers to mill the crystals before the formulation steps (i.e. granulation, lubrication and tabletting) in order to shape them into a desirable CSD (Wieckhusen, 2008). However, part of the milled crystal surface may convert into amorphous solid as a result of the mechanical impact during the milling operation. This amorphous content can absorb moisture and consequently recrystallise into crystals with uncertain properties. The most likely

solution to this problem is to produce crystals with the desired CSD directly by the crystallisation operation (Shekunov and York, 2000); but since the crystals obtained in this way tend to have an inconsistent CSD quality, milling is still used in practice as a final shaping tool (Wieckhusen, 2008). It has been recognised that the uncertainties in the nucleation process is the direct source of the inconsistency in the final product. Most control approaches applied in crystallisation operations, on the other hand, use supersaturation level as the manipulated variable. The supersaturation level however is indirectly related to product properties because it only influences the relative rates of nucleation and crystal growth, which in turn determines the product properties. Therefore the design and development of approaches that are able to directly control the onset of nucleation in the crystallisation process are the way forward. The success of such approaches will eliminate the need for milling, which in turn eliminates the risk of product contamination due to the effect of the operation and saves a considerable amount of material, money and energy.

The application of Process Analytical Technology (PAT), an initiative introduced by the United States Food and Drug Administration (FDA), to pharmaceutical crystallisation processes has been the subject of great interest from both industry and academia, since it is considered as a key tool in elucidating and assessing this often poorly understood process (Birch et al., 2005). The initiative involves the use of *in situ* analysers that are able to measure and monitor product quality and critical process properties in real-time. In addition to the provision of kinetic data that are required in the development of a robust crystallisation process, real-time monitoring also allows appropriate remedial actions to be taken during the process if undesirable product quality or process property are identified (Yu et al., 2003). Examples of the *in situ* analysers that have been used in the crystallisation processes are Lasentec focused beam reflectance measurement (FBRM) and attenuated total reflectance ultraviolet (ATR-UV) spectroscopy. The real-time process information given by these analysers can also be integrated into a control framework to provide an optimal control strategy with the aim of producing drug products with consistent desired quality. This framework satisfies the Quality-by-Design (QbD) approach adopted by the FDA to ensure pharmaceutical product quality. Improved control of pharmaceutical crystallisation processes through the application of PAT and QbD may lead to a better product quality and enhanced process efficiency. The latter helps to make new drugs

available more quickly and at a lower cost; hence providing a significant improvement in the quality of life.

1.2 RESEARCH AIM AND OBJECTIVES

The aim of this research project is to develop and apply PAT-based approaches for the monitoring and control of pharmaceutical crystallisation operations to ensure consistent production of the desired quality of APIs for efficient downstream operation and product effectiveness.

Five objectives have been identified that lead to a logical progression through the research:

a) to gain knowledge and understanding about the crystallisation behaviour and polymorphic properties of the main model compound, sulfathiazole, through a comprehensive literature review, a hands-on *in situ* monitoring of the crystallisation processes of the polymorphs and an application of various solid-state characterisation techniques;

b) to develop and assess a method for investigating polymorphism through a combined approach of differential scanning calorimetry (DSC) and hot-stage microscopy (HSM) with image analysis;

c) to implement and evaluate a novel direct nucleation control (DNC) method approach for controlling the CSD;

d) to develop and assess a temperature cycling method (using feedback control from FBRM probe measurements) for controlling size distribution and polymorphic purity in seeded cooling crystallisation; and

e) to evaluate the capability of FBRM as an *in situ* process analyser in monitoring surface events and detecting changes in surface features of crystals, which can provide link to potential growth mechanism.

1.3 MAIN CONTRIBUTIONS OF THE THESIS

The main contributions of this thesis are summarised in the following lists:

a) A provision of a comprehensive literature review on the crystallisation and polymorphism of sulfathiazole. This includes a compilation of literature methods for isolating a particular polymorph and a reconciliation of various enumerations of the polymorphs that are in use from 1941 to present.

b) A provision of reliable methods of generating sulfathiazole polymorphs through *in situ* monitoring and recording of process properties using FBRM and ATR-UV spectroscopy. It has been suggested that the failure to adequately describe the crystallisation conditions is one of the factors that led to the confusion over the identity of sulfathiazole polymorphs (Hughes et al., 1997). The *in situ* monitoring and recording of the crystallisation processes identify the design range of the process parameters that has been demonstrated to produce the desired crystal quality. By operating within the identified design range, the crystals can be reproduced consistently with a guaranteed quality. The incorporation of the process and product knowledge into the process design is part of the PAT framework and satisfies the QbD concept.

c) Introduction of a combined approach of DSC and HSM with image analysis as an addition to the methods of investigating polymorphism. Light intensity profiles obtained from the HSM images are proposed to be utilised as an alternative way to present the results of the HSM analysis. This is the first time the use of image analysis to evaluate the HSM results in the study of polymorphism is reported.

d) Introduction of a novel direct nucleation control (DNC) approach for controlling the CSD. The approach uses information on nucleation and dissolution, provided by FBRM, in a feedback control strategy that adapts the process variables, so that the desired quality of product is achieved. It does not require concentration measurement and has the advantage of being a model-free approach, requiring no information on nucleation or growth kinetics in order to design an operating curve. It automatically and adaptively detects the boundary of the operating zone; hence it is more robust to the presence of impurities or residual solvent than the supersaturation control approach. The approach has been applied for the crystallisation of glycine and experimental results demonstrate the benefits of DNC of producing larger crystals with narrower CSD compared to the uncontrolled operations.

e) Implementation of seeded cooling crystallisation with temperature cycling for the control of size uniformity and growth of the desired sulfathiazole polymorphs. The study used FBRM and ATR-UV spectroscopy for the *in situ* monitoring and control of the process. Based on the FBRM readings, the process was driven using a feedback control approach that employs alternating cycles of heating and cooling phases so that the number of seed particles is

maintained, whilst the growth of the seeds in the system is increased. This work demonstrates the successful use of a simple non-linear function as a calibration model to relate temperature and absorbance data, obtained using the ATR-UV spectroscopy, to solute concentration during the crystallisation process. Results of the experiments show that the temperature cycling method promoted Ostwald ripening, which helped in accelerating crystal growth and correcting poor seed quality, hence enhancing the size uniformity of the product. Conceptually the method may be able to control the polymorphic purity, but the experimental results so far have shown that the effect is negligible in comparison to the effect of solvent. The insights into the solvent-mediated nucleation/growth behaviour of sulfathiazole crystals were captured very well by FBRM.

f) A provision of a practical demonstration of the capability of FBRM in detecting changes in surface features of crystals with the link to potential growth mechanisms. The finding shows that FBRM may provide useful information related to the surface properties of the crystalline products, which can be used to avoid problems in the downstream processing or in the final product property due to variations in flowability and friability.

1.4 THESIS STRUCTURE

An outline of the subsequent chapters in this thesis is as follows:

Chapter 2 provides a review of literature on the fundamental aspects of pharmaceutical crystallisation, which include solubility, crystallisation mechanisms and crystal properties. Also reviewed are the techniques to characterise the crystal properties and the main approaches for crystallisation operation and control. In order to gain knowledge and understanding about sulfathiazole from the literature, the crystallisation and polymorphism of the compound are reviewed. An overview of PAT, its tools and application in pharmaceutical crystallisation are also presented in this chapter.

In **Chapter 3**, the crystallisations of five different sulfathiazole polymorphs using selected methods available in the literature are evaluated and the results of the solid-state characterisation of the obtained polymorphs are presented. The characterisation techniques used are optical microscopy, scanning electron microscopy, DSC,

thermogravimetry, HSM, Fourier transform infrared spectroscopy and X-ray powder diffraction.

Chapter 4 presents the application of a combined approach of DSC and HSM with image analysis in the investigation of the sulfathiazole polymorphism.

Chapter 5 introduces the novel DNC approach and discusses the application of the approach for the control of CSD in the crystallisation of glycine.

Chapter 6 describes and discussed the implementation of seeded cooling crystallisation with temperature cycling approach to produce uniform size crystals and to grow the desired polymorphic form of sulfathiazole crystals.

Chapter 7 presents the evaluation study on the capability of FBRM as an *in situ* process analyser in monitoring surface events and detecting changes in surface features of crystals.

Chapter 8 concludes the thesis by summarizing results of all the works that have been presented and proposing future works.

CHAPTER 2:
LITERATURE REVIEW

This chapter provides an overview of the fundamentals of pharmaceutical crystallisation that include solubility, crystallisation mechanisms and crystal properties. The techniques to characterise the crystal properties are briefly reviewed. The main approaches for crystallisation operation and control are described. In order to illustrate the principles and the problems associated with the crystallisation of a polymorphic system, the crystallisation and polymorphism of sulfathiazole, which is the main model compound used in this work, are reviewed. Brief reviews on PAT, its tools and application in pharmaceutical crystallisation are also given in this chapter.

2.1 SOLUBILITY

Crystallisation from solution involves at least a two-component system: a solute and a solvent. Design and operation of the crystallisation processes usually require that the solubility of the solute in the solvent be known as a function of the temperature or solvent composition (Tavare, 1995). Although the solubility for some systems can be found in the literature (Mullin, 2001; Dalton and Schmidt, 1933; Dunn and Ross, 1935), the data should be treated cautiously since the presence of impurities, which is typical for industrial crystallisation processes, greatly affects the solubility (Myerson, 2002; Dalton and Schmidt, 1933). Alternatively, the solubility data can be obtained experimentally using a technique known as isothermal method. The technique basically involves the determination of a maximum amount of solute that can dissolve in a solvent at a constant temperature with agitation for a time period between 4 to 24 hours. The analysis for the solute can be done either gravimetrically (Nozaki and Tanford, 1971; Dalton and Schmidt, 1933; Dunn and Ross, 1935) or using spectroscopy (Fujiwara et al., 2002). Some variations of the technique are also available, which are described in detailed by Myerson (2002). Another experimental technique for the solubility determination involves heating up a suspension of solid and solvent to dissolution and detecting the clear point, which is taken as the solubility point, visually or using optical probes (Barrett and Glennon, 2002).

The solubility can also be obtained by calculation using the modified van't Hoff equation that incorporates an activity coefficient, γ to accommodate non-ideal solutions (Mullin, 2001):

$$\ln(x\gamma) = \frac{\Delta H_f}{R}\left[\frac{1}{T_f} - \frac{1}{T}\right] \tag{2.1}$$

where x is the mole fraction of the solute in the solution, ΔH_f is the molar enthalpy of fusion of the solute (J/mol), R is the gas constant, T_f is the fusion temperature of the solute (K) and T is the solution temperature (K).

Equation (2.1) requires a reliable estimation of the activity coefficient in order to obtain a good prediction of the solubility. This may be achieved by using activity coefficient models, such as the Non-Random Two-Liquid - Segment Activity Coefficient (NRTL-SAC) (Chen and Song, 2004) and the UNIQUAC (Universal Quasi-Chemical Activity Coefficient) Functional Group Activity Coefficient (UNIFAC) (Fredenslund et al., 1977). In the latter model, the activity coefficient of a molecule in a mixture is obtained from the sum of the activity coefficients of the constituent functional groups in the mixture, whereas in the former, the component-specific molecular parameters that represent the surface interaction characteristics of the molecules are used to obtain the activity coefficient. These and many other thermodynamic models that can be used to predict solubility have been reviewed by Modarresi et al. (2008) and Frank et al. (1999). The accuracy of the solubility obtained from any of the models, however, depends upon how much the system of interest deviates from the model assumptions and how well the required parameters are known (Frank et al.,1999; Gracin et al., 2002).

2.2 CRYSTALLISATION MECHANISMS

The phase relationship of the solute-solvent system can be illustrated by a phase diagram; a typical example is shown in Figure 2.1. In the figure, a solution whose composition lies on the solubility curve is said to be saturated, whereas those that lie in the regions below and above the curve are termed undersaturated and supersaturated, respectively. The terms indicate the relative amount of dissolved solid as compared to the saturated solution. The supersaturated solution is unstable because the dissolved solid and solvent are not in equilibrium. Like all other non-equilibrium systems, the supersaturated solution tends to reach equilibrium and in doing so it removes the solids in the form of nuclei, which then grow into crystals. The generation of supersaturation is therefore regarded as the first step in the crystallisation process.
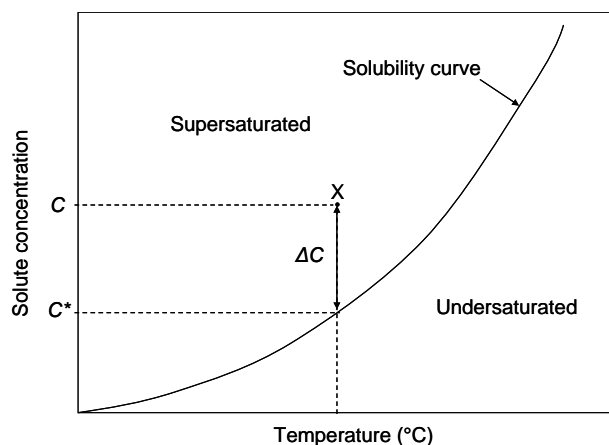
Figure 2.1 A typical phase diagram of a solute in a solvent.

2.2.1 Supersaturation

Supersaturation of the solution may be generated using five main methods. They are listed and briefly described in Table 2.1.

Table 2.1 Methods of supersaturation generation.

No.	Method	Description
1.	Evaporation	Removal of solvent from a solution by evaporation increases the concentration of solute in the solution, which results in supersaturation.
2.	Cooling	If the solubility of a solid increases with increasing temperature, a saturated solution can be prepared at a higher temperature. The solution is then cooled and since the solubility decreases during cooling, the solution becomes supersaturated.
3.	Anti-solvent addition	Addition of a second solvent that reduces the solubility of the solute in the resultant mixture.
4.	Chemical reaction	When a new compound is formed by a chemical reaction, the concentration of this compound is higher than its solubility in a solution. Therefore, the solution becomes supersaturated with respect to the new compound. Variation of pH to produce a less soluble acid or base from a salt, or *vice versa*, can also generate supersaturation.
5.	Freezing	Freezing of solvent from a solution increases the concentration of solute in the solution, which results in supersaturation. The frozen solvent can then be removed from a solution by sublimation under vacuum (Connolly et al., 1996).

There are also combinational methods to generate supersaturation such as combined cooling–evaporation method, known as vacuum crystallisation and combined cooling-anti-solvent addition method (Nagy et al., 2008b). Generally, the choice of method for generation of supersaturation depends on the required product properties, as well as the economic aspects.

With reference to Figure 2.1, the degree of supersaturation of a solution at point X can be defined using the concept of absolute supersaturation, ΔC which is expressed by the difference between the concentration of the supersaturated solution, C, and the saturated concentration, $C*$:

$$\Delta C = C - C*. \tag{2.2}$$

The degree of supersaturation can also be defined as the supersaturation ratio, S, and the relative supersaturation, σ:

$$S = \frac{C}{C*} \tag{2.3}$$

$$\sigma = \frac{\Delta C}{C*} = S - 1. \tag{2.4}$$

It has been shown mathematically that the supersaturation is the driving force for the crystallisation process (Mullin, 2001). It is therefore important to monitor its level and in order to do that; the degree of supersaturation needs to be quantified and measured. Many different methods have been used and developed to measure supersaturation in crystallisation (Loffelmann and Mersmann, 2002). Some of these will be discussed in Section 2.6.

2.2.2 Nucleation

When the supersaturation is increased, eventually a point will be reached at which the formation of nuclei occurs spontaneously. As mentioned before, the formation of nuclei is an attempt of the system to reach equilibrium. The process of forming nuclei is called nucleation, whereas the point at which the nucleation occurs spontaneously is called the metastable limit. The metastable limit depends on kinetic variables, such as

the rate at which supersaturation was created, the agitator speed, and the presence of impurities (Kim and Mersmann, 2001; Titit-Sargut and Ulrich, 2002). The zones in the supersaturation region in which spontaneous nucleation would or would not occur are termed labile and metastable, respectively.

Figure 2.2 shows a possible location of labile zone, metastable zone, metastable limit and metastable width on a concentration against temperature diagram. Knowledge of the metastable zone width (MSZW) is important in crystallisation because it provides information on nucleation kinetics, so that the nucleation behaviour of a system can be understood (Myerson, 2002). The MSZW also can be considered as a characteristic property for each crystallising system (Kim and Mersmann, 2001). In practice it is normally expressed in term of temperature rather than concentration for simplicity.
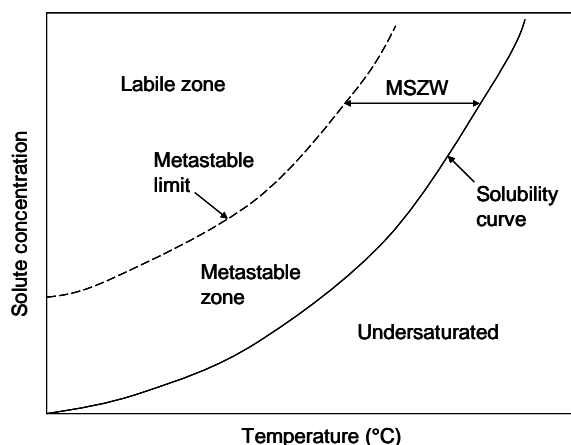
Figure 2.2 A typical phase diagram showing labile zone, metastable zone, metastable limit and MSZW.

The detection of the nucleation event in a system can be done by measuring appropriate properties in the system. These include, *(a)* optical transmittance since nucleation produces a dispersion of fine crystals (Barrett and Glennon, 2002; Titit-Sargut and Ulrich, 2002; Parsons et al., 2003); *(b)* concentration of the solution by direct measurement (Fujiwara et al., 2002) or by measuring a concentration-dependent property such as conductivity, density and refractive index (Titit-Sargut and Ulrich, 2002) since nucleation of the solute is accompanied by a decrease in the solution concentration; *(c)* temperature since during nucleation, heat is normally released because the free energy of the system is reduced (Davey and Garside, 2001); and *(d)* volume of a crystallising system with time since the solid phases have different densities from their mother phases (Davey and Garside, 2001).

Nucleation is commonly classified into either primary or secondary nucleation and can be further divided as shown in Figure 2.3.
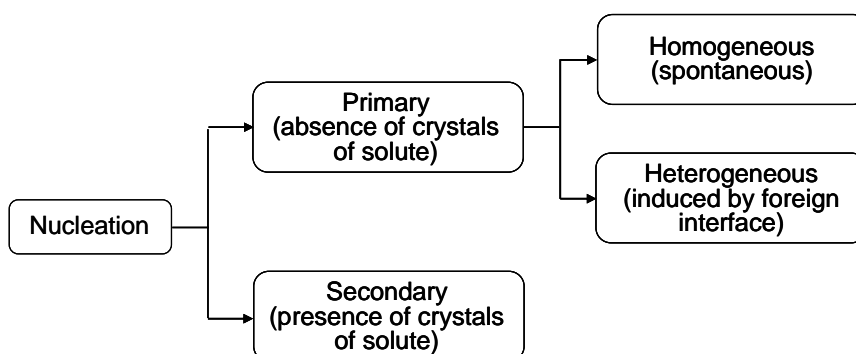
Figure 2.3 Overview of the different types of nucleation.

As shown in Figure 2.3, a nucleation that takes place spontaneously from a clear pure solution is called a homogeneous nucleation, whereas one induced by foreign particles or surfaces is called a heterogeneous nucleation (Rawlings et al., 1993). Homogeneous nucleation, however, rarely occurs in practice because solutions usually contain impurities that act as substrates for nucleation (Giulietti et al., 2001). Since the presence of impurities in a supersaturated solution is known to reduce the energy required for nucleation, nucleation in a heterogeneous system generally takes place at a lower supersaturation than in a homogeneous system (Myerson, 2002). Theoretical aspects of the primary nucleation have been discussed by Mullin (2001) and Myerson (2002).

Secondary nucleation occurs when a supersaturated solution is in contact with seed crystals of the solute. The seeds can either be deliberately added, or unintentionally present in the system. The latter can be the result of initial breeding (the dislodgement of microcrystalline dust particles from the surface of the seed crystals), needle/dendrite breeding (the detachment of weak outgrowths from crystal surfaces), polycrystalline breeding (the fragmentation of a weak polycrystalline mass) or collision breeding, which is also known as contact nucleation (the collision of crystals with one another, with agitator blades, or with crystalliser's wall) (Mullin, 2001). There are other sources of secondary nucleation, which are discussed by Tai et al., (1992). The seed crystals catalyse the nucleation and as a result, nucleation takes place at a lower supersaturation than that for the primary nucleation. For this reason, the secondary nucleation can be controlled more easily (Rawlings et al., 1993).

2.2.3 Crystal growth

Once stable nuclei with sizes greater than a critical size, r_c, have been formed in a supersaturated solution, they begin to grow into crystals of visible size. Crystal growth involves an addition of solute molecules from a supersaturated solution to the crystal surface (Rodriguez-Hornedo and Murphy, 1999). There are three possible sites for the solute molecules to incorporate into the crystal surface, namely flat (F), step (S) and kink (K) (Rawlings et al., 1993). Figure 2.4 schematically distinguishes these three sites. The more number of surfaces available for bonding, the more favourable the site will be for the incorporation of the molecules. For this reason, site K with three surfaces is the most favourable site; hence it grows at the highest rate, whereas site F with only one surface is the least favourite among the sites; hence it grows the slowest (Myerson et al., 2002).
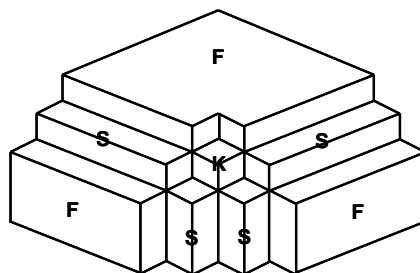
Figure 2.4 Three possible growth sites on a crystal surface.

Crystal growth is generally a two-step process consisting of mass transfer (diffusion) followed by a surface reaction (surface integration), although several researchers have added heat transfer as the third step that occurs in parallel with the other two steps (Hixson and Knox, 1951). The first step involves the diffusion of solute molecules from the bulk liquid through the solution boundary layer adjacent to the crystal surface. In the second step, the adsorbed solute molecules at the crystal surface are integrated into the crystal lattice. The rates of solute diffusion through the boundary layer and surface integration into the crystal surface are given by:

Diffusion $\qquad\qquad \dfrac{dm}{dt} = k_m A(C - C_i)$ $\qquad\qquad\qquad\qquad$ (2.5)

Integration $\qquad\qquad \dfrac{dm}{dt} = k_r A(C_i - C^*)$ $\qquad\qquad\qquad\qquad$ (2.6)

where m is the mass of crystal deposited in time t, A is the surface area of a crystal, k_m is the mass transfer coefficient, k_r the surface integration rate constant, C is the concentration in a bulk liquid, C_i is the solute concentration at the interface between the crystal and the solution, and $C*$ is the saturation concentration. The equations show that the driving force for the diffusion is $(C - C_i)$, whereas that for the surface integration is $(C_i - C*)$. The concentration profiles are described diagrammatically in Figure 2.5.
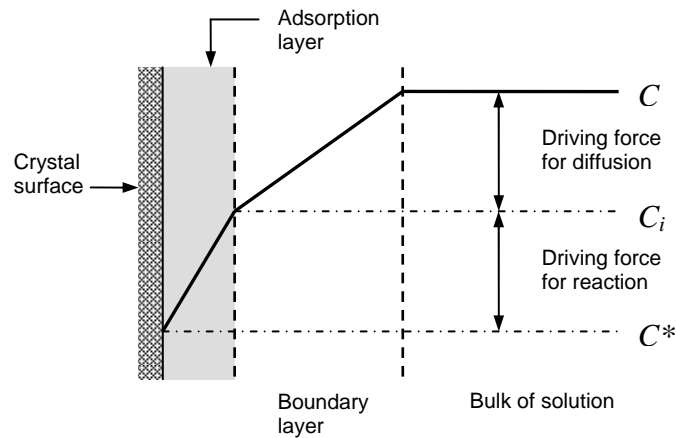
Figure 2.5 Concentration driving forces for crystal growth from solution.

The problem with equations (2.5) and (2.6) is that C_i cannot be determined. Therefore, the term is eliminated by using the overall concentration driving force $\Delta C = (C - C*)$ and introducing an overall crystal growth coefficient, K_G:

$$\frac{dm}{dt} = K_G A (\Delta C)^g \tag{2.7}$$

where g is the order of the growth rate. If $g = 1$, then C_i can be eliminated from equations (2.5) and (2.6) to give:

$$\frac{1}{K_G} = \frac{1}{k_m} + \frac{1}{k_r} \tag{2.8}$$

Based on equation (2.8), if the surface integration resistance $\left(\dfrac{1}{k_r}\right)$ is low, K_G is equal

to k_m and the process is controlled by the diffusion step. In this process, the growth rate will depend on the hydrodynamic conditions such as flow rate or stirring rate (Hixson and Knox, 1951; Rodriguez-Hornedo and Murphy, 1999; Garside, 1985). If

the diffusion resistance $\left(\dfrac{1}{k_m}\right)$ is low, K_G is approximately equal to k_r and the process

is controlled by the surface integration step. For growth controlled by surface integration, various mechanisms exist (Rodriguez-Hornedo and Murphy, 1999; Mullin, 2001; Myerson, 2002; Giulietti et al., 2001). A schematic overview of these mechanisms is given in Figure 2.6. The three most important mechanisms are: (a) continuous growth, (b) Burton-Cabrera-Frank (BCF) model, and (c) birth and spread model. They are briefly described in Table 2.2. Microtopographic observations at the surface of the crystal may reveal growth mechanisms (Rodriguez-Hornedo and Murphy, 1999). This can be done using crystal surface imaging tools, such as atomic forced microscopy (AFM).
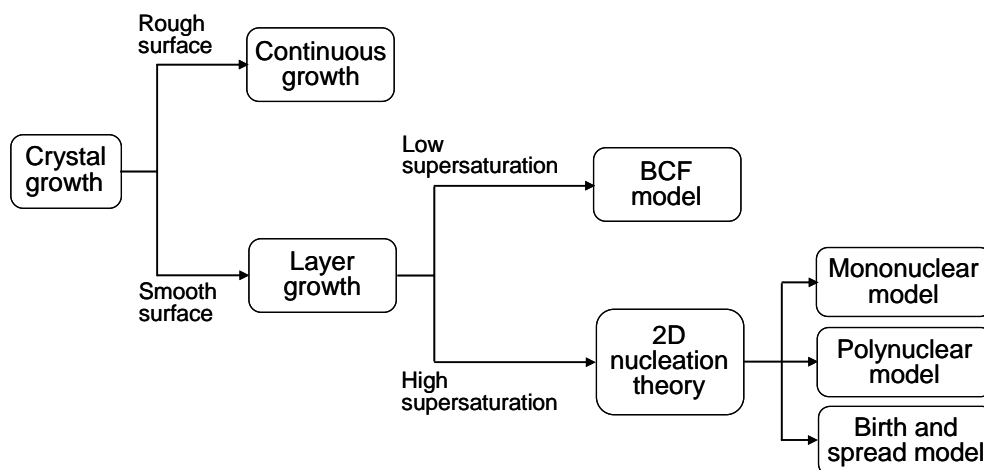
Figure 2.6 Overview of the different mechanisms of surface integration.

Table 2.2 Three important mechanisms of crystal growth by surface integration.

No.	Mechanism	Description
1.	Continuous growth	Also known as rough growth. A rough crystal surface provides many kink sites for growth, so the growth proceeds continuously until all these sites heal over (Jones, 2002). Thereafter, a layer growth mechanism may take over.
2.	BCF model	Also known as spiral growth or screw dislocation. This model accounts for low supersaturation. The presence of defects in the form of screw dislocation on the crystal surface provides a necessary kink site for growth. Growth proceeds layer by layer upon this defect and consequently produces a spiral, which is self-propagating and never dies (Burton et al., 1951).
3.	Birth and spread model	This model accounts for high supersaturation. It is based on the two-dimensional (2D) nucleation theory, which postulates that 2D nuclei should form on the smooth crystal surface to overcome the activation energy for growth, hence providing the necessary kinks for further growth (Jones, 2002). The model assumes the spreading of the surface nuclei as it formed at a finite constant rate and the nuclei can form at any location on the surface (Myerson, 2002). It is between the extremes of the mononuclear model (a model that assumes the spreading of the nuclei across the surface at an infinite velocity) and the polynuclear model (a model that assumes the nucleus does not spread at all as it formed, but the layer formed as a result of the formation of enough nuclei to cover the layer) (Myerson, 2002).

2.2.4 Dissolution

Crystal dissolution is not exactly the reverse of the crystal growth because the former does not require the surface integration step, but it is entirely controlled by the solute diffusion. Crystal dissolution rate, therefore, is of first order with respect to supersaturation and the dissolution occurs at all levels of undersaturations (Mullin and Gaska, 1969). The coefficient for the dissolution rate is a function of the diffusion coefficient, crystal size and local hydrodynamics. During dissolution, crystals are easily rounded off because their edges and corners are sterically favoured and hence are faster to dissolve (Bermingham, 2003).

2.2.5 Ostwald ripening

When crystals of different sizes are dispersed in their saturated solution, the smaller crystals tend to dissolve and the resultant solute subsequently deposits on larger crystals. Eventually, the small crystals disappear whilst the large grow larger. This phenomenon, known as Ostwald ripening, occurs spontaneously as a result of the

difference in solubility between small and large crystals (Boistelle and Astier, 1988; Mullin, 2001). The relationship between crystal size and solubility obeys the Gibbs-Thomson equation:

$$\ln\left(\frac{C(r)}{C_\infty}\right) = \frac{a}{r}$$

(2.9)

where $C(r)$ is the solubility of a crystal of size r, C_∞ is the solubility of a large crystal of infinite size and $a = \frac{2\gamma v}{kT}$, in which γ is the interfacial tension of the solid particle per unit area, v is the molar volume, k is the Boltzmann constant and T is the absolute temperature.

An expansion of equation (2.9) using first order Taylor series gives:

$$C(r) = C_\infty\left(1 + \frac{a}{r}\right)$$

(2.10)

Equation (2.10) is a mathematical demonstration that the solubility of a small crystal is larger than that of a large one (Boistelle and Astier, 1988). The difference in solubility between a crystal with a critical radius, $r*$ and any other, r is

$$C(r) - C_{r*} = aC_\infty\left(\frac{1}{r} - \frac{1}{r*}\right)$$

(2.11)

Equation (2.11) shows that a crystal of size $r < r*$ must dissolve whereas a crystal of size $r > r*$ must grow because neither of them is in equilibrium with the solution (Boistelle and Astier, 1988).

Ostwald ripening can change the crystal size distribution over a period of time, even at a constant temperature, but it can be accelerated with periodic temperature changes or temperature cycling (Mullin, 2001; Kahlweit, 1975).

2.2.6 Agglomeration

Agglomeration occurs when growing nuclei or fine crystals collide and bind to each other by forces such as the Van der Waals. It is a dominating process for very fine particles and negligible for large particles (Mersmann, 1999). The addition of a large number of nuclei to original agglomerates by continuous collisions leads to very large agglomerates. The agglomerates that formed under low supersaturation can be broken because the binding forces are week. This break-up is called disruption. Since the agglomerates that formed under high supersaturation are much stronger, they are not prone to disruption (Paul et al., 2005).

Agglomeration should be avoided because it causes a reduction in effective surface area for crystal growth, a possible entrapment of solvent/impurities in the crystal mass, difficulties in the subsequent downstream processing and friability during dry processing that leads to changes in crystal size distribution (Paul et al., 2005). In order for the agglomeration to be minimized, the rates of supersaturation generation and nucleation should be controlled. The latter can be achieved by operating the crystallisation process within the metastable zone.

2.2.7 Breakage and attrition

Both breakage and attrition can occur as a result of the collision of crystals with one another, with agitator blades, or with crystalliser's wall. Breakage is defined as the fracture of a crystal into two or more pieces, whereas attrition is the fracture of a crystal into many small fragments. The phenomena can have a strong impact on the crystal size distribution and the median crystal size (Qu, 2007).

The discussion to this point shows that the crystallisation mechanisms are highly interactive. In the end, they determine the properties of the final product of the process. These properties are reviewed in the next section.

2.3 CRYSTALLISATION PRODUCT PROPERTIES

The success of the crystallisation processes is indicated by the property and quality of the crystals produced. In addition to purity, the property of crystals is usually defined by crystal size, morphology, and appropriate polymorphic form (Jones, 2002).

2.3.1 Crystal size

Crystal size is important in the pharmaceutical manufacturing applications because if crystals are too fine, they may form agglomerates (as discussed in section 2.2.6) and cakes that can have a detrimental effect on downstream unit operations such as filtration and drying (Barrett et al., 2005). Although the fine crystals are preferred from the bioavailability perspective since they can dissolve faster, but from the manufacturing perspective they may cause a large loss of yield when washed and create handling and environmental problems due to dust formation (Variankaval et al., 2008; Rawlings et al., 1993). Coarser crystals are therefore preferable, but not so coarse that it may affect content uniformity in the formulated product (Variankaval et al., 2008).

Crystals do not form in single sizes, but they form in a range of sizes, from coarse to fine, which is characterised by the crystal size distribution (CSD). The CSD may affect the pharmaceutical processing parameters, such as filtration and drying rates, and product formulation parameters, such as flowability, compactability and segregation, which in the end affect important product properties, such as content uniformity, tablet strength and dissolution rate (Variankaval et al., 2008). It is usually desirable to have a narrow CSD, which means that the size of the crystals produced is almost uniform because the crystals with a broad or multi-modal CSD has a higher tendency to result in slow filtration rate, poor flowability and variable dissolution rate (Berglund, 2002; Variankaval et al., 2008). Examples of crystals with narrow and broad CSD are illustrated in Figure 2.10.
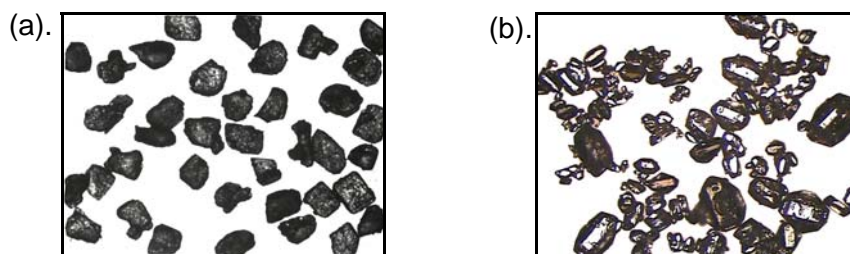
Figure 2.7 Microscopy images of crystals with (a) narrow and (b) broad CSD.

2.3.2 Morphology

As mentioned previously in Section 2.2.3, different sites on the crystal surface would grow at different rates. Consequently, the produced crystals have varied appearances due to the difference in the relative areas of their faces, the lengths of the axes in the

three dimensions, and the angles between faces. This property of the crystals is termed morphology or habit. Figure 2.11 shows some of the typical morphology of sulfathiazole crystals (Blagden et al., 1998a).

(a)   (b)   (c)   (d)
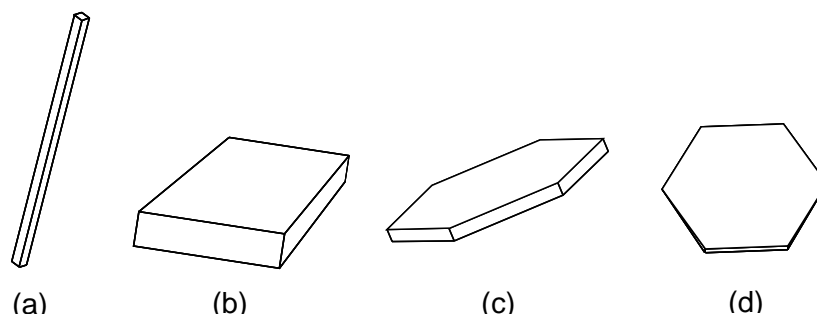
Figure 2.8 Typical morphology of sulfathiazole crystals: (a) needle; (b) cuboid; (c) truncated hexagon; and (c) plate-like hexagonal.

The morphology is determined by the internal structure and external influences on the crystal such as the growth rate, solvent used, and the presence of impurities during the crystallisation growth period (Perry, 1997). It is of technologically importance because different habits will exhibit different product characteristics. As mentioned by Perry (1997), long, needle-like crystals tend to break easily during centrifugation and drying, whereas flat, plate-like crystals are difficult to wash during filtration or centrifugation resulting in low filtration rates. Spherical crystals are desirable compared to cubical shape crystals because they have better flowability and do not form cakes easily. If the final product is a suspension of crystals in a liquid, its rheology is very much dependent on the crystal's morphology (Rawlings et al., 1993).

Shape factors are a convenient mathematical way of describing the geometry of a crystal (Myerson and Ginde, 2002). If the size of a crystal is defined in terms of a characterisation dimension L, two shape factors can be defined: the volume shape factor, α, and the area shape factor, β:

$$\alpha = V/L^3 \tag{2.12}$$

$$\beta = A/L^2 \tag{2.13}$$

Values of shape factors for common materials and geometries are available in the literature (Mullin, 2001).

2.3.3 Polymorphic form

When polymorphism occurs, the molecules arrange themselves into at least two different structural arrangements; either they may be packed differently in the crystal lattice or they may be different in the orientation or conformation of the molecules at the lattice sites (McCrone, 1965). The different crystalline forms exhibited by one substance are called polymorphs.

For a substance that exhibits polymorphism, each of its polymorphs has its own solubility curve. Within the limits imposed by the curves, the embryos of the various polymorphs compete for solute molecules. The embryos that present at the highest concentration, for which the activation energy is the lowest, will form the first nucleus leading to the crystallisation of that particular polymorph (Grant, 1999). This is in accordance to the suggestion made by Etter et al. (1991) that the polymorph favoured to crystallise is the one that nucleates the fastest. Etter et al., (1991) also suggested that more than one polymorph may all nucleate simultaneously and, as a result, a mixture of polymorphs is obtained as product. This, according to Bernstein (2002), may be due to a condition in which the nucleation rates of the polymorphs are equal; hence there is a higher probability of the polymorphs to appear together. Recent studies, however, have found that an existing polymorph that initially nucleated in a system can then initiate the nucleation of another polymorph (Yu, 2007). The phenomenon is called the "cross-nucleation between polymorphs". Compared to the existing polymorph, the newly nucleated one can be thermodynamically more or less stable but has a higher or equal growth rate (Yu, 2007). These show that the selective crystallisation of a polymorph depends not only on the initial nucleation as commonly known, but also on the cross-nucleation between polymorphs and the relative growth rates of the polymorphs (Yu, 2007).

Besides forming polymorphs, some substances can also crystallise into a structure in which the solvent is present as part of the crystal lattice. These crystals are known as solvates. If the solvent is water, the crystals are known as hydrates. The solvates and hydrates are commonly referred to as *pseudo*polymorphs (Myerson and Ginde, 2001), but the term, which literally means false polymorphs, is said to be ambiguous (Desiraju, 2003) and scientifically inaccurate (Rogers, 2003); hence its usage is proposed to be discontinued (Seddon, 2004). The solvates and hydrates are typically

discussed together with the polymorphs since they share many of their behaviours (Morris, 1999).

The crystallisation of polymorphs is governed by Ostwald's rule of stages, which states that upon crystallisation, an unstable polymorph will appear first and subsequently transforms stepwise to other more stable forms until the most stable form has been achieved. This polymorphic transformation is the consequence of the thermodynamic drive towards minimising the Gibbs free energy of the system in order to reach equilibrium (Cardew and Davey, 1985). The change in Gibbs free energy, ΔG, acts as the driving force for the polymorphic transformation. The most stable form is therefore the one with the lowest ΔG and those forms that exist but do not have the lowest ΔG are called metastable forms. The relationship between metastable polymorphs and their more stable forms can be either monotropic or enantiotropic. Figure 2.13 shows the solubility curves for monotropic and enantiotropic systems. For a monotropic system, the solubility curves of Form I and Form II do not cross, so no reversible transformation between polymorphs can be observed below the melting point. The polymorph with the lowest solubility is the stable form. Therefore, based on Figure 2.14(a), Form II is the most stable form. For an enantiotropic system, a reversible transformation can be observed at a definite transition temperature, T_x, at which the curves cross before the melting point is reached (Grant, 1999).
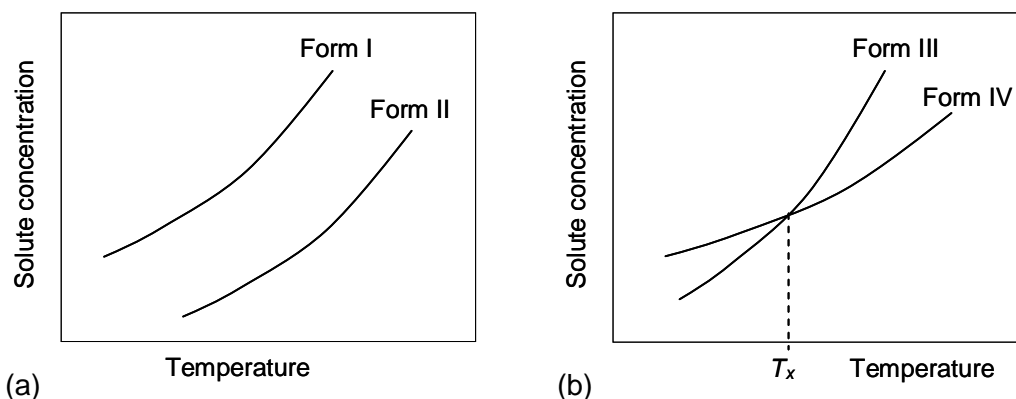
Figure 2.9 Solubility curves for (a) monotropic, and (b) enantiotropic systems.

There are two proposed mechanisms for polymorphic transformation: (a) solid-state transformation, and (b) solvent-mediated transformation. In the solid-state transformation, nucleation and growth of the stable phase take place in crystals of the metastable phase. This transformation is slower (Beckmann, 2003) and it is often

reversible when the temperature is raised or reduced from the transition temperature (Davey and Garside, 2000). Solvent-mediated transformation, sometimes also called solution-mediated transformation, occurs in the present of a solvent and is usually driven by the difference in solubility between the two forms. The mechanism of transformation typically involves three steps: (a) dissolution of the metastable phase into solution to reach and exceed the solubility of the stable form; (b) nucleation of the stable phase; and (c) crystal growth of the new stable nuclei together with the continuous dissolution of the metastable phase (Zhang et al., 2004).

Polymorphs of a substance will have the same chemical properties because they have the same chemical composition but their physical properties, which depend on the structural arrangement of atoms, may be widely different. Since polymorphs usually have different crystal habits, they will also exhibit different properties that are influenced by the shape of the crystal such as flowability and compressibility (Verma, 1966). Due to the wide variation in the properties of the polymorphs of the same substance, it is very important to achieve control over which polymorph is produced in crystallisation processes. It is thus essential to know and understand the formation conditions of the different polymorphs as well as their characteristics so that these can be accounted for in the crystallisation process design.

2.4 SOLID-STATE CHARACTERISATION OF CRYSTAL PROPERTIES

2.4.1 Crystal size and morphology

Crystal size is usually defined by a single linear dimension and it is quantified by the techniques of measurement (Berglund, 2002). There are a large number of techniques available for crystal size analysis (Barth and Sun, 1985). The major techniques commonly used in practice can be categorised into mass-based (or volume-based) and number-based. The mass-based techniques include sieving, sedimentation and light scattering/diffraction. These techniques however have a difficulty in measuring small crystals in the presence of larger ones, which makes it unable to determine the nucleation rates from CSD measurements. The number-based techniques, as the name implies, are based on crystal number. The techniques include electrical sensing zone, focused beam reflectance measurement (FBRM) and microscopy. FBRM, used in this work for *in situ* measurement, is described in detail in section 2.6.2. Microscopy techniques such as optical microscopy and scanning

electron microscopy (SEM) can be used to characterise crystal size and morphology simultaneously. The SEM is particularly useful for examining morphology as well as surface features of crystals (Bernstein, 2002). The static images provided by optical microscopy can only handle a small sample size at a time; therefore the provision of statistically relevant data is an arduous and time consuming work (Pollanen et al., 2006). There are several image analysis techniques that provide dynamic images including Sympatec's QICPIC dynamic image processing system (Witt et al., 2004) and Retsch Technology's Camsizer. The systems image a flow of moving crystals and the images are then analysed to give information about the sample's size and shape parameters (aspect ratio or sphericity). They have been successfully utilised by researchers such as Patchigolla and Wilkinson (2009) and Ho et al. (2009).

2.4.2 Polymorphic form

Different polymorphs can be identified and differentiated using many characterisation techniques. These techniques have been extensively reviewed in the literature (Brittain, 2006; 1999; Stephenson et al., 2001; Bugay et al., 2001; Threlfall, 1995; Yu et al., 1998). Table 2.3 summarises the typical off-line characterisation techniques for the study of polymorphism.

Table 2.3 Typical off-line characterisation techniques for polymorphic form.

No.	Technique	Description
1.	Microscopy:	
	a. Optical microscopy	Provides visual information on the morphological properties of crystals, which can be used to roughly differentiate between different polymorphs (Rodriguez-Spong et al., 2004). If viewed under polarised light, different polymorphs can be distinguished from each other by their optical properties such as birefringence (Brittain et al., 1999).
	b. Scanning electron microscopy (SEM)	Gives a two-dimensional morphological image and a higher resolution compared to optical microscopy. These make it an ideal complementary technique to optical microscopy (Yu et al., 1998).

2.   Thermal analysis:

     a.   Differential scanning calorimetry (DSC) — Involves placing the solid sample in a metal pan along with a reference pan (normally an empty pan) in a furnace. Then heating or cooling at a control rate is applied and subsequently, the heat flow required to keep the equality in the temperature of the sample and reference is measured. A DSC curve is obtained as the differential rate of heat flow (in W/g) against temperature. If there are any thermal events such as melting, polymorphic transformation and crystallisation, peaks are shown on the curve. The area under the peak is directly proportional to the heat absorbed or released by the event and by integrating the area, the enthalpy change of transformation is obtained (Brittain et al., 1999).

     b.   Hot-stage microscopy (HSM) — Allows observation of the behaviour of a solid during heating or cooling, which permits observation of phase transitions such as melting and polymorphic transformation, and the recording of their optical properties changed (Threlfall, 1995). It easily distinguishes a polymorphic transformation from the melting process (Marthi et al., 1992); hence provides confirmation of thermal events that are observed using other techniques. Some examples of its application in the analysis of pharmaceuticals have been presented by Vitez and Newman (2007).

     c.   Thermogravimetry (TG) — Measures the thermally induced weight loss of a solid as a function of temperature. Commonly used to identify solvates or hydrates qualitatively as well as quantitatively since it can determine the total volatile content of a solid (Brittain et al., 1991). It however cannot provide a chemical identification of the volatile (Bugay et al., 2001).

3.   Vibrational spectroscopy:

     a.   Fourier transform infrared (FT-IR) — When an IR radiation is passed through a sample, some of the wavelengths are absorbed by the sample and some are transmitted. The resultant infrared spectrum represents a fingerprint of a sample with absorption peaks that correspond to the frequencies of vibrations between the bonds of the atoms making up the compound. Since different polymorphs have different hydrogen-bonding patterns, which in turn may shift the affected functional groups in varying degrees, no two polymorphs produce the same spectrum (Rodriguez-Spong et al, 2004). The technique is used to confirm the identity of the polymorphs by comparing the spectra of the sample with a reference (Brittain et al., 1991).

	b. Raman	When a sample is irradiated with monochromatic light, a small fraction of the light is scattered at frequencies different from that of the incident light. This inelastic scattering process is due to an effect called Raman. The molecule's vibrational energy levels determine the size of the frequency shift and the number of different shifts that will occur. This gives information about the state and identity of molecular bonds, which in turn help to identify the sample and its structure (Vankeirsbilck et al., 2002).
4.	Solid-state nuclear magnetic resonance (ssNMR) spectroscopy	Operates based on the principle that nuclei resonate at different frequencies and these changes in chemical shift can be connected with changes in chemical environment of the compound (Rodriguez-Spong et al., 2004). The technique provides detailed information on the three-dimensional structure of the compound. It is however a non-routine technique due to its complexity. Some reviews devoted to its application in pharmaceuticals include Bugay (1993) and Geppi et al. (2008).
5.	X-ray diffractometry (XRD)	Operates based on Bragg's law: $n\lambda = 2d\sin\theta$, where n is the order of the diffraction pattern; λ is the wavelength of the incident beam; d is the distance between the planes in the crystal; and θ is the angle of beam diffraction. When a monochromatic X-ray beam strikes a plane of atoms at an angle θ, the rays are diffracted at the same angle θ. These angles are corresponding to spaces between planes of molecules in the crystal lattice. Since no two compounds would form crystals in which their three-dimensional spacing of planes is the same in all directions, the technique is considered as the most conclusive by itself alone (Brittain et al., 1991). If a single crystal is used, the technique is able to clearly differentiate between polymorphs, but high quality crystals of adequate size are hard to obtain. Crystalline powder (XRPD) is routinely used instead although it cannot easily differentiate between polymorphs (Rodriguez-Spong et al., 2004). If X-ray diffraction patterns are obtained while the sample is subjected to a controlled temperature program, the technique is called variable temperature XRD (Rastogy et al., 2001). It allows observation of phase transitions such as polymorphic transformation and dehydration.

Since the properties of different polymorphs are very often only marginally different, a variety of characterisation techniques should be employed to avoid making erroneous conclusions (Vippagunta et al., 2001). The use of more than one characterisation technique is also needed because some techniques require sample preparation steps that could induce polymorphic transformation (Threlfall, 1995).

The discussion up to this point highlights the well-known notion that the properties of the crystals are defined during crystallisation process; therefore, the production of crystals with the desired quality requires a careful selection of crystallisation operation and control. These issues will be reviewed in the next section.

2.5 CRYSTALLISATION OPERATION AND CONTROL

Crystallisation can either be operated in a batch or continuous mode. However, batch operation is a typical mode of choice for pharmaceutical crystallisations because their production rates are generally small and losses must be kept as low as possible, since the materials are very expensive (Myerson, 2002). In addition, the operation offers the flexibility of execution with changing recipes (Costa and Filho, 2005). Batch crystallisation operations are classified based on the methods by which supersaturation is generated as previously discussed in Section 2.2.1. In order to determine which method is suitable for a particular system, the shape of its solubility curve should be examined. If the solubility curve is steep, which means that the solute solubility sharply increases with temperature, a cooling crystallisation might be suitable. However, if the metastable zone width is wide, addition of seed crystal might be necessary (Jones, 2002). If the curve is relatively flat, which means that its solubility increases only slightly with an increase in temperature, a reasonable yield of crystals can be produced either by evaporative or by freeze crystallisations. However, since most APIs have limited temperature stability, the use of evaporative crystallisation is precluded (Fujiwara et al., 2005). Besides application to heat sensitive APIs, freeze crystallisation is also useful for those APIs that exhibit poor stability in solution (Connolly et al., 1996). Anti-solvent crystallisation can always be used if the yield of other crystallisation operations is low. Two types of crystallisation operation that will be employed in this research work are cooling crystallisation and anti-solvent crystallisation.

2.5.1 Cooling crystallisation

The main advantage of the cooling crystallisation operation is that no additional raw material is required that could affect the product purity and would increase operating and capital costs (Nagy et al., 2006a). However, as mentioned previously, this type of operation is only applicable to systems, in which the solute solubility sharply increases with temperature.

Supersaturation in the cooling crystallisation is generated by decreasing the temperature of the solution using a particular cooling mode. There are three cooling modes that can be employed to control cooling rate during batch, namely natural, linear and programmed cooling (Pollanen, 2006). Figure 2.4 shows the difference in the profile of the natural, linear and the programmed cooling curves. In natural cooling, the crystallisation process depends directly on the heat transfer capacity of the system operating at a constant coolant temperature (Yang, 2005). In this case, the temperature driving force will be high initially and then will decrease with time. As for linear cooling, the cooling rate of the process is constant throughout the batch. In these two cooling modes, often there will be a rapid initial cooling, which will result in the solution crossing the metastable limit and producing enormous nucleation. This can lead to a poor quality product, with a small mean size and a wide CSD (Yang, 2005). In order to produce crystals with a desired quality, an optimal cooling profile needs to be followed. Many studies have dealt with finding the optimal temperature profile as exemplified by the works of Hu et al., (2005), Costa and Filho (2005), Choong and Smith (2004) and Yang (2005). This is where a programmed cooling mode comes into play. It is employed to follow the optimal temperature profile. Typically in this mode, a very low cooling rate is applied in the early stage of the process, while the concentration of crystals, and hence surface area for growth, is low. The cooling rate gradually increases with time as the concentration of crystals and the surface area increases.

Batch cooling crystallisation is often operated using the programmed cooling mode. There are two main approaches used to determine the optimal cooling profile, namely model-based and direct design.
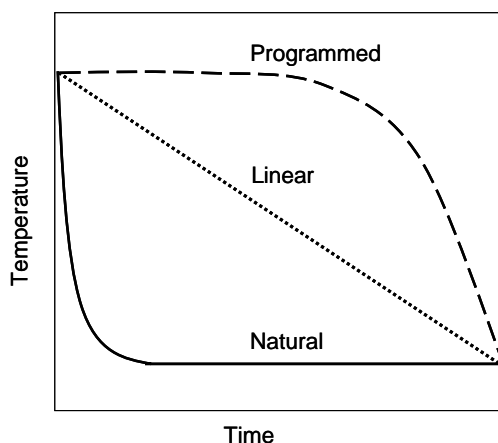
Figure 2.10 Typical profiles of natural, linear and programmed cooling operations.

Model-based approach

The model-based approach is a theoretical prediction of the cooling profile to reach different control targets. The control targets can be to maintain a constant supersaturation course during operation, or to attain the desired crystal properties using optimisation methods (Yang, 2005). The simplified cooling model to maintain a constant supersaturation level is expressed as

$$T = T_0 - (T_0 - T_f)\left(\frac{t}{\tau}\right)^x \tag{2.14}$$

where T_0, T_f and T are the temperatures at the beginning, end, and any time t during the process, respectively, τ is the overall batch time, $x = 4$ for the unseeded solution with nucleation and $x = 3$ for the seeded solution with ignored nucleation (Mullin, 2001). The subject of seeded operation is discussed in more detail later in this section. There are some assumptions made in obtaining this simplified cooling model equation: (a) constant growth and nucleation rates; (b) size of initial seeds or nuclei is negligible compared to the corresponding size of the product; and (c) linear solubility curve for the crystallised compound (Mullin, 2001).

If the control targets of the crystallisation process are defined in terms of desired properties of final crystal products, the temperature profiles used are usually based on *a priori* knowledge of nucleation and growth kinetics as a function of supersaturation. This approach is often referred to as the first-principle approach (Braatz, 2002). However, the results of the approach depend on the accuracy of the kinetic models

used. Therefore, as mentioned by Choong and Smith (2004), and Matthews and Rawlings (1998), in order to obtain the correct optimal cooling profile, the work should firstly focus on getting accurate kinetic models. Several approaches have been proposed to obtain the kinetic models. For example, Rawling et al., (1993) proposed non-linear optimisation approaches to estimate the parameters in the kinetic models.

In addition to the effects of the potential deviations from the model assumptions, Nagy et al. (2004a) pointed out that the effects of parameter uncertainties and disturbances also have to be taken into consideration to ensure that the model-based approach produces the expected optimised product quality. Miller and Rawlings (1994), Zhang and Rohani (2003) and Mohameed et al. (2003) are among many other research groups that used the approach to develop the cooling profiles. According to Chew et al. (2007a), although the model-based approach has the benefit of improving process understanding and potential use in process scale-up, the considerable expertise required in process modelling and optimisation has limited its application to small scale laboratory studies.

Direct design approach

The direct design approach investigates the cooling profile experimentally using a feedback control strategy on the basis of a real-time measurement of supersaturation and/or product properties, such as the CSD, during a batch. With the understanding that the desired region of operation is within the metastable zone, this approach can be implemented based on the automated determination of the solubility curve and the metastable limit (Nagy et al., 2004b). It means that the approach does not require kinetic information at all. However, the reliability of control depends on the accuracy of the in-line measurement and on a good performance of the controller (Yang, 2005). In addition, compared to the model-based approach, this approach may be more time-consuming and costly as a large number of experiments is sometimes required. Various feedback control strategies based on in-line measurement of supersaturation have been presented (Chew et al., 2007b; Nagy et al., 2004b; Liotta and Sabesan, 2004; Feng and Berglund, 2002; Fujiwara et al., 2002). This is mainly due to its simplicity as it requires only a simple mathematical tool, which makes it amenable for large-scale implementation in industry (Chew et al., 2007a).

2.5.2 Anti-solvent crystallisation

In an anti-solvent crystallisation, a solute is crystallised from a primary solvent by the addition of a second solvent, known as an anti-solvent. The anti-solvent chosen must be a poor solvent for the solute and must also be fully miscible with the primary solvent (Nagy et al., 2007). These would result in a solubility decrease of the solute in the resulting binary solvent mixture. Consequently, the solute precipitates out. Addition of the anti-solvent can be done either at the beginning of the crystallisation process to induce nucleation, or at the end of a cooling crystallisation period to enhance yield (Barrett et al., 2005). The later technique known as combined cooling-anti-solvent addition was employed successfully by Nagy et al. (2007) in the crystallisation of lovastatin.

An anti-solvent crystallisation can be operated at ambient temperature, which is useful when dealing with heat sensitive products. It also does not require energy to cool the solution, as in the case of cooling crystallisation, which will lower the operating costs of the process. The anti-solvent crystallisation operation however, requires large operating costs for the solvent separation and large capital costs for a large volume crystalliser, and an additional solvent recovery system (Nagy et al., 2007). In addition, time scale of response is much shorter than for cooling crystallisation.

The anti-solvent addition has a profound effect on the crystal habit or polymorphic form due to changes in solvent activity, which is important when crystals with a particular required habit or polymorphic form are to be produced. Different polymorphs will have a different solubility in the mixed solvents with the stable polymorph having the lowest solubility (Roelands et al., 2006). Due to the difference in solubility, the driving force toward the forms is different and so is the interfacial energy between the crystals and solution. As a result, the polymorphs nucleate and grow at different rates. The polymorphic form that is obtained depends on how these competitive rates vary. Several research groups that studied the formation of different polymorphs in anti-solvent crystallisation processes described the formation as a function of the ratio solution/anti-solvent (Roelands et al., 2006; Beckmann, 1999; Toth et al., 2004).

Mixing is a critical issue for all crystallisation operations but in the anti-solvent crystallisation, adequate mixing is required to incorporate the anti-solvent into the bulk solution and maintain a constant supersaturation throughout the crystalliser (O'Grady

et al., 2007). O'Grady et al. (2007) investigated the effect of mixing on the MSZW of benzoic acid in ethanol-water mixture, with water as the anti-solvent. They found that the higher the anti-solvent addition rate, the wider the MSZW, which is typical of most crystallisation systems since the increase in the supersaturation generation, will increase the MSZW. When the anti-solvent was added close to the impeller, this effect was more pronounced. This is due to the mixing conditions at that location, which allow rapid incorporation of the anti-solvent and a homogeneous mixture of anti-solvent and solution. However, increase in agitation speed at the same location resulted in a narrower MSZW for all addition rates. This is, according to them, possibly due to the increased probability of contact between solute molecules. They also found that, when anti-solvent was added close to the vessel wall, the MSZW was significantly narrower. The reason is that, at this location, the poor mixing conditions produce areas of high supersaturation that leads to a premature nucleation. When the agitation was increased, a wider MSZW was produced since the local areas of supersaturation dissipated.

For controlled operation of the anti-solvent crystallisation, the rate at which the anti-solvent is added can be used as a control variable to achieve desired crystal properties since it influences the level of supersaturation. Normally, the supersaturation during operation should be at a level where the nucleation rate is minimised while the crystal growth is maximised. According to Mersmann (1999), nucleation typically occurs at a rather high supersaturation level, whereas crystal growth can occur and proceed at a considerably lower level of supersaturation. Based on these considerations, it is expected that at a slower addition rate of anti-solvent, the resultant low level of supersaturation will result in growth being favoured over nucleation and in the end, a larger crystal size is produced; the reverse is true if a faster addition rate of anti-solvent is employed.

Similar to the case of finding an optimal cooling profile, the determination of an optimal anti-solvent addition profile may also be done using either model-based or direct design approaches.

Model-based approach

Tavare (1995) described an optimal anti-solvent addition profile using a model equation similar to equation 2.14:

$$\frac{U - U_i}{U_f - U_i} = \left(\frac{t}{\tau}\right)^4 \qquad\qquad (2.15)$$

where U_i, U_f and U are the anti-solvent concentrations at the beginning, end, and any time t during the process, respectively, and τ is the overall batch time. This model treats anti-solvent crystallisation in a similar manner as cooling crystallisation and uses the following assumptions: no seed, linear solubility relation, and constant growth and nucleation rates, which are independent of the solution composition. However, as Nonoyama et al. (2006) found out, the assumptions are not always satisfied for all compounds.

Alternatively, Nonoyama et al. (2006) introduced a model, based on the fundamental crystallisation equations using a numerical simulation. The simulation was applied using kinetic parameters obtained from experiments. This model takes into account only growth and ignores nucleation, agglomeration and breakage. It also assumes size-independent crystal growth and uniformity within the crystalliser.

A population balance model, as mentioned previously, is able to describe the evolution of the CSD in a system. Its usage in the modelling of the crystallisation process requires a reformulation of the model into a computationally more affordable form than the direct numerical solution (Nagy et al., 2006b). There are many different approaches of the reformulation, but Nagy et al. (2006b) developed a population balance model for the anti-solvent crystallisation of lovastatin using the method of moments. The method is based on the fact that the dominant dynamics of the crystalliser can be described by a small number of degrees of freedom. The model is used to obtain optimal control strategies through simultaneous cooling and anti-solvent addition with different product quality targets.

As mentioned previously, mixing is a critical issue in the anti-solvent crystallisation. In order to take into account the imperfect mixing of anti-solvent crystallisation process, several research groups adopted approaches based on a computational fluid dynamics (CFD) simulation (Liu et al., 2006; Woo et al., 2006; Choi et al., 2005). For example, Woo et al. (2006) incorporated in the turbulent CFD simulations a multi-environmental probability density function model, which captures the macromixing between the different components, and the population balance equation, which models

the evolution of the CSD. These modelling studies provide valuable understanding of the effects of mixing on crystallisation and would offer a scientific basis for the design and scale-up of crystallisers (Chew et al., 2007a).

Direct design approach

The direct design approach for the anti-solvent crystallisation follows the same principle with the approach previously described under cooling crystallisation. It utilises a feedback control system in which the crystalliser follows the set-point profile by adjusting the anti-solvent addition rate based on the *in situ* measurement of the supersaturation and/or the product properties. This approach partly overcomes the problem associated with imperfect mixing in the crystalliser as the implementation of supersaturation control and *in situ* measurement are able to absorb disturbances in operating conditions. Partly because if the crystalliser is imperfectly mixed, the measurement sensor may not reflect the true vessel's average supersaturation. Zhou et al. (2006) used the approach for the concentration control of the anti-solvent crystallisation of paracetamol from acetone-water. The study demonstrates the ability of the approach to be automated. The automation enables the rapid testing of various supersaturation profiles, hence rapid development of crystallisation processes.

2.5.3 Seeding

In addition to supersaturation control, the seeding technique can also play a critical role in defining the properties of crystal products. It is known that the technique is able to improve the CSD (Warstat and Ulrich, 2006; Yu et al., 2006b; Kubota et al., 2001; Patience and Rawlings, 2001; Lol Mi Lung-Somarribaa et al., 2004) and to control polymorphism (Beckmann, 1999; 2001; Doki et al., 2004a). A guide on the use of seeds to control the formation of polymorphs is provided by Beckmann (2000). Seed crystals can be generated either directly from recrystallisation, or from subsequent particle-size reduction processes including sifting, screening, sonication, super-critical fluid extraction and particle-size reduction followed by ripening (ageing).

Basically, the introduction of seeds in the supersaturated solution at the start of the crystallisation circumvents the uncertainties in the spontaneous primary nucleation, since the system is not allowed to become labile (Yu et al., 2006b). With the presence of seeds in the system, secondary nucleation is expected to take place and the supersaturation is mainly used for the growth of seeds. Typical operating curves, on a

phase diagram, for unseeded and seeded controlled operations of both cooling and anti-solvent crystallisations, are shown in Figure 2.11. In the figure, the *x*-axis represents the temperature for cooling crystallisation, and the percentage of solvent in the mixture for anti-solvent crystallisation.
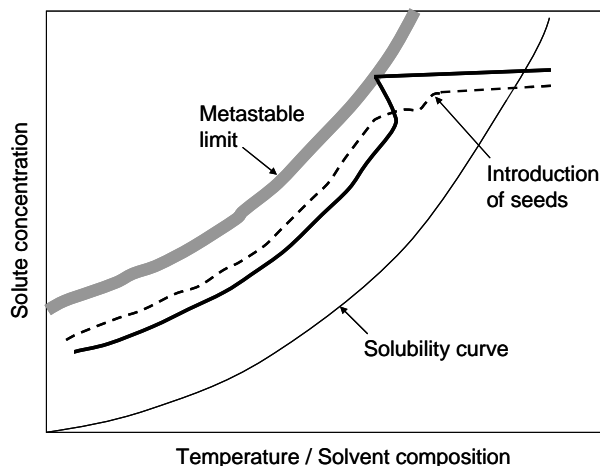
Figure 2.11 Typical operating curves for unseeded (thick continuous line) and seeded (dashed line) controlled operations.

Research on seeding techniques has mainly focussed on how to determine the seed size and loading. Mullin (2001) proposed the following expression to determine the size of seed:

$$M_S = \frac{Y \bar{L}_S^3}{\left(\bar{L}_P^3 - \bar{L}_S^3 \right)}$$

(2.16)

where M_S is the mass of seeds, $\bar{L}_S$ and $\bar{L}_P$ are the average sizes of seeds and final products, respectively, and Y is the required crystal yield. $\bar{L}_S$ and $\bar{L}_P$ are number-mean sizes, defined based on the first moment of the normalised population density function. The expression is derived from a mass balance of the crystallisation batch by assuming the number of product crystals to be equal to that of seeds. It means that nucleation is restrained to such an extent that almost all solute molecules deposit on the seed surfaces.

Yu et al. (2006b) utilised equation 2.16 to study the effects of seed loading and seed size distribution for anti-solvent crystallisation of paracetamol from a water-acetone

mixture operated at constant supersaturation. Their results indicate that seed loading can be used to refine the CSD of the final product and the ratio of target product size to initial seed size should not be too high to avoid excessive secondary nucleation.

Kubota et al. (2001) emphasised the importance of seed loading to ensure the narrow size distribution of final products. Their work showed that desired size distribution of final products could be achieved with a wide range of supersaturation generation rates when seed loading exceeded a critical value, which was determined empirically. Lol Mi Lung-Somarriba et al. (2004) put forward a procedure to determine seed size and seed loading that took into account the attrition of large crystals. They proposed that the seed size should be smaller than one-quarter of the maximal product size over which attrition will hinder crystal growth. Similar to the critical seed loading proposed by Kubota et al. (2001), they used a critical surface area obtained empirically to determine the size and mass of seeds. Doki et al. (2004b) have demonstrated that a selective crystallisation of a metastable polymorphic form can be performed based on the identification of a critical level of seed loading in order to suppress the secondary nucleation of the stable and other metastable forms.

Combination of seeding technique and manipulation of supersaturation profile is expected to increase the likelihood in producing crystals with the desired qualities. Therefore, instead of treating seeding policy separately from supersaturation profile, Yang et al. (2006b), and Choong and Smith (2004) included seeding conditions as the optimised variables along with temperature profile in the formulation of the optimal profiles. This approach is capable of absorbing some disturbances in operating conditions, such as growth rate dispersion and agglomeration (Yu et al., 2006b).

In this study, the direct design approach will be used due to its simplicity in application as it does not require a kinetics study, process models, and optimisation. Moreover, application of *in situ* monitoring techniques could lead to better prediction and control of the applied supersaturation and in the end, better control of the final product quality. Factors that affect the product quality however are system-specific and it is a challenge to control a system that has multiple polymorphic forms. In the next section, the literature information on the crystallisation and polymorphism of sulfathiazole, the main model compound used in this work, are reviewed. Besides to gain a background knowledge about the system of interest, which is a prerequisite in the development of

its crystallisation operation, the review illustrates some of the principles and the difficulties associated with the crystallisation of a polymorphic system.

2.6 CRYSTALLISATION AND POLYMORPHISM OF SULFATHIAZOLE

Sulfathiazole, a chemical structure shown in Figure 2.12, is an antimicrobial agent. Since its discovery in 1939 (Fosbinder and Walter, 1939; Lott and Bergeim, 1939), numerous works in isolating, generating and characterising its different polymorphic forms have been carried out and communicated to the scientific community.
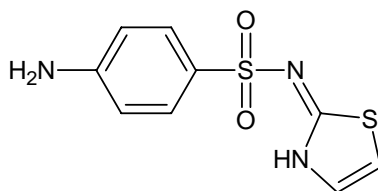
Figure 2.12 Chemical structure of sulfathiazole.

True to a famous suggestion by Walter McCrone, that the number of polymorphic forms known for a given compound is proportional to the time and money spent in research on that compound (McCrone, 1965), the official knowledge on the number of sulfathiazole polymorphic forms has progressed from two in 1941 (Grove and Keenan, 1941) to five from 1999 (Hughes et al., 1999; Chan et al., 1999) until present. Sulfathiazole is also reported to form an amorphous phase (Mesley and Houghton, 1967; Lagas and Lerk, 1981), a hydrate (Kuhnert-Brandstatter and Wunsch, 1969) and over one hundred solvates (Bingham et al., 2001).

The extensive and repeated works on sulfathiazole polymorphism have produced inconsistent nomenclatures in the naming of the polymorphs. This inconsistency may cause confusion and difficulty in identifying and interpreting the literature information on the polymorphs and, as highlighted by Bernstein (2002), is due to the lack of attempts by authors to reconcile their own work with previous studies. Some authors, however, have corresponded and/or referred to their polymorphs using the notations of the Cambridge Structural (CS) Database reference codes (refcodes) (Blagden et al., 1998a; Aaltonen et al., 2003; Karjalainen et al., 2005; Hakkinen et al., 2005; Gelbrich et al., 2008; Alvarez et al., 2009). The refcodes can be considered as standards since each of them represents specific crystallographic properties. There are currently twenty four crystal structures of sulfathiazole available in the database to represent

five different polymorphs. These structures are contributed by various researchers. A summary of the structures with their cell data and depositor are given in Appendix A. A large number of structures to represent only five different polymorphs means that some of them are repeated. However, the later deposited data are expected to provide improved quality in their structural representations, particularly with respect to the hydrogen atom positions. This is due to the improved XRD's capability as a result of the technological advances. In order to differentiate between different polymorphs, the CS Database also uses the enumeration scheme adopted by the earlier crystal structures' depositors. Table 2.4 relates the scheme to the corresponding refcodes. In this thesis, the enumeration of the sulfathiazole polymorphs follows this scheme. Attempts to reconcile the literature enumeration of sulfathiazole polymorphs have been made by Burger and Dialer (1983), and Anwar et al. (1989). Here, their works were updated and extended to include all five known polymorphs as well as the un-cited and later literature. Table 2.4 also relates the literature enumeration of the sulfathiazole polymorphs to the enumeration scheme and refcodes adopted by the CS Database.

2.6.1 Crystallisation of sulfathiazole polymorphs

Since the polymorphism of sulfathiazole has been extensively and repeatedly investigated by various researchers as shown in Table 2.4, various recipes for generating a particular polymorph have become available.

Form I

Literature recipes for isolating Form I are presented in Table 2.5. It can be seen from the table that all of the solvents that have been used to crystallise Form I are alcohols containing between three to five carbon atoms, which satisfy a suggestion made by Mesley (1971) that recrystallisations from alcohols containing three or more carbon atoms should produce Form I. In accordance to the Ostwald's Rule of Stages, Blagden et al. (1998a) suggested that any solvent should be able to initially produce Form I as it is the least stable form, followed by a stepwise conversion, through the other metastable forms, to the thermodynamically most stable form. An example of this stepwise conversion had been observed by Grove and Keenan (1941) during their attempt to isolate rod-like Form I crystals from hot ethanol. In order to prevent any polymorphic conversions, n-propanol was chosen as the solvent since it has a higher boiling point than ethanol, which they reckoned will allow enough time for the crystals to be removed from the hot solution before the conversion can take place; hence the

Table 2.4 Literature enumeration of sulfathiazole polymorphs and the corresponding CS Database enumeration and refcode.

CS Database enumeration	Equivalent CS Database refcode	Literature enumeration and reference.
Form I	Suthaz01, Suthaz07, Suthaz08, Suthaz16, Suthaz23.	Rod form (Grove and Keenan, 1941); β (Miyazaki, 1947); B (Mesley and Houghton, 1967); II (Milosovich, 1964; Higuchi et al., 1967; Guillory, 1967; Moustafa and Carless, 1969; Shenouda, 1970; Shami et al., 1972; Carless and Jordan, 1974; Jordan and Carless, 1976); I (Lagas and Lerk, 1981; Anwar et al., 1989; Mesley, 1971; Kruger and Gafner,1971;1972; Gelbrich et al., 2008; Burger and Dialer, 1983; Shaktshneider and Boldyrev, 1993; Khoshkhoo and Anwar, 1993; Apperley et al., 1999; Luner et al., 2000; Blagden, 1998a; Zeitler et al., 2006; Parmar et al., 2007; Drebushchak et al., 2008).
Form II	Suthaz, Suthaz03, Suthaz09, Suthaz10, Suthaz18, Suthaz20.	Hexagonal form (Grove and Keenan, 1941); α (Miyazaki, 1947); A (Mesley and Houghton, 1967); I (Shami et al., 1972); II' (Babilev et al., 1987); II (Blagden et al., 1998a; Kruger and Gafner,1971;1972; Blagden, 2001; Parmar et al., 2007; Drebushchak et al., 2008); IV (Anwar et al., 1989; Burger and Dialer, 1983; Khoshkhoo and Anwar, 1993; Apperley et al., 1999; Zeitler et al., 2006; Gelbrich et al., 2008).
Form III	Suthaz02, Suthaz11, Suthaz12, Suthaz17, Suthaz21.	α' (Miyazaki, 1947); C (Mesley and Houghton, 1967); IIA (Mesley, 1971); I ((Milosovich, 1964; Higuchi et al., 1967; Guillory, 1967; Moustafa and Carless, 1969; Shenouda, 1970; Carless and Jordan, 1974; Jordan and Carless, 1976); III (Lagas and Lerk, 1981; Blagden et al., 1998a; Anwar et al., 1989; Kruger and Gafner,1971;1972; Gelbrich et al., 2008; Burger and Dialer, 1983; Shaktshneider and Boldyrev, 1993; Khoshkhoo and Anwar, 1993; Apperley et al., 1999; Luner et al., 2000; Blagden, 2001; Zeitler et al., 2006; Parmar et al., 2007; Drebushchak et al., 2008; Ali et al., 2009).

Form IV	Suthaz04, Suthaz13, Suthaz14, Suthaz19, Suthaz22.	*IIB* (Mesley, 1971); *II* (Khoshkhoo and Anwar, 1993); *IV* (Blagden, 1998a; Babilev et al., 1987; Blagden, 2001; Parmar et al., 2007; Drebushchak et al., 2008); *V* (Apperley et al., 1999; Zeitler et al., 2006; Gelbrich et al., 2008).
Form V	Suthaz05, Suthaz06, Suthaz15.	*V* (Hughes et al., 1999; Chan et al., 1999); *II* (Lagas and Lerk, 1981; Anwar et al., 1989; Burger and Dialer, 1983; Apperley et al., 1999; Zeitler et al., 2006; Gelbrich et al., 2008).

origin of Method 1. However, it was reported much later that Form I crystallised from n-propanol did not transform to other forms up to one year of storage as slurry at 30°C (Blagden et al., 1998a).

All of the cited researchers that utilised Method 1 and Method 2 in Table 2.5 implied no presence of any other polymorphic forms besides Form I, but more recent researchers reported otherwise. Anderson et al. (2001) reported that although crystallisations from n-propanol at various cooling rates in stirred and unstirred 50 mL reactors consistently produced Form I, traces of Form V were also found within some samples. The crystals obtained by Aaltonen et al. (2003) through cooling crystallisation from n-propanol at a constant rate of 35°C/hour in a 100 mL reactor were mainly Form I, but Form II and Form III were also present. Through a cooling crystallisation experiment conducted at a constant rate of 27.5°C/hour in a 4 L reactor, Hakkinen et al. (2005) obtained crystals of mainly Form I together with some portions of Form III and Form V. More recently, Alvarez et al. (2009) produced Form I, Form III and Form IV from cooling crystallisation experiments using n-propanol as a solvent at various initial concentrations and cooling rates.

Method 7 in Table 2.5 was first applied by Miyazaki (1947). The method can be considered as the most reliable one because at the heating temperature, crystals of Form II, or Form III, or the commercial raw material, which is typically composed of Form II or Form III, or a mixture of the two, are expected to transform into Form I since it is the most stable sulfathiazole polymorph at high temperature. Although the heating

process may turn the crystals into a slight off-white colour, it was found that this did not interfere with the subsequent characterisation studies (Apperley et al., 1999).

Table 2.5 Methods of producing Form I.

No.	Procedure	Reference
1	Seeded cooling crystallisation from a saturated n-propanol solution at 80-90°C. After a crop of rod-like crystals has formed, the hot supernatant solvent was decanted and drained off. The crystals were washed with ether to remove solvent and then dried in the air at room temperature.	Grove and Keenan (1941); Higuchi et al. (1967)
2	Cooling crystallisation from a saturated n-propanol solution at 80-90°C.	Mesley and Houghton (1967); Shenouda (1970); Kruger and Gafner (1971); (1972); Lagas and Lerk (1981); Burger and Dialer (1983); Anwar et al. (1989); Khoshkhoo and Anwar (1993); Blagden et al. (1998); Blagden (2001); Karjalainen et al. (2005); Parmar et al. (2007).
3	Cooling crystallisation from a saturated solution of amyl alcohol.	Miyazaki (1947); Moustafa and Carless (1969);
4	Cooling crystallisation from a saturated solution of isobutanol.	Miyazaki (1947); Mesley and Houghton (1967)
5	Cooling crystallisation from a saturated solution of n-butanol at its boiling temperature..	Shakhtshneider et al. (1993); Parmar et al. (2007); Drebushchak et al. (2008).
6	Cooling crystallisation from a saturated solution of sec-butanol.	Higuchi et al. (1967); Moustafa and Carless (1969); Shenouda (1970).
7	Heating a commercial raw material or Form II or Form III at a temperature between 170 to180°C for 15-40 minutes.	Miyazaki (1947); Milosovich (1964); Moustafa and Carless (1969); Shami et al. (1972); Carless and Jordan (1974); Shakhtshneider et al. (1993); Apperley et al. (1999); Luner et al. (2000); Zeitler et al. (2006).

Form II

Table 2.6 summarises methods of producing Form II. Although Method 1 was the method used by the researchers that contributed the crystallographic data for Form II

(Kruger and Gafner, 1971); it is not a reliable method to produce Form II crystals based on a recent work by Alvarez et al. (2009), which showed that cooling crystallisation experiments from initial temperature of 30°C produced only Form III at a slow cooling rate and no crystals at all when a fast cooling rate was applied. In addition, as mentioned previously, only a small portion of Form II was obtained by Aaltonen et al. (2005) through their cooling crystallisation experiment from n-propanol at a constant rate of 35°C/hour. Based on the same set of works by Alvarez et al. (2009), Method 2 is also not a reliable method of producing Form II because only Form III and Form IV were obtained in their cooling crystallisation experiments with water as the solvent (Alvarez et al., 2009). On the same note, Blagden et al. (1998a) also reported that crystallisation from water only favours the formation of Form IV crystals. Although Form II was produced by cooling crystallisation experiments from both acetone and a mixture of acetone and chloroform, as reported by Alvarez et al. (2009), it always formed as a mixture with Form III. On the other hand, based on a report by Mesley (1971), recrystallisation from a mixture of acetone and chloroform did not produce Form II at all, but a mixture of Form III and Form IV. For these reasons, Method 3 and Method 4 are not reliable methods of generating Form II crystals. Method 5 was the method used by Babilev et al. (1987), the contributor of the crystallographic data of Suthaz03 (Form II). Slightly over a decade later, Blagden et al. (1998a) also used the same method to produce Form II crystals in their study on the effect of solvent to the polymorph appearance. In the same study, they also generated Form II crystals from nitromethane (Method 6). Method 7, Method 8 and Method 9 are also believed to be reliable since Parmar et al. , Apperley, Drebushchak and their co-workers were able to produce crystals with X-ray diffraction parameters consistent with literature values of Form II.

Form III

Methods of producing Form III are presented in Table 2.7. Method 1, Method 2 and Method 3 involve fast evaporation, slow evaporation and cooling crystallisation, respectively, using the same solvent i.e. a diluted ammonium hydroxide. Method 2 was used by Kruger and Gafner (1971) in their work, which the crystallographic data of Form III originated. Method 4 is basically similar to one of the reliable methods of producing Form II (Method 5 in Table 2.6); therefore its reliability to generate Form III at the same time is suspicious. Method 5 uses the same solvent as another reliable method of producing Form II (Method 7 in Table 2.6) and although their mode of

Table 2.6 Methods of producing Form II.

No.	Procedure	Reference
1	Cooling crystallisation from a saturated n-propanol solution at room temperature.	Kruger and Gafner (1971); (1972); Burger and Dialer (1983).
2	Cooling crystallisation from water to room temperature.	Grove and Keenan (1941); Miyazaki (1947)
3	Cooling crystallisation from a saturated acetone solution to room temperature.	Grove and Keenan (1941); Miyazaki (1947)
4	Cooling crystallisation from a mixture of acetone and chloroform. A saturated acetone solution was cooled to room temperature and diluted with chloroform.* A 1:1* or 3:2[†] mixture of acetone:chloroform was used.	Mesley and Houghton (1967); Shami et al. (1972); Anwar et al. (1989)*; Khoshkhoo and Anwar (1993)[†]
5	Slow[†] cooling crystallisation from a saturated ethanol solution to room temperature. Store in the slurry for a month at 30°C*.	Grove and Keenan (1941); Miyazaki (1947); Babilev et al. (1987)[†]; Blagden et al. (1998a)*.
6	Cooling a saturated solution of sulfathiazole in nitromethane (26g/L) to 30°C and store in the slurry for a month at that temperature.	Blagden et al. (1998a)
7	Cooling crystallisation from a saturated methanol solution to room temperature.	Grove and Keenan (1941); Miyazaki (1947); Parmar et al. (2007).
8	Cooling crystallisation from a saturated acetonitrile solution.	Apperley et al. (1999); Zeitler et al. (2006).
9	Slow concentrating a solution in a methanol-acetonitrile mixture.	Drebushchak et al. (2008).

supersaturation generation is different – evaporation for Method 5 and cooling for the other; the method is still suspect since in determining the formation of a particular polymorph, the effect of solvent often dominates the effect of supersaturation (Khoshkhoo and Anwar, 1993). Method 6 is also a suspicious method because it was reported that crystallisations from water produced either a mixture of Form III and Form IV (Alvarez et al., 2009) or Form IV (Blagden et al., 1998). Crystallisation from a mixture of acetone and chloroform, as mentioned earlier, always favour the formation of a mixture of polymorphs; either Form II and Form III (Alvarez et al., 2009) or Form III and Form IV (Mesley, 1971). For this reason, Method 7 is not a reliable method of

producing Form III. The reliability of Method 8, first implemented by Shenouda (1970), has never been verified by later researchers. In that work, the obtained crystals were made to undergo inconclusive solid-state characterisation analyses, which subject the outcome of the application of the method to speculation. Method 9 was used by Parmar et al. (2007) to produce Form III and they found that the x-ray diffraction parameters of the obtained crystals match well to the literature values of the intended polymorph. The same method was also applied by Luner et al. (2000), who found that the measured density of the obtained crystals corresponded very well to the literature value of Form III. Method 10 and Method 11 were used by Burger and Dialer (1983) and Apperley et al. (1999), respectively. The methods are believed to be reliable since they have successfully differentiated different polymorphs they generated using a combination of solid-state characterisation techniques. Drebushchak and co-workers (2008) showed that the crystals they obtained using Method 12 gave X-ray diffraction parameters that are consistent with the literature values for Form III. This verifies the reliability of Method 12 to produce Form III.

Form IV

There are three methods of producing Form IV as shown in Table 2.8. Method 1 and Method 2 are basically the same in that both use water as the solvent; only Method 2 is clearer in describing the crystallisation conditions. Based on the work by Alvarez et al. (2009), cooling crystallisations from saturated water solutions at 90°C with both fast (5°C/min) and slow (1°C/min) cooling rates consistently produced Form IV crystals. These findings proved the reliability of Method 2. Babilev et al. (1987) used Method 1 to come up with the crystallographic data for Form IV. Two decades later, Parmar et al. (2007) confirmed the repeatability of the same method to produce Form IV by showing that the crystals they obtained using Method 1 gave x-ray diffraction parameters that are consistent with the values given by Babilev et al. Drebushchak et al. (2008) were also able to produce crystals that give x-ray diffraction data similar to those given by Babilev et al.; in this case, however, the crystals were produced using Method 3. Although Method 3 in Table 2.8 may appear to be similar to Method 10 in Table 2.7, but it should be noted that different compositions of ethanol:water ratio have to be considered as different solvents.

Table 2.7 Methods of producing Form III.

No.	Procedure	Reference
1	Dissolving in a cold dilute ammonium hydroxide solution, followed by warming up the solution surface to obtain the crystals.	Miyazaki (1947)
2	Slow evaporation of a diluted ammonium hydroxide solution at room temperature.	Kruger and Gafner (1971); Shakhtshneider et al. (1993);
3	Cooling crystallisation from a dilute ammonium hydroxide solution (1% or 10% or 20%). Store in the slurry for a month at 30°C.	Mesley and Houghton (1967); Moustafa and Carless (1969); Shenouda (1970); Blagden et al. (1998); Milosovich (1964);
4	Slow crystallisation from warm ethanol.	Higuchi et al. (1967); Shenouda (1970); Lagas and Lerk (1981)
5	Evaporation of methanol solution.	Mesley and Houghton (1967)
6	Cooling crystallisation from water (cooling rate of 5-10°C/hr).	Moustafa and Carless (1969); Mesley (1971); Jordan and Carless (1976); Lagas and Lerk (1981); Anwar et al. (1989); Khoshkhoo and Anwar (1993); Karjalainen et al. (2005).
7	Cooling crystallisation from a mixture of acetone-chloroform (3:1).	Moustafa and Carless (1969); Shenouda (1970); Lagas and Lerk (1981)
8	Cooling crystallisation from a mixture of benzene:ethanol (3:1).	Shenouda (1970)
9	Cooling crystallisation from isopropanol.	Shenouda (1970); Luner et al. (2000); Parmar et al. (2007)
10	Slow cooling crystallisation from aqueous ethanol (95% or 40%).	Moustafa and Carless (1969); Carless and Jordan (1974); Lagas and Lerk (1981); Burger and Dialer (1983);
11	Replacement of acetone by dichloromethane in boiling solution.	Apperley et al. (1999)
12	Slow evaporating of a solution of ethanol-water-ammonia mixture.	Drebushchak et al. (2008).

Table 2.8 Methods of producing Form IV.

No.	Procedure	Reference
1	Cooling a saturated solution of sulfathiazole in water. Store in the slurry for a month at 30°C.	Babilev et al. (1987); Blagden et al. (1998); Parmar et al. (2007).
2	Rapid quenching a boiling solution of sulfathiazole in water to 4°C.	Khoshkhoo and Anwar (1993)[†];
3	Cooling crystallisation from aqueous ethanol.	Drebushchak et al. (2008).

Form V

As shown in Table 2.9, most of researchers used Method 1 to generate Form V; most notably among them are Hughes, Chan and their co-workers, who are the contributors of the crystallographic data for Form V and Form V, respectively. In order to ensure a successful outcome of the execution of Method 1, the transfer of the crystals to the hot air oven after the water has just evaporated must be quick enough; otherwise Form III will be formed instead (Anwar et al., 1989). The immediate transfer also prevents overheating of the crystals, which may turn them brown or decompose them. Method 2 is not a reliable method to produce Form V since n-propanol is a solvent known to favour the crystallisation of Form I or at least the crystals of mainly Form I. With the exception of Hakkinen and co-workers (2005), whose detected the presence of a small portion of Form V together with Form I and Form III, no other researchers reported the formation of Form V from n-propanol.

Table 2.9 Methods of producing Form V.

No.	Procedure	Reference
1	Boiling a supersaturated solution of sulfathiazole in water to dryness. As soon as the water evaporated, crystals are immediately dried in a hot air oven at 105°C for 15 minutes.	Lagas and Lerk (1981); Anwar et al. (1989); Khoshkhoo and Anwar (1993); Hughes et al. (1999); Chan et al. (1999); Apperley et al. (1999); Anderson et al. (2001); Zeitler et al. (2006).
2	Dissolving in n-propanol at 97°C and cooled very slowly without rotation or agitation.	Burger and Dialer (1983)

Despite the availability of these recipes, however, it remains difficult to provide guaranteed recipes for producing single polymorph (Hughes et al., 1997); most of the

time, the desired polymorph contains impurities from at least one other form (Anderson et al., 2001; Aaltonen et al., 2003; Hakkinen et al., 2005; Alvarez et al., 2009).

2.6.2 Solid-state characterisation of sulfathiazole polymorphs

Numerous characterisation methods, which vary from traditional to advanced instrumentations, have been utilised to examine and differentiate between different sulfathiazole polymorphs. The methods and the corresponding literature are presented in Table 2.10. Results of these solid-state characterisation studies will be referred, discussed and analysed appropriately in Chapter 3.

Table 2.10 Methods of characterising sulfathiazole polymorphs.

No.	Method
1.	Density measurement:
	- Flotation (Kruger and Gafner,1971)
	- Pyknometry (Burger and Dialer, 1983)
2.	Refractive indices (Grove and Keenan, 1941; Miyazaki, 1947)
3.	Solubility measurement (Lagas and Lerk, 1981; Milosovich, 1964; Burger and Dialer, 1983; Khoshkhoo and Anwar, 1993)
4.	Microscopy:
	- Optical (Grove and Keenan, 1941; Blagden et al., 1998; Miyazaki, 1947; Parmar et al., 2007)
	- Scanning electron (Hakkinen et al., 2005; Parmar et al., 2007)
5.	Thermal analysis:
	- DSC (Lagas and Lerk, 1981; Anwar et al., 1989; Mesley, 1971; Anderson et al., 2001; Moustafa and Carless, 1969; Shenouda, 1970; Burger and Dialer, 1983; Shaktshneider and Boldyrev, 1993; Luner et al., 2000; Zeitler et al., 2006; Parmar et al., 2007; Ali et al., 2009);
	- TG (Lagas and Lerk, 1981);
	- HSM (Grove and Keenan, 1941; Anwar et al., 1989; Milosovich, 1964; Higuchi et al., 1967; Guillory, 1967; Shenouda, 1970; Burger and Dialer, 1983; Zeitler et al., 2006).

6.   Spectroscopy:

- IR (Mesley and Houghton, 1967; Lagas and Lerk, 1981; Anwar et al., 1989; Mesley, 1971; Anderson et al., 2001; Moustafa and Carless, 1969; Burger and Dialer, 1983; Shaktshneider and Boldyrev, 1993; Parmar et al., 2007);

- NIR (Aaltonen et al., 2003; Luner et al., 2000; Ali et al., 2009);

- Raman (Anwar et al., 1989; Anderson et al., 2001; Zeitler et al., 2006; Ali et al., 2009);

- Terahertz pulsed (Zeitler et al., 2006).

7.   NMR (Anwar et al., 1989; Apperley et al., 1999)

8.   X-ray diffraction:

- Powder (Chan et al., 1999; Anwar et al., 1989; Mesley, 1971; Aaltonen et al., 2003; Hakkinen et al., 2005; Kruger and Gafner, 1971; Higuchi et al., 1967; Shaktshneider and Boldyrev, 1993; Parmar et al., 2007; Ali et al., 2009);

- Single crystal (Hughes et al., 1999; Anwar et al., 1989; Kruger and Gafner, 1971; 1972; Babilev et al., 1987; Parmar et al., 2007);

- Variable temperature powder (Lagas and Lerk, 1981; Karjalainen et al., 2005);

- Variable temperature single crystal (Drebushchak et al., 2008).

Table 2.11 shows calculated density values for each of the polymorphs. The values were obtained from the unit cell dimensions and mass. Since the most stable structure corresponds to the one with the most efficient packing, which in turn corresponds to the structure with the highest density, the density values can be used to rank the relative stability of the polymorphs. Based on the values; the ranking of the stability of the sulfathiazole polymorphs at ambient conditions is in the order of Form IV > Form III > Form II > Form V > Form I. The melting and transformation temperatures obtained from the literature, as shown in Table 2.11, indicate that at high temperature, Form I is the most stable polymorph since all other forms transformed to Form I above 105°C. The values shown in the table will be referred and discussed accordingly in Chapter 3.

Some of the analytical techniques in Table 2.10, such as Raman, NIR and X-ray diffraction, have been used for monitoring polymorph transformations in real-time (Yu et al., 2003). The use of *in situ* analysers in real-time is one of the important elements in the application of process analytical technology, which is the subject of the following section.

Table 2.11 Summary of literature calculated density, melting temperature and polymorphic transformation from one form to another that is stable at high temperature.

Polymorph	Calculated density (g/cm^3)	Melting temperature (°C)	Transformation temperature into Form I (°C)
I	1.499 (Kruger and Gafner, 1972)	200-202 (Lagas and Lerk, 1981; Anwar et al., 1989; Mesley, 1971; Anderson et al., 2001; Zeitler et al., 2006)	-
II	1.550 (Kruger and Gafner, 1971)	173-175 (Grove & Keenan, 1941; Anwar et al., 1989; Apperley et al., 1999)	150-170 (Anwar et al., 1989); 138 (Zeitler et al., 2006)
III	1.567 (Kruger and Gafner, 1971)	173 (Miyazaki, 1947; Anwar et al., 1989; Lagas and Lerk, 1981; Shenouda, 1970; Moustafa and Carless, 1969) 175 (Apperley et al., 1999)	105-170 (Lagas and Lerk, 1981); 150-170 (Anwar et al., 1989); 159 (Zeitler et al., 2006)
IV	1.595 (Babilev et al., 1987)	179 (Shenouda, 1970); 175 (Apperley et al., 1999)	160 (Zeitler et al., 2006)
V	1.510 (Hughes et al., 1999)	196-197 (Lagas and Lerk, 1981; Anwar et al., 1989; Anderson et al., 2001).	When Form V melts it immediately recrystallises into Form I (Lagas and Lerk, 1981)

2.7 PROCESS ANALYTICAL TECHNOLOGY IN CRYSTALLISATION OPERATION

2.7.1 Basic concepts of PAT

Traditionally, pharmaceutical production involves the manufacture of the finished products, followed by laboratory analysis to verify the products' quality. This approach, known as Quality by Testing (QbT), requires a continuous process optimization, and the possibility of producing failed batches is high (Yu, 2008). The concept of Quality by Design (QbD) was introduced to fill the need of the pharmaceutical industries to have a more efficient manufacturing approach. It is based on a notion that "quality

cannot be tested into products, i.e., quality should be built in by design" (FDA, 2006). Prior to that, the US Food and Drug Administration (FDA) introduced the Process Analytical Technology (PAT) initiative, defined as "a system for designing, analyzing, and controlling manufacturing through timely measurements (i.e. during processing) of critical quality and performance attributes of raw and in-process materials and processes, with the goal of ensuring final product quality" (FDA, 2004). The goal of PAT is consistent with that of QbD. In fact, PAT can be considered as a tool or system that help in the implementation of QbD.

PAT focuses on the utilisation of real-time measurement tools as a primary mean in process monitoring. The term "analytical" in PAT includes chemical, physical, microbiological, and statistical analysis conducted in an integrated manner (Yu et al., 2003). The science of relating measurements and analysis made on a system or process to the state of the system through the application of mathematical or statistical methods is called chemometrics. It is very useful in the interpretation of the multivariate data by in-situ process monitoring devices (Yu et al., 2003). The tools derive a mathematical relationship between the desired properties, such as CSD, with various contributing variables that affect them, such as the solute concentration. The derivation is done using multivariate data analysis, such as multiple linear regression (MLR), principle component analysis (PCA), principle component regression (PCR), partial least squares (PLS), and different variations of these approaches. MLR is the most straightforward analysis method since the variable to be modeled is described as a linear combination of dependent variables. Instead of using the original variables of the model, PCA uses linear algebra to derive a new set of variables that have a linear combination of the original variables. The derived variables are determined based on variability in the data. PCR and PLS are actually the combination of MLR and PCA. They are different in the way the derived variables are selected.

Applications of PAT to crystallisation processes have been reviewed by Yu et al. (2003). The review emphasizes the importance of using sensor technologies that can measure critical process properties, such as supersaturation, and desired product qualities, such as size, shape and polymorphic form. This real-time process information, according to the review, can be integrated into the control plan to provide an optimal control strategy. The monitoring of multiple process and quality properties

at the same time, rather than one at a time, is also possible by utilising chemometrics to its full potential.

The use of PAT helps to identify the critical parameters that affect the process and therefore result in a more in-depth understanding of the process as exemplified by the work of Birch et al. (2005). In their work to develop an API at Pfizer's Sandwich laboratories, the implementation of PAT was found to help to identify the best solvent media and the best approach to crystallisation. They however, stress that PAT is not a substitute for traditional characterisation techniques, but it is a tool for an in-situ process understanding. In fact, a combination of on-line and off-line analyses would provide a full assessment of the process.

2.7.2 Overview of PAT tools

PAT requires sensor technologies that are able to measure and monitor the indications of product quality and critical process properties in real-time. As a result of the recent scientific advances, many such measurement and monitoring tools are available. The measurement and monitoring of the crystallisation processes can be classified into two aspects: liquid phase and solid phase. According to Barrett et al. (2005), the monitoring of liquid phase concentration will provide information about the degree of supersaturation and thus can reveal the potential yield of the process as well as problems due to, for instance, high supersaturation level. The monitoring of the solid phase, on the other hand, will highlight the process kinetics due to nucleation and growth as well as a way to understand how the operating conditions affect the system.

Liquid Phase Monitoring

Many different methods have been used and developed to measure liquid phase concentration in the crystallisation process. These include direct concentration measurement methods, as well as measurement of concentration-dependent properties, such as density and electrical conductivity.

One of the most common methods for concentration measurement in analytical chemistry is a spectroscopy method. It provides a spectrum, which is a plot of interaction between electromagnetic radiation and the absorbing species of a substance (Atkins and de Paula, 2005). Concentration can be calculated from the spectral data using the Beer-Lambert law. However, in order for the spectrometer,

which is the instrument that detects the interaction, to give a spectrum of the liquid phase in the slurry without being disturbed by the solid phase, an attenuated total reflection (ATR) accessory needs to be fitted on the immersion probe. The principle of ATR is illustrated in Figure 2.13.
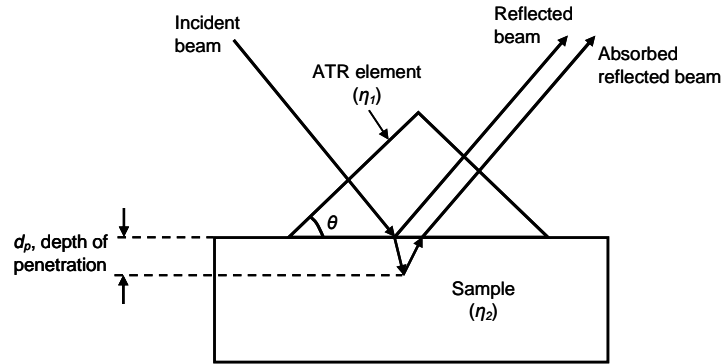
Figure 2.13 ATR measurement geometry (adapted from Lewiner et al., 2001).

With reference to Figure 2.13, a transparent ATR element with a refractive index η_1 is shown with one surface in contact with a sample (refractive index η_2). When a radiation beam is transmitted at a certain incidence angle of θ through the ATR element, the beam will undergo a total reflection at the interface of the ATR element and sample. The absorption of the sample causes the attenuation of the reflected beam, which is then transmitted to the detector to produce a spectrum (Lewiner et al., 2001). The spectrum is a function of the solution concentration and temperature. The depth of the penetration, d_p is related to θ, η_1, η_2 and the radiation wavelength, λ by the following relation:

$$d_p = \frac{\lambda}{2\pi\eta_1 \left[\sin^2\theta - \left(\frac{\eta_2}{\eta_1}\right)^2 \right]^{\frac{1}{2}}} \qquad (2.17)$$

Based on the relation, d_p increases with decreasing θ, increasing λ and increasing $\left(\frac{\eta_2}{\eta_1}\right)$. The value of d_p for most solution samples is very small, and hence it can be postulated that the measurement is limited within the liquid phase only (Doyle and Tran, 1999). As a result, the ATR is not sensitive to the presence of solid phase.

ATR UV/Vis Spectroscopy

UV/Vis spectroscopy uses a radiation beam in the UV/Vis region (200-900 nm). Absorbance, A obtained from the UV/Vis absorption spectra is directly proportional to the concentration of an absorbing species in solution according to the Beer-Lambert law:

$$A = \varepsilon \lambda c \qquad\qquad (2.18)$$

where ε is the molar absorption coefficient, λ is the path length of the absorbing solution, and c is the concentration of the absorbing species.

The absorbance however is temperature dependent because the change in temperature changes the refractive index and hence the path length for the ATR element. For this reason, a temperature correction is required to be applied to the absorption spectra before the development of a calibration model (Thompson et al., 2005). Alternatively, temperature terms can be incorporated into the calibration model (Abu Bakar et al., 2009).

ATR-UV/Vis spectroscopy has been used quantitatively for the in situ monitoring and detection of the nucleation event (Simon et al., 2009; Nagy et al., 2007; Anderson et al., 2001) and the polymorphic transformation (Howard et al., 2009; Nagy et al., 2007; Gillon et al., 2005). It also has been used quantitatively in the monitoring and measurement of supersaturation levels during crystallisation processes (Billot et al., 2010; Abu Bakar et al., 2009; Thompson et al., 2005). The use of ATR-UV/Vis spectroscopy in the pharmaceutical crystallisation, however, is not as popular as the ATR-FTIR. This is probably due to the limitation of its application only to compounds that contain a chromophore, which is a functional group that causes absorption at the UV's wavelength range. However, Billot et al. (2010) have recently demonstrated that the technique can also be applied to non-absorbing molecules through the reliance of internal reflection on refractive index. The technique is expected to gain more interest to be implemented in industrial environment since it is relatively simple and cheaper compared to other spectroscopy techniques.

ATR-FTIR Spectroscopy

The basic operation of the ATR-FTIR is similar to ATR-UV/Vis but it uses a radiation beam in the infrared region. The IR regions include the near-IR 12800-4000 cm^{-1}, mid-IR 4000-200 cm^{-1} and far-IR 200-10 cm^{-1}. Since most compounds absorb radiation in the mid-IR range, its applicability to different systems is widespread. It operates by imposing the radiation beam on a sample and measuring the amount of IR light absorbed at different frequencies. The frequencies at which absorption occurs indicate the identity of chemical species present, while the absorption magnitudes indicate the concentrations of these species. A mathematical treatment, the Fourier transformation, is used to interpret the data and produce a spectrum. ATR-FTIR has been widely used and proven to be a reliable technique for liquid phase monitoring in crystallisation processes (Dunuwila and Berglund, 1997; Lewiner et al., 2001; Feng and Berglund, 2002; Togkalidou et al., 2002; Fujiwara et al., 2002; Liotta and Sabesan, 2004; Barrett et al., 2005; Polanen, 2006; Yu et al., 2006a; Zhou et al., 2006; Nonoyama et al., 2006; Scholl et al., 2006; Chew et al., 2007a; Kee et al., 2009a;b).

Transformation of the ATR-FTIR spectral data measured from crystallisation process into reliable concentration information is a critical issue (Polanen, 2006). The simplest way of doing this is by correlating the height or area of the specific band in the spectrum to the solute concentration by regular linear regression as performed by Dunuwila and Berglund (1997), Feng and Berglund (2002) and Lewiner et al. (2001). Another approach of analysing the spectral data is through a chemometrics approach, which takes into account the spectra over a wide range of wavenumbers, using either principal component regression or partial least squares (Togkalidou et al., 2002; Fujiwara et al., 2002; Liotta and Sabesan, 2004; Zhou et al., 2006 and Chew et al., 2007). Although the chemometrics approach was shown to produce a remarkably high accuracy of concentration measurement, as reported by Togkalidou et al. (2002) and Fujiwara et al. (2002), the use of the former approach was motivated by the fact that simple measurements performed on well defined absorption bands have a clearer physical and chemical meaning (Lewiner et al., 2001).

ATR-FTIR spectroscopy however, is considerably more expensive than other techniques of *in situ* concentration measurement. Another disadvantage of ATR-FTIR spectroscopy is the susceptibility of its probe's optical material to chemical attack and fouling (Doyle, 2005).

Raman spectroscopy

Raman spectroscopy differs from other spectroscopic techniques discussed previously in that it is concerned with the scattering of the radiation by the sample, rather than an absorption process. It imposes a monochromatic radiation beam on a sample and measures the amount of light scattered at different wavelengths. The difference in wavelength between the incident light and the scattered light is a fingerprint for the types of chemical bonds in the sample. Raman spectroscopy can be used for monitoring both liquid and solid phases. Falcon and Berglund (2003) and Hu et al. (2005) have successfully monitored and measured liquid concentrations using this instrument during crystallisation processes. The Raman spectroscopy's sampling probe is less chemically sensitive than an ATR-FTIR probe, but like ATR-FTIR, the instrument is expensive.

Densitometry

Density measurement has been successfully used in the monitoring of the liquid phase concentration during crystallisation processes. It is applicable for a single component system (Gutwald and Mersmann, 1990) as well as for a two-component solution system (Zhu et al., 2004). Since the solution to be measured needs to be free from crystals, the sample is passed to an external density measuring cell through a sampling loop (oscillating U-tube). This however may produce temperature fluctuations and is subject to filter clogging.

Electrical conductivity

The supersaturation evolution during a crystallisation process can also be followed by measuring the electrical conductivity of the liquid phase. The technique has been applied by Sessiecq et al. (2000), in which a conductivity meter probe was used in a study of ammonium chloride crystallisation. The correlation between electrical conductivity and concentration is only valid for crystal-free solution, because the presence of solid particles may alter the conductivity value of the solution; as demonstrated by Maxwell in his early work, the conductivity of a liquid is proportional to the volume fraction of particles (Maxwell, 1998). Other limitations associated with this technique are its limited applicability to organic systems since they are not usually conductors and the results are temperature dependent and sensitive to impurities (Mullin, 2001).

Solid Phase Monitoring

Many techniques have been utilised and developed for the *in situ* monitoring of solid phase in the crystallisation processes. The choice of the technique depends mainly on the targeted quality of the solid's property to be produced. The measurable properties or events of the solid phase include crystal size, shape or habit, polymorphic form, optical, nuclei formation, and turbidity.

Image analysis

Image analysis is the simplest technique to monitor crystal size and shape in the crystallisation processes. The simplicity is due to the fact that it is a direct observation technique. A non-automated image analyser was once used to measure size of crystals as a function of time by manually sampled the crystal slurry placed under the microscope (Puel et al.,1997). In more recent years, many applications of real-time image analysis for crystal size and shape measuring and monitoring have been reported, for example by Li et al. (2005), Calderon De Anda et al. (2005), Wang et al. (2008), Patience et al. (2004) and Simon et al. (2009). A Lasentec particle and vision measurement (PVM) system has been utilised, for example by Barrett and Glennon (2002), Gillon et al. (2006) and Scholl et al. (2006) to provide images of crystals and crystal structures during crystallisation processes. It is a probe-based high resolution in-situ video microscope that uses laser light to illuminate an area within the slurry; the light scattered back towards the probe is used together with a CCD element to generate an image. The system however was mainly used to validate the result of other in-situ solid characterisation techniques since it provides two-dimensional crystal images in random orientation that limit the ability of imaging software to automatically identify individual crystals (Braatz and Hasebe, 2001).

Raman spectroscopy

Raman spectroscopy has been reported to be an efficient method for monitoring solid phases during crystallisation, particularly the polymorphic or phase transformation (Starbuck et al., 2002; Wang et al., 2000; Scholl et al., 2006; Ono et al., 2004). Caillet et al. (2007) used it to continuously monitor the overall solid concentration and the composition of the solid phase in the solvent-mediated phase transformation of citric acid. They validated the results using off-line analytical methods and found the accuracy of Raman measurements was of the order of 5%. Besides that, Raman spectroscopy has also been used to monitor the dehydration of crystal hydrates over

time (Falcon and Berglund, 2003). However, as mentioned previously, Raman spectroscopy is expensive. In addition, calibration of the Raman signal for quantitative polymorphic composition measurements can be difficult because the signal intensity is affected by the particle size distribution (O'Sullivan et al., 2003).

Ultrasonic spectroscopy

Ultrasonic spectroscopy, which is a comparatively new solid characterisation technique, has been successfully applied for the on-line crystal size measurement by Mougin et al. (2002) and Mougin et al. (2003). The technique is based on measurement of the attenuation of ultrasonic waves through the slurry. It is capable of measuring crystal sizes within the range of 0.01 to 1000 µm for slurries of solid concentration in the range of 0.1 to 50 vol. %. In addition to crystal size determination, the technique is also able to detect nucleation, crystal growth and crystal breakage on-line and in real time.

Turbidimetry

The presence of solid particles in a liquid changes its optical properties. Hence the detection of the solid particles can be done using optical instruments such as a turbidity meter. Turbidity is a measure of the amount of particles in a liquid. For in-situ determination of turbidity, a turbidity probe is required. The probe transmits near-infrared light into the slurry. The light is scattered by the particles present and returns to the analyser, which provides a relative measure of the liquid turbidity. This technique has been used by Parsons et al. (2003) to detect nucleation and measure metastable zones of pharmaceutical compounds. Howard et al. (2009) have reported the capability of the turbidity probe to detect a nucleation and a possible polymorphic transformation event during the anti-solvent crystallisation of sodium benzoate from IPA/water mixture. The turbidity meter however, is only able to provide a qualitative information since it practically measures bulk properties to note the cloud and clear points, but it is unable to give any quantitative information related to the size or number of particles.

Laser diffraction

Laser diffraction technique has been applied to measure the crystal particle size and shape in the crystallisation processes by Ma et al., (2001). A laser diffraction instrument works by passing a beam of monochromatic laser light to illuminate the

particles. The scattered as well as the unscattered light then pass through a lens to a detector, located in the focal plane of the lens. Then, by processing the signals using an appropriate approach, a spectrum can be obtained to represent either particle size or shape. In their work, Ma and co-workers used two-dimensional pixel arrays as a detector so that diffraction pattern for both size and shape could be obtained.

Laser backscattering

Another solid phase measurement technique based on the optical properties of the system being studied is laser backscattering such as Lasentec focused beam reflectance measurement (FBRM). It is the main instrument used for solid phase monitoring in this study, and therefore, its operation and application will be discussed in detail here.

FBRM uses a laser beam sent through fibre optics to an immersion probe tip where it is finely focused by a rotating lens, which causes the beam to scan in a circular path through a sapphire window at a fixed high speed. The beam then passes into the solution under study and when it hits a crystal suspended in the solution, light is scattered in many directions, but only light scattered back towards the probe is collected. The crystal continues to back-scatter the light until the beam reaches the opposite edge of the crystal. The time period of the backscattering (Δt) is recorded and multiplied by the scan speed of the beam (v_b) to give the distance between one edge of the crystal to the other (s). This distance measured by FBRM is called a chord length. Figure 2.14 shows a schematic diagram of backscattered light pulses detection and chord length measurement.
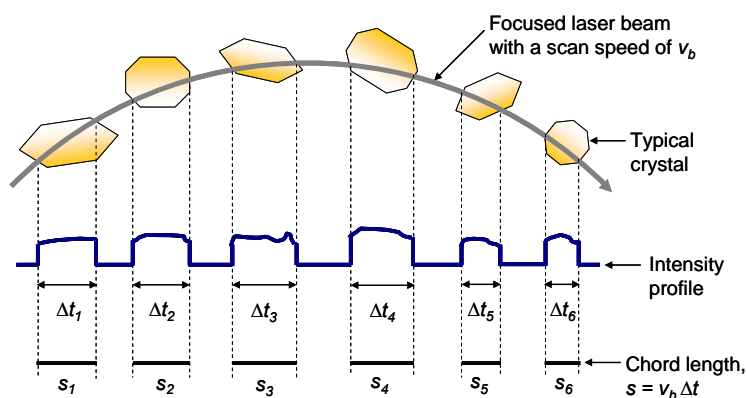
Figure 2.14 A schematic diagram of backscattered light pulses detection and chord length measurement of typical crystals.

Typically, a large number of chords of different sizes can be obtained from any given particle. These chord lengths are classified into a series of size ranges, known as channels, to produce a chord length distribution (CLD). The number and measured length of these chords are related to the solids concentration, particle diameter and particle shape. FBRM also allows the monitoring of the change in CLD for different chord size classes (fine, intermediate and coarse) of the crystals as a function of time. The software that accompanies the FBRM not only provides the chord length by number distribution, but also calculates the unweighted mean chord and the length, length-squared, and length-cubed weighted mean values. Basically, each weighted mean chord value is, successively, more heavily affected by the presence of large particles than the unweighted mean chord length value.

FBRM has been used extensively in the crystallisation processes to provide qualitative as well as quantitative information on nucleation and crystal growth. Since a sudden increase in the chord counts of FBRM indicates the onset of nucleation; Chew et al., (2007a), Zhou et al. (2006), Liotta and Sabesan (2004), and Barrett and Glennon (2002) have successfully used FBRM to detect the MSZW. Fujiwara et al. (2002) compared MSZW determination by FBRM with that by visual observation and ATR-FTIR and found that FBRM detected nucleation the earliest among the three methods. Liotta and Sabesan (2004) also showed that the onset of secondary nucleation in the crystallisation process can be detected by a rise in the FBRM small particle counts. Besides the detection of nucleation event, Barrett and Glennon (2002) and Zhou et al. (2006) have proved that FBRM can also be used to determine the solubility curve since a reduction in the chord counts may indicate the dissolution of crystals.

Since CLD data measured by FBRM provide an approximate correlation to the CSD in slurry, many research groups used FBRM to monitor the CSD on-line (Chew et al., 2007a; Barthe and Rousseau, 2006; and Barrett et al., 2005). The effects of process conditions on CSD can also be monitored using FBRM. Yu et al. (2005) used FBRM to monitor the effects of agitation speed and feeding rate on CSD. Yu et al. (2006b) again used FBRM to monitor the effects of seed loading and seed size distribution on the average crystal size of the same system operated at constant supersaturation. Yi and Myerson (2006) utilised FBRM to study the role of vessel size on the size of the crystals produced.

In crystallisation control applications, the CLD data obtained from FBRM have been used by Doki et al. (2004a) to devise an alternating temperature profile as a process control strategy to produce crystals with a desired mean size. Chew et al. (2007b), Abu Bakar et al. (2009) and Woo et al. (2009) also used FBRM in a feedback closed-loop to improve crystal product quality. The approach involves nucleation detection, followed by a holding time to internally generate seeds through primary nucleation and then controlled conditioning of the seeds using the CLD obtained from FBRM.

FBRM can also be used to monitor polymorphic forms, as exemplified by the works of O'Sullivan et al. (2003), O'Sullivan and Glennon (2005), Shaikh et al. (2005), Scholl et al., (2006) and Barthe et al., (2008). The successful monitoring of polymorphic transformation by FBRM requires the crystals to have a distinct change of shape upon transformation (Mangin et al., 2009). Doki et al. (2004a) have successfully devised a process control strategy using FBRM to selectively crystallised a metastable polymorph.

Since FBRM provides a CLD rather than a conventional diameter distribution, some studies have been conducted to find the relationship between them (Tadayyon and Rohani, 1998; Ruf et al., 2000; Worlitschek et al., 2005; Li and Wilkinson, 2005). For example, Tadayyon and Rohani (1998) developed a model to infer CSD using the measured CLD. The model showed that the measured CLD is reasonably accurate for spherical particles but it progressively deteriorates as the shape of particles changes from spherical to ellipsoidal. Ruf et al. (2000) produced a model that allows conversion of CSD into CLD, but the geometry of the crystal must be known otherwise the mapping cannot be inverted.

Instead of finding a relationship between CLD and CSD, Heath et al. (2002), Chew et al. (2007a) and Yu and Erickson (2008) empirically compared the FBRM outputs with those obtained from more conventional particle sizing techniques. They found that one of the FBRM statistics, the square weighted chord length, resembles more closely the Sauter mean diameter measured using laser diffraction instrument (Heath et al., 2002; Yu and Erickson, 2008) and optical microscopy (Chew et al., 2007a; Yu and Erickson, 2008). However, since the instruments are based on different principles of measurement, the FBRM data do not correspond quantitatively to laser diffraction or

optical microscopy data, but the comparison should only be used to evaluate the trend of the dynamic change of the crystallisation process.

Many research groups describe FBRM as a powerful tool for *in situ* solid phase measurement and monitoring. However, like all other PAT tools, it is not a completely perfect tool. Kougoulos et al. (2005) found out that FBRM is not a suitable technique to measure the crystallisation kinetics for an organic fine chemical, because FBRM is not sensitive to particles of size less than 1 μm. However, this is not just a limitation for organic compounds. In fact, the smallest size of particle that FBRM can measure is 0.5 μm. Besides that, as pointed out by Abbas et al. (2002), another disadvantage of FBRM is the noise that comes with the data. As a result, data filtering would be required before using the technique for control purposes. In addition, there is also a concern that solids could coat the probe window and hinder accurate particle size measurements. According to the Lasentec manual (Mettler Teledo, 2006), the probe window is self-cleaning, if it is positioned into the flow direction at a 45° angle as the fluid flow passing the probe window will wash its surface. This depends on the fluid velocity passing at the window. However, Heath et al. (2002) observed that fine particles are prone to adhere to the probe window so they performed window cleaning regularly to give a total background count of less than 50 counts per second in air.

The PAT tools described in this section benefit the development of crystallisation control approaches, since with their presence the *in situ* measurement of key process variables, such as supersaturation and desired crystal quality can be used as an input signal for feedback control. In the next section, the application of PAT in crystallisation control will be reviewed.

2.7.3 Application of PAT in crystallisation control

Application of PAT in the process control involves a combinational use of appropriate *in situ* measuring tools, chemometrics, and feedback control approach. In crystallisation, the three important product properties that measure the success of the process are CSD, crystal habit and polymorphic form. The available literatures on the successful application of PAT to control each of these aspects of product quality are reviewed here.

CSD

The feedback control approach for CSD can be based on *in situ* measurement of either concentration or CSD. Several research groups including Liotta and Sabesan (2004) and Feng and Berglund (2002) have demonstrated that a concentration measurement based control approach, also known as supersaturation control or concentration control, in cooling crystallisation is able to produce APIs within a desired crystal size range. For example, Liotta and Sabesan (2004) used FBRM to generate MSZW and ATR-FTIR to determine the evolution of supersaturation. The information was used as a guide to operate a process that favours growth over nucleation. Real time supersaturation control was then implemented using a feedback control approach to determine a set-point limit for the cooling rate and to manipulate the heater/cooler to maintain the specified cooling rate. The successful application of the same approach to anti-solvent crystallisation has been demonstrated by Yu et al. (2006a) and Zhou et al. (2006). In this case, the feedback control was implemented to determine a set point for anti-solvent addition rate and manipulate the pump to maintain the specified rate.

Reports on the use of feedback control approaches for CSD, based on CSD measurement indicates that only FBRM has been utilised for the purpose. Tadayyon and Rohani (2000) designed a control system for a continuous cooling crystallisation using FBRM counts of chord lengths smaller than 125 μm to adjust the flow rate of fine dissolution stream, thus increasing the average crystal size. Woo et al. (2009), Abu Bakar et al. (2009), Doki et al. (2004) and Chew et al. (2007b) are other research groups that utilised FBRM to control CSD via feedback control.

Morphology

The literature on the application of PAT in the control of morphology is scarce. This is probably due to the limited availability of measurement tools for the purpose and the complexity in extracting detailed shape information. Patience and Rawlings (2001) demonstrated the use of a commercially available image analysis software to produce noise-free signal that was sent to a controller to regulate the flow rate of a habit modifier (additive) stream to maintain a desired morphology. Wang et al. (2005) enhanced the reliability of the shape information by using a combinational approach of on-line imaging, multi-scale image analysis and crystal morphology modeling.

Polymorphic form

The *in situ* monitoring of polymorph is very useful because of the dynamic nature of polymorphic transformation and instability of certain polymorphs (Chew et al., 2007a). This kinetic information can be utilised to design techniques for the selective crystallisation of a desired polymorph. In order to further ensure that the obtained polymorph is the right form, seeds of the desired polymorph are introduced. Doki et al. (2004b) reported a selective crystallisation method by introducing seeds and then based on the information given by the ATR-FTIR and FBRM, an alternating temperature profile was implemented to dissolve fine crystals unavoidably produced or to grow the crystals. Kee et al. (2009a; 2009b) have successfully implemented concentration feedback control to grow seeds of a metastable form. In this method, the regulation of the cooling rate based on the solute concentration measured by ATR-FTIR, prevents secondary nucleation of both the stable and the metastable forms.

Although, many of *in situ* measurement tools reviewed in the previous section have been used for the monitoring of polymorphic form, they have not been utilised directly for the control of polymorphic crystallisation. According to Chew et al. (2007a), this is probably due to the difficulty in the use of polymorphic information measured by those tools as input signal for feedback control.

2.8 CONCLUSIONS

The literature on crystallisation is voluminous. All of them imply that the crystallisation mechanisms (particularly supersaturation, nucleation and growth) are highly interactive and in the end, define the properties of the final crystalline product. The production of crystals with the desired properties (i.e. appropriate crystal size, morphology, and polymorphic form), therefore, requires a careful selection of crystallisation operation and control. Approaches that are gaining popularity nowadays involve the application of *in situ* monitoring techniques, which is a part of the PAT initiative. A review of some of the application of the techniques shows that the approach could lead to better prediction and control of the applied supersaturation and in the end, better control of the final product quality. The literature also reveals that the knowledge and understanding about the formation conditions of the different polymorphs as well as their characteristics are essential so that these can be accounted for in the crystallisation process design. For this reason, a comprehensive literature review on the crystallisation and polymorphism of the main model compound, sulfathiazole was

carried out. This work resulted in the production of a compilation of literature methods for isolating a particular polymorph and a reconciliation of various enumerations of the polymorphs that are in use from 1941 to present. In the next chapter, crystallisations of sulfathiazole polymorphs using the selected literature methods are evaluated.

CHAPTER 3:
CRYSTALLISATION AND CHARACTERISATION OF SULFATHIAZOLE POLYMORPHS

This chapter presents a discussion of the crystallisations of sulfathiazole polymorphs using selected literature methods. The crystallisation processes were monitored using PAT tools, such as FBRM and ATR-UV spectroscopy. The obtained crystals were examined using various solid-state characterisation techniques and whenever possible, the results are compared with those in the literature.

3.1 INTRODUCTION

Since the discovery of sulfathiazole as an antimicrobial agent in 1939, numerous works have reported on the screening for its different polymorphic forms, which is an essential part of drug development. These works consequently result in the availability of various methods for generating a particular polymorph. By following these methods, however, one cannot be guaranteed to obtain the intended pure polymorph because most of them do not clearly and adequately describe the crystallisation conditions, such as cooling rates and initial solute concentrations. The implementation of PAT, which involves the use of *in situ* analysers that are able to measure, monitor and record the process properties and the indication of product quality in real-time, is one of the strategies to fully describe the crystallisation conditions. This chapter presents the work in generating sulfathiazole polymorphs using crystallisation methods that were selected from the literature. The crystallisations were performed with the processes monitored using FBRM and ATR-UV spectroscopy. In order to assess the success of these polymorph crystallisations, the obtained crystals were examined using various characterisation techniques including optical microscopy, SEM, DSC, TG, HSM, FT-IR spectroscopy and PXRD and whenever possible the results were compared with those of previous workers.

The works presented in this chapter were undertaken with the following objectives: (a) to provide reliable methods of generating sulfathiazole polymorphs through *in situ* monitoring and thorough recording of process properties using PAT tools; (b) to understand and differentiate sulfathiazole polymorphs properly – an essential prior knowledge in the design and development of a polymorphic control approach; and (c)

to illustrate some of the principles and the difficulties associated with development of a polymorph crystallisation process.

3.2 EXPERIMENTAL METHODS

3.2.1 Materials

Sulfathiazole was purchased from Sigma-Aldrich with a purity of 98%. Results of PXRD analysis show that the received sulfathiazole is a mixture of Form III, Form IV and the amorphous form. The PXRD patterns are presented in Appendix B. The solvents used are *sec*-butanol, acetonitrile, isopropanol and deionised water. Except water, all other solvents were analytical reagent grade purchased from Fisher Scientific.

3.2.2 Solubility measurements

The solubilities of sulfathiazole in the respective solvents were determined at temperatures ranging from 25°C to 70°C using isothermal method, which is detailed in Appendix C.

3.2.3 Crystallisation of sulfathiazole polymorphs

Different polymorphs were generated using the methods shown in Table 3.1. Methods 1 - 4, which utilized unseeded cooling crystallisations, were performed in a jacketed 500 ml glass vessel. The temperature in the vessel was controlled with a PTFE sheathed thermocouple connected to a thermo fluid circulator bath (Huber Variostat CC-415 vpc). The temperature readings were recorded every 20 seconds on a computer by a control interface written in LabVIEW (National Instruments). An overhead stirrer with a PTFE four pitch-bladed turbine was used to agitate the system between 220 to 320 rpm. The agitation speed was reduced to 150 rpm after nucleation in order to minimize damage to the crystals. An FBRM probe (model D600, Lasentec) was inserted into the solution to measure chord length distributions. The distributions were collected every 20 seconds and averaged during collection. They were monitored using the FBRM control interface software (version 6.7). The UV system used was a Zeiss MCS621 spectrometer with a CLD600 lamp module. Absorbance spectra were obtained through a Hellma 661.822 Attenuated Total Reflectance (ATR) UV/Vis probe, which was directly immersed in the solution. The spectral range was 242 – 360 nm, and a spectrum of the solution was recorded every 20 seconds using a data acquisition software, Aspect Plus (version 1.76). A schematic

representation of the experimental set-up is shown in Figure 3.1. Method 5, which involved evaporative crystallisation, was performed in a 250 ml glass beaker on a Stuart CB162 heat-stir plate (Bibby Sterlin Ltd.).

Table 3.1 Methods to produce different polymorphs of sulfathiazole.

Method no.	Polymorph to be produced	Procedure
1.	Form I	Based on Method 6, Table 2.5 in Chapter 2. A saturated solution at 70°C was prepared by heating 2.4g of sulfathiazole in 300g of sec-butanol in a 0.5L double jacketed crystalliser to dissolution, followed by natural cooling to 20°C.
2.	Form II	Based on Method 8, Table 2.6 in Chapter 2. A saturated solution at 60°C was prepared by heating 6.0g of sulfathiazole in 240g of acetonitrile in a 0.5L double jacketed crystalliser to dissolution, followed by natural cooling to 20°C.
3.	Form III	Based on Method 9, Table 2.7 in Chapter 2. A saturated solution at 70°C was prepared by heating 3.0g of sulfathiazole in 240g of isopropanol in a 0.5L double jacketed crystalliser to dissolution, followed by natural cooling to 25°C.
4.	Form IV	Based on Method 2, Table 2.8 in Chapter 2. A saturated aqueous solution of sulfathiazole at 80°C (3.0g in 300g water) was cooled rapidly to 4°C at a set rate of 10°C/min in a 0.5L double jacketed crystalliser.
5.	Form V	Based on Method 1, Table 2.9 in Chapter 2. A saturated aqueous solution of sulfathiazole (4.0g in 200g water) was boiled to evaporate in a beaker on a hot plate until almost dry.
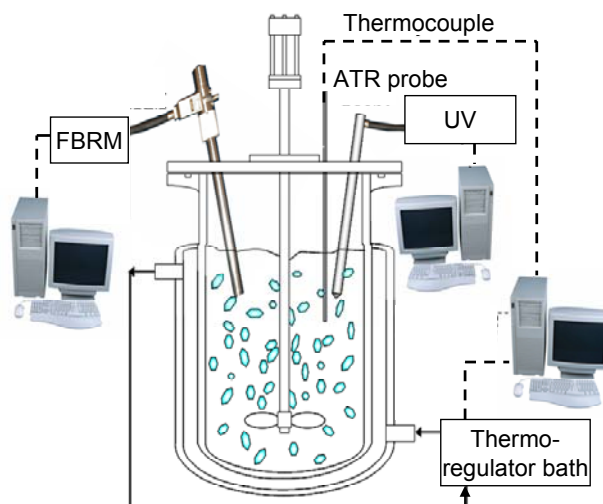
Figure 3.1 A schematic representation of the experimental set-up.

At the end of the crystallisation runs, the crystallised solids were vacuum filtered and subsequently, those crystals obtained from water, were immediately dried in a hot air oven at 105°C for 15 minutes, whereas crystals obtained from other solvents were dried in a desiccator.

3.2.4 Characterisation of sulfathiazole polymorphs

Optical microscopy

The morphology of the crystals was observed using a Leica DMLM microscope. The captured microscopic images were analyzed using Leica QWin (Leica Microsystems Digital Imaging).

SEM

Samples were sparsely sprinkled onto carbon tape attached to metal stubs before thinly being coated with gold. The samples were then imaged using an SEM (Cambridge Streoscan 360) fitted with an Inca X-Sight (Oxford Instruments) detector. An accelerating voltage of 10 kV was used during imaging.

DSC

The thermal behaviour of the polymorphs was examined using a TA Instruments DSC Q10. About 8 mg of sample was weigh into an aluminium pan and sealed hermetically. Analysis was carried out by heating the sample from 100 to 240°C at a heating rate of 10°C/min under constant purging of nitrogen at 40 mL/min. An empty aluminium pan was used as a reference in all the runs. Results were analysed using TA Instruments Universal Analysis 2000.

TG

A Perkin Elmer Pyris 1 TGA system was used for the TG analysis of the polymorphs. The analysis was conducted by heating the sample with a weight range of 2-10 mg from 25°C to 200°C at a constant heating rate of 10°C/min.

HSM

The thermal behaviour of the polymorphs was visually examined using a Mettler Toledo FP90 hot-stage system and a Leica DMLM microscope with a 10X objective lens from 100 to 250°C at a heating rate of 10°C/min. Microscopic observations during experiments were displayed on a computer screen and recorded using a JVC colour video camera.

FT-IR spectroscopy

FT-IR spectra of the polymorphs were acquired using a Shimadzu FT-IR-8400S system at room temperature (approximately 25°C). Spectra over a range of 4000-600 cm^{-1} with a resolution of 2 cm^{-1} were recorded using potassium bromide (KBr) discs. The discs were prepared earlier by mixing approximately 2 mg of sample in 300 mg of KBr (IR spectroscopy grade purchased from Fisher Scientific) and grinding them together using pestle and mortar. The resulting powder mixture was then pressed into disc using a laboratory hydraulic press.

PXRD

The XRD data were collected on powdered samples using a Bruker D8 X-ray powder diffractometer. The instrument used monochromated CuKα$_1$ radiation and a position sensitive detector (PSD). Samples were mounted in Perspex flat plate sample holders and analysed through a 2θ range of 5-35° using a step size of 0.014767° over a period of 60 min at a constant temperature of 25°C. Theoretical diffraction patterns generated using the ATOMS 5.0 programme from the crystallographic data of each polymorph obtained from the CS Database are used as reference data.

3.3 RESULTS AND DISCUSSION

3.3.1 Solubility measurements

The obtained solubility data for sulfathiazole in *sec*-butanol, acetonitrile, isopropanol and water, provided in Appendix D, were used to construct linearised van't Hoff solubility curves, as presented in Figure 3.2 below. Linear regression analysis of the curves gave R-squared values between 0.97 and 0.99, which indicates the consistency and reliability of the experimental solubility data.

Based on van't Hoff equation, which is similar to equation (2.1), but without the activity coefficient, γ, a plot of $\ln C$ against $1/T$ should give a straight line with a slope of $(-\Delta H_f / R)$ and an intercept of $(\Delta H_f / RT_f)$. For simplicity, the slope and intercept are now referred to as a and b, respectively. Rearrangement of the equation gives:

$$C = e^b \times e^{\frac{a}{T}} \tag{3.1}$$
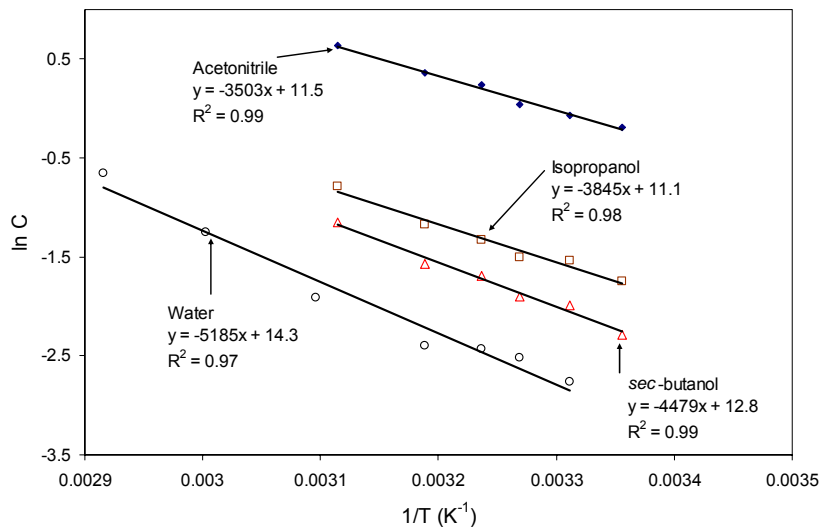
Figure 3.2 Linearised van't Hoff solubility curves for sulfathiazole in *sec*-butanol, acetonitrile, isopropanol and water.

The coefficients of the best-fit linear equations of the curves in Figure 3.2 were substituted into equation (3.1) to relate concentration to absolute temperature as presented in Table 3.2.

Table 3.2 Van't Hoff equations for sulfathiazole in various solvents.

Solvent	Van't Hoff equation
sec-butanol	$C = 3.52 \times 10^5 e^{\left(\frac{-4479}{T}\right)}$
Acetonitrile	$C = 1.03 \times 10^5 e^{\left(\frac{-3503}{T}\right)}$
Isopropanol	$C = 0.68 \times 10^5 e^{\left(\frac{-3845}{T}\right)}$
Water	$C = 16.58 \times 10^5 e^{\left(\frac{-5185}{T}\right)}$

Based on the equations in Table 3.2, van't Hoff solubility curves were plotted along with the experimental solubility points, as shown in Figure 3.3. It can be inferred from the position of the solubility curves in the figure that the relative solubility of sulfathiazole in the selected solvents is in the order of acetonitrile > isopropanol > *sec*-butanol > water. The solubility values of sulfathiazole in *sec*-butanol and water at 30°C were reported by Higuchi et al. (1967) as 0.149 g/100g and 0.114 g/100g, respectively. The values obtained in this work, however, are found to be 0.134 g/100g and 0.061g/100g, respectively. Although deviates by almost 87% from Higuchi et al.'s, the solubility of sulfathiazole in water at 30°C obtained in this work agrees well with the

one extracted from the solubility curve given by Khoshkhoo and Anwar (1993) i.e. 0.066 g/100g. The discrepancy between the solubility data is probably due to the difference in polymorphic form of the crystals. Based on the extensive literature review, this is the first time the solubility data for sulfathiazole in acetonitrile and isopropanol have been reported.
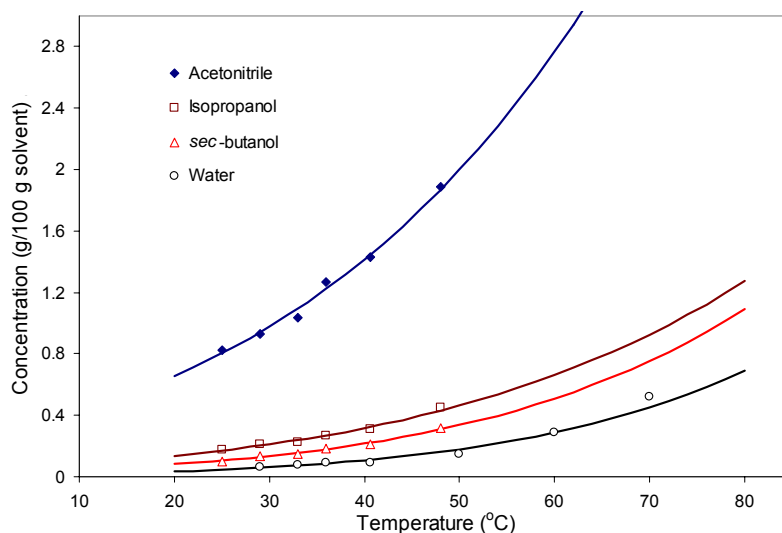
Figure 3.3 Experimental solubility points (shown as markers) and the corresponding van't Hoff solubility curves for sulfathiazole in *sec*-butanol, acetonitrile, isopropanol and water. Solid lines represent van't Hoff solubility curves.

3.3.2 Crystallisation of sulfathiazole polymorphs

UV absorbance spectra at the highest peak, 291 nm, as marked by a dashed line in Figure 3.4, were used directly to qualitatively indicate the change of sulfathiazole concentration during the crystallisation processes, with the assumption that the absorbance is directly proportional to the concentration. Although the absorbance is also affected by the temperature; however, very often the impact can be differentiated easily from those of the nucleation, dissolution and polymorphic transformation events, which are normally characterised by the sudden change in the absorbance. As discussed in section 2.7.2, the ATR-UV spectroscopy has been used quantitatively for the *in situ* monitoring and detection of nucleation event (Simon et al., 2009; Nagy et al., 2007; Anderson et al., 2001), as well as the polymorphic transformation (Howard et al., 2009; Nagy et al., 2007; Gillon et al., 2005).
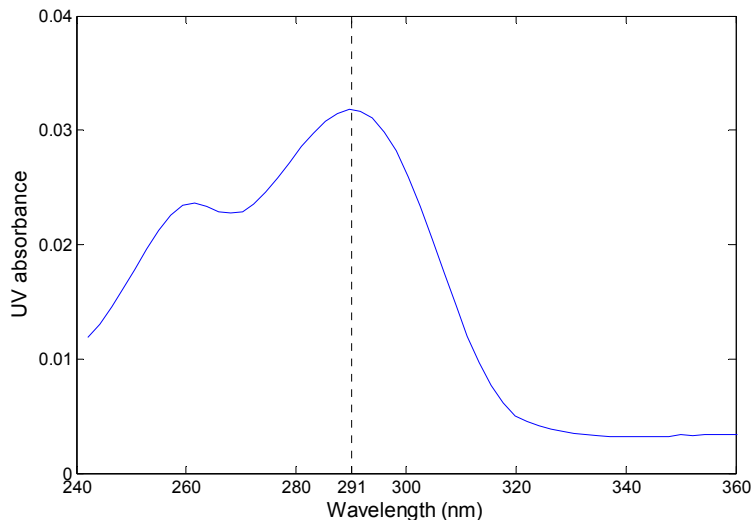
Figure 3.4 Typical absorbance spectra of sulfathiazole in *sec*-butanol saturated at 80°C.

The profiles of temperature, FBRM total number of counts/s and UV absorbance at 291 nm for cooling crystallisations performed in Method 1, Method 2, Method 3 and Method 4 are shown in Figure 3.5. The temperature profile of the natural cooling was pre-determined from the actual natural cooling experiment performed in a 250 ml conical flask from 80°C to ambient temperature, which was 25°C. As can be observed in Figure 3.5(a) for Method 1, when the system reached approximately 48°C upon cooling, the FBRM total number of counts/s showed a sudden increase while the absorbance showed a sudden drop, which indicates the occurrence of nucleation event. Since the solution was prepared to be saturated at 70°C, the MSZW of the system was calculated to be 22°C. Once the number of counts/s eventually stabilised at approximately 3500 counts/s, the absorbance continued to drop slowly. This indicates that the growth dominated process has taken over the nucleation dominated phase of the process. A similar trend was also shown by the crystallisation processes for Method 2, Method 3 and Method 4 as can be seen in Figure 3.5(b), (c) and (d), respectively. In these cases, the nucleation events were detected at approximately 31°C for Method 2, 50°C for Method 3, and 75°C for Method 4 which gave the MSZWs of 29°C, 20°C and 15°C, respectively. It can also be observed that prior to all the nucleation events, the absorbance was increasing on cooling, which is due to the effect of temperature change. In a solution at constant concentration, the absorbance generally increases with decreasing temperature. Hence for quantitative concentration measurement, the temperature effect has to be taken into account in the calibration as described in Chapter 6.

In addition to the provision of the clear and adequate initial crystallisation conditions, such as solute concentrations and temperatures, the *in situ* monitoring and thorough recording of the process properties in real-time would define the design range of the process parameters (temperature, FBRM total number of counts/s and UV absorbance) that has been demonstrated to provide the required crystal quality. By operating within this design range, the crystals can be reproduced with the same desired quality.
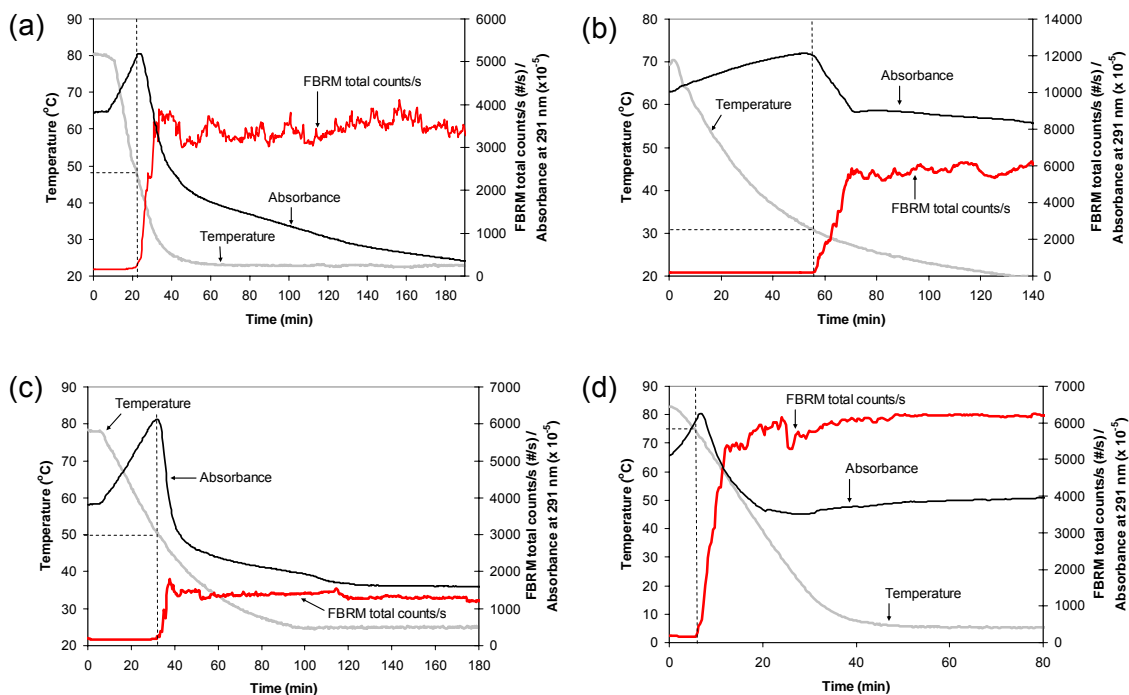
Figure 3.5 Profiles of temperature, FBRM total number of counts/s and UV absorbance at 291 nm during cooling crystallisations for (a) Method 1; (b) Method 2; (c) Method 3, and (c) Method 4.

3.3.3 Characterisation of sulfathiazole polymorphs

Optical Microscopy and SEM

Figure 3.6 shows the optical microscopy and SEM images of crystals produced by (a) Method 1; (b) Method 2; (c) Method 3; (d) Method 4; and (e) Method 5. Based on the images given by these two microscopy techniques, the morphology of the crystals can be accurately described. It was found that the crystals that were recrystallised from *sec*-butanol (Method 1), as shown in Figure 6(a), have a rod-like structure with an average length of approximately 400 µm. Form I crystals are normally reported to exhibit this morphology regardless of the crystallising solvent (Blagden et al., 1998a; Parmar et al., 2007). This, according to Blagden and co-workers, implies that the available solvent-surface interactions cannot inhibit the growth of the fastest growing

{010} faces. The crystals produced by Method 2, in which acetonitrile was the crystallising solvent, were found to exhibit a mixture of morphology: rectangular plates and truncated rectangular rods as can be seen in Figure 3.6(b). Images in Figure 3.6(c) show that the crystals produced from isopropanol (Method 3) generally have a
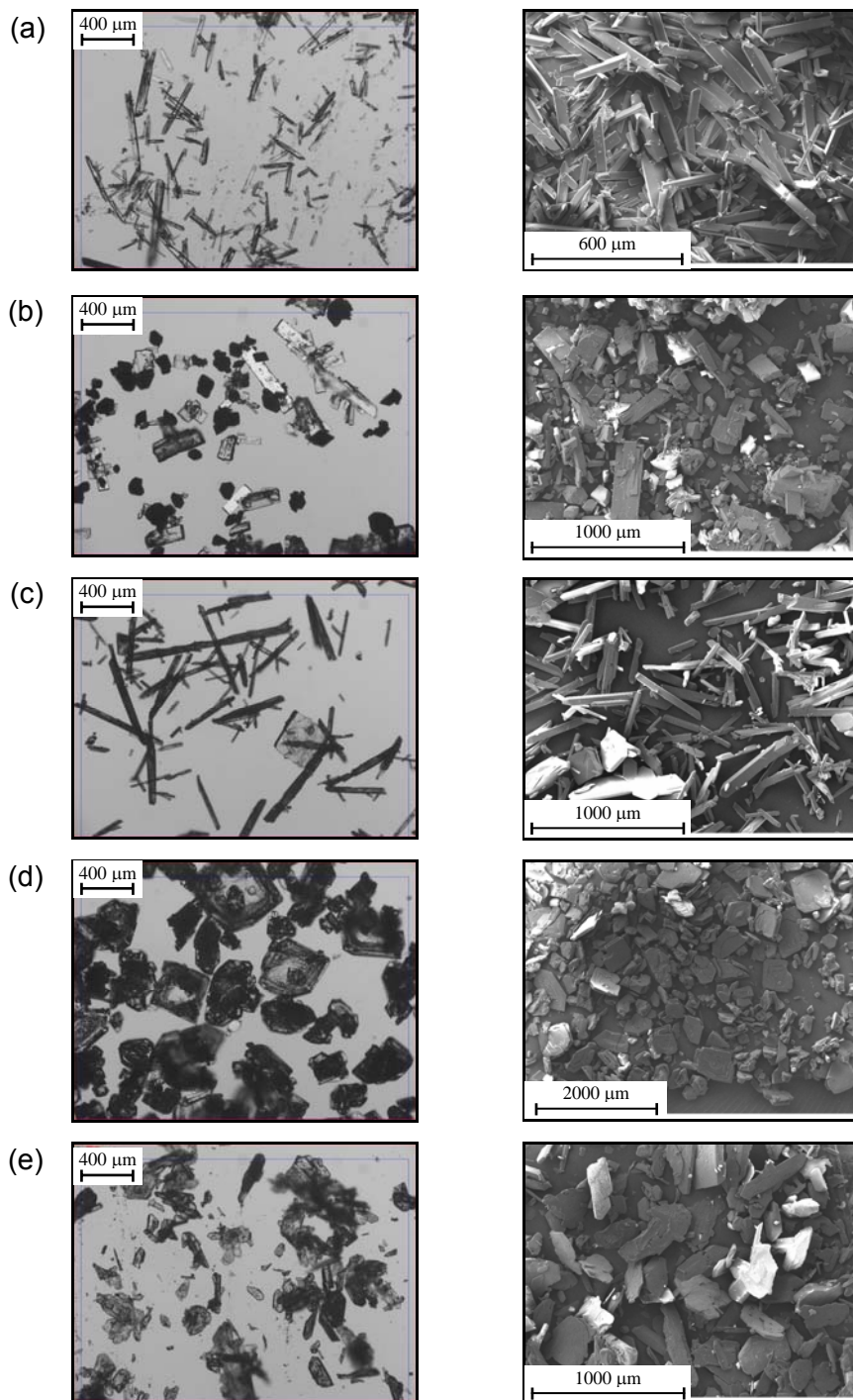
Figure 3.6 Optical microscopy and SEM images of crystals obtained from (a) Method 1; (b) Method 2; (c) Method 3; (d) Method 4; and (e) Method 5.

rod-like morphology, although the presence of square plate crystals was also observed. According to the work of Parmar et al., (2007), sulfathiazole initially crystallised from isopropanol as needles and very small square plates. The square plates then grew in size and the needles vanished. They also reported that the rate of crystal growth was slow and this may explain the appearance of the crystals produced in this work, which is mostly rod-like since the crystals were suspended in the crystallising solvent for only about 150 min. The morphology of the crystals obtained from water by fast cooling crystallisation (Method 4), shown in Figure 3.6(d), can be categorized as a mixture of square and hexagonal plates. This is consistent with that reported in the literature for Form IV crystals (Blagden et al., 1998a). On the other hand, the crystals obtained from water by evaporative crystallisation (Method 5), with their images presented in Figure 3.6(e), were found to be irregular-shaped plates. Since the morphology of crystals depends very much on the crystallising solvent, as well as other factors including the degree of supersaturation and the state of agitation of the crystallisation system, morphology is not normally used to differentiate between polymorphs.

DSC, TG and HSM

The curves of the DSC and TG, and some snapshots during HSM analysis of the crystals obtained by Method 1 are presented in Figure 3.7 and Figure 3.8, respectively. The DSC curve shows one endothermic peak with an onset temperature of 201.6 ± 0.4°C and a latent heat of 109.3 ± 5.9 J/g. It is widely known that Form I is the most stable sulfathiazole polymorph at high temperature and for the heating at 10°C/min, it was reported to melt at a temperature between 200°C to 202°C (Lagas and Lerk, 1981; Anwar et al., 1989; Mesley, 1971; Anderson et al., 2001; Zeitler et al., 2006) and released a latent heat of fusion between 81.8 J/g to 108.5 J/g (Lagas and Lerk, 1981; Zeitler et al., 2006). Although a melting event should not be detected by TG, however, as can be observed from Figure 3.7, the obtained derivative TG curve shows a very small weight change at approximately the same temperature as the melting peak on the DSC curve. This probably due to the loss of trapped solvent, or sublimation of sample during the melting process. The HSM analysis was found to agree very well with the results of the DSC and TG analyses. As shown by the snapshots of the crystals during the HSM analysis in Figure 3.8(c), most of the crystals started to melt when the hot-stage temperature reached 200.4°C. A complete melting of the crystals was observed slightly above 200.7°C, as can be seen in Figure 3.8(d). The absence

of other thermal events prior to the melting of Form I, as shown by all three thermal analysis methods, indicates that Method 1 is a reliable method to produce pure Form I crystals.

Figure 3.7 DSC and derivative TG curves of crystals obtained by Method 1.
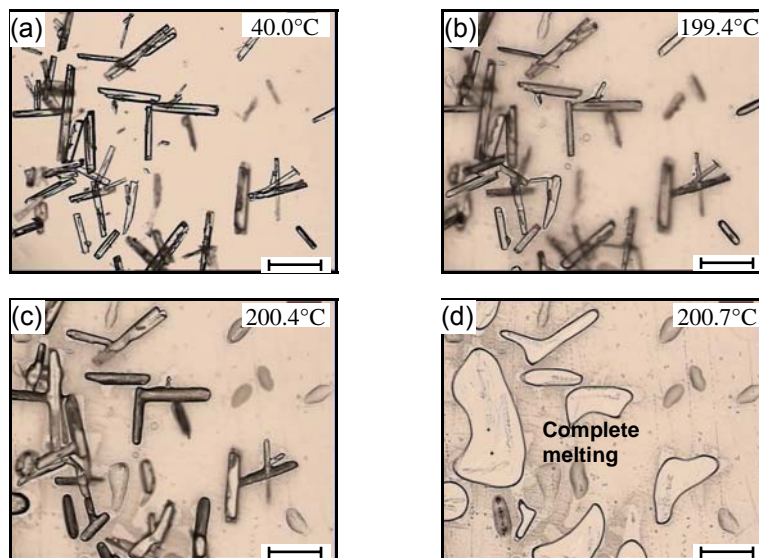
Figure 3.8 Images of crystals obtained by Method 1 during HSM analysis taken at (a) 40.0°C; (b) 199.4°C; (c) 200.4°C; and (d) 200.7°C. The scale bars represent 200 μm.

The DSC and derivative TG curves of the crystals obtained by Method 2 are shown in Figure 3.9, while some snapshots of the crystals during HSM analysis are presented in Figure 3.10. The DSC curve shows the presence of two major and one minor endothermic peaks. The first major peak at an onset temperature of 155.2 ± 0.6 °C and a latent heat of 21.1 ± 2.1 J/g was contributed by the change in the optical properties of the crystals, as shown by the difference in the brightness of the

highlighted crystals between (b) and (c) in Figure 3.10, which can be associated with a solid-solid transformation event.   It was reported that a transformation from one polymorph to another could be accompanied by a striking change in birefringence (Miller and Sommer, 1966).   The temperature of the presumed transformation event observed in this work is consistent with a previous report.   Anwar et al., (1989) reported that Form II crystals may transform into Form I in a temperature range of 150 - 170°C.   Zeitler et al. (2006), on the other hand, reported a slightly lower transformation temperature i.e. 138°C and a higher heat of transformation i.e. 32.4 J/g. The derivative TG curve in Figure 3.9 shows an increase in the rate of weight change between 131 to 165°C, which is almost in the same vicinity as the first DSC peak. Since the calculated mole fraction of the solvent presents in the sample is very small i.e. 0.0035; there is no reason to suppose that the crystals are solvates. The change in the weight was believed to be due to a polymorphic transformation.   The transformation involves rearrangement of the crystal structures and in doing so may remove some volatile impurities that are trapped in the structures.   The snapshots of the crystals during the HSM analysis in Figure 3.10(d) and (e) show that all crystals, except those that had undergone optical property change, melted between 173.3°C to 182.0°C.   This event, however, only registered as a minor endothermic peak at 172.9°C with a latent heat of 0.2 J/g on the DSC curve, which suggests that only small quantity of crystals were involved.   The melting of Form II at a temperature between 173°C to 175°C has been reported by previous researchers (Grove & Keenan, 1941; Anwar et al., 1989). The melting of the remaining crystals at 201.7°C, as shown by the HSM analysis in Figure 3.10(f), is consistent with the second major peak on the DSC curve, which lies at an onset of 201.9 ± 0.0 °C with a latent heat of 109.9 ± 1.7 J/g. The results of the DSC, TG and HSM analyses imply that some of the crystals obtained by Method 2 have transformed to Form I in a temperature range of 155.2°C to 165°C.   Those crystals that were not transformed melted at a temperature between 172.9°C to 173.3°C, while the newly formed Form I crystals melted at a temperature between 201.7°C and 201.9°C.   This is actually one of the two reasonable explanations suggested by Anwar et al. (1989), who also observed similar behaviour exhibited by sulfathiazole crystals other than Form I and Form V. Another explanation is that two polymorphs were initially formed; one melted at a temperature between 172.9°C to 173.3°C and another transformed to Form I in a temperature range of 155.2°C to 165°C.

Figure 3.9 DSC and derivative TG curves of crystals obtained by Method 2.
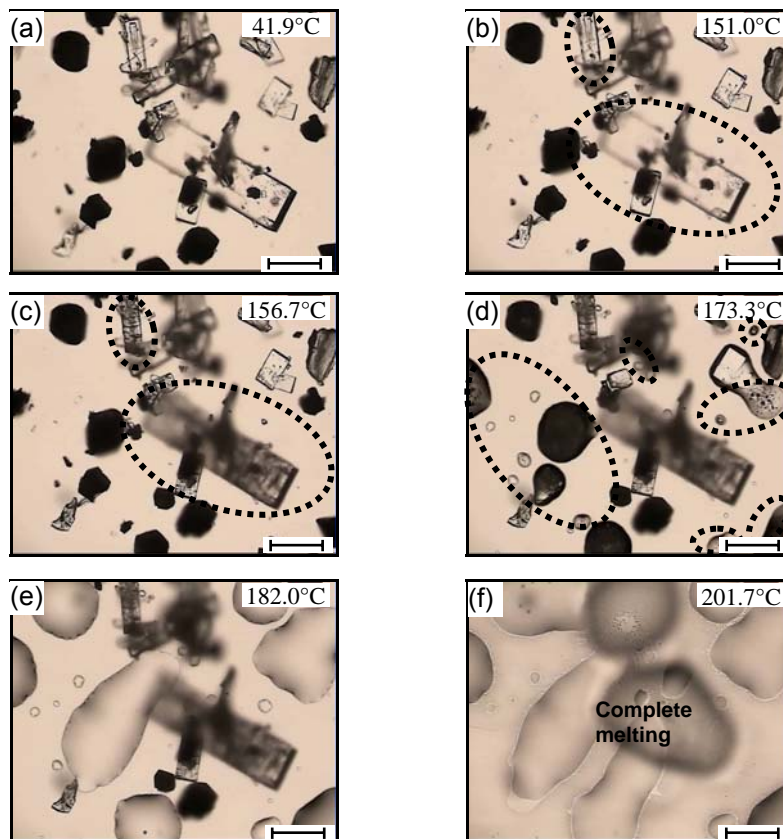
Figure 3.10 Images of crystals obtained by Method 2 during HSM analysis taken at (a) 41.9°C; (b) 151.0°C; (c) 156.7°C; (d)173.3°C; (e) 182.0°C; and (f) 201.7°C. The scale bars represent 200 μm.

The DSC curve of the crystals obtained by Method 3 presented in Figure 3.11 demonstrates the presence of two endothermic peaks. The first peak with an onset temperature of 142.3 ± 0.4°C and a latent heat of 19.0 ± 1.9 J/g was contributed by a possible polymorphic transformation, which was indicated by a slight movement of some of the crystals during HSM analysis as shown by the highlighted crystals in Figure 3.12(b) and (c). Besides an optical property change, a polymorphic transformation may also result in a movement of the crystals since the transformation events may be accompanied by a change in the crystals' volume (Warrington, 2002). The temperature of the transformation event observed in this work lies within the 105 - 170°C range, in which Form III crystals may transform into Form I, as reported by Lagas and Lerk (1981), but outside the 150 - 170°C range reported by Anwar et al. (1989). Zeitler et al. (2006) also reported a higher transformation temperature i.e. 159°C and a higher heat of transformation i.e. 27.3 J/g. The derivative TG curve in Figure 3.11 indicates an increase in the rate of weight change between 130 to 155°C. The increase corresponds well with the endothermic peak that is associated with the polymorphic transformation. The mole fraction of the solvent presents in the sample was calculated to be 0.0023; too small to consider the crystals as solvates. The second peak on the DSC curve has an onset temperature of 201.8 ± 0.1°C and a latent heat of 102.9 ± 7.5 J/g was the result of the melting of Form I crystals. The melting was confirmed by the HSM analysis, as shown in Figure 3.12(f), Although the HSM analysis showed the melting of a few tiny crystal fragments at 173.9°C, as highlighted in Figure 3.12(d), the DSC curve does not show any melting peak in the vicinity of that temperature, due to either a negligible impact of the event on the overall thermal process or a complete absence of the melting species in the DSC samples. However, both results are consistent with the reports by the previous researchers (Miyazaki, 1947; Anwar et al., 1989; Lagas and Lerk, 1981; Shenouda, 1970; Moustafa and Carless, 1969) about the behaviour of Form III crystals during thermal analysis, which were summarized by Anwar et al. (1989) as either melted at 173°C, or transformed to Form I between 150°C to 170°C before melting at 201°C, or showed a combined behaviour. The single melting at 173°C was postulated to be obtained only if the crystals are purely Form III (Lagas and Lerk, 1981). If the slightest amount of Form I was present, some, if not all Form III crystals will transform to Form I. Since Form I is expected to always be initially crystallised in accordance to the Ostwald's Rule of Stages, the likelihood of the contamination of the crystallisation product with Form I is very high. In general, the results of the DSC, TG and HSM indicate that
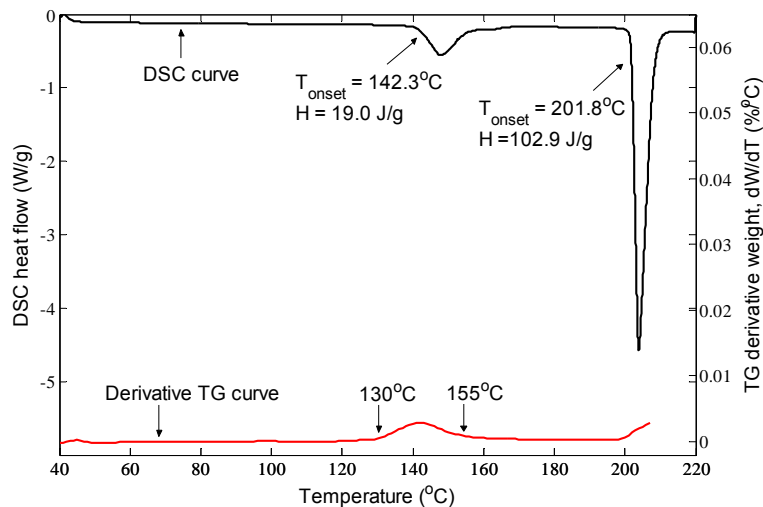
Figure 3.11 DSC and derivative TG curves of crystals obtained by Method 3.
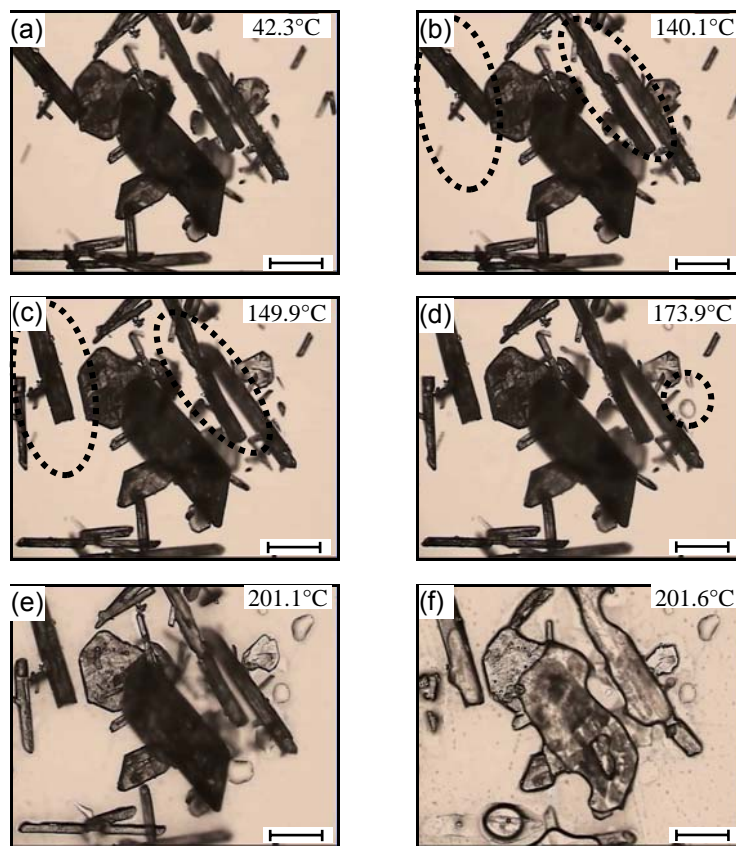
Figure 3.12 Images of crystals obtained by Method 3 during HSM analysis taken at (a) 42.3°C; (b) 140.1°C; (c) 149.9°C; (d)173.9°C; (e) 201.1°C; and (f) 201.6°C. The scale bars represent 200 μm.

Method 3 was able to produce Form III crystals. If the suggestion by the previous researchers about the effect of the presence of Form I on the transformation of Form III is true, then Method 3 also produced Form I crystals along with Form III crystals.

The presence or absence of Form I crystals can be confirmed by the PXRD analysis, as shown later.

The results of the DSC and TG analyses of the crystals obtained using Method 4 are presented in Figure 3.13. Three endothermic peaks are shown by the DSC curve. The first peak was formed at an onset of 118.9 ± 0.0°C, the second at 160.8 ± 2.3°C and the third at 201.8 ± 0.2°C. Their enthalpies are 1.3 ± 0.6 J/g, 24.9 ± 0.9 J/g and 115.6 ± 4.2 J/g, respectively. The HSM analysis, however, only confirmed the last two events as shown by the snapshots of the crystals during the HSM analysis in Figure 3.14. A polymorphic transformation was detected at 168.3°C based on the optical property change of the highlighted crystals in Figure 3.14(b) and (c). This is consistent with the second peak on the DSC curve. The transformation of Form IV crystals to Form I was also detected by Zeitler et al. (2006) at almost the same onset temperature i.e. 160°C, but it produced a slightly higher heat i.e. 29.5 J/g. The HSM detected a melting event at 180.8°C, as shown by the highlighted crystal fragments in Figure 3.14(d). This event may be too small to be detected by the DSC, or the melting species was not present in the DSC samples. The temperature of the melting was slightly higher than those found previously (in crystals obtained by Method 2 and Method 3), but Shenouda (1970) have also reported melting events at 179°C, given by the DSC analysis. Form IV, as well as Form II and Form III, have been reported to melt in the vicinity of 175°C (Apperley et al., 1999). The melting of Form I crystals was shown by the HSM at 203.3°C as depicted in Figure 3.14(f). This is consistent with the third peak on the DSC curve. In contrast to the result of the DSC analysis, no thermal event was detected by the HSM in the vicinity of 118.9°C. It was reported recently that the DSC peak that lies in the vicinity of that temperature corresponds to the dehydration of a hydrate (Howard et al., 2009). In order to confirm the presence of hydrates, the crystals were heated while immersed in silicone oil. Some of the images during the analysis were presented in Figure 3.15. It was found that some bubbles were liberated at 120.1°C, as highlighted in Figure 3.15(b). The evolution and movement of these bubbles were seen in the subsequent snapshots in (c) and (d) in Figure 3.15. This liberation of bubbles is believed to correspond to the escape of water vapour during the vaporisation process, which would never be visually detected without the use of oil.
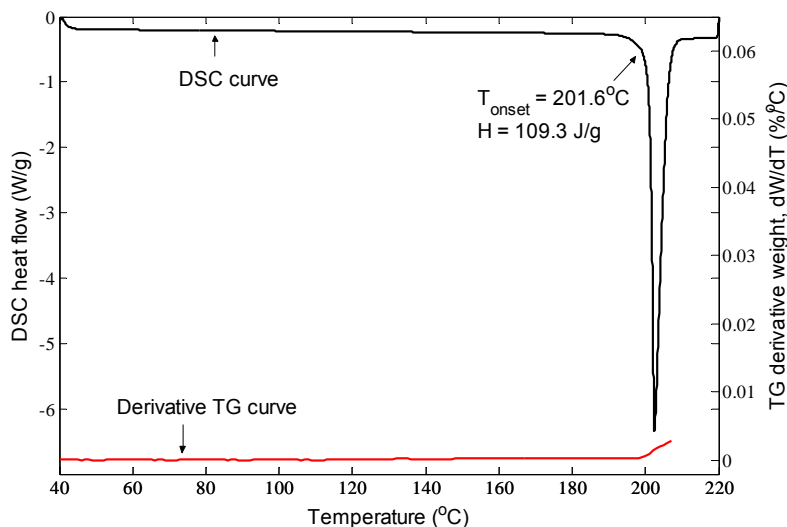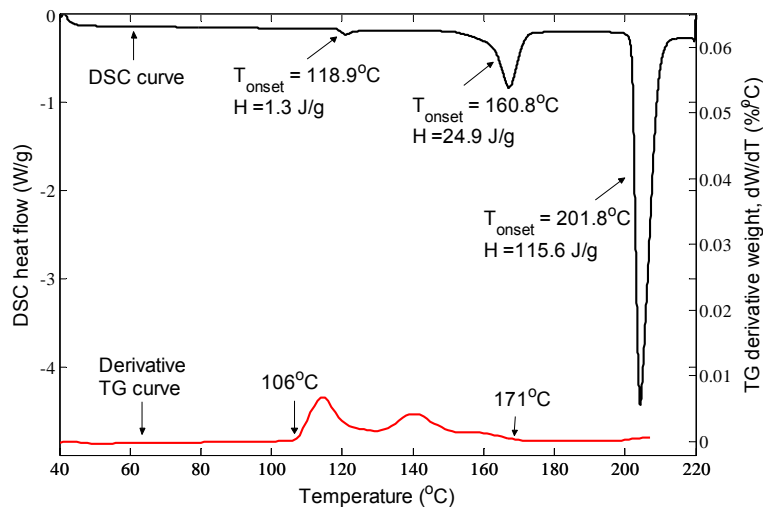
Figure 3.13 DSC and derivative TG curves of crystals obtained by Method 4.
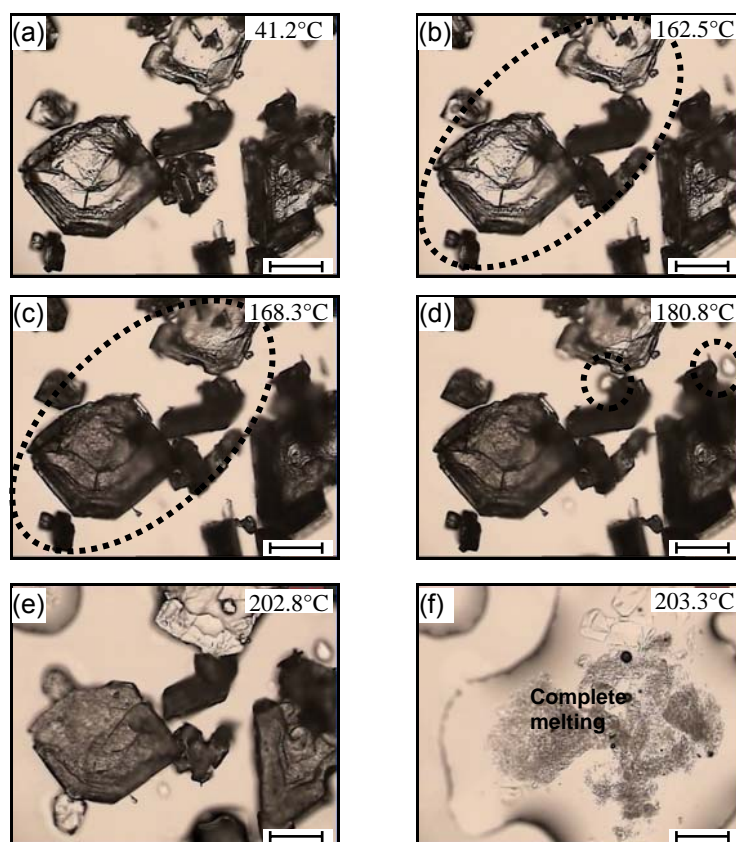
Figure 3.14 Images of crystals obtained by Method 4 during HSM analysis taken at (a) 41.2°C; (b) 162.5°C; (c) 168.3°C; (d)180.8°C; (e) 202.8°C; and (f) 203.3°C. The scale bars represent 200 µm.
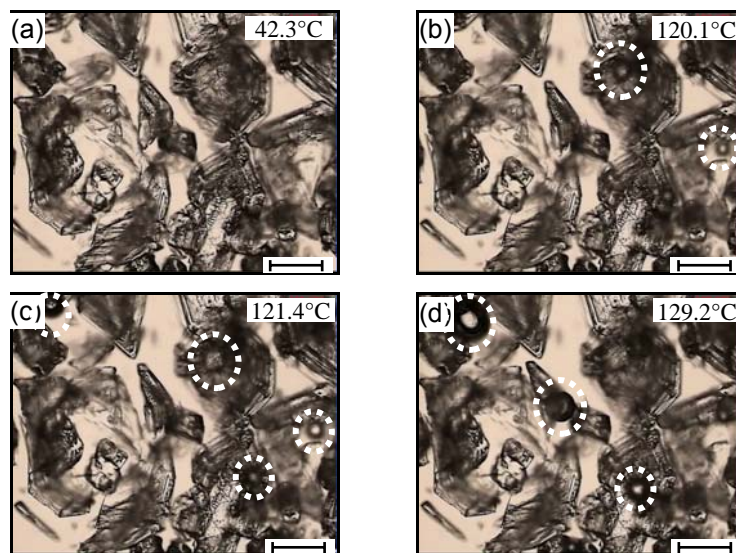
Figure 3.15 Images of crystals obtained by Method 4 immersed in silicon oil during HSM analysis taken at (a) 42.3°C; (b) 120.1°C; (c) 121.4°C; and (d) 129.2°C. The scale bars represent 200 μm.

The derivative TG curve as shown in Figure 3.13 indicates the removal of volatile impurities between 106°C to 171°C, which requires close examination. For this reason, the curve was re-plotted together with the TG curve and they are presented in Figure 3.16. Below 200°C, the curves can be divided into three parts according to different reactions: (A) 106 - 129°C: dehydration of a hydrate species called isolated site hydrate with loosely bound water; (B) 129 - 153°C: dehydration of tightly bound water from the sulfathiazole hydrate; and (C) 153 - 171°C: removal of the trapped volatile impurities due to polymorphic transformation. The mole fraction of the solvent removed by the dehydration processes (A and B) is calculated to be 0.0206, while that removed by the polymorphic transformation is 0.0024. The results of the DSC, TG and HSM analyses indicate that some of the crystals obtained by Method 4 are hydrates, while some transformed to Form I at a temperature between 160.8°C and 168.3°C. Those few crystals that have not transformed to Form I, melted at 180.8°C. The newly formed Form I melted at a temperature between 201.8°C and 203.3°C.

Results of the DSC and TG analyses of the crystals obtained by Method 5 are shown in Figure 3.17. The DSC curve shows two endothermic peaks. The onset of the first peak is at 196.5 ± 0.1°C, while that of the second is at 202.0 ± 0.0°C. Two thermal events were also shown by the HSM analysis. As can be seen from a snapshot of the crystals during HSM analysis in Figure 3.18(c), all crystals, except the highlighted
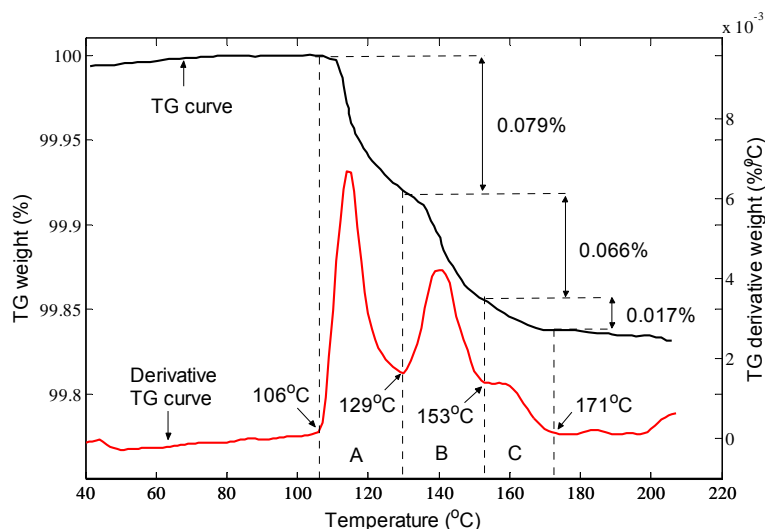
Figure 3.16 TG and derivative TG curves of crystals obtained by Method 4.

ones, melted at 198.2°C. The highlighted crystals started to melt at 201.8°C, as can be observed in Figure 3.18(d). A complete melting of Form V crystals at a temperature between 196.0°C to 196.5°C was previously reported (Lagas and Lerk, 1981; Anwar et al., 1989), but this would only be observed if the crystals were very pure. According to Lagas and Lerk (1981), if the slightest amount of Form I was present, Form I crystallised during the melting of Form V, which was indicated by the appearance of an exothermic peak immediately after the endothermic melting peak and before the newly formed crystals melted. The presumed exothermic crystallisation peak was also observed in this work, as can be seen in Figure 3.17. The presence of two melting peaks in this work is consistent with the work of Anderson et al. (2001). In their work, the melting peaks were observed at the onsets of 197°C and 202°C. In addition to the two melting peaks at the onsets of 197°C and 201°C, Zeitler et al. (2006) detected another endothermic peak at 156°C. The derivative TG curve in Figure 3.17 shows the increase in the rate of weight change started at the temperature corresponding to the onset of the first DSC melting peak, i.e. 196.5°C. These results show that Method 5 has successfully produced crystals of Form V (that melted at 196.5°C), but some of them have transformed to Form I undetected at some points during heating, or as suggested by Lagas and Lerk (1981) have melted and immediately recrystallised as Form I. However, there is also a possibility that Form I has formed together with Form V from the beginning; which is based on the suggestion by Lagas and Lerk (1981) that the presence of Form I may induce the recrystallisation of Form I from the melt of Form V.
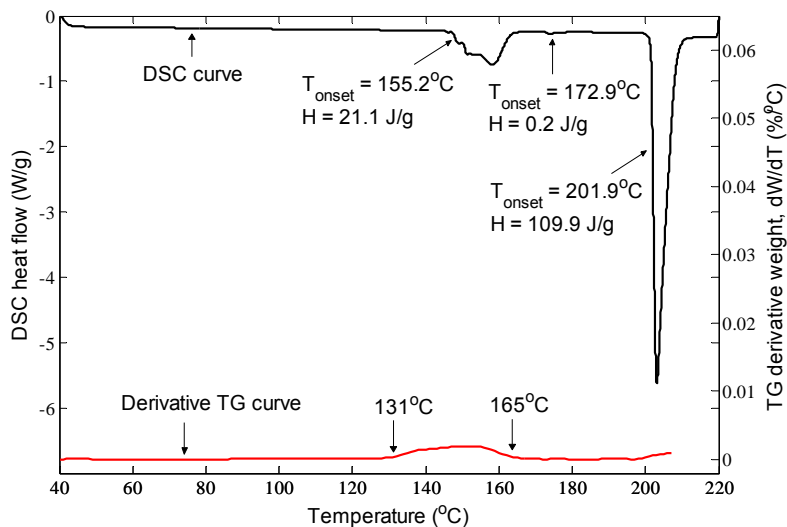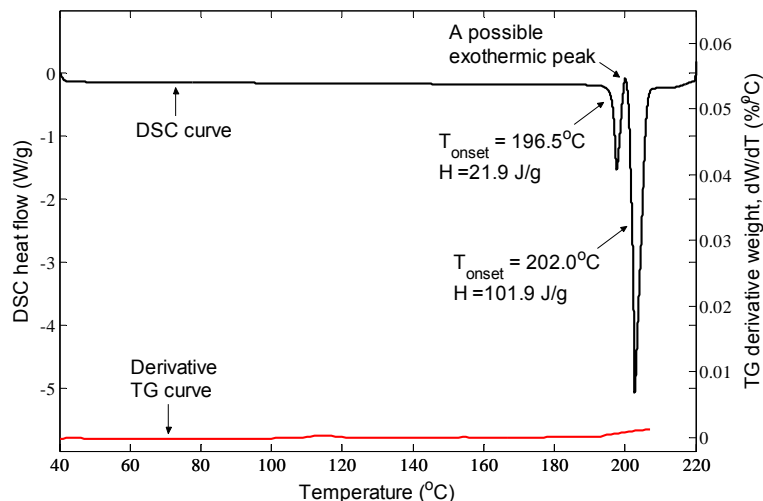
Figure 3.17 DSC and derivative TG curves of crystals obtained by Method 5.
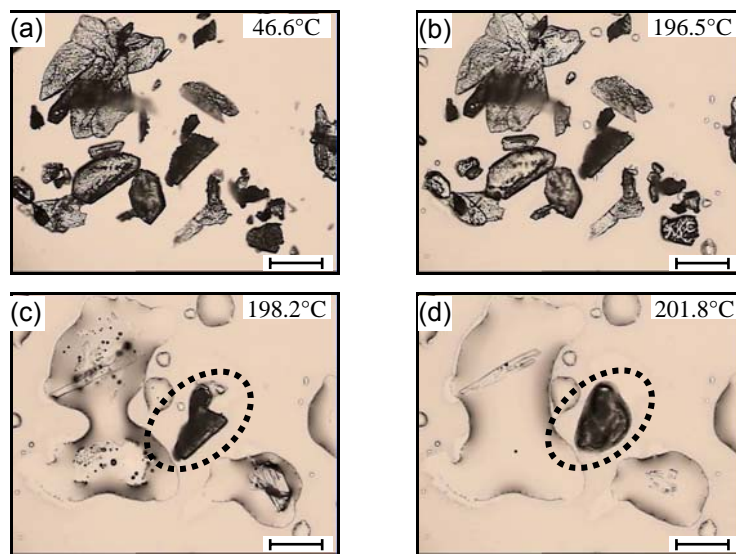
Figure 3.18 Images of crystals obtained by Method 5 during HSM analysis taken at (a) 46.6°C; (b) 196.5°C; (c) 198.2°C; and (d) 201.8°C. The scale bars represent 200 μm.

FT-IR spectroscopy

The FT-IR spectra (600-4000 cm^{-1}) and (600-1600 cm^{-1}) of crystals obtained by all methods are presented in Figure 3.19.   The spectra are sufficiently distinct to characterise crystals obtained by Method 1 and Method 5 only; the others, however, are practically indistinguishable. As can be observed in Figure 3.19(a), the presence of bands at 3466 and 3368 cm^{-1} is unique for the spectrum of the crystals obtained by Method 1.
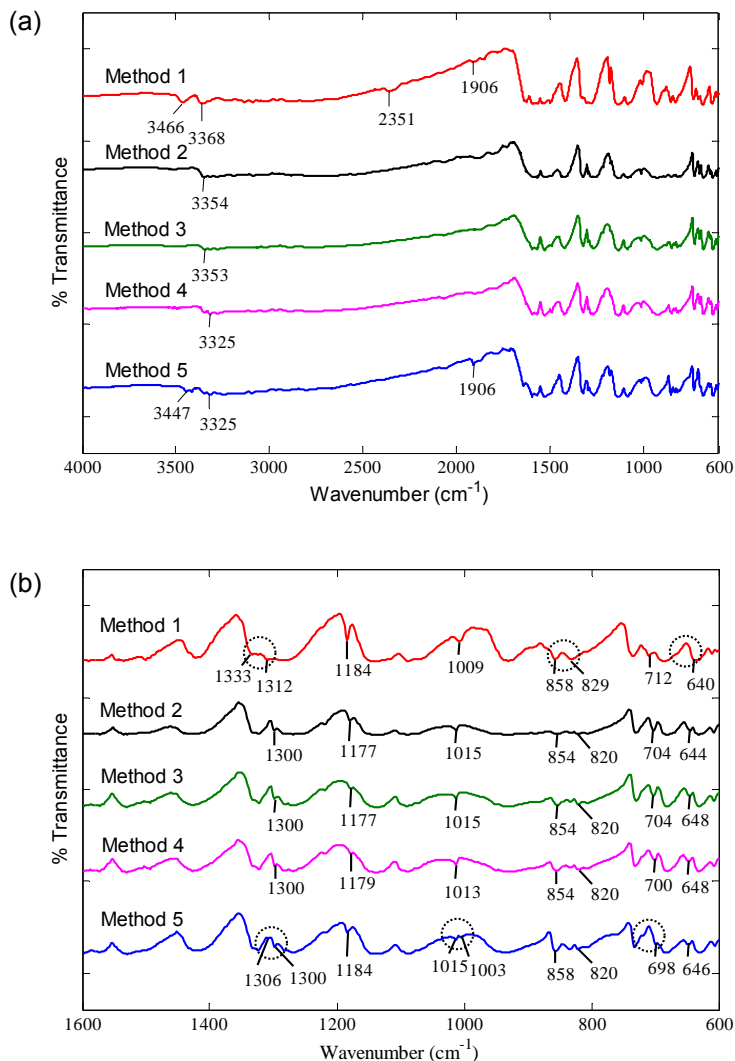
Figure 3.19 FT-IR spectra of crystals obtained from Method 1, Method 2, Method 3, Method 4 and Method 5 arranged in order from top to bottom between (a) 600 and 4000 cm^{-1} and (b) 600 and 1600 cm^{-1}.

Although slightly shifted, the bands are consistent with the NH$_2$ bands in Form I that occurred at 3460 and 3355 cm^{-1}, as reported by Mesley (1971). They are also consistent with the characteristic bands for Form I crystals identified by Burger and Dialer (1983) at 3365 cm^{-1}, as well as with those identified by Anderson et al. (2001) at 3462 and 3355 cm^{-1}.

The FT-IR spectrum of the crystals obtained by Method 5, on the other hand, is found to possess distinctive bands at 3447 and 3418 cm^{-1}. They are very close to the characteristic bands for Form V crystals at 3345 and 3417 cm^{-1} as reported by Anderson et al. (2001). One of the bands also matched the characteristic band of

Form V crystals reported by Burger and Dialer (1983) at 3445 cm^{-1}. A further examination of the FT-IR spectra in the range of 600-1600 cm^{-1}, presented in Figure 3.19(b), also revealed the distinctive patterns of the spectra given by the crystals obtained by Method 1 and Method 5. As highlighted in the figure, the distinctive pattern for the crystals obtained by Method 1 are observed between 1330 to 1290 cm^{-1}, 935 to 820 cm^{-1} and 662 to 630 cm^{-1}, whilst those for the crystals obtained by Method 5 are detected between 1330 to 1290 cm^{-1}, 1017 to 965 cm^{-1} and 730 to 684 cm^{-1}. It has been reported in the literature that the IR spectra may not be able to distinguish clearly between sulfathiazole polymorphs (Hughes el al., 1997), particularly between Form II and Form III (Anwar et. al., 1989). It was found in this work that, besides being unable to differentiate between crystals obtained by Method 2, Method 3 and Method 4, the FT-IR spectra also showed no evidence of the presence of water in the crystals obtained by Method 4. The presence of water should show interference from NH$_2$ absorptions near 3300 and 1650 cm^{-1} where water absorptions are expected (Mesley, 1971). The result may indicate that the presence of water in the crystals was so small that it escaped detection by the FT-IR.

PXRD

PXRD patterns of the crystals obtained by all five methods are shown in Figure 3.20 below. It can be observed that each of the patterns has its own distinctive features. Although PXRD is always able to distinguish unequivocally between different polymorphs, its use in this work has some challenges. Firstly, the five polymorphs of sulfathiazole have very closely related structures, differing only in the hydrogen bonding arrangements and inter-relation between the molecules in the asymmetric unit (Blagden et al., 1998a). This resulted in many of the strong reflections of each polymorph lie within the same 20-30° region, as can be seen in Figure 3.20. Low angle (<20°) data, where there are fewer overlapping reflections, therefore contain the most information for distinguishing between the different polymorphs. However these may be relatively weak and hence require careful scrutiny. Secondly, there is a case called preferred orientation, which is generated when crystals line up preferentially along particular directions due to their morphology. In the case of sulfathiazole, several polymorphs exist where the crystals have plate-like or rod-like morphology. Platelets typically line up in a stacking sequence, whilst rods line up parallel similar to matchsticks in a box. This partially organised set-up is far from the totally random arrangement of the crystals required to observe the expected intensities of the

reflections, which should be observed based on the unit cell lattice parameters and arrangement of the atoms within it. Generally the plate-like and rod-like crystals demonstrated preferred orientation along the long axis direction, which means these reflections are unexpectedly strong. However, by using the presence of the reflections, rather than their intensity, the occurrence of each polymorph can be evaluated.
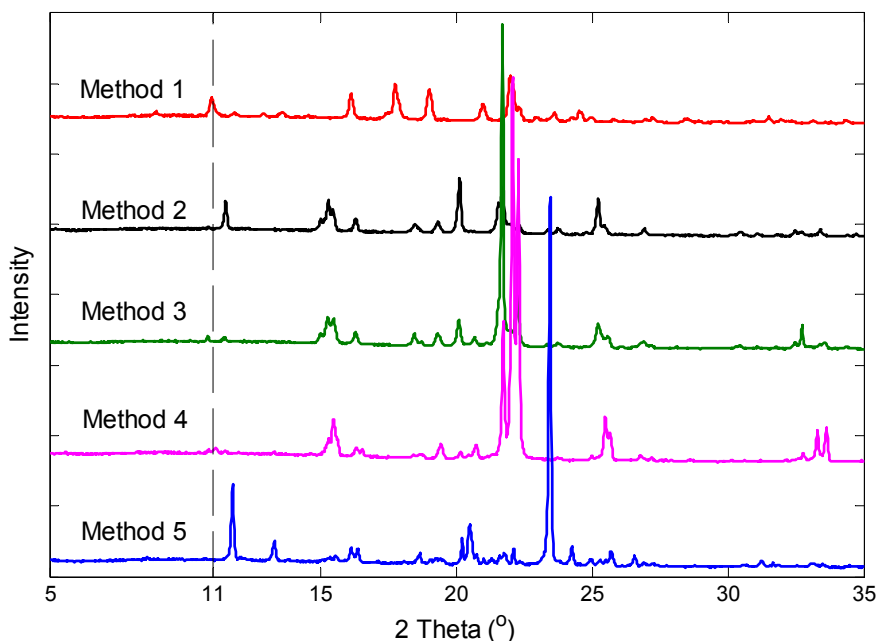
Figure 3.20 PXRD patterns of crystals obtained from Method 1, Method 2, Method 3, Method 4 and Method 5 arranged in order from top to bottom. A vertical dash-line to assist in the observation for the presence of peaks at 11° 2θ.

Anwar et al. (1989) and Blagden (2001) have reported that the pattern of Form I can be distinguished by its characteristic peak at a 2θ value of 11°. With the assistance of a vertical dash-line, as shown in Figure 3.20, it can be observed that peaks at 11° 2θ are only present on the PXRD patterns of Method 1 and Method 4. The peak on the latter pattern, however, is so tiny that it may require close examination. The patterns in Figure 3.20 are individually analysed and discussed in the subsequent paragraphs.

Figure 3.21 shows the PXRD pattern of the crystals obtained from Method 1 in comparison with some major reflections ($\geq$10% relative intensity) in the PXRD data of Form I (Suthaz01) contributed by Kruger and Gafner (1972), obtainable from the CS Database. It can be seen from the figure that the pattern of the crystals obtained from Method 1 concurs very well with the reference data. As previously mentioned, the

characteristic peak of Form I at 11° 2θ is present on the pattern. This confirms the results of other characterisation techniques that pure Form I crystals have been successfully produced by Method 1.
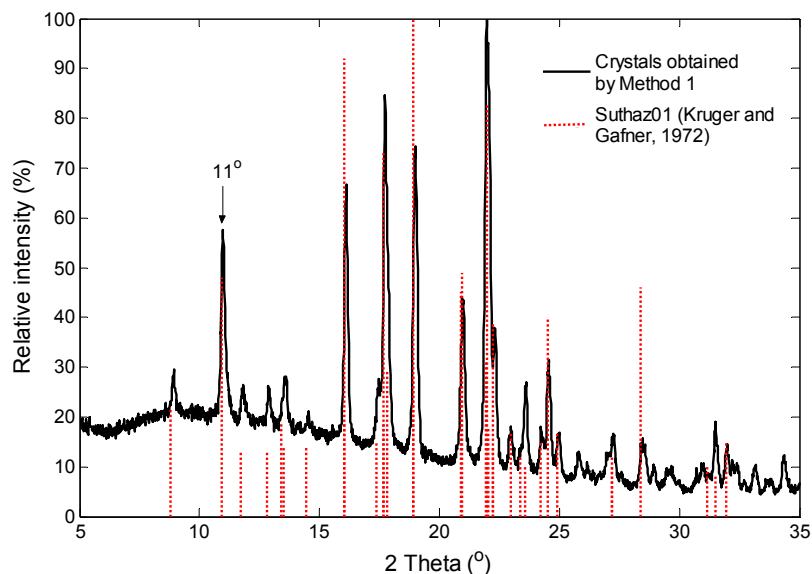
Figure 3.21 PXRD pattern of crystals obtained from Method 1 in comparison with some major reflections in the reference pattern of Form I (Suthaz01).
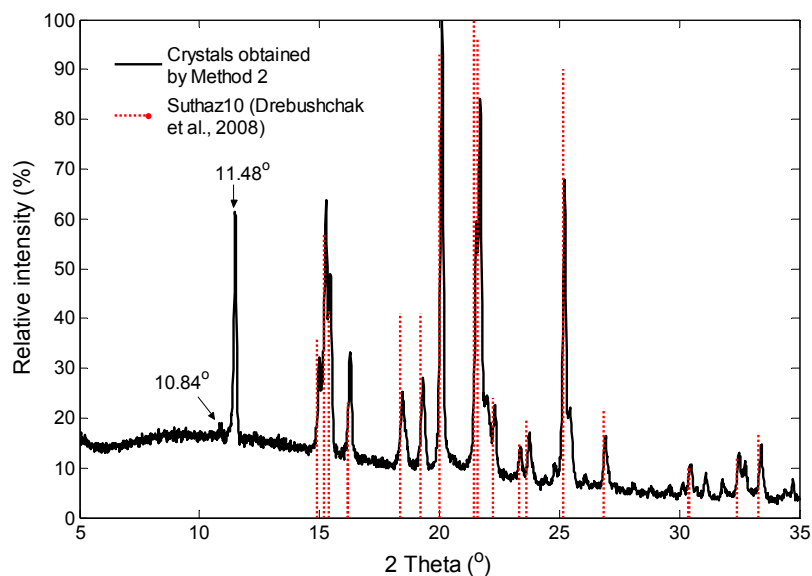
Figure 3.22 PXRD pattern of crystals obtained from Method 2 in comparison with some major reflections in the reference pattern of Form II (Suthaz10).

Figure 3.22 presents the PXRD pattern of the crystals obtained from Method 2 in comparison with the CS Database's PXRD data of Form II (Suthaz10) contributed by Drebushchak et al. (2008). This data reference was chosen instead of the earlier one

by Kruger and Gafner (1971) because of its better quality of the structure determination. Except a reflection at 11.48°, all other major reflections in the PXRD pattern of the obtained crystals concur very well with those of the reference data. The reflection at 11.48° however corresponds to a peak at 11.40° in the reference data, only that the latter relative intensity is only 2% (hence it is not shown in the figure), while the former is 61%. This extreme difference in the relative intensity may be contributed by the preferred orientation as mentioned previously. The absence of a peak at 11° 2θ on the pattern indicates the absence of Form I in the sample. Since in this case almost all peaks in the PXRD pattern of the obtained crystals agree well with the reference data, it can be confirmed that Method 2 is a reliable method of producing Form II crystals.
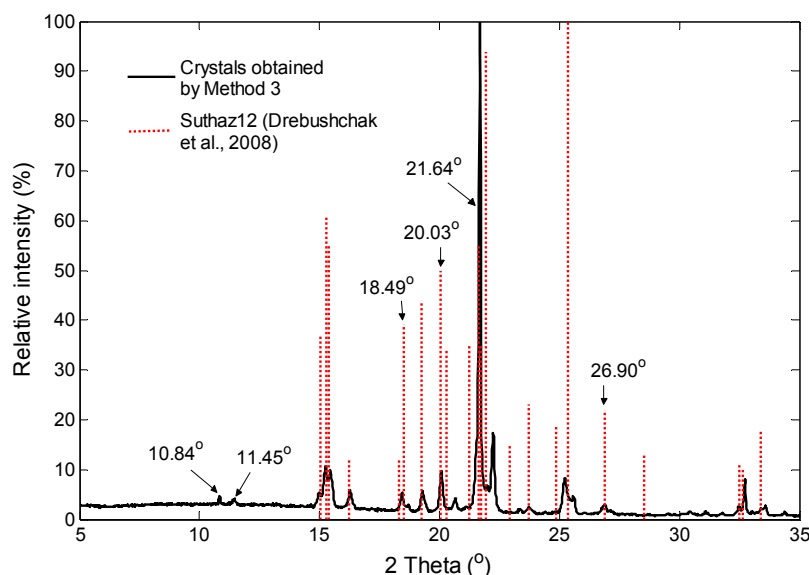
Figure 3.23 PXRD pattern of crystals obtained from Method 3 in comparison with some major reflections in the reference pattern of Form III (Suthaz12).

The comparison of the PXRD pattern of crystals obtained from Method 3 with the major reflections in the reference data for Form III (Suthaz12), supplied by Drebushchak et al. (2008) in the CS Database, is presented in Figure 3.23. In this case, the difference in intensity is very large; most reflections of the obtained crystals are much less intense compared to the reference. Extreme cases may contribute to the complete absence of a few reflections in the crystals' PXRD pattern, which are present in the reference's. However, since most of the reflections present in the crystals' PXRD pattern concur very well with those of the reference, particularly at the characteristic reflections of Form III at 18.49°, 20.03°, 21.64° and 26.90°, it confirms that Method 3 has successfully produced Form III crystals. Since Form I is not present

in the sample as can be inferred from the absence of the characteristic peak of Form I at 11° 2θ, the transformation of Form III to Form I crystals, as shown by the DSC and the derivative TG curves in Figure 3.11, can proceed without any contamination of Form III with Form I.
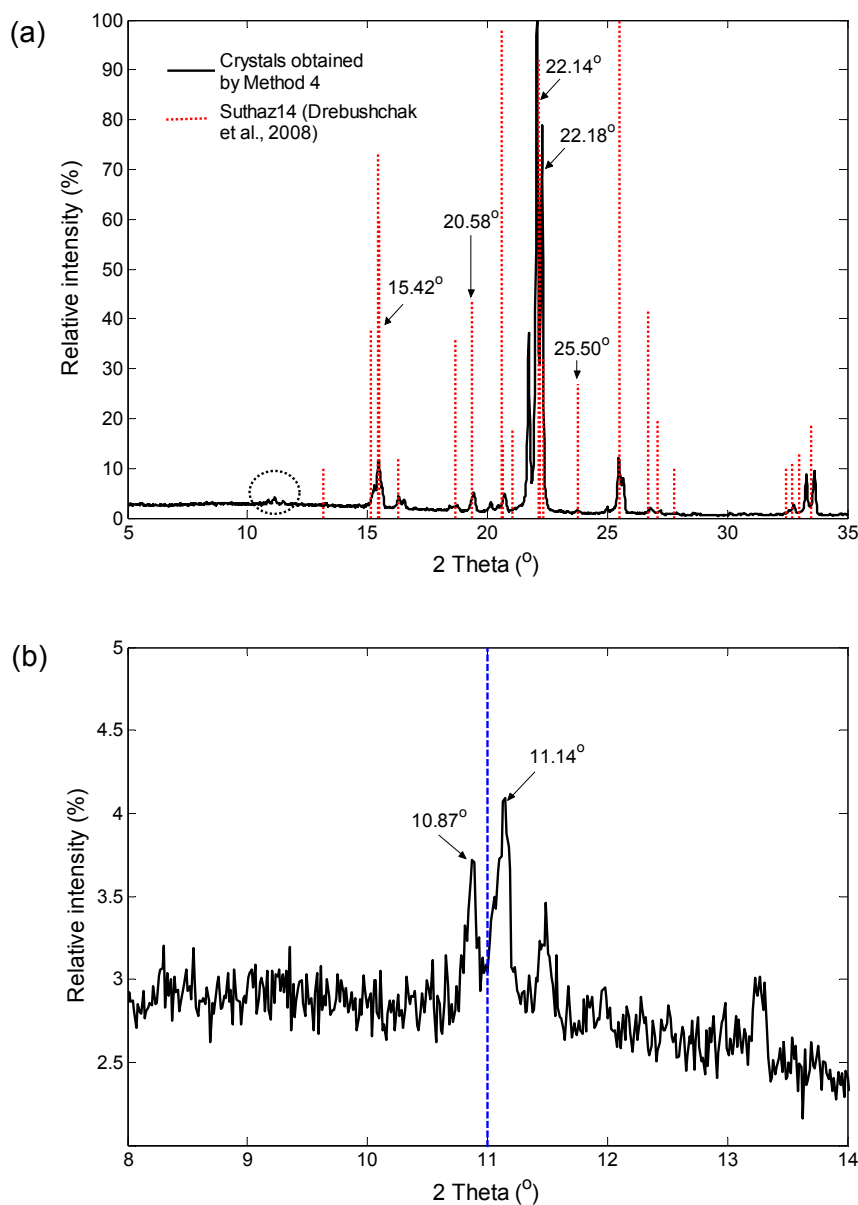
Figure 3.24 (a) PXRD pattern of crystals obtained from Method 4 in comparison with some major reflections in the reference pattern (Suthaz14); and (b) zoom-out view of the circled part on the PXRD pattern in (a).

The PXRD pattern of crystals obtained from Method 4 as depicted in Figure 3.24(a) also shows that most of its reflections are less intense compared to the reference data of Form IV (Suthaz14) given by Drebushchak et al. (2008) in the CS Database. There are also an absence of a few of the reflections in the crystals' PXRD pattern that are

present in the reference. Form I is not present in the crystals since its characteristic peak at 11° 2θ is absent from the pattern, as can be seen from Figure 3.24(b), which shows a zoom-out view of the circled part on the PXRD pattern in Figure 3.24(a). The concurrence of most of the reflections in the crystals' pattern with those of the reference, particularly at the characteristic reflections of Form IV at 15.42°, 20.58°, 22.14°, 22.18° and 25.50° as shown in Figure 3.24(a), proves that Method 4 is a reliable method to produce Form IV crystals.
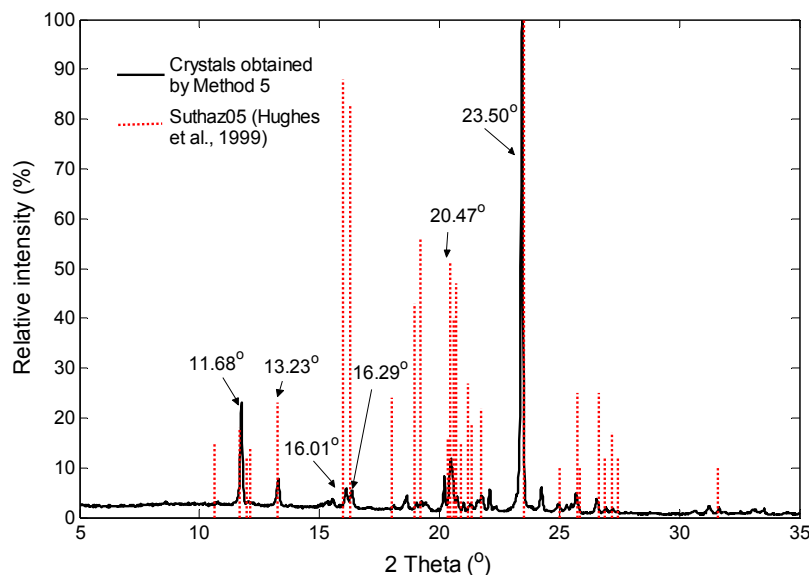
Figure 3.25 PXRD pattern of crystals obtained from Method 5 in comparison with some major reflections in the reference pattern (Suthaz05).

Figure 3.25 shows the PXRD pattern of crystals obtained from Method 5 together with the CS Database's pattern of Form V (Suthaz05) contributed by Hughes et al. (1999). It was found that the pattern of the crystals under investigation shares the characteristic reflections of Form V at 11.68°, 13.23°, 16.01°, 16.29°, 20.47° and 23.50°. No peak at 11° 2θ is observed, which indicates the absence of Form I crystals. Therefore, the possibility that Form I has formed together with Form V from the beginning, as suggested earlier, can be eliminated. It can now be confirmed that Method 5 is a reliable method to produce Form V crystals.

In this work, although the normal procedure of grinding samples to a fine powder to present the crystals in a random orientation to the incident x-ray beam was followed, the results of the PXRD analysis indicates that no polymorphic transformations had occurred. This is in agreement with Anwar et al. (1989), who studied the effect of

grinding of a sulfathiazole polymorph on the PXRD pattern. Besides the absence of polymorphic transformation, they also found that the PXRD pattern improved significantly with the increase in grinding.

3.4 CONCLUSIONS

The crystallisations of sulfathiazole polymorphs using selected literature methods were carried out with their processes monitored and recorded using FBRM and ATR-UV spectroscopy. Various solid-state characterisation techniques have been utilised to assess the success of these crystallisation processes. The results of the thermal analysis (DSC, TG and HSM), FT-IR spectroscopy and PXRD have shown that the crystals obtained from Method 1 and Method 5 are pure Form I and Form V, respectively. For the crystals obtained from Method 2, Method 3 and Method 4, the results of the thermal analysis have indicated that some of the crystals have transformed to Form I in a temperature range of 130°C to 168°C. Those crystals that were not transformed melted at a temperature between 173°C to 182°C, while the newly formed Form I crystals melted at a temperature between 201.7°C and 203.3°C. The results of the thermal analysis also indicate that some of the crystals obtained by Method 4 are hydrates. The FT-IR spectra of the crystals obtained by Method 2, Method 3 and Method 4 were found to be identical; therefore it is not possible to differentiate between them. The obtained PXRD patterns for the crystals obtained by Method 2, Method 3 and Method 4 matched well with the CS Database patterns for Form II, Form III and Form IV, respectively. The patterns also showed the absence of Form I in the obtained crystals, which indicates the presence of Form I detected by the thermal analysis was the result of the polymorphic transformation during heating. The results show that all of the selected crystallisation methods are able to produce the desired pure polymorphs.

The *in situ* monitoring and recording of the crystallisation processes of the polymorphs allow the design range of the process parameters that has been demonstrated to produce the desired crystal quality to be defined. The process parameters in this case refer to the evolution of the temperature, FBRM total counts/s and UV absorbance. By operating within the defined design range, the crystals can be reproduced with a guaranteed quality and minimum risk. The incorporation of the process and product knowledge into the process design is part of the PAT framework and satisfies the QbD concept. The ultimate aims are to reduce wastage, manufacturing error, time to

market and costs of drugs. In the context of the present work, it is hoped that the availability of the defined design range of the process parameters will contribute towards the availability of clear and adequate description of the crystallisation conditions that are able to consistently produce the intended pure sulfathiazole polymorph. This work has also successfully illustrated basic principles associated with the development of a polymorph crystallisation process.

CHAPTER 4:
A COMBINED APPROACH OF DSC AND HSM WITH IMAGE ANALYSIS IN THE INVESTIGATION OF SULFATHIAZOLE POLYMORPHISM

The application of a combined approach of DSC-HSM with image analysis in the investigation of sulfathiazole polymorphism is presented in this chapter. The approach provides a unique insight into the polymorphic transformations and thermal behaviour exhibited by the compound. The use of light intensity profiles obtained from the HSM images, as an alternative way to present the results of the HSM analysis, was found to be useful in describing and verifying thermal events.

4.1 INTRODUCTION

DSC and HSM are two of the most widely used thermal analysis techniques for the investigation of polymorphism. The popularity of DSC is due to its simplicity and rapidity of measurement, requirement for a small sample size and ability to provide detailed information about the physical and energetic properties of a sample (Clas et al., 1999). HSM combines microscopy and thermal analysis, and allows visual observation of the thermal behaviour of a sample (Giron, 1998). This visual technique easily distinguishes thermal events, such as a polymorphic transformation from a melting process (Marthi et al., 1992); hence HSM is very useful to confirm the thermal events that are observed using other techniques, such as DSC. Recent technological advances have expanded the capabilities of the visual techniques, for example with the use of software, which not only captures the image, but also performs an image analysis, for example by computing the total light intensity. The latter may be calculated as the sum or average of the grey levels in all pixel (pixel value ranges from black = 0 to white = 255). As the image becomes brighter, the light intensity value becomes higher. The application of image analysis to evaluate HSM results is very attractive because of its ability to translate visual effects, which other techniques may not be able to provide, into quantitative information. The introduction of an alternative way of presenting results may broaden the application of HSM, since it is conventionally used only to confirm results of other thermal analysis techniques. Although image analysis has been used to extract crystallisation growth and nucleation data from a sequence of HSM images (Stapley et al., 2009), the use of image analysis to evaluate HSM results in the study of polymorphism has never been reported.

In this chapter, examples are presented of a complementary application of DSC and HSM with image analysis in the investigation of sulfathiazole polymorphism. The image analysis tool used in this work allows the selection of regions of interest (ROI) and restricts image analysis to each selected region only. The aim of this work is two-fold: (a) to give a contribution to the methods of investigating polymorphism through a combined approach of DSC-HSM with image analysis, and (b) to gain more understanding about the polymorphism of sulfathiazole.

4.2 EXPERIMENTAL METHODS

4.2.1 Materials

Sulfathiazole was purchased from Sigma-Aldrich with a purity of 98%. The solvents used are deionised water, n-propanol, acetone and chloroform. Except water, all other solvents were analytical reagent grade purchased from Fisher Scientific.

4.2.2 Crystallisation of the polymorphs

Different methods were followed to generate different polymorphs, as shown in Table 4.1. Although similar to Method 4 and Method 5 in Chapter 3, Method 2 and Method 5 in this work, were operated at lower initial concentrations.

Table 4.1 Preparation methods to produce different polymorphs of sulfathiazole.

Method no.	Polymorph to be produced	Procedure
1	Form I	Based on Method 2, Table 2.5 in Chapter 2. Heating 0.5g of sulfathiazole in 50 mL of *n*-propanol in a flask on a hot plate to dissolution, followed by natural cooling to 25°C. Note that *n*-propanol is used here, which is different from "Method 1" in Chapter 3.
2	Form IV	Based on Method 2, Table 2.8 in Chapter 2. Rapid cooling of a saturated aqueous solution of sulfathiazole at 60°C (0.5g in 100 mL water) from 80°C to 4°C at a set rate of 10°C/min in a crystalliser.
3	Form III	Based on Method 6, Table 2.7 in Chapter 2. Slow cooling of a saturated aqueous solution of sulfathiazole (0.5g in 100 mL water) at a rate of 0.1°C/min from 80°C to 20°C in a crystalliser.
4	Form II	Based on Method 4, Table 2.6 in Chapter 2. Natural cooling to 20°C a saturated solution of sulfathiazole in a 50:50 mixture of acetone: chloroform at 50°C (1.3g in 100 mL).
5	Form V	Based on Method 1, Table 2.9 in Chapter 2. Boiling to evaporate a saturated aqueous solution of sulfathiazole at 60°C (0.8g in 50 mL water) in a beaker on a hot plate until almost dry.

Note that lower initial concentrations were used for Method 2 and Method 5 here compared to Method 4 and Method 5 in Chapter 3, although the methods are similar. All of the crystallised solids were vacuum filtered and subsequently, those crystals obtained from water, were immediately dried in a hot air oven at 105°C for 15 minutes, whereas crystals obtained from other solvents were dried in a desiccator.

4.2.3 Thermal analysis of polymorphs

The DSC and HSM systems and procedure were the same, as described in Chapter 3, Section 3.2.4, except that for DSC, heating rates of 2, 10 and 20°C/min were used here.

4.2.4 HSM image analysis

The MATLAB image processing toolbox (Mathworks, Inc.) was used to compute mean values of light intensity of greyscale images in the HSM video clips. The computation was based on the average of grey levels in all pixels (pixel value ranges from black = 0 to white = 255). An algorithm for the computation is presented as a flowchart in Figure 4.1.
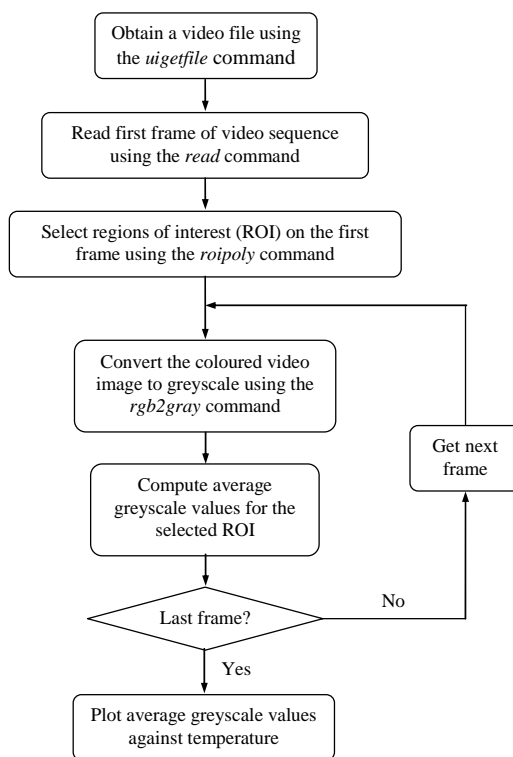
Figure 4.1 An algorithm for the computation of mean light intensity values of greyscale images in the HSM video clips.

In this work, the mean light intensity values of the HSM greyscale images is presented as percentage HSM light intensity, defined as a percentage of an average greyscale intensity value divided by the largest value of average greyscale intensity.

4.3 RESULTS AND DISCUSSION

4.3.1 Crystals obtained by Method 1

The DSC curves of the crystals obtained by method 1 at various heating rates are presented in Figure 4.2. The onset of the first peak was observed between 121 and 131°C, with the peak maxima increased from 124 to 136°C, with increasing heating rates. The shifting of the onset of the peak and the peak maximum to higher temperatures as the heating rate increases is due to the effect of ''thermal lag'' within the system. The effect is the result of the thermal lag between the DSC's furnace and the bottom of the sample pan, and/or the lag between the bottom of the sample pan and the sample, and/or the lag throughout the sample (Lever, 2007). Therefore, although the use of a higher heating rate will reduce the experimental time, the thermal lag may affect the accuracy of the results. It can also be observed from Figure 4.2 that the baseline of the curves is increasingly offset with an increase in the heating rate. The height and width of the peak are also increased, which consequently increased the detection limit, but reduced the resolution as demonstrated by the appearance of an unresolved peak for the run at a heating rate of 20°C/min, whereas for the run at a heating rate of 2°C/min, the peak is undetected. In order to find a compromise, a heating rate of 10°C/min was chosen for the subsequent thermal analysis experiments.
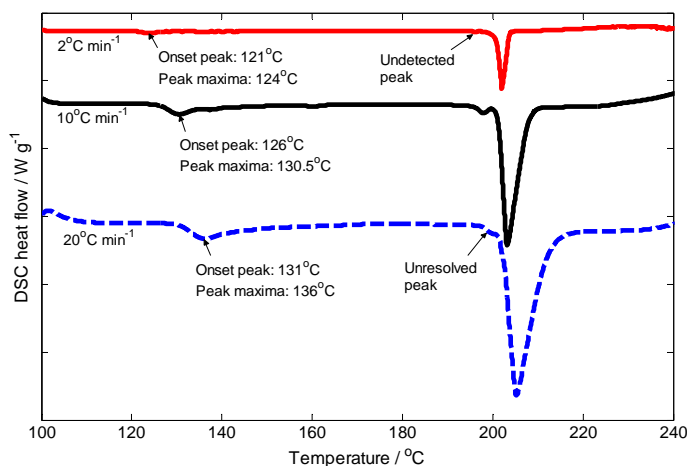
Figure 4.2 DSC curves of sulfathiazole crystals obtained by Method 1 at various heating rates.

Figure 4.3 shows the DSC curve and the HSM light intensity of the crystals obtained by Method 1, whilst Figure 4.4 shows snapshots of selected crystals during HSM analysis. Both experiments, DSC and HSM, were conducted at a heating rate of 10°C/min. Based on the DSC curve in Figure 4.3, it can be seen that there are three major peaks. The peak with a maximum at 203.2°C corresponds to the melting peak of Form I, while the peak at a maximum of 197.9°C corresponds to the melting peak of Form V. The formation of the peak at the maximum of 130.5°C may correspond to the polymorphic transformation of either Form II, Form III or Form IV crystals into Form I, since such transformations were observed to occur in a temperature range of 130°C to 168°C, as reported in Chapter 3. These events, which were implied by the results of the DSC analysis, were verified by the HSM analysis. HSM shows no melting at the expected polymorphic transformation peak at 130.5°C, but it shows an optical property change, as can be observed by the difference between the highlighted crystals in Figure 4.4(a) and (b). The change reduced the brightness and thus the light intensity of the crystals, as indicated in Figure 4.3, by the reduction in the HSM light intensity from 130.5°C onwards. The same visual observation through a HSM had been reported in the case of lithium sulphate salt in which a transformation of one of its polymorphs to another was accompanied by a striking change in birefringence (Miller and Sommer, 1966). Melting of Form V was indicated by a small increase in the value of the light intensity, while melting of Form I was shown by the continuous increase in the value of the light intensity as all the crystals have melted. Figure 4.4 shows the melting of Form V and Form I in (c) and (d), respectively.
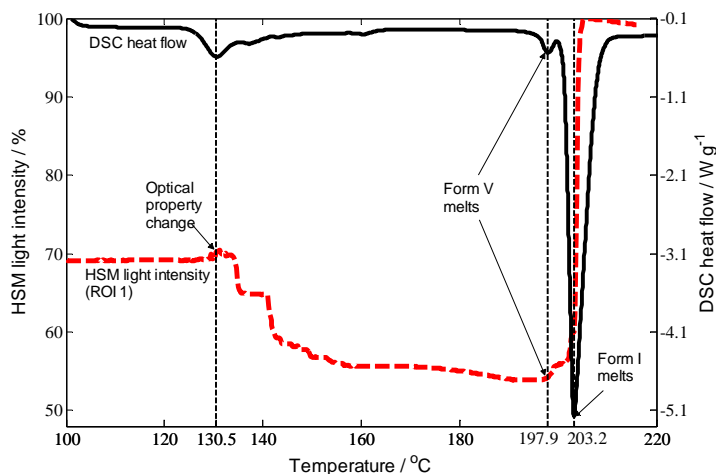
Figure 4.3 DSC curve and HSM light intensity of sulfathiazole crystals obtained by Method 1.

Figure 4.4 Images of sulfathiazole crystals obtained by Method 1 during HSM analysis taken at (a) 100.0°C; (b) 142.6°C; (c) 198.8°C; and (d) 203.9°C.

The profile of the HSM light intensity shown in Figure 4.3 was computed from all crystals on the frame (ROI 1), which is fairly comparable to the profile of the sample's DSC curve. In order to investigate the capability and sensitivity of the HSM light intensity in describing thermal events of individual crystals, two other ROI were selected; one was selected around a crystal that melts at 197.9°C (ROI 2) and another around a crystal that melts at 203.2°C (ROI 3), as highlighted in Figure 4.4(c) and (d), respectively. The computed profiles of light intensity are shown in Figure 4.5. It can be seen that all profiles indicate an optical property change with a decrease in the light intensity from 130.5°C onwards. The profile of ROI 3, however, shows a larger decrease in the light intensity compared to the profile of ROI 2, but this is believed to be due to the difference in the appearance of the images since ROI 2 is more blurred than ROI 3. The absolute changes in the HSM light intensity depend on the fraction of ROI pixels that are filled with the crystal. The ROI 2 and ROI 3 profiles show the melting of crystals at 197.9°C and 203.2°C, respectively, with a sharp increase in the light intensity. The ROI 3 profile also shows a small peak that corresponds to the melting of a crystal in ROI 2, which demonstrates the sensitivity of the HSM light intensity to the changes happening on the surface of the crystals due to the melting of adjacent crystals. The results of DSC and HSM with image analysis show that the sulfathiazole crystals obtained by Method 1 initially contain crystals of either Form II, Form III or Form IV, and Form V. The crystals of either Form II, Form III or Form IV were completely transformed into Form I. Form I crystals may also initially present. It is worth to note again that the method presented here used *n*-propanol as the solvent; whereas the method presented in Chapter 3 used *sec*-butanol.

Figure 4.5 HSM light intensity profiles of sulfathiazole crystals obtained by Method 1 at three different ROIs; all crystals on the frame (ROI 1); a crystal that melts at 197.9°C (ROI 2) and a crystal that melts at 203.2°C (ROI 3).

4.3.2 Crystals obtained by Method 2

Figure 4.6 shows the profiles of the DSC curve and the HSM light intensity of the crystals produced by Method 2. Figure 4.7 shows snapshots of the crystals during HSM analysis. Based on Figure 4.6, the DSC curve indicates the presence of three major endothermic peaks. The first peak at a maximum of 168.5°C was not a melting peak as verified by the HSM analysis. The peak resulted from a change in the optical properties of the crystals, as shown by the difference in the appearance of the highlighted crystals between (a) and (b) in Figure 4.7. The phenomenon was indicated by fluctuations in the HSM light intensity profile between 159.3°C to a temperature slightly above 168.5°C and it was probably due to a transformation of either Form II, Form III or Form IV into Form I, as previously suggested. The second peak at a maximum of 197.2°C on the DSC curve corresponds to a melting peak of Form V, whilst the third peak at a maximum of 202.5°C corresponds to a melting peak of Form I. The melting of Form I and Form V were verified by HSM analysis as shown in Figure 4.7(d) and (e), respectively, and the subsequent increase in the HSM light intensity value at the corresponding melting temperatures in Figure 4.6. The HSM analysis was able to detect the melting of a crystal at 174.5°C, as shown in Figure 4.7(c) and as indicated in Figure 4.6 by a small increase in the HSM light intensity value at the same temperature. This melting event was barely detected by the DSC. This indicates that the crystals obtained by Method 2 are also a mixture of either Form II, Form III or Form IV, Form V and probably Form I.

Figure 4.6 DSC curve and HSM light intensity of sulfathiazole crystals obtained by Method 2.

Figure 4.7 Images of sulfathiazole crystals obtained by Method 2 during HSM analysis taken at (a) 120.1°C; (b) 169.1°C; (c) 176.1°C; (d) 198.8°C; (e) 202.6°C and (f) 204.0°C.

The HSM light intensity profiles for various ROI were presented in Figure 4.8. ROI 2 was selected to represent a crystal that melts at 174.5°C as highlighted in Figure 4.7(c), ROI 3 represents crystals that melt at 197.2°C as shown in Figure 4.7(d) and ROI 4 represents a crystal that melts at 202.5°C as shown in Figure 4.7(e). All profiles

show a sharp increase in the light intensity at the corresponding melting temperatures of their represented crystals. Although there are some discrepancies between the temperature values representing melting at inflection points shown by the HSM light intensity and the DSC heat flow peak maximum, the relative errors are very small, i.e., between 0.1% and 0.7%. The fluctuation of the HSM light intensity profile between 159.3 and 169.4°C that corresponds to the change in the optical properties of the crystals was shown by ROI 3 and ROI 4, but it was not shown by ROI 2. This result confirms that the phenomenon shown by the crystal in ROI 4 between 159.3 and 169.4°C was due to a transformation of either Form II, Form III or Form IV into Form I. A similar phenomenon displayed by a crystal in ROI 2, on the other hand, was probably just due to a surface property change, since the crystal should not undergo a polymorphic transformation as it melted at its melting temperature of 197.2°C (corresponding to melting temperature of Form V crystals). Nevertheless, the HSM light intensity profiles of individual crystals in this case have been demonstrated to help in confirming the potential presence of either Form II, Form III or Form IV, as well as Form I and Form V.

Figure 4.8 HSM light intensity profiles of sulfathiazole crystals obtained by Method 2 at three different ROIs; a crystal that melts at 174.5°C (ROI 2); crystals that melt at 197.2°C (ROI 3) and a crystal that melts at 202.5°C (ROI 4).

4.3.3 Crystals obtained by Method 3

The obtained DSC curve and the HSM light intensity for the sulfathiazole crystals from Method 3 are presented in Figure 4.9. Three endothermic peaks were shown by the DSC curve. The first peak had a maximum of 121°C, the second at 162°C and the third at 203.5°C. The third peak corresponds to the melting peak of Form I. The formation of the second peak may be the result of a polymorphic transformation, as it

lies in the reported range of temperatures for the event, presented in Chapter 3. This polymorphic transformation event implied by the results of the DSC analysis was confirmed by the HSM analysis. No melting, but a change in optical property of the crystals, was observed as shown by the difference between the highlighted crystals in Figure 4.10(a) and (b). The formation of the first peak lies within a range of temperatures that were recently reported to correspond to the dehydration of a hydrate (Howard et al., 2009). The HSM analysis confirmed this by showing no thermal event in the vicinity of 121°C. This can be explained by the fact that the liberation of water vapour during vaporization process could not be visually detected unless the sample was heated whilst immersed in silicone oil. The HSM light intensity profile of all crystals in the frame (ROI 1) presented in Figure 4.9 shows that the responses to the thermal events that occurred below 170°C were slightly disturbed by noise caused by the slight movement of some of the crystals, which has been observed to occur during heating. It is reported that besides an optical property change, a polymorphic transformation may also result in a movement of crystals since the transformation events may be accompanied by a change in volume of the crystals (Warrington, 2002). This observation demonstrates a limitation of the HSM light intensity profile in that it can be very sensitive to noise due to crystal movements.
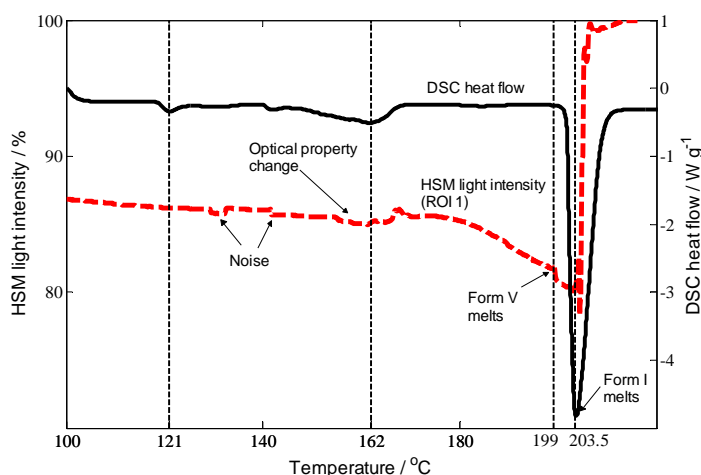
Figure 4.9 DSC curve and HSM light intensity of sulfathiazole crystals obtained by Method 3.

Figure 4.11 compares the HSM light intensity profiles computed from three different ROIs: all crystals on the frame (ROI 1), a crystal that melts at 199°C (ROI 2) and a crystal that melts at 203.5°C (ROI 3). As was expected, ROI 2 does not show any

light intensity change at 121°C as detected by the DSC since the crystal should not undergo polymorphic transformation. Besides showing a sharp increase in the light
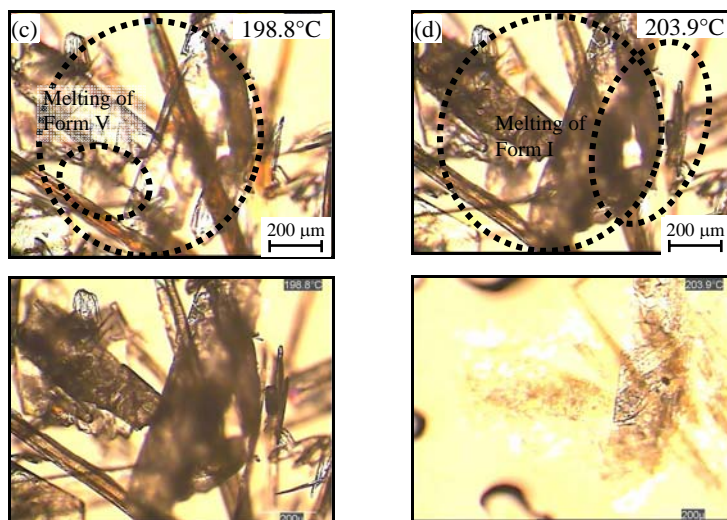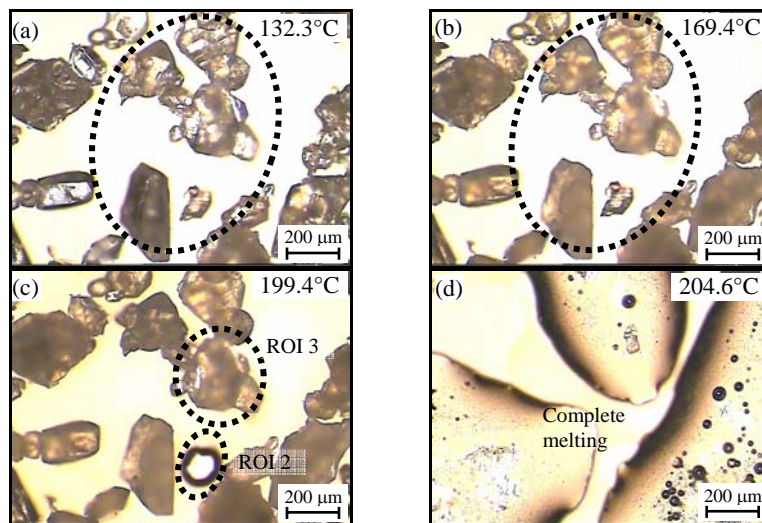

Figure 4.10 Images of sulfathiazole crystals obtained by Method 3 during HSM analysis taken at (a) 132.3°C; (b) 169.4°C; (c) 199.4°C; and (d) 204.6°C.

intensity due to melting at 197.5°C, ROI 2 also shows a sharp increase in the light intensity at 170.8°C, which corresponds to a change in the crystal's optical property. This result implies that the change in optical property may not necessarily be due to the polymorphic transformation, but could also be due to a change in the surface property of the crystals due to the effect of increasing temperature. ROI 3, on the other hand, shows an increase in the light intensity profile at 165°C, which is 5.8°C lower than in ROI 2, but within the temperature range for transformation of either Form II, Form III or Form IV into Form I crystals, as reported in Chapter 3. It is therefore possible that the sharp increase in the HSM light intensity for ROI 2 and ROI 3 at 170.8°C and 165°C, respectively, was caused by two different events. ROI 3 also shows a change in the HSM light intensity due to melting at 203.5°C, but the change shows a sharp decrease instead of a sharp increase. This peculiarity may be due to the presence of shadow, which darkens the selected region. However, in this case, only the change of the profile is of interest; the direction of the change is not important. The profiles of ROI 2 and ROI 3 seemed to be smoother compared to the profile of ROI 1. These results demonstrate that the HSM light intensity profile is strongly affected by the ROI sample location; the effect of noise and disturbances to the profile could be minimised through a proper selection of the ROI. The results of DSC and HSM with image analysis indicate that the sulfathiazole crystals obtained by Method 3

may initially comprise a hydrate, either Form II, Form III or Form IV, Form V and Form I crystals.
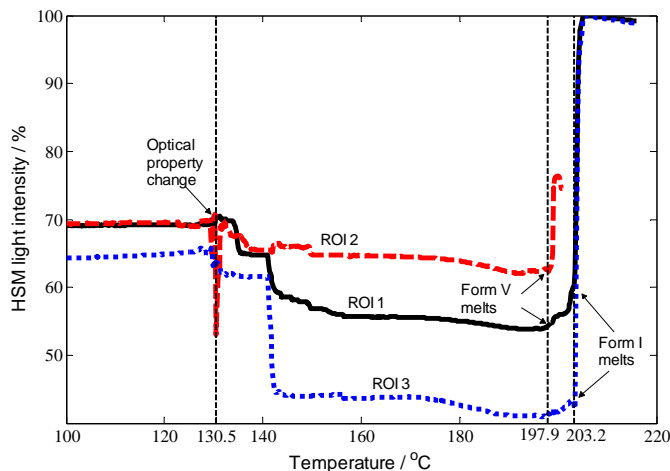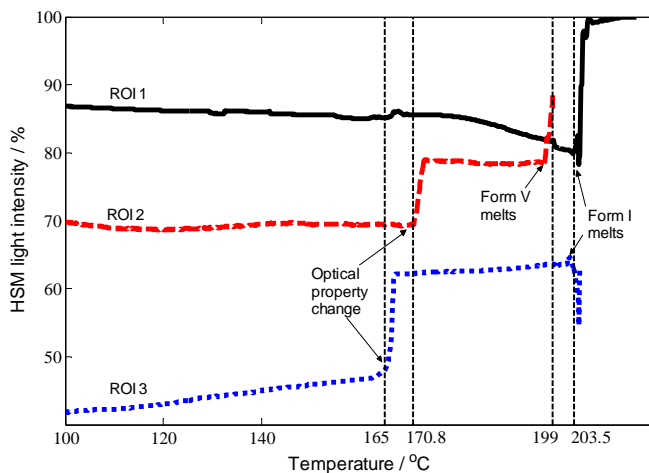

Figure 4.11 HSM light intensity profiles of sulfathiazole crystals obtained from Method 3 at three different ROIs; all crystals on the frame (ROI 1); a crystal that melts at 199°C (ROI 2) and a crystal that melts at 203.5°C (ROI 3).

4.3.4 Crystals obtained by Method 4

The results of the DSC and HSM analyses of the sulfathiazole crystals obtained using Method 4 are presented in Figure 4.12. Some images of the crystals during HSM analysis are shown in Figure 4.13. The DSC curve indicates the presence of two endothermic peaks. The first peak maximum occurs at 142.5°C, whereas the second peak maximum occurs at 203°C. As previously suggested, the first peak may be due to the transformation of either Form II, Form III or Form IV into Form I, whereas the second peak indicated the melting of Form I. The HSM analysis confirmed that the first peak was not a melting peak since no melting was observed between 100 and 149°C, as indicated by the images of the crystals in Figure 4.13(a) and (b). There was, however, a change in the crystals' optical property as clearly shown by the difference in brightness of the highlighted crystals between (a) and (b) in Figure 4.13. The HSM light intensity profile presented in Figure 4.12 shows a decrease from 140°C upwards, until it stabilised above 150°C. A slow decrease of light intensity value is shown from 180°C until suddenly the value increased very fast starting from a temperature that corresponds to the melting of Form I. The result signifies the capability of the light intensity profile to identify the beginning of the melting event earlier, since it is very sensitive to the changes happening on the surface of the crystals. The HSM analysis was able to detect a crystal that melts at 175.1°C, as shown by the highlighted crystal in Figure 4.13(c). It was not detected by either the

DSC analysis or the HSM light intensity profile computed from all crystals in the frame (ROI 1) presented in Figure 4.12.
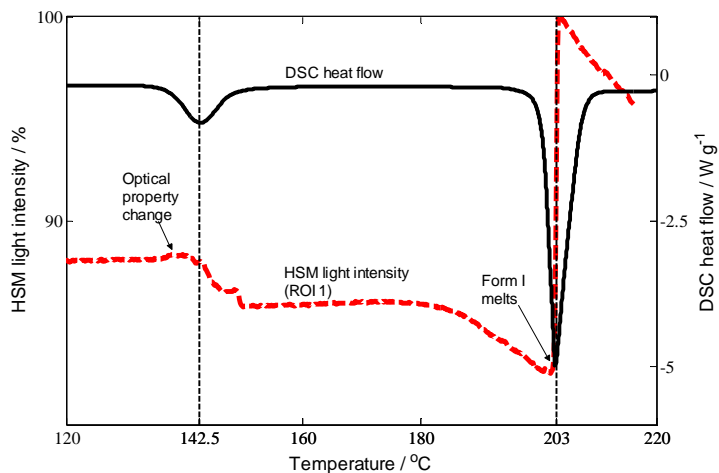
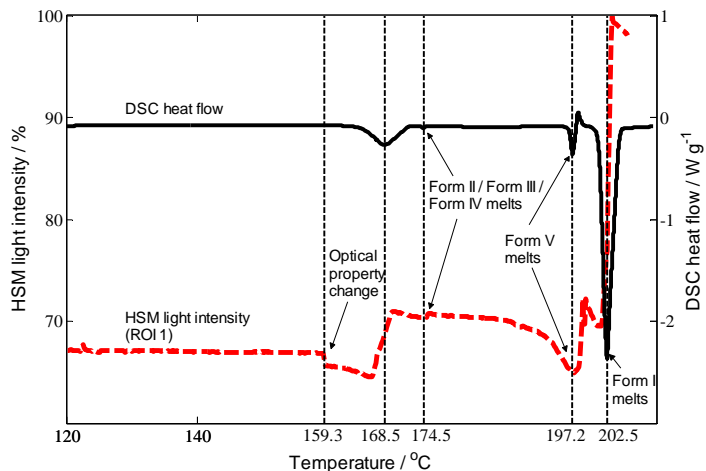**Figure 4.12** DSC curve and HSM light intensity of sulfathiazole crystals obtained by Method 4.
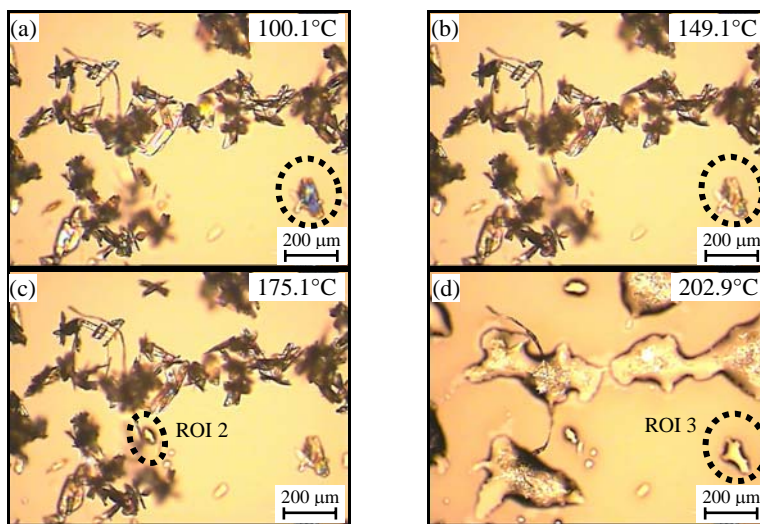
Figure 4.13 Images of sulfathiazole crystals obtained by Method 4 during HSM analysis taken at (a) 100.1°C; (b) 149.1°C; (c) 175.1°C; and (d) 202.9°C.

Figure 4.14 shows the HSM light intensity profiles computed from three different ROIs: all crystals on the frame (ROI 1); a crystal that melts at 175.1°C (ROI 2), which is highlighted in Figure 4.13(c) and a crystal that melts at 203°C (ROI 3), which is highlighted in Figure 4.13(d). Generally, ROI 3 and ROI 1 are similar in the pattern of their profiles. This implies that most of the crystals in the sample had similar properties to the selected crystal in ROI 3. The profile of ROI 2 displays a sharp increase from 175.1°C that corresponds to the melting of the crystal of either Form II, Form III or Form IV. It also displays a slight fluctuation between 140 and 145°C, but

no significant decrease in light intensity was observed, which indicates the crystal did not undergo a polymorphic transformation. Despite its sensitivity to noise, the results illustrate the capability of the HSM light intensity to describe the thermal events of an individual crystal. The results of DSC and HSM with image analysis show that the sulfathiazole crystals obtained by Method 4 initially contain crystals of either Form II, Form III or Form IV. Some of the crystals transform into Form I, but few of them were unchanged until they melted at 175.1°C as observed through the HSM. There is also a possibility that Form I crystals were also present initially.
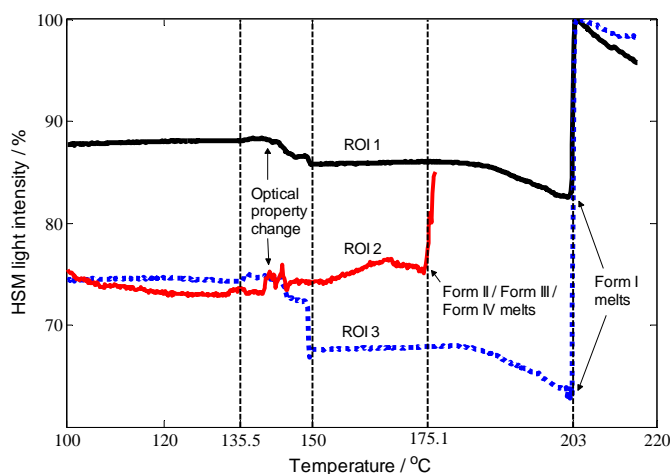
Figure 4.14 HSM light intensity profiles of sulfathiazole crystals obtained by Method 4 at three different ROIs; all crystals on the frame (ROI 1); a crystal that melts at 175.1°C (ROI 2) and a crystal that melts at 203°C (ROI 3).

4.3.5 Crystals obtained by Method 5

Figure 4.15 shows the profiles of the DSC curve and the HSM light intensity of the crystals from Method 5, while Figure 4.16 shows snapshots of the crystals during HSM analysis. The DSC curve indicates the presence of three major endothermic peaks. The first peak at a maximum of 161°C corresponds to a change in the optical properties of the crystals. This is verified by the HSM analysis as shown by the difference in the brightness of the highlighted crystals between Figure 4.16(a) and (b). As mentioned previously, a peak formation in a temperature range of 130–168°C may be due to a transformation of either Form II, Form III or Form IV into Form I. However, the HSM light intensity profile computed from all the crystals on the frame (ROI 1) presented in Figure 4.15 does not show any change in the optical property of the crystals. This may be due to the averaging-out effect that makes the event undetectable in the HSM light intensity profile. The melting of the crystals at 197°C

and 203°C are illustrated by the HSM light intensity profile in Figure 4.15 as two consecutive sharp increases.

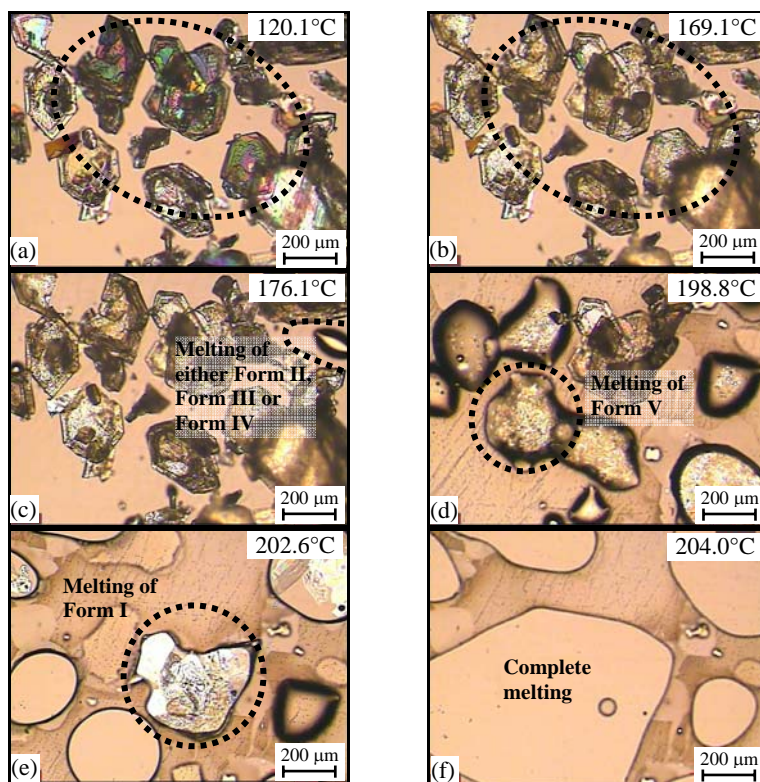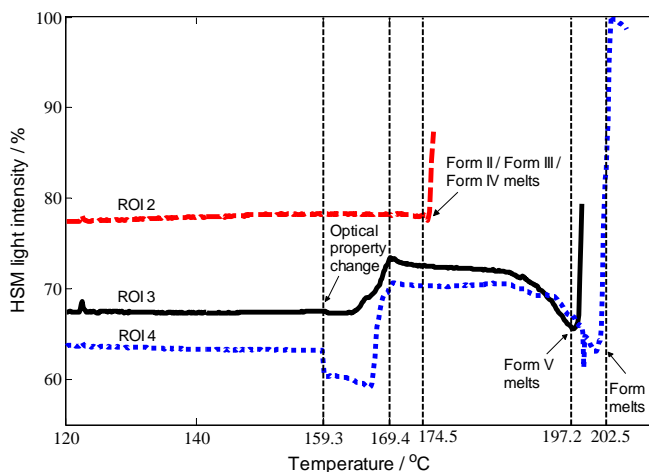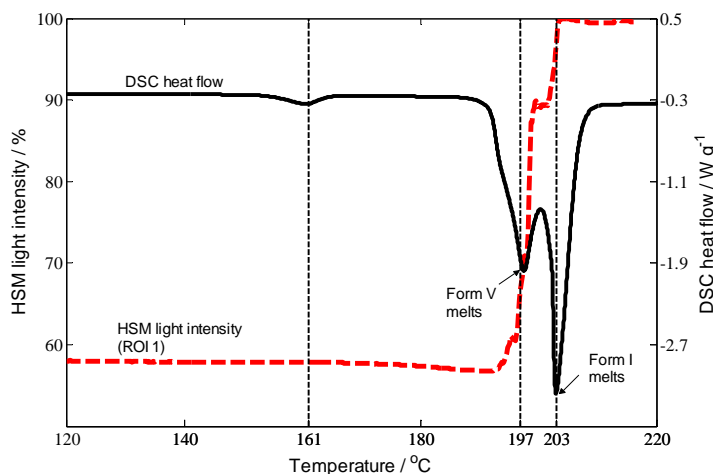**Figure 4.15** DSC curve and HSM light intensity of sulfathiazole crystals obtained by Method 5.
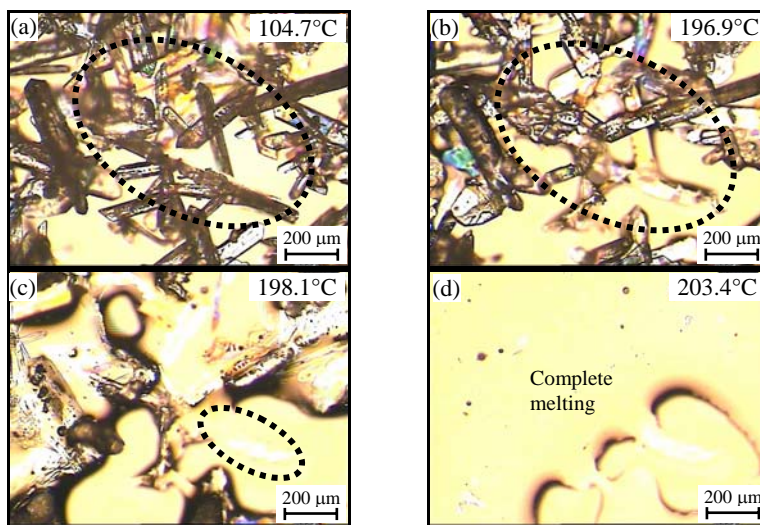
Figure 4.16 Images of sulfathiazole crystals obtained by Method 5 during HSM analysis taken at (a) 104.7°C; (b) 196.9°C; (c) 198.1°C; and (d) 203.4°C.

Figure 4.17 compares the HSM light intensity profiles between the one computed from all crystals in the frame (ROI 1) with another from a crystal that melts at 197°C (ROI 2), as highlighted in Figure 4.16(c). The HSM light intensity profile of ROI 2 differentiates itself from the profile of ROI 1 by not indicating melting at 203°C. The results signify the potential of the HSM light intensity profile to provide a unique description of the changes happening to individual crystals. The results of a combined approach of DSC and HSM with image analysis imply that the sulfathiazole crystals obtained by Method

5 initially contain crystals of either Form II, Form III or Form IV, Form V and probably Form I.
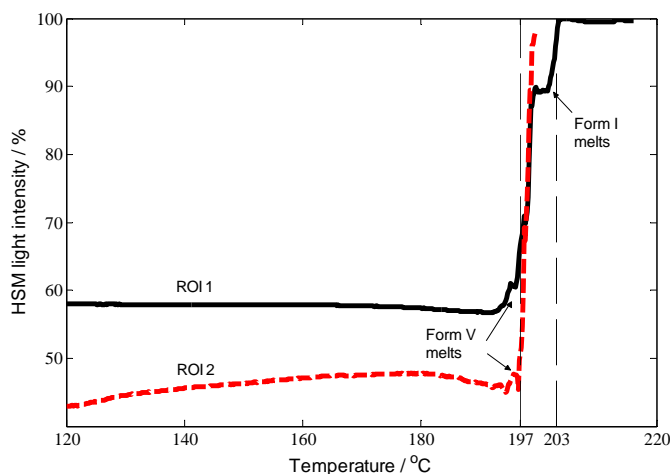
Figure 4.17 HSM light intensity profiles of sulfathiazole crystals obtained by Method 5 at three different ROIs; all crystals on the frame (ROI 1); a crystal that melts at 197°C (ROI 2) and a crystal that melts at 203°C (ROI 3).

4.4 CONCLUSIONS

The crystallisation of sulfathiazole polymorphs was investigated by a combined DSC-HSM with image analysis approach. The approach provides synergistic benefits of two characterisation techniques and the use of image analysis gives a unique insight into the thermal behaviour of the polymorphic system. The capability of the HSM image analysis to provide alternative and quantitative ways of presenting the HSM results has been demonstrated. It translates visual effects, which other characterisation techniques may not be able to provide, into quantitative information. Despite its sensitivity to noise, the light intensity profile obtained from HSM image analysis was found to be capable of describing thermal behaviour of individual crystals and very sensitive to the changes happening on the surface of these crystals. With these unique capabilities, the HSM image analysis allows verification of thermal events, particularly in confirming the formation of mixtures of polymorphs. Although Method 2 and Method 5 presented in this chapter are in general similar to Method 4 and Method 5 in Chapter 3, respectively; however, their initial concentrations are slightly different. The results of the experiments show that this variation affects the polymorphic purity of the produced crystals. The results of the experiments also show the tendency of sulfathiazole to crystallise as mixtures of polymorphs.

CHAPTER 5:
DIRECT NUCLEATION CONTROL APPROACH

In this chapter, a novel direct nucleation control approach is introduced that directly controls the onset of nucleation in the case of (i) anti-solvent and (ii) combined cooling and anti-solvent crystallisation processes. A desired number of FBRM counts, which indicates the number density of crystals, is maintained during the entire duration of crystallisation using a feedback control strategy that adapts the anti-solvent/solvent addition, and/or cooling/heating rate, to directly control the nucleation or dissolution rates. Experimental results from the implementation of the approach for the crystallisation of glycine are reported.

5.1 INTRODUCTION

The direct nucleation control (DNC) approach, as the name implies, directly controls the onset of nucleation based on the number of counts measured by an FBRM using a feedback control strategy. By definition, the total number of counts/s (#/s) measured by an FBRM is the sum of the number of chord length measurements detected in all the channels (1 through 38 in the FBRM model used) that represents a chord length range from 0.8 to 1000 μm, and is approximately proportional to the nucleation rate, which is the predominant mechanism in changing the number of particles. Figure 5.1 shows the schematic block diagram of the DNC approach for an anti-solvent crystallisation system. A similar structure can be used for cooling crystallisation.
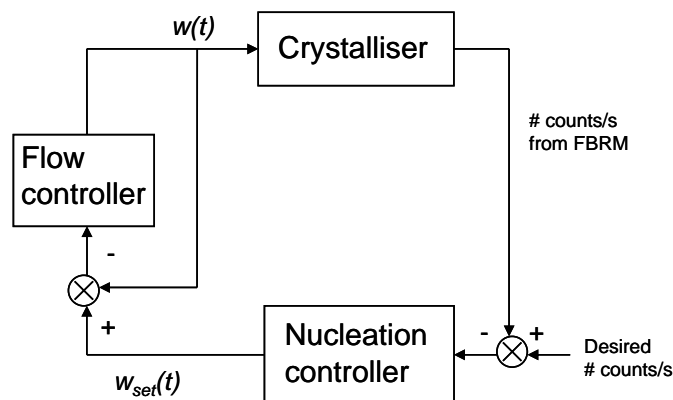
Figure 5.1 A block diagram of the DNC approach. $w(t)$ is the actual anti-solvent/solvent flowrate into the crystalliser; $w_{set}(t)$ is the anti-solvent/solvent flowrate set-point given by the DNC to the pump.

A typical operating profile during DNC, represented in the phase diagram, is illustrated in Figure 5.2. The DNC approach automatically switches between heating and cooling, solvent and anti-solvent addition, or a combination of the two, to generate nucleation, or fines dissolution, to maintain the desired number of counts/s. If the number of counts/s exceeds the desired value, the excess particles are dissolved by solvent addition, or an increase in temperature, which drives the process into the undersaturated zone until the number of counts/s decreases. The proposed DNC approach provides *in situ* fines removal through the operating protocol, rather than having additional equipment and external recycle loops. The method extends the fines removal strategy proposed by previous workers (Lewiner et al., 2002) in which the on-line measurement signal is not only used for the monitoring purposes, but also as an input for a continuous feedback control methodology.
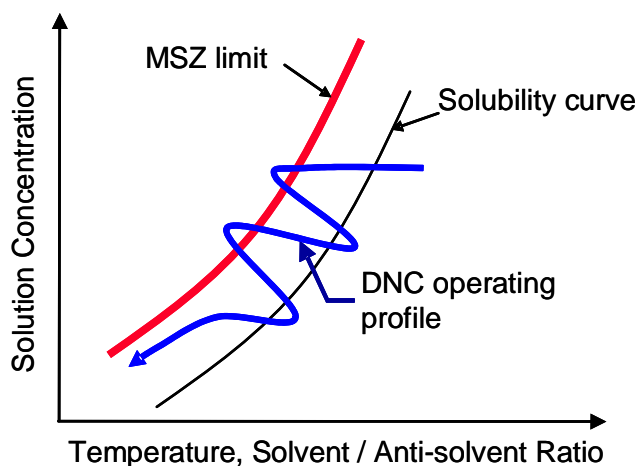
Figure 5.2 Typical DNC operating profile.

An additional novel characteristic of the DNC is that it does not use predetermined heating or cooling polices. The heating/cooling rates (or solvent/anti-solvent addition rates) are automatically determined during the entire duration of the crystallisation in correlation with the extent of nucleation detected. The DNC approach has the benefit of automatically driving the crystallisation process toward the optimal operating curve by automatically and adaptively detecting the metastable zone limits. It provides a very robust methodology for crystallisation scale-up, through FBRM feedback control, which requires virtually no *a priori* information about the model, kinetics or metastable zone width of the process. For an unseeded system, the approach however requires at least one uncontrolled experiment to establish a suitable desired number of counts/s; whilst for a seeded system, the number of counts/s measured after seed

loading is maintained. Since the approach tends to operate at high supersaturation, the problems related to solvent-inclusion, impurities and agglomeration may be facilitated. Usually in these cases it is recommended to operate at lower supersaturation. However, the repeated and controlled dissolutions have a de-agglomeration effect on the system with the potential additional benefit of minimizing solvent or impurity inclusion due to agglomeration. The approach provides a simple and robust inferential control method of the size distribution by maintaining the number of counts per second constant, hence eliminating the difficulties related to the conversion of chord length distribution (CLD) to CSD, which would be required by more sophisticated algorithms, such as non-linear model predictive control (Nagy and Braatz, 2003).

5.2 EXPERIMENTAL METHODS

5.2.1 Material and experimental set-up

Materials

In all experiments, aqueous glycine (> 99.5% purity, Fisher BioReagents) solutions were prepared to be saturated, which based on the solubility curve provided in Appendix E, corresponds to a solubility of 22.5 g of glycine per 100 g of water at 20°C. Since the minimum starting volume of the crystallisation vessel is 300 mL (approximately 300 g), 67.5 g of glycine and 300 g of water were used. Glycine was dissolved into water in the crystallisation vessel by heating to 35°C at a rate of 5°C/min. After the solution equilibrated at 35°C for 10 minutes, the temperature of the solution was lowered to 30°C with a cooling rate of -1°C/min, after which the temperature was further reduced to 25°C at -0.3°C/min. The temperature of the solution was maintained at 25°C prior to the start of experiment. Ethanol (99.99% purity, analytical reagent grade, Fisher Scientific) was used as an anti-solvent, while acetone (general purpose grade, Fisher Scientific) was used in the cleaning of the apparatus that were in contact with the solution, before and after each experiment.

Experimental set-up

The crystallisation experiments were performed in a jacketed 1000 mL cylindrical-shaped vessel. The temperature in the vessel was controlled with a stainless steel Pt100 thermocouple connected to a thermofluid (Dow Corning® 200/20 cS) circulator bath (Huber Ministat 125). The temperature readings were recorded every 4 seconds

on a PC by a control interface written in LabVIEW (National Instruments). A snapshot of the control interface is shown in Appendix F.

An overhead stirrer with a stainless steel three-blade marine type impeller was used to agitate the system at 400 rpm. This agitation speed was chosen to be high enough to guarantee that particles are well suspended throughout the process, but low enough to avoid attrition or generation of bubbles due to vortex formation. A FBRM probe (model A100, Lasentec) was inserted into the solution to measure chord length distributions in the range 0.8 to 1000 μm (the lower limit therefore requires nucleation plus some growth to occur before detection occurs in the FBRM) using 38 bins. The position and orientation of the probe were chosen according the standard recommendations to avoid particles adhering to the probe and provide suitable sampling. The distributions were collected every 6 seconds and averaged during collection. They were monitored using the control interface software (version 5.3). The solvent and anti-solvent were pumped into the vessel by a MasterFlex console driver with EasyLoad II peristaltic pump, calibrated before the experiments. Two-way solenoid valves were used for the alternate addition of solvent/anti-solvent, which was controlled by the computer. A schematic representation of the experimental set-up is shown in Figure 5.3.
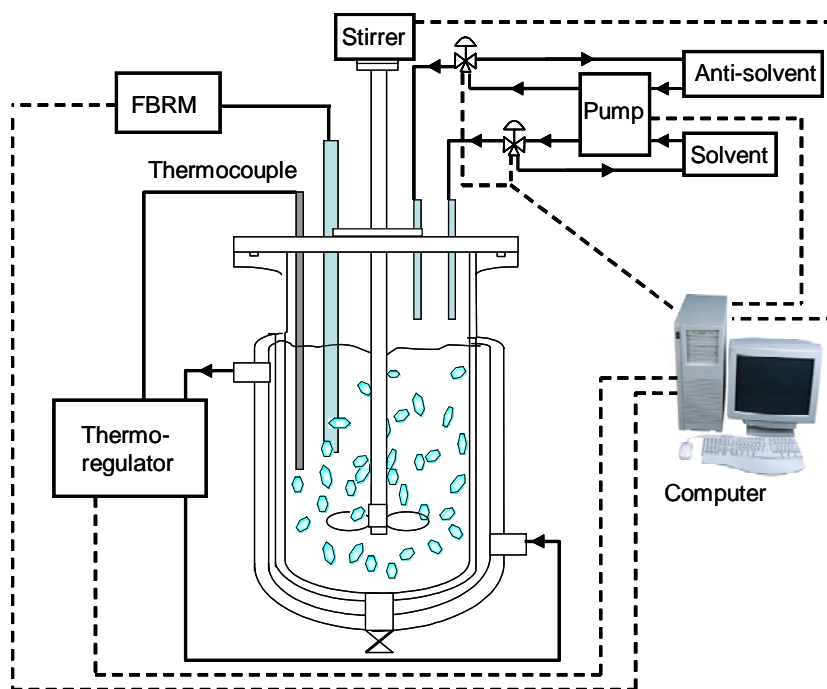
Figure 5.3 A schematic representation of the experimental set-up for DNC experiments.

5.2.2 Solubility of glycine in water-ethanol mixture

In some of the experiments, which examine the application of the DNC, anti-solvent (ethanol) additions were used to alter the supersaturation in the crystalliser, whilst maintaining constant temperature. To interpret these data, it was necessary to measure the solubility of glycine in water-ethanol mixtures.

Glycine was dissolved in excess into 10 g of deionised water in a glass tube with cap. Into another glass tube, 10 g of ethanol was weighted and the same as before, glycine was dissolved in excess into it. The procedure was repeated with a mixture of water-ethanol, instead of pure water or pure ethanol, at different weight compositions of water:ethanol: 10:90, 20:80, 30:70, 40:60, 50:50, 60:40, 70:30, 80:20, and 90:10. This method was based on the one described by Nozaki and Tanford (1971). The general solubility measurement procedure specified in Appendix D was followed.

5.2.3 Uncontrolled Anti-solvent Addition

This experiment was conducted to see the maximum total counts/s the system could achieve, so that the value could be used as an upper limit, below which a suitable desired values of counts/s could be selected for the subsequent controlled experiments. The procedure involved the continuous addition of anti-solvent to an aqueous glycine solution at two fixed rates of 8 g/min and 10 g/min until the number of counts/s stabilized.

5.2.4 DNC by Anti-solvent/Solvent Addition

In this experiment, the desired number of counts/s was selected based on the maximum counts/s achieved in the uncontrolled anti-solvent addition experiment described previously. Anti-solvent was added to the aqueous glycine solution until primary nucleation occurred and was detected by the FBRM, after which the addition rate was reduced or stopped to avoid an overshoot from the desired number of counts/s. Once the number of counts/s exceeded the desired value, the addition of anti-solvent was stopped and sequentially, solvent was added to dissolve the fine particles, thus correcting the number of counts/s. The anti-solvent was continuously added at a slow rate towards the end of the batch to ensure that the supersaturation in the system is maintained without triggering nucleation. The experiment was stopped once the suspension reached the 1000 mL mark on the vessel. The crystals produced were filtered and dried for subsequent analysis. This procedure was repeated with different desired number of counts/s. The solvent/anti-solvent addition rate was

determined according to a proportional control algorithm based on the error between the desired and measured number of counts/s. According to this approach, as the number of counts/s starts to increase, the anti-solvent addition rate is decreased and switched to solvent addition as soon as the number of counts/s exceeds the desired value. Similarly, during the solvent addition, the addition rate was also in correlation with the error between the desired and measured number of counts/s. The decrease in the number of counts/s due to the dilution effect during solvent/anti-solvent addition was also considered.

5.2.5 DNC by Combined Anti-solvent Addition and Heating-Cooling

This experiment follows the same procedure as described in 5.2.4 but instead of adding solvent, heating was used to correct the nuclei count, should the generation of nuclei exceed the desired number of counts/s. Once the desired number of counts/s was achieved, the supersaturation was continuously generated through either cooling or anti-solvent addition.

5.2.6 Characterisation of CSD

Verification of the validity of FBRM statistics was done by comparing them with the trend of the CSD observed under an optical microscope (Leica DMLM). The images were captured and processed using Leica QWin software (version 3.0, Leica Microsystems Digital Imaging). The CSD of the obtained crystals was also obtained using QICPIC particle size analyser (Sympatec GmbH). The size evaluation given by the analyser is based on an equivalent projected circle (EQPC).

5.3 RESULTS AND DISCUSSION

5.3.1 Solubility of glycine in water-ethanol mixture

As mentioned in Section 2.1, solubility characteristics are the first information that should be known about the crystallising system. Besides providing useful guidelines for the method of supersaturation generation, they also help to determine the maximum possible yield of crystals. In this work, the solubility values are required to indicate the lower limits for the crystallisation operating profiles where solvent addition or heating must be done slowly for controlled dissolution. The solubility values obtained in this experiment are compared with the literature values from the work of Dunn and Ross (1935), and Nozaki and Tanford (1971), as shown in Figure 5.5. Based on the figure, the experimental values appear to be in agreement with results

obtained by Dunn and Ross, but slightly below the results obtained by Nazaki and Tanford. However, since very high precision values of solubility are not demanded by the DNC approach, the experimental solubility values obtained are acceptable and will be used in this work. A trajectory of solution concentration due to dilution as a result of the anti-solvent addition, calculated based on mass balance, is also shown in the figure. A derivation of the trajectory calculation is given in Appendix G. The trajectory indicates the theoretical maximum supersaturation limit that would be achieved assuming no change in concentration due to nucleation or growth.
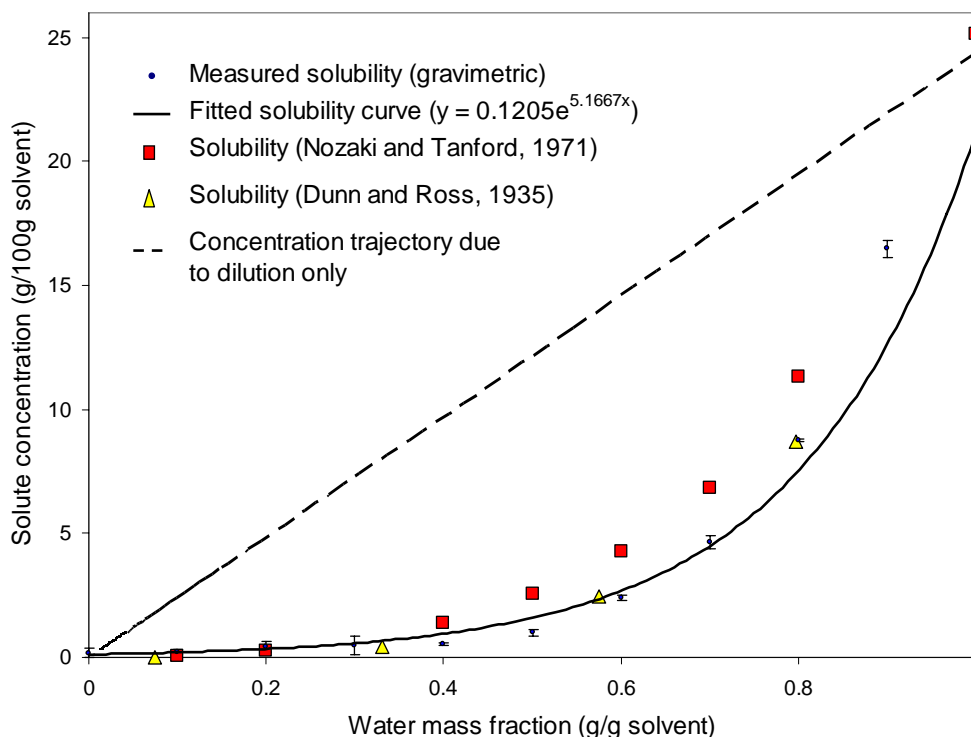
Figure 5.4 Solubility data and trajectory of the solute concentration due to the dilution as a result of the addition of anti-solvent.

5.3.2 Continuous anti-solvent addition

Continuous (uncontrolled) anti-solvent addition experiments were conducted to fulfil two objectives: (a) to see the maximum total counts the system could achieve, so that the value can be used as an upper limit, below which suitable desired values of counts could be selected; and (b) to investigate the behaviour of the system without control; in which case the data obtained could be used for comparison with the control approach.
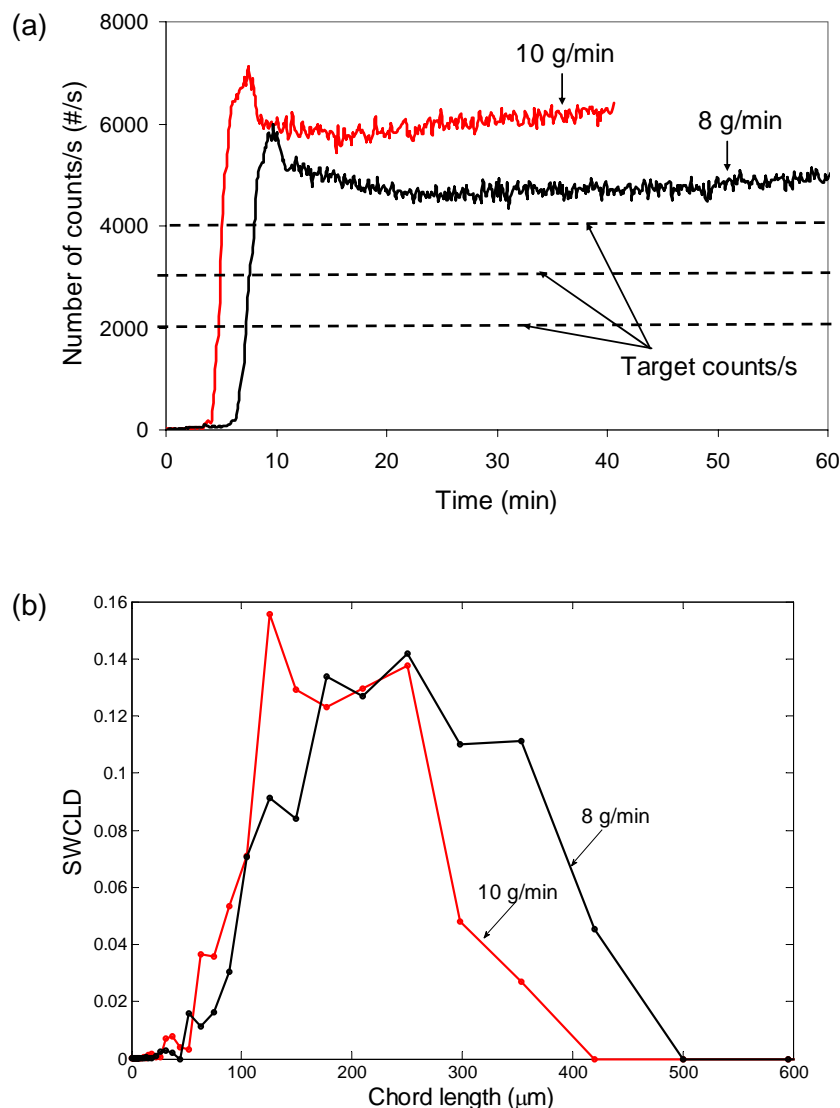
Figure 5.5 Profiles of (a) number of counts/s and (b) SWCLD for the uncontrolled experiments with anti-solvent addition rates of 8 g/min and 10 g/min.

Figure 5.5(a) shows the evolution of the number of counts/s measured by FBRM from the start of the anti-solvent addition (at t = 0). Once nucleated, the number of counts/s increased very rapidly to almost 7000 #/s for the higher addition rate of anti-solvent and 6000 #/s for the lower addition rate, after which they dropped slightly and eventually stabilized at 6000 #/s and 5000 #/s, respectively. This result is to be expected because the higher the supersaturation generation rate, the greater the number of nuclei that will form. The subsequent drop in counts/s may be due to a combined effect of Ostwald ripening and dilution. The drop may also be the result of the agglomeration since the collision between particles may result in permanent attachment if the particles are small enough for the van der Waals forces to exceed the

gravitational forces. Based on the result of this experiment, three target numbers of counts/s for the subsequent DNC experiments were selected i.e. 2000, 3000 and 4000 #/s, as shown in Figure 5.5(a).

In order to obtain information about the size of the crystals, the square-weighted mean chord length (SWMCL) statistic was used, defined as

$$SWMCL = \frac{\sum_{i=1}^{k} n_i M_i^3}{\sum_{i=1}^{k} n_i M_i^2} \qquad (5.1)$$

where M_i is the midpoint length of an individual channel i, k is the number of measurement channels (in this work k =38) and n_i is the number of counts/s in an individual measurement channel. The square-weighted chord distribution (SWCLD) is defined as

$$SWCLD = \frac{n_i M_i^2}{\sum_{i=1}^{k} n_i M_i^2} \qquad (5.2)$$

As indicated by the SWCLD in Figure 5.5(b), due to the more intense nucleation rate for the higher anti-solvent addition rate, the competition between growth and nucleation for the solute molecules increases and as a result, the size of the crystals produced is smaller.

5.3.3 DNC by Anti-solvent/Solvent Addition

At this conceptual stage, the controlled addition of anti-solvent/solvent was done manually to give an idea how the algorithm can be written for automation in the future. Many trials were required for this manual control, as it depends on the user's experience. Some problems were encountered during the first few trials of the experiment, including a high initial base-line, overshoot and undershoot from the desired counts and the presence of artefacts on the probe's window.

The problem with the high initial baseline was solved by performing manual cleaning of the probe using a lint-free tissue paper and acetone before the start of each experiment to give a total background count of less than 300 counts/s in air.

The elimination of the overshoot and undershoot are very difficult to achieve, but their presence, however, could be minimised by proper control. It may require the initial addition of anti-solvent to be stopped, and solvent addition to be started, sequentially, at certain value of counts/s below the desired value. Although undershoot can be corrected by adding anti-solvent, this will promote a secondary nucleation, which is undesirable as it may generate fines and consequently a product with a wide CSD is produced. This problem can also be minimised by the application of an automated feedback control strategy that would adapt the solvent/anti-solvent addition rate according to the errors between the measured counts/s and the target.

The presence of artefacts on the probe's window may create a critical problem as they give a false event that will trigger the controller to react wrongly. In a preliminary experiment controlled at 3000 #/s, after the system stabilised at the desired total count, a sudden increase in the number of counts was detected by FBRM as shown in Figure 5.6. With the assumption that the increase was due to nucleation, solvent was added to correct it. However, although the number of counts was corrected, due to the unnecessary addition of solvent, the solution became diluted and some crystals were dissolved.
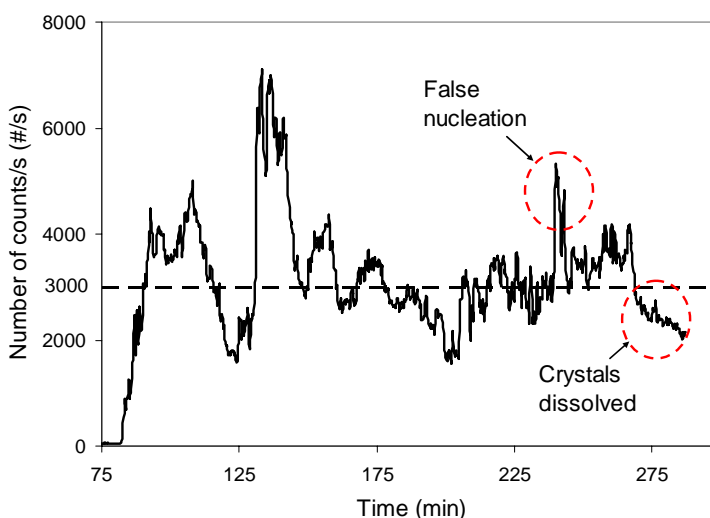
Figure 5.6 A false nucleation detected by FBRM.

Figure 5.7(a) shows the profiles of the number of counts/s and the anti-solvent/solvent addition rate for a DNC target of 2000 #/s. It can be seen from the profile that there were a couple of overshoots and undershoots before the system finally reached the desired number of counts/s. It was found that primary nucleation is always difficult to control as the increase in number of counts/s after the onset of nucleation is very fast.
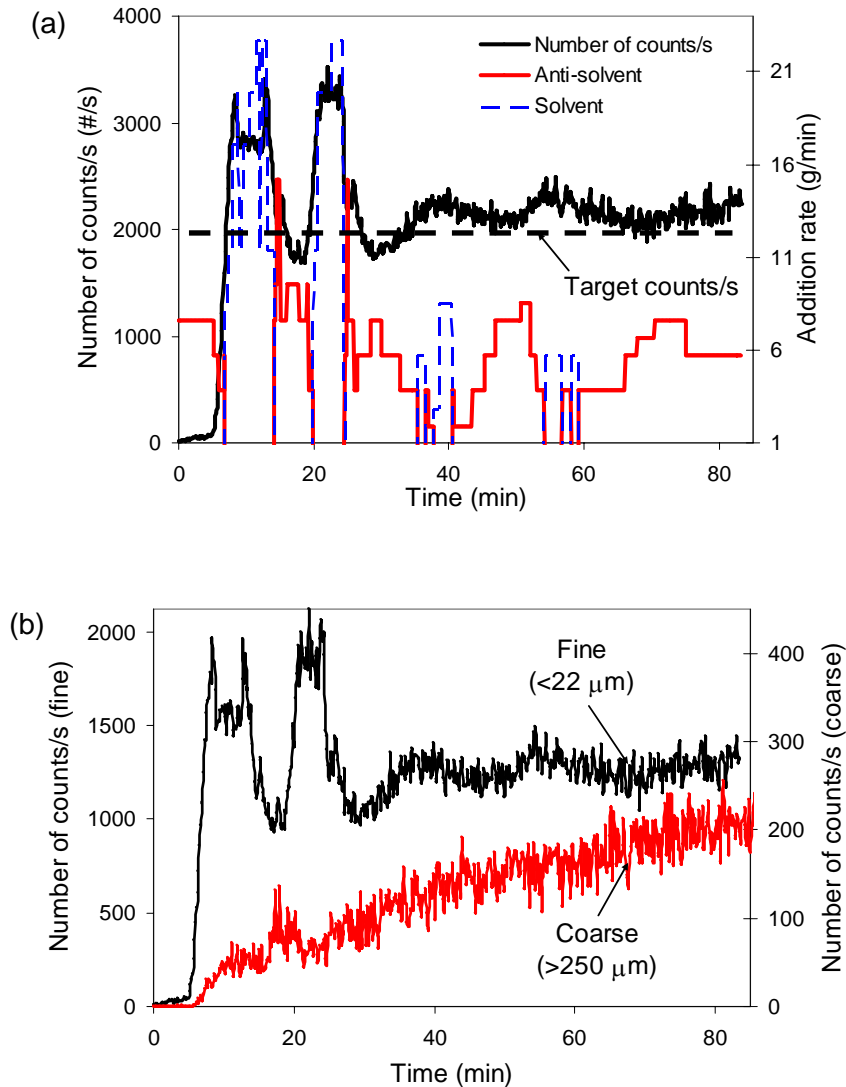
Figure 5.7 Profiles of (a) number of counts/s and anti-solvent/solvent addition rate, and (b) number of fines and coarse for DNC experiment at a desired number of counts/s of 2000 #/s.

Figure 5.7(b) shows the evolution of fine and coarse crystals during the DNC. The trend shows that solvent addition decreases the amount of fines, whilst having little effect on the number of coarse crystals. The continuous increase in the number of coarse crystals indicates growth of smaller crystals into the range > 250 µm, rather

than nucleation events. This result, which is in accordance to the mechanism of Ostwald ripening, shows that DNC is able to provide *in situ* automatic fine removal without the need for additional equipment or design.

The DNC experiments at 3000 and 4000 #/s also produced similar results and trends. Figures 5.8(a) and (b) show the profiles of number of counts/s with the addition of anti-solvent/solvent and the evolution of fine and coarse crystals, respectively, during the DNC experiment at 3000 #/s.   As before, after a couple of overshoots and undershoots, the system eventually reached the desired number of counts/s.
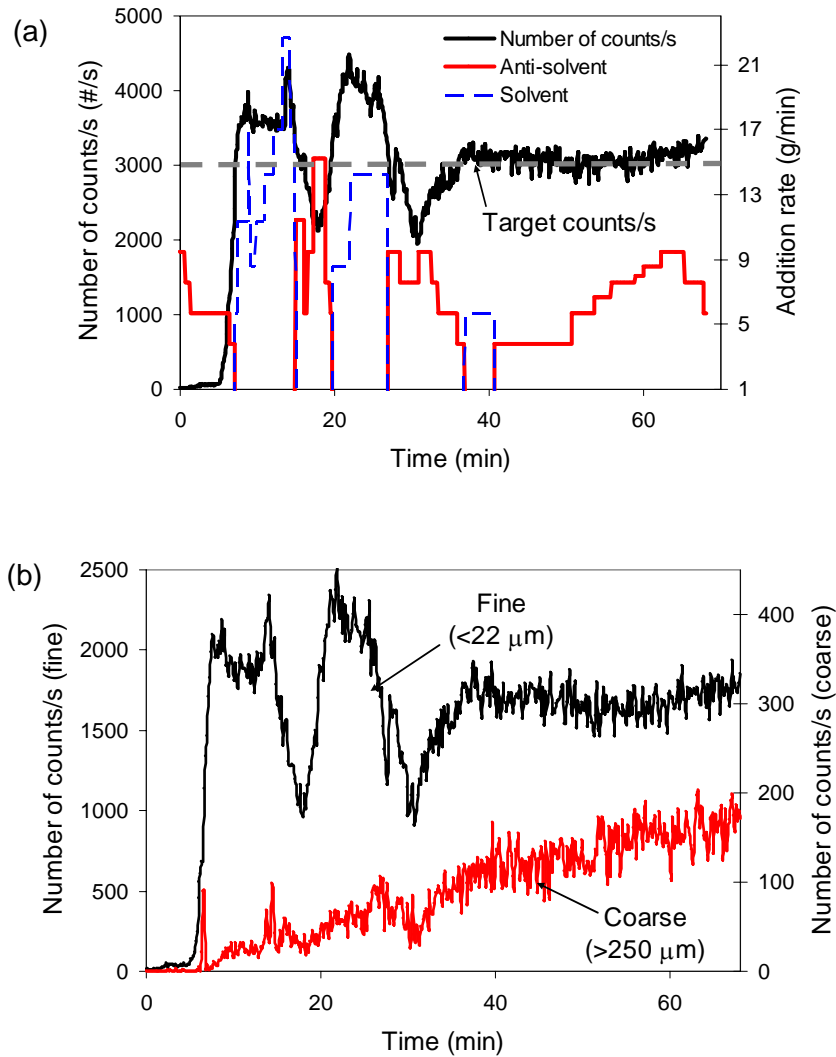
Figure 5.8 Profiles of (a) number of counts/s and anti-solvent/solvent addition rate, and (b) number of fines and coarse for DNC experiment at a desired number of counts/s of 3000 #/s.

Figure 5.9 shows the profile of number of counts/s for all the controlled experiments. It was found that the smallest desired number of counts/s was more difficult to control and it gave higher noise due to the smaller particle concentration. The results show that different set-points consistently produced similar solvent/anti-solvent addition output profiles. This suggests that an iterative learning control approach (Lee and Lee, 2003) could be used to eliminate the over- and undershoots during the first part of the batch and to enhance the overall control performance of the DNC. According to this approach, a feed-forward plus feedback controller could be implemented, in which the feed-forward law given by the solvent/anti-solvent addition profile would be iteratively improved in a batch-to-batch manner so that the overall control error would decrease throughout consecutive batches. The feed-forward component of the iterative learning control would provide batch-to-batch performance improvement, whereas the feedback control component would minimize the effects of within batch disturbances. The iterative learning control approach would improve performance and would provide increased robustness for industrial implementation. However, the benefits of DNC in producing higher quality crystals at the end of the batch are evident already from the implementation demonstrated here.
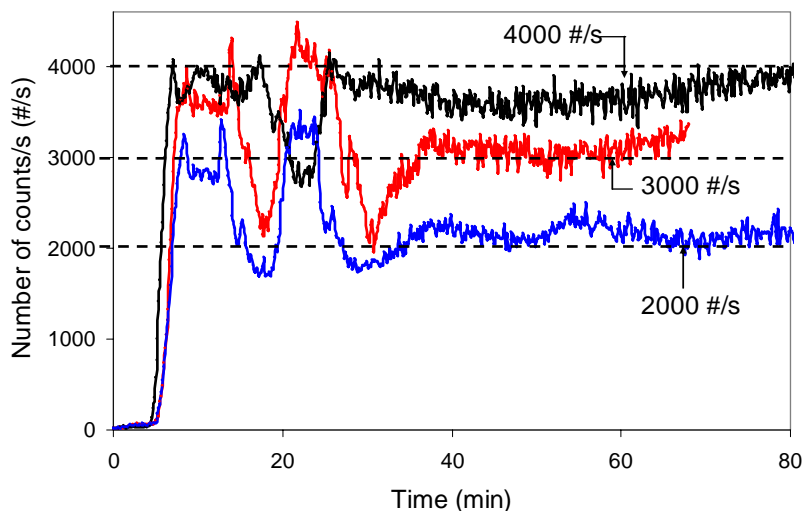
Figure 5.9 Profile of the number of counts/s for DNC experiments at 2000, 3000 and 4000 #/s.

Figure 5.10 compares the plots of SWMCLs for the uncontrolled and DNC experiments at 2000 and 4000 #/s. The plot of SWMCL for the DNC experiment at 3000 #/s is omitted to prevent overcrowding, but it was found to stabilize between those of 2000 and 4000 #/s. Based on Figure 5.10, the growth of the crystals was a maximum in the experiment with the lowest counts/s set-point, and a minimum in the uncontrolled

experiment. The averaged values of the SWMCL for the controlled number of counts/s at 2000 #/s, 3000 #/s, 4000 #/s and uncontrolled experiments are 281, 268, 263 and 232 µm respectively. The SWMCL values shown in Figure 5.10 are more scattered since the smaller the number of particles in the system, the higher the noise in the statistics of the CSD, leading to an increased difficulty in controlling the system at lower counts/s set-points. This is exemplified by the controlled experiment at 2000 #/s, which has the most scattered SWMCL values. The smaller the number of particles, the larger the crystals will grow, however the corresponding increased noise in the measurement requires a suitable compromise when selecting the set-point counts/s values for the DNC.
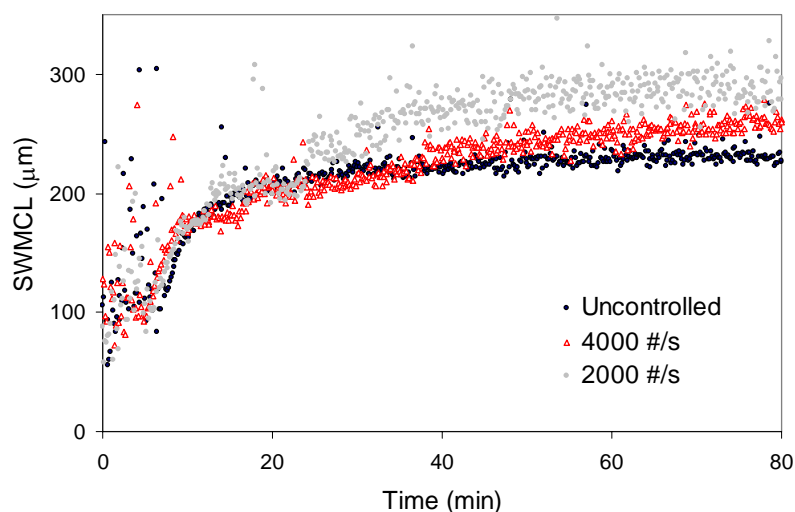
Figure 5.10 Profile of the SWMCLs for the uncontrolled and DNC experiments at 2000 and 4000 #/s.

Figure 5.11 shows the microscopic images of the crystals at the end of the experiments, which confirmed the results obtained from FBRM. Based on the images, the size of crystals obtained from the controlled experiment at the lower counts/s i.e. 2000 #/s was generally found to be the largest, whilst those obtained from the uncontrolled experiments was found to be the smallest. This was also confirmed by the plots of the differential mass fraction, dQ_3 of the EQPC diameter volume distribution of the crystals measured by the QICPIC particle size analyser. The plots for the two extreme cases (uncontrolled and controlled at the lowest counts/s) are presented in Figure 5.12.

The DNC by anti-solvent/solvent addition requires a large volume crystalliser since it involves addition of anti-solvent and solvent. This limitation of the approach may be

critical as it requires additional cost for a large volume vessel. Furthermore, the large volume of suspension which results from the addition of anti-solvent and solvent may lead to mixing problems. Another problem is the generation of large volumes of waste materials that are costly to separate and recycle.
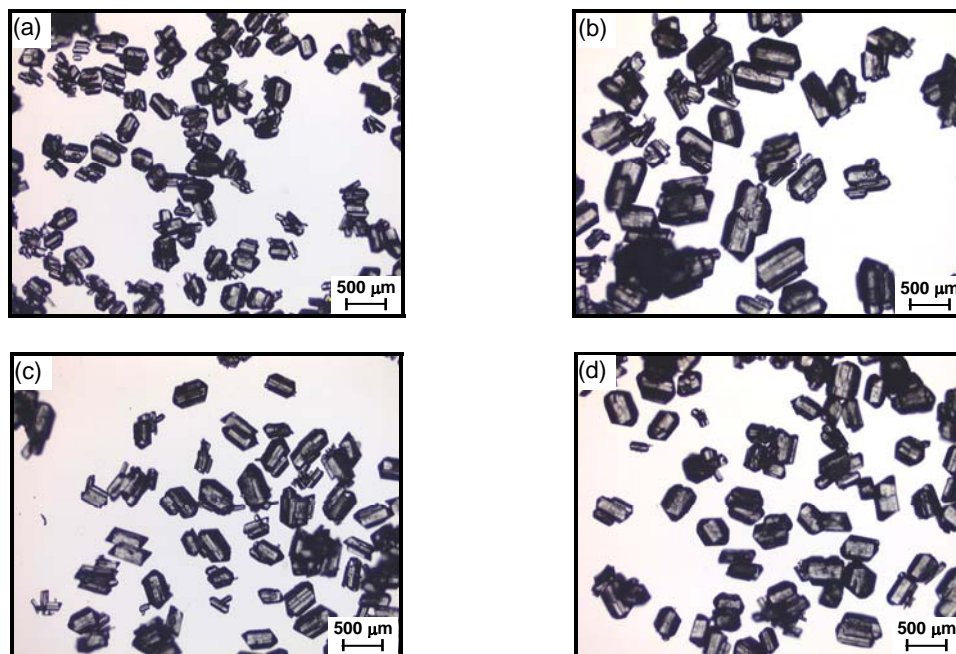
Figure 5.11 Microscopic images of crystals obtained from (a) uncontrolled, (b) DNC at 2000 #/s, (c) DNC at 3000 #/s and (d) DNC at 4000 #/s experiments.
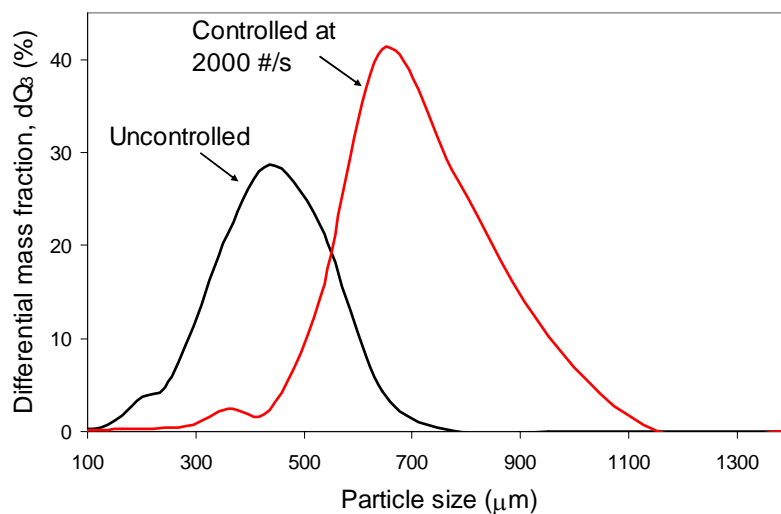
Figure 5.12 Plots of the differential mass fraction, dQ_3 of the EQPC diameter volume distribution of the crystals obtained from the uncontrolled and the DNC at 2000 #/s measured by the QICPIC particle size analyser.

5.3.4 DNC by Combined Anti-solvent Addition and Heating-Cooling

In these experiments the limitation due to vessel capacity was addressed by using heating/cooling to control the level of supersaturation instead of solvent/anti-solvent additions. In this approach, the vessel's volume requirement is only to accommodate the initial anti-solvent addition for generating the nuclei.

Figure 5.13(a) shows the profiles of number of counts/s, SWMCL, process temperature, and anti-solvent addition rate for the experiment using the combined approach of anti-solvent addition and heating–cooling, with a target number of counts/s of 3000 #/s. Initially, when the total counts/s went beyond the desired value upon nucleation as a result of the anti-solvent addition, the addition was stopped and subsequently, the temperature was increased gradually, depending on the error between the measured and desired number of counts/s, to dissolve the excessive nuclei. The total counts/s gradually decreased as the temperature was increased. As soon as the total counts/s went below 4000 #/s, cooling was initiated. The total counts/s eventually settled at 3000 #/s. They remained approximately at the same level throughout the process, even when the system was cooled down to 15°C at the maximum rate, set to 0.3°C/min. This continuous cooling was required to generate the supersaturation for crystal growth.

The profile of SWMCL of the system during the experiment shows that the mean size of the crystals was not affected very much by the heating, only reduced slightly at high temperature (approximately at 38°C). As confirmed by the trends of the evolution of fines and coarse crystals during DNC in Figure 5.13(b), the heating dissolves only fine crystals, which do not contribute significantly to the SWMCL. As the cooling continues, the mean size of the crystals increased significantly as shown by the steady increase of the SWMCL in Figure 5.13(a). It can also be seen that during cooling, there was a slight increase in the number of counts/s due to secondary nucleation. However, during the second part of the batch the process is dominated by growth and the amount of fines generated was not significant enough to trigger the dissolution mechanism of the DNC. In this experiment, the amount of ethanol consumed was very little (53 g), as it was only used to initiate the nucleation.
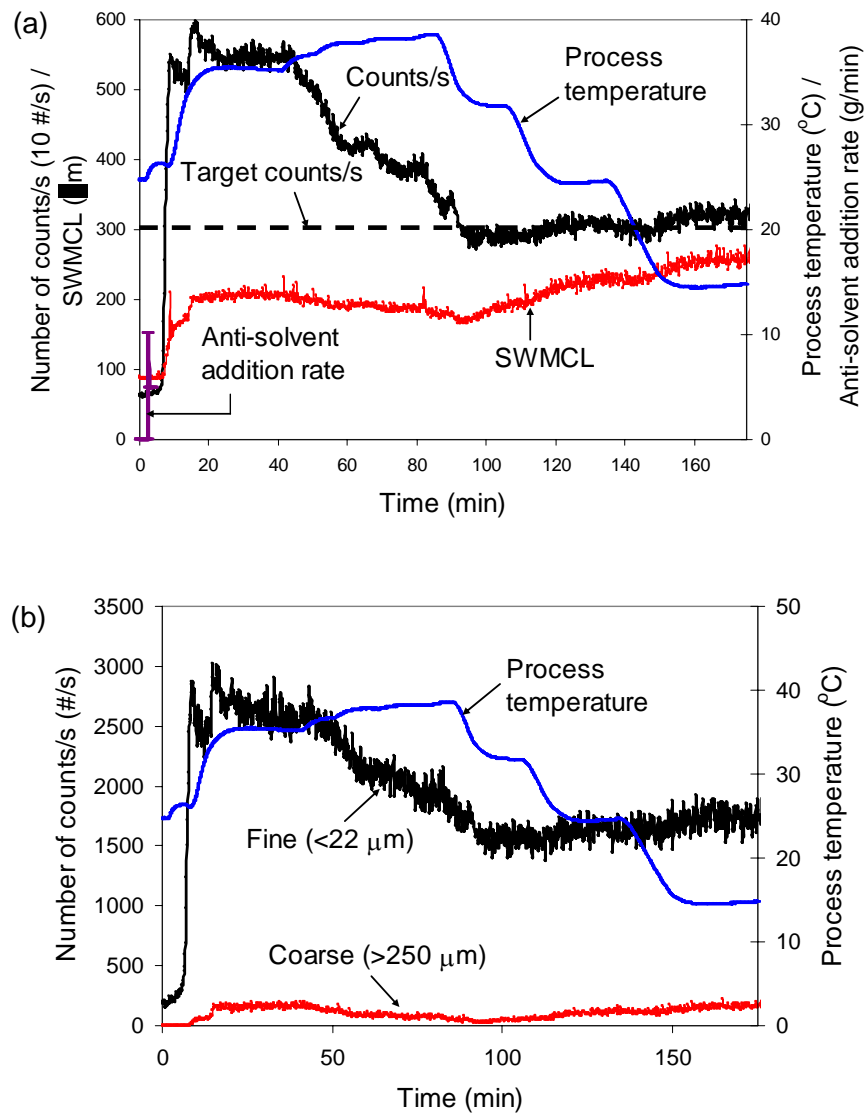
Figure 5.13 Profiles of (a) number of counts/s, SWMCL, process temperature, and anti-solvent addition rate, and (b) number of fine and coarse particles, and process temperature in the DNC experiment by a combined approach.

As an alternative to cooling towards the end of the batch for supersaturation generation, hence promoting growth, the application of anti-solvent addition was also tested. Figure 5.14 shows the profiles of the number of counts/s, SWMCL, process temperature and anti-solvent addition rate during the last 100 minutes of the experiment.
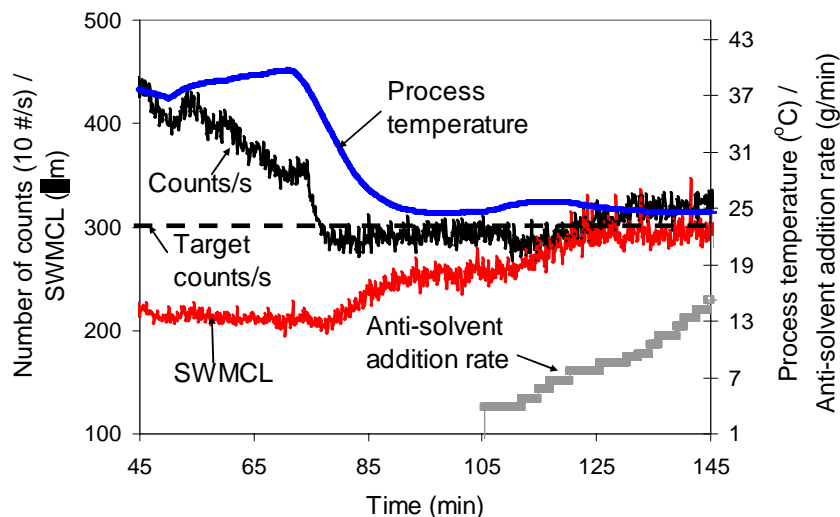
Figure 5.14 Profiles of number of counts/s, SWMCL, process temperature, and anti-solvent addition rate in the DNC by an alternative combined approach.

The figure shows that the crystals started to grow in size with cooling and then further growth was promoted with the addition of anti-solvent. Although anti-solvent was continuously added, the growth rate decreased significantly after about 125 minutes. The solubility of glycine has a lower sensitivity to the solvent/anti-solvent ratio as the amount of anti-solvent increases in the system, which can be inferred from the trend of the concentration trajectory due to dilution plotted in Figure 5.4. The decrease in the growth is probably due to the fact that as the sensitivity of the solubility decreases, the dilution effect becomes predominant in decreasing the supersaturation, thus depleting the driving force for growth (see Figure 5.4).

In comparison, the calculated SWMCL for the crystals obtained from anti-solvent addition towards the end is 297 μm, whereas that obtained from cooling alone towards the end is 258 μm. However, the former consumed a significantly larger amount of ethanol (730 g). The batch time of DNC by the combined approach was longer than that of DNC by anti-solvent/solvent addition because heating/cooling gave a slower response. Table 5.1 compares the outcomes of applying different DNC strategies to reach a stabilized desired counts/s of approximately 3000.

Table 5.1 Different DNC strategies to reach a stabilized desired counts/s of approximately 3000 and their resultant batch times, amount of anti-solvent used and SWMCL of the crystals obtained.

DNC Strategy	Batch time (min)	Amount of anti-solvent used (g)	*SWMCL* of crystals obtained (µm)
Addition of anti-solvent to nucleate; control of counts/s by additions of solvent and anti-solvent; anti-solvent addition towards the end to promote growth.	68	370	268
Addition of anti-solvent to nucleate; control of counts/s by heating and cooling; cooling towards the end to promote growth.	168	53	258
Addition of anti-solvent to nucleate; control of counts/s by heating and cooling; anti-solvent addition towards the end to promote growth.	145	730	297

Suitable automatic control of the solvent/anti-solvent addition or heating and cooling is difficult especially during the initial part of the batch when the first nucleation events are generated. The initial overshoot can be minimized by automatically stopping the anti-solvent addition when a continuous increase in the number of counts/s has been detected, but before the desired set-point is achieved. The overshoots can be minimized by using a control structure with anti-windup which allows an immediate switch from anti-solvent addition to solvent addition (or from cooling to heating), and vice-versa when the desired set-point is achieved. An iterative learning control approach could lead to batch-to-batch improvement in the performance of the DNC.

Although in the case of the model system used in this work (glycine in water) attrition or agglomeration were not observed, these are common phenomena in the case of industrial crystallisation systems, and are not accounted for neither by the supersaturation control nor by the classical open-loop control approaches. The DNC approach could have the additional benefits in the control of systems exhibiting these phenomena. The fines generated by attrition would be detected as an increase in the number of counts per second and hence would be eliminated by the DNC, by controlled dissolution. Additionally, the particular feature of the DNC approach of generating partial dissolution by repeatedly driving the process into the under-saturated regime has a beneficial de-agglomeration effect.

The DNC approach can also be extended to control polymorphic transformations. This however requires the polymorphic system to exhibit a distinguishable shape change upon transformation, or show a separate nucleation event, which can be correlated with the FBRM signal.

The approach is different from the recently published robust model based approaches (Hermanto et al., 2007) that it is model-free and does not require model development, parameter estimation and optimization. The DNC approach could be more favourable in an industrial environment as the iterative way of modelling and experiment may consume significantly more resources and time.

5.4 CONCLUSIONS

The DNC approach implemented in this work controls directly the amount of nuclei present using information provided by FBRM, in a feedback control strategy through (a) addition of anti-solvent or reduction of the suspension temperature, to generate nuclei up to a desired number of counts/s and (b) addition of solvent or increase of the suspension temperature to correct the nuclei count, should excess nucleation occur. It has been found that the DNC approach implemented in these experiments, using glycine in water-ethanol mixture as a model system, was able to produce crystals with a larger size than those obtained from uncontrolled experiments. Results also suggest that the lower the desired number of counts/s, the larger the size of the crystals produced. In the experiments which used the application of the combined approach, the results indicate that the crystals produced were even larger. In some cases better control of nuclei generation and correction are still needed, but nonetheless the approach has proved to provide a robust crystallisation control strategy.

CHAPTER 6:
SEEDED COOLING CRYSTALLISATION WITH TEMPERATURE CYCLING

In this chapter, experimental results from a seeded cooling crystallisation with temperature cycling approach, implemented using sulfathiazole in n-propanol and in water as model systems, are presented. The capability of the approach to produce uniform size crystals and to grow the desired polymorphic form is evaluated. FBRM was used for the in situ detection and monitoring of unwanted primary nucleation, dissolution of fine particles and growth evolution of the seed crystals, whilst ATR-UV spectroscopy was utilised for the in situ and in-process monitoring of the solute concentration in the system. The conditions under which various polymorphic forms of sulfathiazole can grow in the system are also corroborated in this chapter via a set of seeded temperature cycling experiments.

6.1 INTRODUCTION

Seeding crystallisation, as mentioned in 2.5.3, is widely used in the control of CSD and has been successfully applied in the control of polymorphism. The quality of the seed crystals are crucial, but it is often difficult to guarantee the quality of the CSD and the polymorphic purity of the seed. This is because the generation of seed crystals typically involves particle-size reduction processes that may produce seeds with a broad CSD and a significant amount of fines. The fines may also form due to attrition, which is often observed in the case of crystals with needle morphology commonly encountered for pharmaceutical compounds. The seed crystals can also be present as mixtures of polymorphs, since many polymorphic systems tend to crystallise in mixtures (Abu Bakar et al., 2010). In these cases, it is possible to correct the quality of the seed crystals in-situ and consequently improving the quality of the product by applying alternating cycles of heating and cooling phases. These temperature fluctuations increase the kinetics of Ostwald ripening since the dissolution of fine particles (and/or unwanted polymorphic forms) is accelerated during heating phases, whilst the growth of the larger crystals is accelerated during cooling phases. This is known as the temperature cycling method and was previously implemented by Carless and Foster (1966) to accelerate growth of sulfathiazole crystals. A similar method was also applied by Loi Mi Lung-Somarribaa et al. (2004) to control the CSD.

Figure 6.1 shows the hypothetical operating profile of the proposed approach on a phase diagram of a monotropic system with two polymorphs, Form I and Form II. In this case, Form II is the desired polymorph and the seed crystals are un-sieved and contain both polymorphs. Once the seeds are loaded, some of the seeds of Form I dissolve because the seed loading point lies in the undersaturated region of Form I. This results in a slight increase in the solute concentration during seed loading as depicted in the figure. In order to eliminate the presence of Form I as well as fine particles from the seed crystals, temperature cycling, which is a succession of heating and cooling phases, is applied after the seed loading. Ideally the operating profile should at all times lie below the solubility curve of Form I, but in the supersaturation region of Form II. However this is very difficult to achieve since most of the solubility curves of different polymorphs of a system are very close to each other. For this reason, the heating and cooling phases may cross the solubility curve of Form I, as shown in Figure 6.1. On cooling, the supersaturation is expected to be used for the growth of the seeds, and hence the profile of the cooling phases shows a decreasing trend in solute concentration. On heating, the fine particles and the unwanted polymorph are expected to dissolve, and hence the profile of the heating phases shows an increasing trend in solute concentration. The transition between heating and cooling phases creates loops, as shown in the figure. Figure 6.1 also shows that the temperature cycling is continued progressively stepping down towards a low temperature. This is to maintain the supersaturation in the system, so that the seed crystals can continuously grow. The crystallisation process should be stopped and the end product should be collected only when the profile lies in the undersaturated region of Form I but in the saturated region of Form II in order to ensure that no crystals of Form I are present in the product.

The temperature cycling method can provide a more practical approach with superior performance compared to supersaturation control based approaches. This is because for systems with very slow growth rates and when the desired form is the metastable polymorph, controlling the process at constant high supersaturation may induce secondary nucleation and hence generate unwanted fines and/or another polymorph. On the other hand, if the system is controlled at low supersaturation to avoid secondary nucleation, crystallisation times will be excessively long and may lead to the transformation of the metastable form into the thermodynamically more stable form. In addition, for most pharmaceutical systems, the solubility curves of the various

polymorphs are very close and operation within a narrow zone between the solubility curves using a supersaturation control approach may be impractical, due to the very low supersaturation, or due to errors in concentration measurement or limitations in the cooling system.
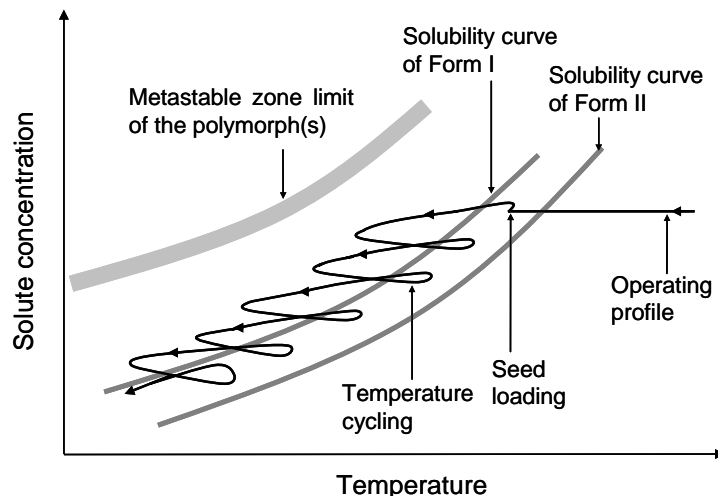
Figure 6.1 The hypothetical operating profile of the proposed seeded cooling crystallisation with temperature cycling.

In this chapter, the application of a seeded cooling crystallisation with temperature cycling approach using sulfathiazole in n-propanol and in water as model systems is presented.   Previous studies have found that the crystallisation of sulfathiazole polymorphs were dependent mainly on the solvent; for examples, Form I was found to crystallise from n-propanol (Khoshkhoo and Anwar, 1993), whereas Form III and Form IV were found to crystallise from water (Alvarez et al., 2009). The work used FBRM and ATR-UV spectroscopy for the *in situ* monitoring and control of the process. The aim of the work is to evaluate the capability of the approach to simultaneously control the CSD and the polymorphic purity of the sulfathiazole crystals.

6.2 EXPERIMENTAL METHODS

6.2.1 Materials

Sulfathiazole was purchased from Sigma-Aldrich with a purity of 98%. The solvents used were n-propanol (analytical reagent grade, Fisher Scientific), water (ultrapure, generated from a Milli-Q reversed osmosis unit) and ammonium hydroxide (analytical reagent grade, Fisher Scientific).

6.2.2 Experimental setup

The crystallisation experiments were performed in a jacketed 500 mL glass vessel. The temperature in the vessel was controlled with a PTFE sheathed thermocouple connected to a thermo fluid circulator bath (Huber Variostat CC-415 vpc). The temperature readings were recorded every 20 seconds on a computer by a control interface (Crystallisation Process Information System – CryPRINS v.2.0) written in LabVIEW (National Instruments). An overhead stirrer with a PTFE three-bladed marine type impeller was used to agitate the system at 320 rpm. An FBRM probe (model D600, Lasentec) was inserted into the solution to measure the CLD using 90 bins. The distributions were collected every 20 seconds and averaged during collection. They were monitored using the FBRM control interface software (version 6.7). The UV system used was a Zeiss MCS621 spectrometer with a CLD600 lamp module. Absorbance spectra were obtained through a Hellma 661.822 ATR-UV probe, which was directly immersed in the solution. The spectral range was 242 – 360 nm, and a spectrum of the solution was recorded every 20 seconds using a data acquisition software, Aspect Plus (version 1.76). A schematic representation of the experimental set-up is shown in Figure 6.2.
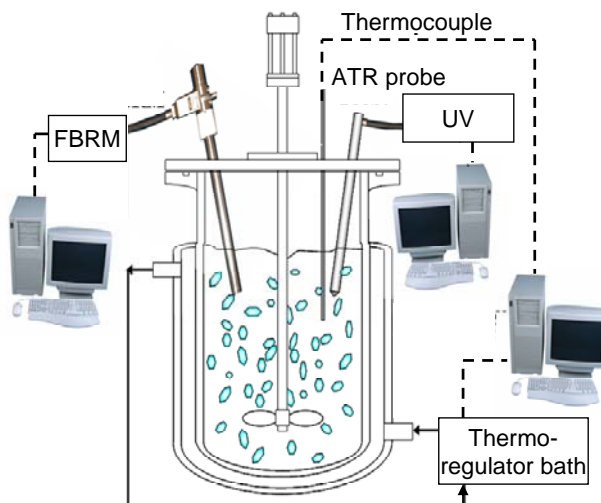
Figure 6.2 A schematic representation of the experimental set-up.

6.2.3 Solubility of Sulfathiazole in n-propanol

The solubility of sulfathiazole in its raw form in n-propanol was determined using the method as described in Appendix C. It was determined at five different temperatures ranging from 30 to 70°C.

6.2.4 Calibration for Solution Concentration

Specified amounts of sulfathiazole and n-propanol were placed in a 500 mL jacketed glass vessel and with the overhead stirrer agitating the system, the slurry was heated to about 10°C above its saturation temperature. The slurry was kept at this elevated temperature for at least 20 minutes to ensure all crystals had dissolved. The clear solution was then subjected to a negative step change of 5°C and was left to equilibrate at the set temperature for 10 minutes. The procedure was continued for five other different set temperatures or until the FBRM detected a nucleation event. In the latter case, the system was brought back to dissolution by heating and then the negative step change procedure was repeated down to a temperature slightly above the nucleation point. In order to investigate any hysteresis effect between cooling and heating runs on the absorbance spectra measurement, the solution was subsequently subjected to positive temperature step changes to repeat the measurement at all temperatures. Once the cooling-heating cycle was completed, a specific amount of sulfathiazole was added to the solution to change the solution concentration, and the procedure was repeated, stepping up to a progressively higher concentration systems. Stepping up, instead of stepping down of the system concentration was performed because throughout the experiment, the solvent needs to be kept at the vessel's maximum capacity in order to prevent the formation of crust on the vessel wall. For calibration purposes, absorbance spectra were collected for six different solution concentrations ranging from 0.20 to 1.03 g per 100 g n-propanol, over temperatures in the range from 20 to 65°C. The position of the calibration points on the phase diagram is shown schematically in Figure 6.3.

6.2.5 Preparation of Seeds

Seed crystals of different sulfathiazole polymorphs were prepared based on methods available in the literature. Form I was prepared by heating a saturated n-propanol solution at 80°C (7.2 g of sulfathiazole in 300 g of n-propanol) in the crystallisation vessel to dissolution, followed by natural cooling to 20°C (Method 2, Table 2.5, Section 2.6.1). Form IV was generated by rapid cooling of an aqueous solution of sulfathiazole (6.0 g of sulfathiazole in 600 g of water) from 80 to 4°C (Method 2, Table 2.8, Section 2.6.1). Form III was prepared by slow evaporation of ammonium hydroxide solution at room temperature (Method 2, Table 2.7, Section 2.6.1). All of the obtained crystals were vacuum filtered and subsequently, the crystals prepared from water, were

immediately dried in a hot air oven at 105°C for 15 minutes, whereas crystals obtained from other solvents were dried in a desiccator.

6.2.6 Sulfathiazole in n-propanol system

Seeded with Linear Cooling Crystallisation

In this crystallisation run, the initial solution of sulfathiazole in n-propanol was prepared to have a concentration corresponding to a saturation temperature at 60°C, which is equivalent to a solute concentration at 1.0 g of sulfathiazole per 100 g of n-propanol. The solubility of sulfathiazole in n-propanol is low; for this reason the solute concentration used in this work is considerably more dilute than typical concentrations used in industry. After all sulfathiazole crystals were dissolved by heating and maintaining at 70°C for 15 minutes, the resultant clear solution was cooled to 55°C and equilibrated at this temperature before seeds of Form I (preferred form for n-propanol) were loaded. The amount of seeds used was about 10% of the amount of solute in the solution. After the seeds were loaded, the solution was cooled at a slow rate of 0.05 °C/min.

Seeded with Temperature Cycling Crystallisation

In this crystallisation run, the procedure was the same as in the previous section, but after seeds of Form I were loaded, the system was subjected to temperature cycling with temperature fluctuations between 2 to 4°C at heating/cooling rates of 1°C/min, progressively stepping down towards lower temperature. The experiment was repeated with seeds of Form IV and Form III.

6.2.7 Sulfathiazole in water system

Seeded with Linear Cooling Crystallisation

The solubility of sulfathiazole in water is lower than in n-propanol; for example at 30°C, the solubilities are 0.1 g and 0.2 g per 100 g in water and n-propanol, respectively (Khoshkhoo and Anwar, 1993). For a system with lower solubility, the initial solution was prepared to have a concentration corresponding to a higher saturation temperature, in this case at 80°C (i.e. 1.0 g of sulfathiazole per 100 g of water). After it was heated to complete dissolution, the resultant clear solution was cooled to 78°C and equilibrated at this temperature prior to the loading of Form IV seeds (preferred form for water). The same amount of seeds as in previous experiments was used (i.e. 10% of the amount of solute). After the seeds were loaded, the solution was cooled at a linear rate of 0.03°C/min to 20°C.

Seeded with Temperature Cycling Crystallisation

The procedure was the same as in the previous section, but after the seeds of Form IV were loaded, the system was subjected to temperature cycling with temperature fluctuations between 6 to 8°C at heating/cooling rates of 0.5°C/min, progressively stepping down towards 20°C. At the end of the run, the crystals were vacuum filtered and dried for characterisation. The experiment was repeated with seeds of Form I.

6.2.8 Characterisation of Crystal Properties

The obtained crystals were characterised for their size uniformity and polymorphic form using optical microscopy and DSC, respectively. The instruments and procedure were the same with those used in Chapter 3.

6.3 RESULTS AND DISCUSSION

6.3.1 Solubility of sulfathiazole in n-propanol and calibration points

The solubility data of sulfathiazole in n-propanol were measured at various temperatures ranging from 30 to 70°C. The data were fitted by a van't Hoff equation, as described in Section 3.3.1, with a linear least square of 0.967. The solubility points and the fitted curve are presented in Figure 6.3. The solubility curve is produced to provide guidance in the selection of calibration points. The system would be better described if some of the points lie within supersaturated region and some lie within undersaturated region. The selected calibration points in this work are shown in Figure 6.3.
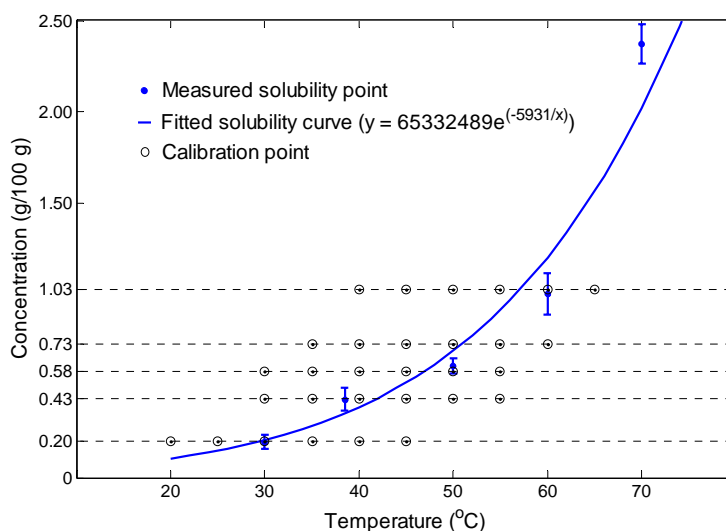
Figure 6.3 An experimental solubility curve of sulfathiazole in n-propanol and calibration points.

6.3.2 Calibration model

Temperature and the absorbance spectra at the highest peak, 291 nm as marked by a dashed line in Figure 6.4, were correlated with the sulfathiazole concentration. Analysis of the calibration data as shown in Figure 6.5 indicates that the effect of temperature on the absorbance was linear for a given concentration, however the slopes increased with increasing concentration, indicating the need for an overall non-linear calibration model.
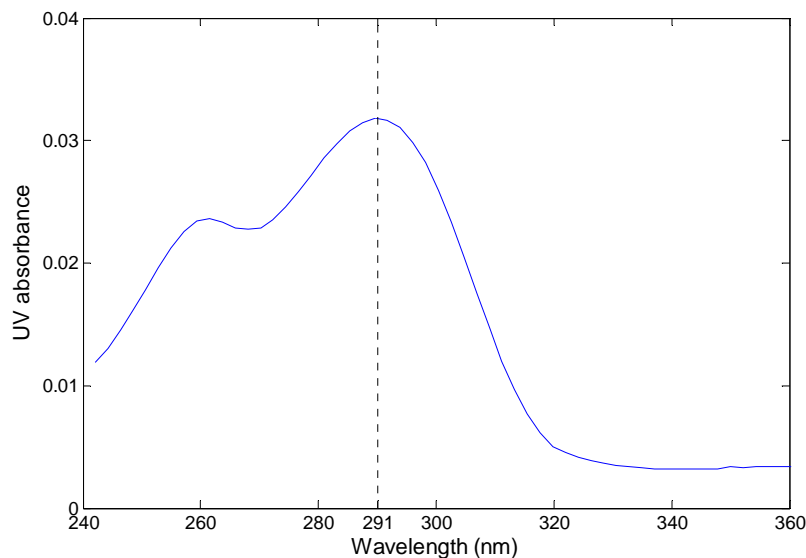
Figure 6.4 A typical absorbance spectra of sulfathiazole in n-propanol.
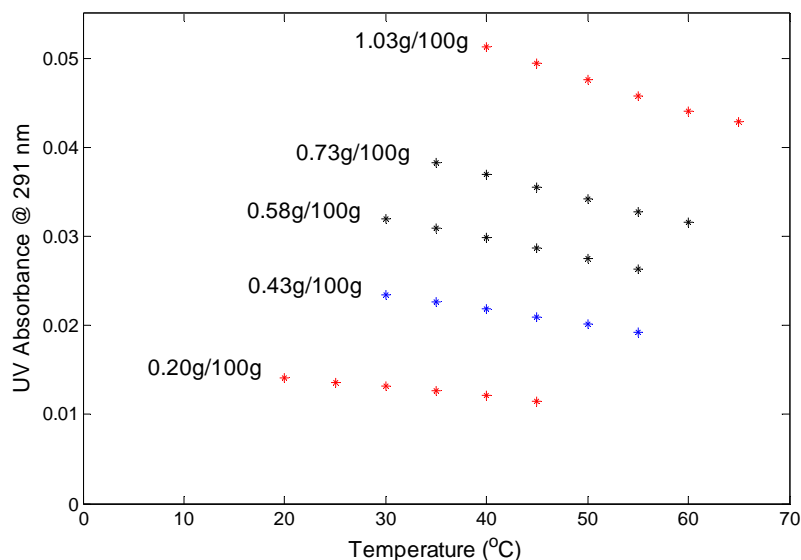
Figure 6.5 Plots of absorbance at 291 nm against temperature for various concentration of sulfathiazole in n-propanol.

Standard linear robust chemometrics approaches (e.g. based on partial least squares or principal component regression) do not work in this case, hence the following simple non-linear function was used for the calibration:

$$C = p(1)T + p(2)A + p(3)AT + p(4) \qquad\qquad (6.1)$$

where C denotes solution concentration, T represents temperature (in °C), and A represents the absorbance at 291 nm. The parameters of the calibration model, $p(1)$, $p(2)$, $p(3)$ and $p(4)$ were computed as 0.0006, 14.8480, 0.1509 and -0.0618, respectively, through least squares optimization implemented in Matlab using the fmincon function, by minimizing the sum-square errors between the experimental concentrations and the concentrations obtained from equation (6.1). The value of the minimized sum-square error is 0.0016.

As shown in Figure 6.6, the difference between experimental and simulated concentrations using the calibration model is very small and the maximum error was calculated to be less than 5%, judging from the two validation points, which were not part of the data set used to obtain the parameters in equation (6.1). In the subsequent analysis of this work, equation (6.1) was used as a calibration to relate temperature and absorbance spectra to the sulfathiazole concentration.
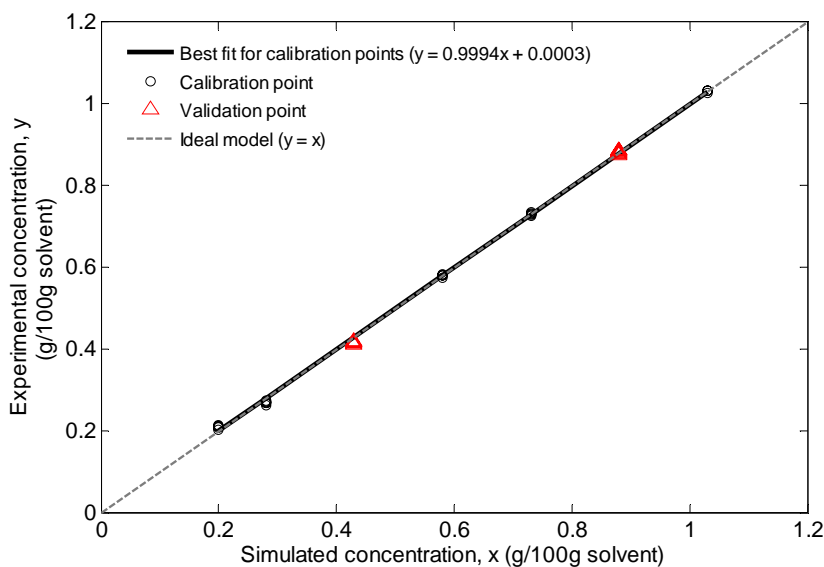
Figure 6.6 A plot of experimental concentrations against simulated concentrations.

6.3.2 Sulfathiazole in n-propanol system

Seeded with linear cooling crystallisation

Figure 6.7(a) shows the profile of temperature and the evolutions of fine and coarse crystals and the square weighted mean chord length (SWMCL) during crystallisation. Fines were defined to be crystals with chord lengths of < 20 µm, whereas coarse were defined to be crystals with chord lengths of > 100 µm. It can be seen that about 30 minutes after seed loading, the number of fines reduced until it stabilized approximately 60 minutes later. At the same time and over the same period, the number of coarse and the SWMCL increased. This indicates the occurrence of Ostwald ripening in which some fine seed crystals dissolved and immediately recrystallised on the surface of the remaining larger crystals. This however can also be due to the effect of a morphology change of the seed crystals that affected the FBRM readings - the microscopy images of seed and product, presented later in Figure 6.10(a), show that the product appears to be more plate-like, whereas the seed is more rod-like. The crystallisation was stopped after a nucleation event was detected, as indicated by a sudden change in the number of fines at about 44°C (marked by dashed lines in Figure 6.7(a)).

Figure 6.7(b) shows the solute concentration profile of the crystallisation on the phase diagram. The solubility curve of Form I, shown by a dashed line in Figure 6.7(b), was plotted based on literature value (Khoshkhoo and Anwar, 1993), whereas the solubility curve of raw sulfathiazole, shown by a solid line in the same figure, was determined in this work (see Section 6.3.1). It can be observed that the solute concentration reduced continuously during cooling but remained in the supersaturation region of Form I. This continuous reduction in the solute concentration corresponds very well with the continuous increase of the SWMCL during cooling as shown in Figure 6.7(a), indicating that the seed crystals were continuously growing. This was confirmed by the profiles of the chord length distribution (CLD) during the crystallisation run as depicted in Figure 6.7(c), where crystal growth was indicated by slight shift of the CLD for the end product and that for the crystals before the primary nucleation to the right. The occurrence of nucleation towards the end of the run however resulted in a bimodality of the end product's CLD.
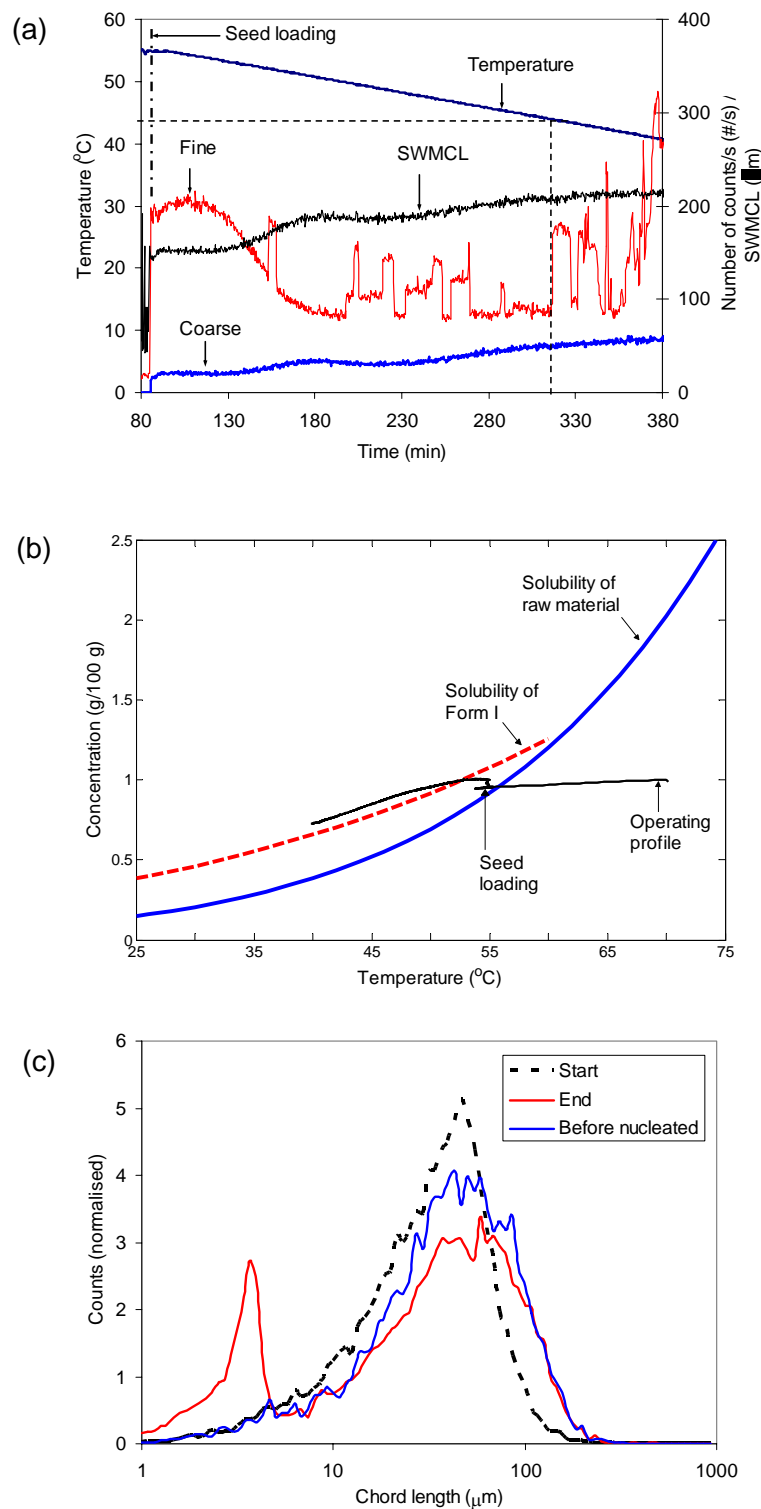
Figure 6.7 Profiles of (a) temperature, number of fine and coarse, and SWMCL; (b) solution concentration on the phase diagram; and (c) CLDs (normalised counts to 100) at the start, the end and before the nucleation of the seeded cooling crystallisation of Form I in n-propanol with linear cooling.
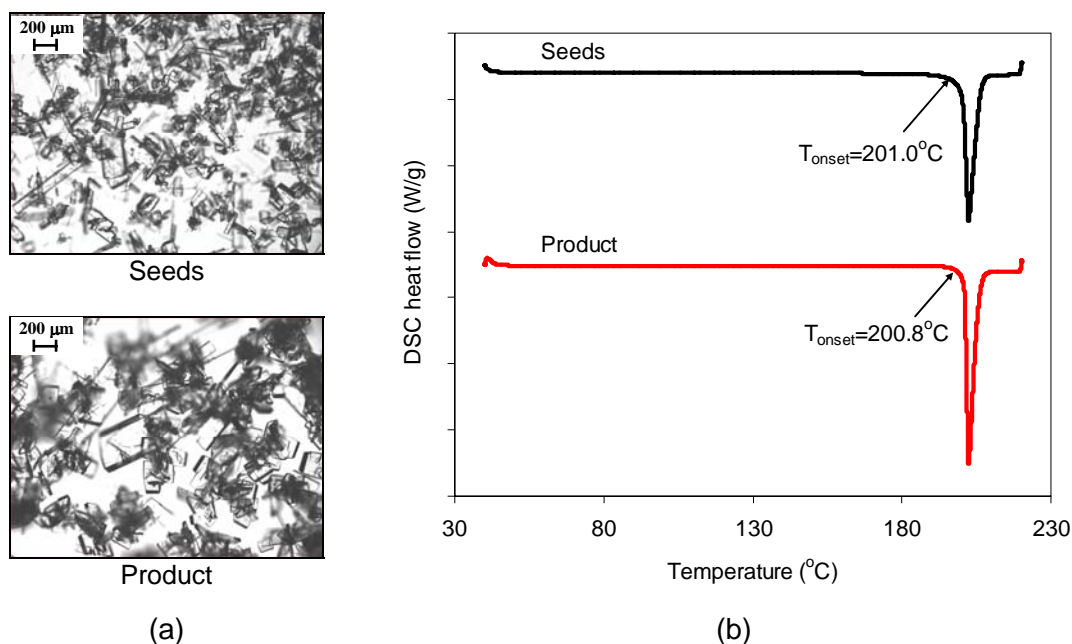
Figure 6.8 (a) Microscopy images and (b) DSC curves of the seeds and product of the seeded cooling crystallisation of Form I in n-propanol with linear cooling.

Microscopy images of the seed and product crystals, shown in Figure 6.8(a), confirmed the inference made based on the profiles of SWMCL, solute concentration and CLD that there was crystal growth. It can also be seen from the images that the product is characterised by more plate-like crystals compared to the seed, which appears to have more rod-like crystals. This may be the reason for the change in number of fine, coarse and SWMCL about 30 minutes after the seed loading, since the FBRM is sensitive to changes in the shape of the monitored particles. The microscopy images also showed that the seed crystals propagated their poly-dispersed CSD to the end product. This underscores the importance of having a controlled manipulation of temperature after seed loading, to correct for the poor quality of the seed crystals. The DSC curves of the seed crystals and the product in Figure 6.8(b) show the presence of single peaks, with onsets at 201.0°C and 200.8°C, respectively. These DSC curves are the characteristic of Form I crystals. The results indicate that both seed crystals and product were pure Form I.

Seeded with temperature cycling crystallisation

Seeding with Form I

The profiles of temperature, total number of counts/s and SWMCL during crystallisation run are presented in Figure 6.9(a). The total number of counts/s represents a total number of crystals with a chord length range from 1 to 1000 μm and

is sensitive to changes in fines since crystals with the fine size range are predominant. It can be seen that the evolutions of the total number of counts/s and the SWMCL for the first 200 minutes after seed loading are very similar to the profiles shown previously in Figure 6.7(a). This indicates the consistency of the occurrence of Ostwald ripening. Temperature cycling was started when the temperature of the suspension reached 48°C. This temperature was chosen based on the onset of nucleation in the previous crystallisation run. However, as can be seen in Figure 6.9(a), the nucleation occurred at around 49°C. Although the temperature cycling was started around 25 minutes after the nucleation, the total number of counts/s in the system has successfully been brought as close as possible to the initial number of seed crystals. During the implementation of temperature cycling, the amplitudes of temperature change were varied accordingly (between 2 to 7°C) in order to keep approximately the same number of counts/s in the system, whilst the heating/cooling rates were maintained at 1°C/min. It can be seen in Figure 6.9(a) that the overall trend of the total number of counts/s is increasing. This is probably due to the nature of Form I crystals; they tend to grow in elongated form, which subsequently were broken and consequently the total number of counts/s increased. The profile of the solute concentration on the phase diagram in Figure 6.9(b) follows the hypothetical operating profile very well. The continuous growth of the crystals in the system can be inferred from the increasing trend of the SWMCL profile in Figure 6.9(a) and the decreasing trend of the solute concentration in Figure 6.9(b). The profiles of the CLD at the start and at the end of the crystallisation run, as shown in Figure 6.9(c), also indicate crystal growth since the CLD at the end of the run is slightly shifted to the right of the CLD at the start, after the seed was introduced in the system.

The growth of the crystallisation product inferred by the profiles of SWMCL and solute concentration was confirmed visually by microscopy images as shown in Figure 6.10(a). The images also show the improvement of size uniformity in comparison to the seed crystals. The DSC curves in Figure 6.10(b) show that the seed crystals of Form I have grown into the same polymorphic form.

Figure 6.9 Profiles of (a) temperature, total number of counts/s and SWMCL; (b) solution concentration on the phase diagram; and (c) CLD (normalised counts to 100) at the start and the end of the seeded cooling crystallisation of Form I in n-propanol with temperature cycling.

Figure 6.10 (a) Microscopy images and (b) DSC curves of the seeds and product of the seeded cooling crystallisation of Form I in n-propanol with temperature cycling.

Seeding with Form IV

The profiles of temperature, total number of counts/s and SWMCL during seeded cooling crystallisation of Form IV with temperature cycling are shown in Figure 6.11(a). Unlike in the previous crystallisation run, no drop in the total number of counts/s was observed within the first 200 minutes after seed addition. The seed crystals were suspended in the solution without showing any growth for about 5 hours. The temperature cycling was started when the suspension reached 48°C and continued through to 36°C with temperature fluctuations of 2°C and heating/cooling rates of 1°C/min. The total number of counts/s showed a sudden increase when the suspension reached 39°C, which indicates the occurrence of nucleation. At the same time, the SWMCL showed a slight drop, which is influenced by the presence of fine crystals (nuclei). In order to eliminate the newly formed fine crystals and maintain the number of seed crystals, the suspension was heated to 53°C. Once the total number of counts/s returned to the initial value, the suspension was subjected to a slow cooling at 0.05°C/min. The temperature cycling was started again when the suspension reached 43°C and continued through to 30°C with temperature fluctuations of 4°C and heating/cooling rates of 1°C/min. The total number of counts/s showed a sudden increase again at 42°C, which indicates the start of another nucleation. The presence of polymorphic impurities produced from the previous nucleation may act as seeds which results in the earlier occurrence of nucleation. Although the temperature cycling

was implemented, the heating phases were not able to bring the total number of counts/s back to the initial value and for this reason when the total number of counts/s exceeded 1000 #/s, the suspension was heated to 53°C. This time the heating was too much and the total number of counts/s dropped to below the initial value. Immediately, the suspension was cooled linearly and in the process, the total number of counts/s increased to slightly below the initial value. The run was stopped at 43°C to avoid another nucleation. Other than showing slight decreases when nucleation events were detected, the profile of the SWMCL was generally flat during the run, which indicates no crystal growth. Figure 6.11(b) shows the operating profile of the crystallisation run on the phase diagram. The solubility curve of Form IV in the figure was plotted according to literature data (Khoshkhoo and Anwar, 1993). It can be seen from the figure that the crystallisation run was operated in the supersaturated regions of both Form I and Form IV.   The operating profile showed a decreasing trend in concentration due to the formation of nuclei during the nucleation events, but returned close to the initial concentration towards the end due to the dissolution of the nuclei as shown in Figure 6.11(b). The inability of the Form IV crystals to grow was also shown by the almost overlapping profiles of the CLD at the start and the end of the crystallisation run in Figure 6.11(c).

No size change between the seed crystals and the product was visually observed based on the microscopy images in Figure 6.12(a). This confirmed the result inferred from the profiles of SWMCL and CLD. The DSC curve of the seed crystals shown in Figure 6.12(b) has two peaks; one at 154.4°C and another at 201.6°C, which is a characteristic DSC curve for Form IV crystals. The DSC curve of the product, on the other hand, shows the presence of a major peak at an onset temperature of 201.3°C and poor resolution peak(s) that lie between 140 to 160°C. The difference between the DSC curves of the seed and the product indicates that the crystals produced by the nucleation events have contaminated the seed crystals.   Nucleation is thought to produce Form I crystals, because the intensity of the transition peaks of Form IV were swamped by the melting peak of Form I. It was reported that Form I always crystallises from n-propanol and although it is the least stable form in the solvent, it did not transform to other forms even after a month of storage as slurry at 30°C (Blagden et al., 1998a). Above the nucleation temperature, seeds of Form IV are expected to stay as Form IV without transformation because it is more stable than Form I in n-

propanol, as can be inferred from the position of their solubility curves in Figure 6.11(b).
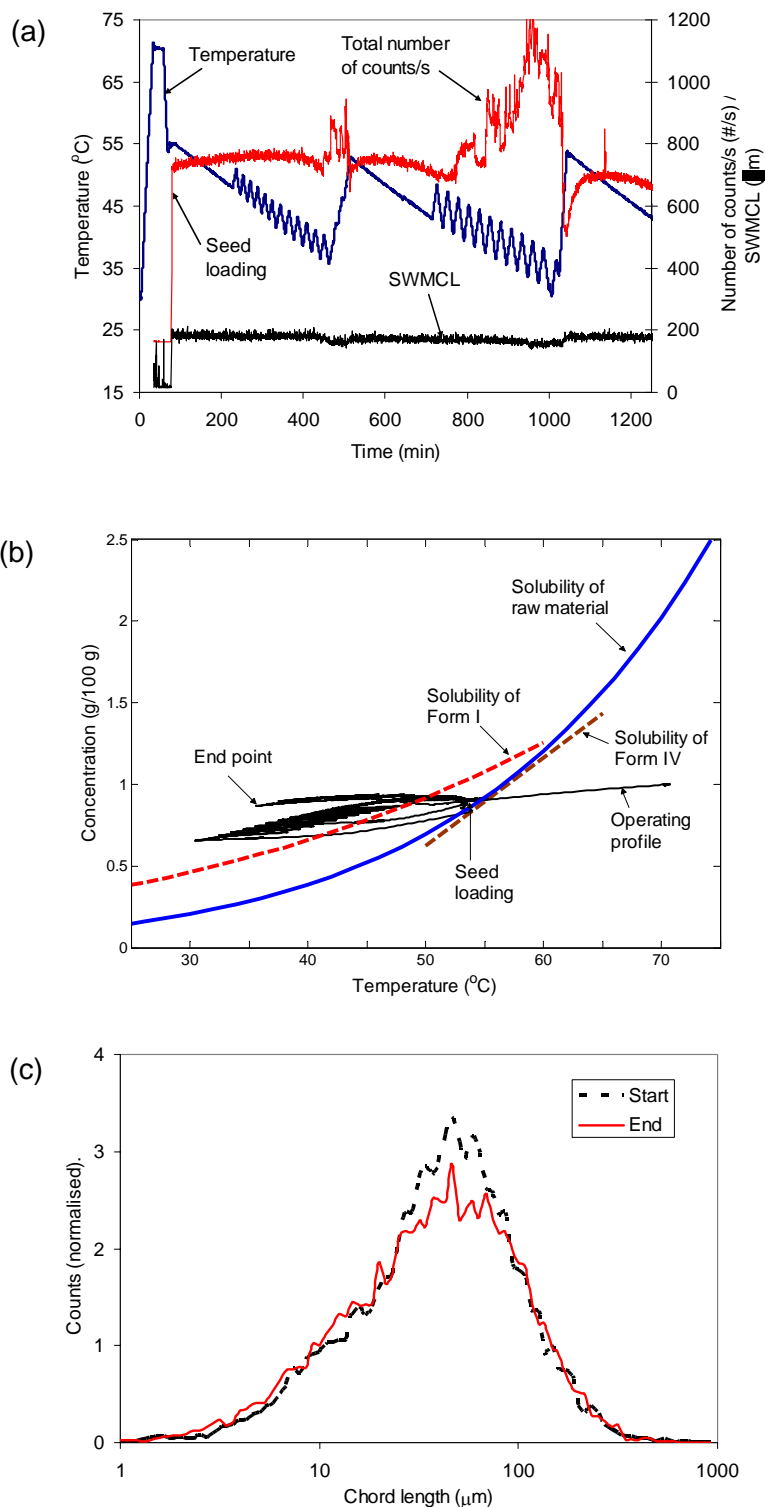
Figure 6.11 Profiles of (a) temperature, total number of counts/s and SWMCL; (b) solute concentration on the phase diagram; and (c) CLD (normalized to 100) at the start and the end of the seeded cooling crystallisation of Form IV in n-propanol with temperature cycling.

Figure 6.12 (a) Microscopy images and (b) DSC curves of the seeds and product of the seeded cooling crystallisation of Form IV in n-propanol with temperature cycling.

Sudo et al. (1991) made the same observation, in which seed crystals of one polymorph did not grow, but instead the system nucleated another polymorphic form. In their work on the crystallisation of cimetidine, they found that one of its polymorphic forms, which is a thermodynamically metastable form in IPA solution, was crystallised from high supersaturated IPA solution with or without seed and regardless of the polymorphic form of seed.

Seeding with Form III

Figure 6.13(a) depicts the profiles of temperature, total number of counts/s and SWMCL during seeded cooling crystallisation of Form III with temperature cycling. The temperature cycling with amplitudes between 5 to 7°C and heating/cooling rates of 1°C/min was started when the temperature of the suspension reached 44°C and continued until the total number of counts/s started to increase at approximately 33°C. In order to suppress the nucleation and return the total number of counts/s to the initial value, the suspension was then heated to 50°C at a rate of 1°C/min. Thereafter a couple of cycles with maximum temperatures of 48°C and 50°C were applied, but since this was still unable to reduce the total number of counts/s, the suspension was further heated to 55°C, the same temperature as was used for the initial seed loading. The heating reduced the total number of counts/s to below the initial value, but the

cooling process performed after that brought the total number of counts/s closer to the initial value. The cooling was conducted at two rates; 0.05°C/min from 55 to 50°C, and 0.10°C/min from 50°C and below. The crystallisation run was stopped at 40°C in order to avoid a nucleation event that may affect the quality of the product. It can be seen from Figure 6.13(a) that after the seed loading, the profile of SWMCL was completely flat, which indicates no crystal growth. The same can be inferred from the profile of solute concentration on the phase diagram in Figure 6.13(b), which shows the system stayed in the supersaturated region without any significant change in the solute concentration. The solubility curves of Form I and Form III in the figure were plotted according to literature data (Khoshkhoo and Anwar, 1993). Figure 6.13(c) shows profiles of the CLD at the start and at the end of the crystallisation run that are almost overlapped, which also indicates the absence of crystal growth.

Microscopy images in Figure 6.14(a) show that there was no significant difference in size between seed and product crystals. This confirmed the result inferred from the profiles of SWMCL and CLD and also confirmed the similar behaviour of the sulfathiazole in n-propanol system to cimetidine in IPA, as mentioned in the previous section. It can also be seen from the microscopy images that the product appears to have fewer fine particles than the seed, which may be due to the effect of the temperature cycling. The DSC curve of seed crystals shown in Figure 6.14(b) indicates the presence of three endothermic peaks. The first peak at the onset of 117.5°C is in the vicinity of the temperature corresponds to the dehydration of a hydrate, as mentioned in Section 3.3.3. The presence of a hydrate is possible since the crystals were prepared from ammonium hydroxide solution, which contains water. The second peak is within the range of temperatures for the transformation of Form III into Form I crystals. The product crystals have all the same peaks as the seed crystals, but with lower intensity. This may be due to a slight contamination of seed crystals with the products of nucleation.
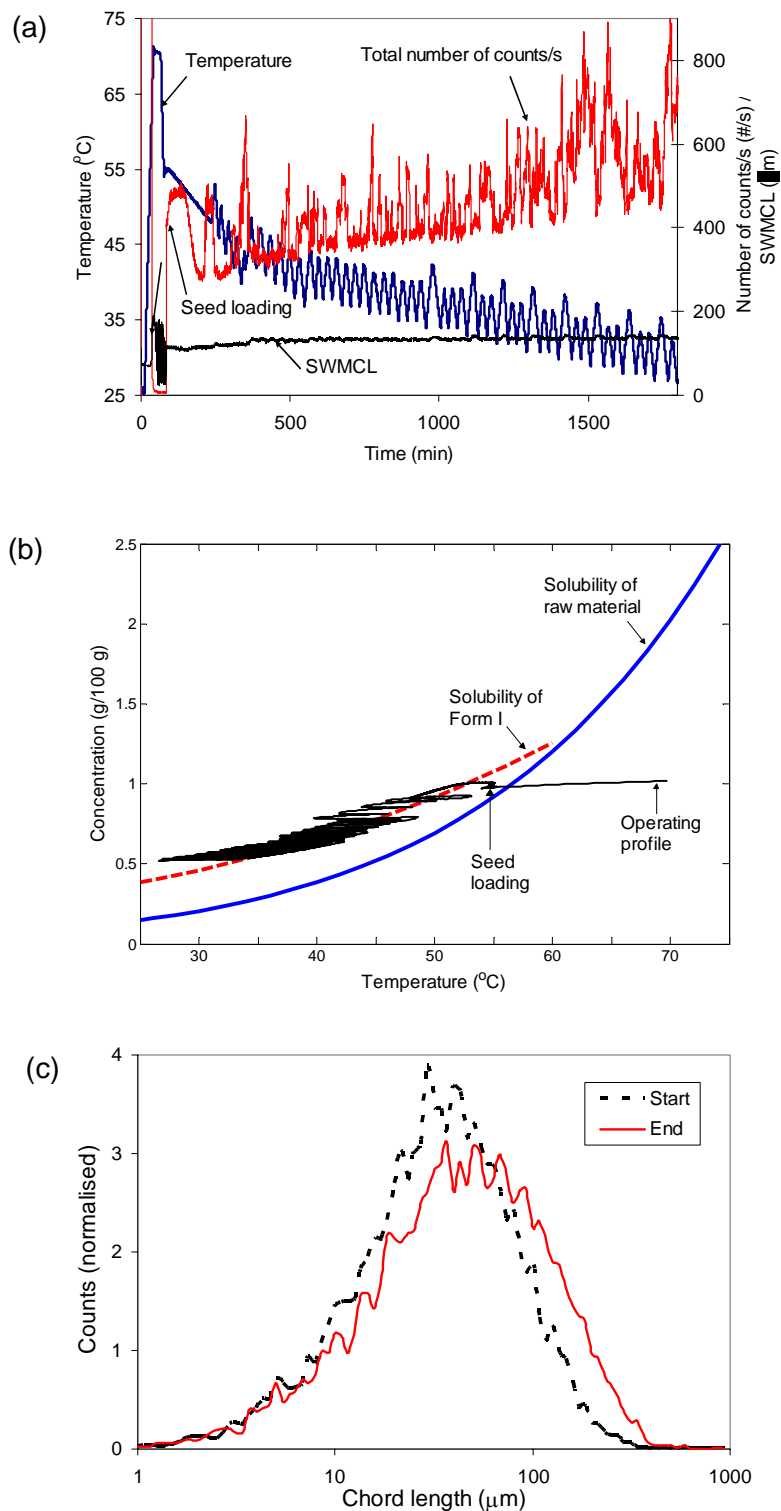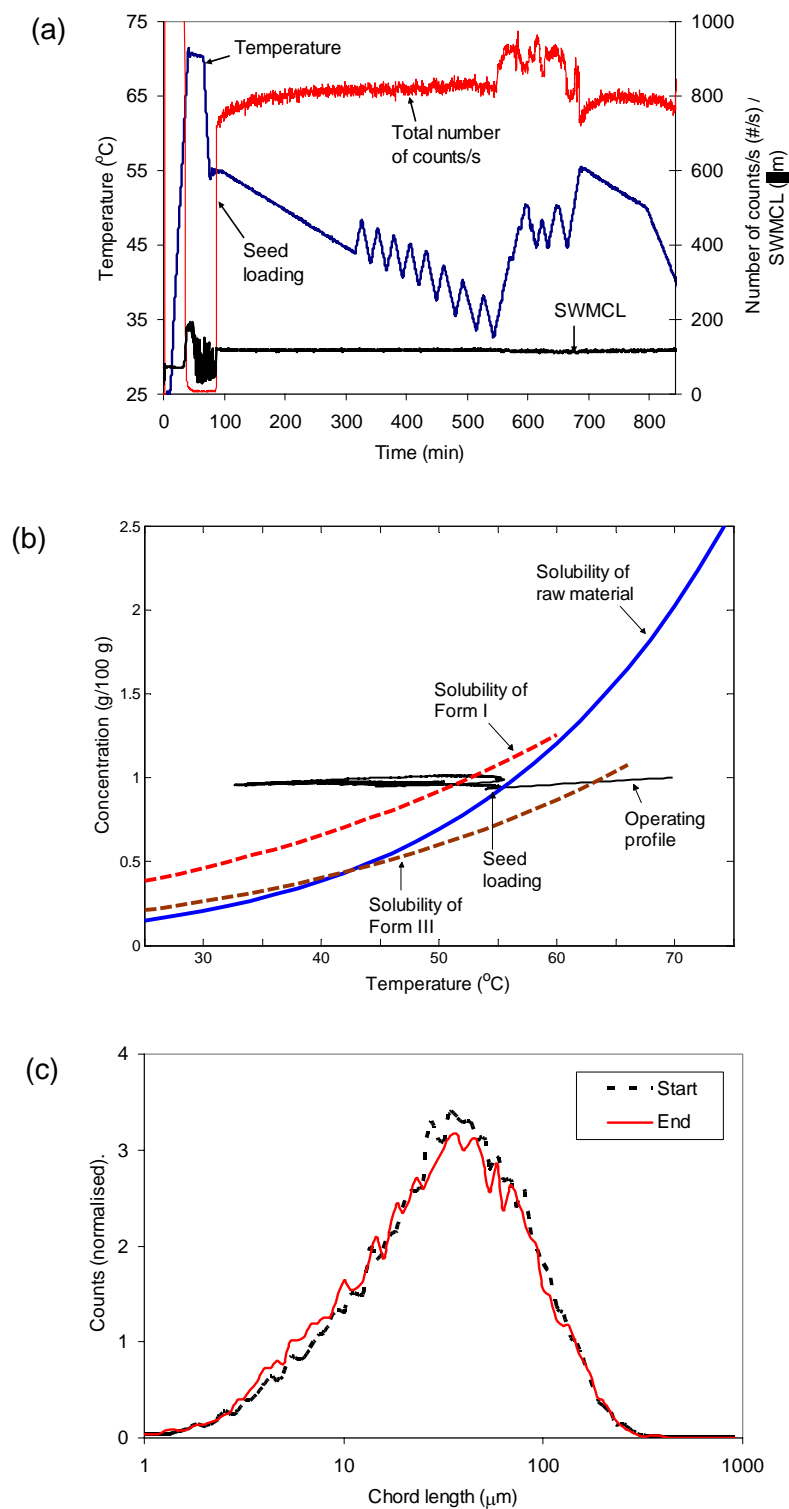
Figure 6.13 Profiles of (a) temperature, total number of counts/s and SWMCL; and (b) solution concentration on the phase diagram; and (c) CLD (normalized to 100) at the start and the end of the seeded cooling crystallisation of Form III in n-propanol with temperature cycling.
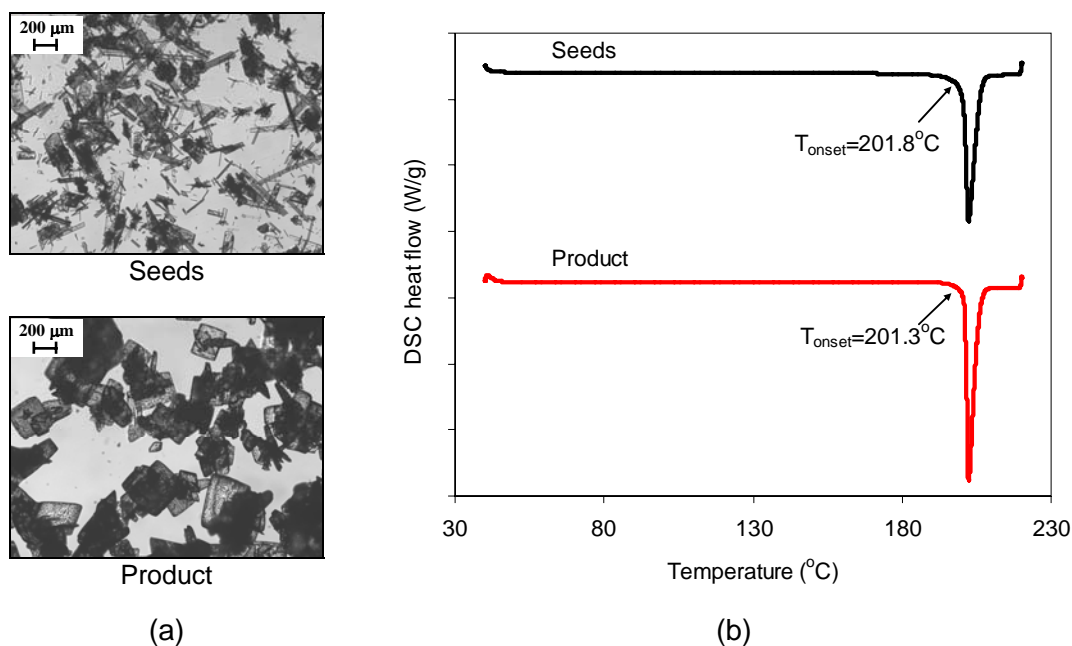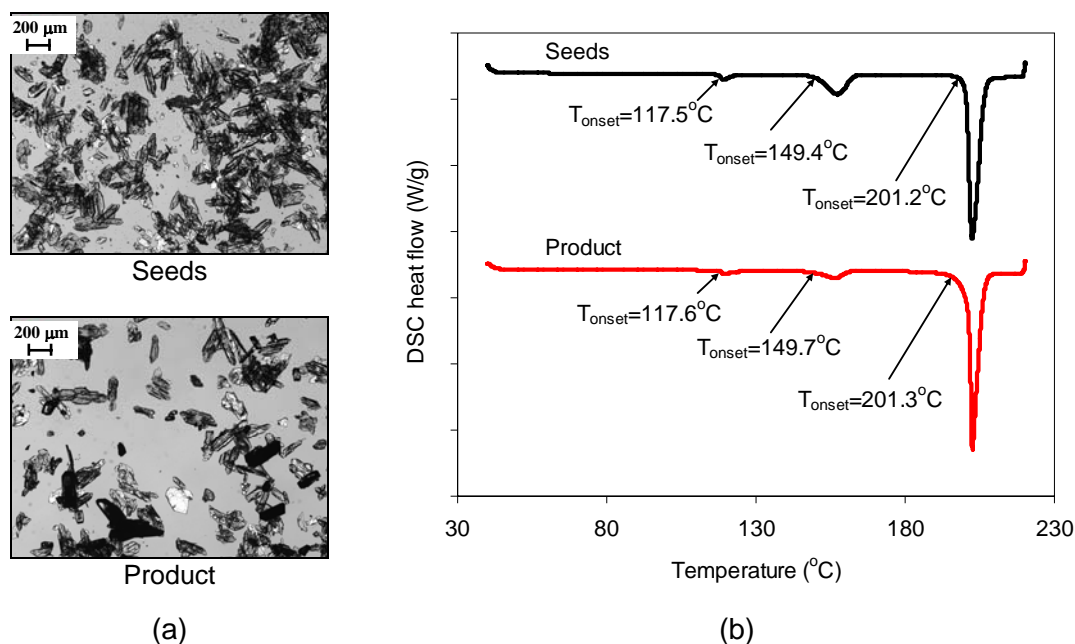
Figure 6.14 (a) Microcopy images and (b) DSC curves of the seeds and product of the seeded cooling crystallisation of Form III in n-propanol with temperature cycling.

6.3.3 Sulfathiazole in water system

Seeded with linear cooling crystallisation

Figure 6.15(a) shows the profile of temperature and the evolutions of the number of fine and coarse crystals, and the SWMCL for the seeded cooling crystallisation of Form IV in water with linear cooling. During cooling after seeds loading at 100 min, the number of fines continuously fluctuated due to nucleation event and noises of the FBRM signal. The nucleation events kept producing fine particles and as a result, the trend of the overall profile of the fine particles increases. The profiles of numbers of counts/s of coarse particles and the SWMCL also show a continuous increase, which indicates a continuous growth of the crystals present in the system. The difference in the profiles of the CLDs at the start and at the end of the experimental run as shown in Figure 6.15(b) provides further evidence of the crystal growth.
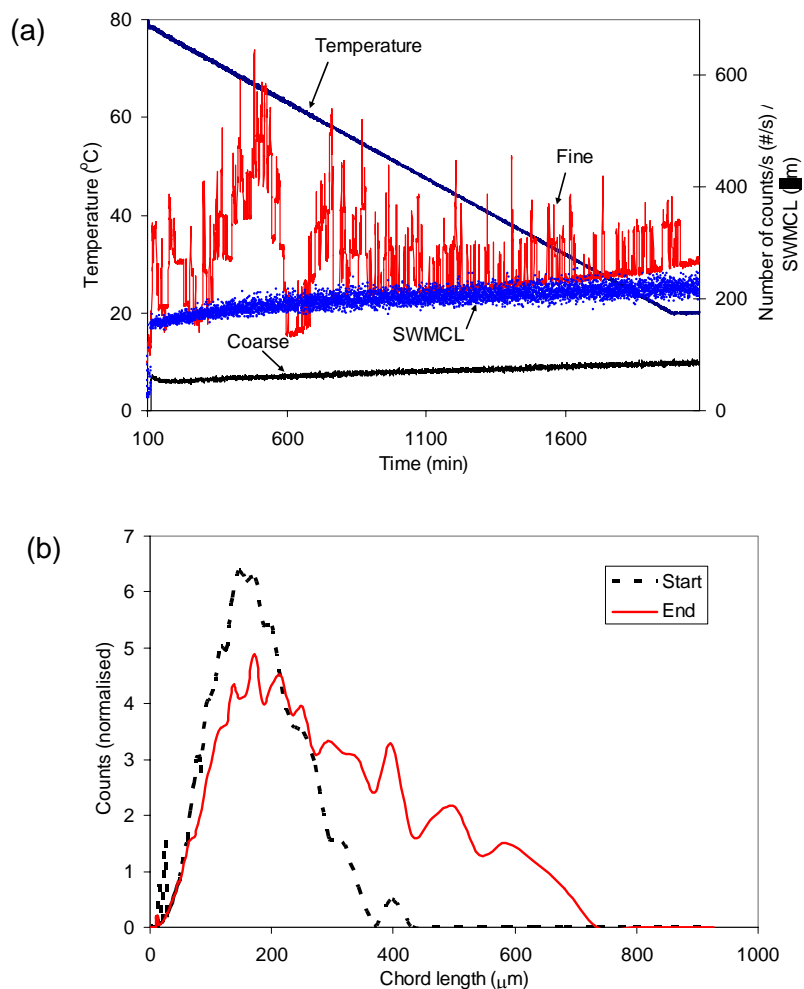
Figure 6.15 Profiles of (a) temperature, fine, coarse and SWMCL; and (b) CLD (normalized to 100) at the start and the end of the seeded cooling crystallisation of Form IV in water with linear cooling.

The nucleation and growth events inferred from the profiles of fine, coarse, SWMCL and CLD are confirmed by the microscopy images in Figure 6.16(a). The microscopy images show that there is a significant difference in size between seed and product crystals, which indicates growth. The image of the product shows the presence of much smaller crystals among the larger ones. These smaller crystals are most likely the products of nucleation events that had occurred during the cooling process. This shows that besides correcting the effects of poor quality of the seed crystals, as shown in section 3.2.1, a controlled manipulation of temperature after seed loading is necessary to prevent unwanted nucleation, or in cases where nucleation cannot be prevented, to eliminate nuclei so that they could not contribute to the poor size uniformity of the end product. DSC curves presented in Figure 6.16(b) show that seeds and product are of the same polymorph. It can be confirmed from the results of

microscopy and DSC analyses that water is the preferred solvent for Form IV crystals to grow as well as to nucleate, whereas in n-propanol (preferred solvent for Form I) the Form IV seeds do not grow at all.
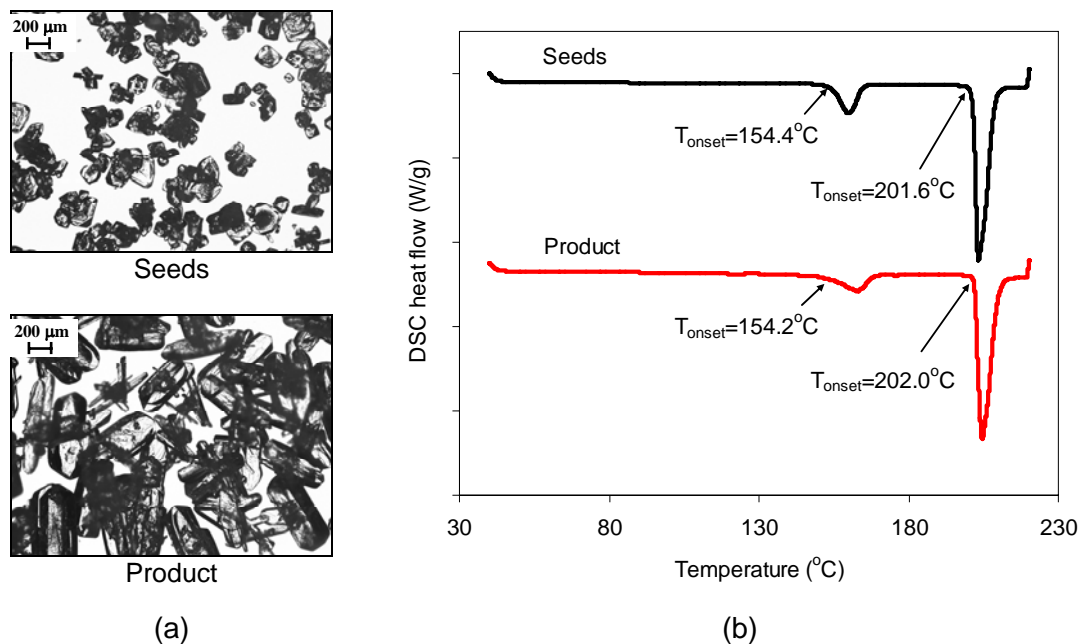
Figure 6.16 (a) Microcopy images and (b) DSC curves of the seeds and product of the seeded cooling crystallisation of Form IV in water with linear cooling.

Seeded with temperature cycling crystallisation

Seeding with Form IV

The profiles of temperature, number of fine, number of coarse and SWMCL during seeded cooling crystallisation of Form IV with temperature cycling in water are shown in Figure 6.17(a). The figure shows that the number of fines fluctuated with the change in temperature due to nucleation and dissolution events whilst maintaining almost the same number of counts/s throughout the batch. The number of coarse particles was similarly fluctuating and as can be seen more clearly from a zoom out view of a part of the profiles of fine, coarse and temperature in Figure 6.17(b), the number of fine and coarse responded to temperature change out of phase with each other: on heating, the number of fines dropped while the number of coarse increased, whereas on cooling, the fines increased while the coarse reduced. These responses of fine and coarse to temperature change may indicate the occurrence of Ostwald ripening. The responses are the subject of a thorough investigational study that will be presented in Chapter 7. Since the temperature fluctuations increase the kinetics of Ostwald ripening, the application of temperature cycling after seed loading is a

beneficial method to accelerate the growth of crystals and to eliminate the fine particles. Figure 6.17(a) also shows that the amplitude of the fluctuations of coarse reduces with time. It can also be observed that the first half of the coarse profile shows a decreasing trend, whilst during the second half it shows an increasing trend. These observations may be due to a transition of the crystallisation process from a nucleation-dominated to a growth-dominated process. The profile of the SWMCL in Figure 6.17(a) shows a continuous increase, which indicates a continuous growth of the crystals in the system. The difference between the CLDs at the start and at the end of the batch presented in Figure 6.17(c) provides further evidence of the crystal growth.

The growth of the crystals in the system is confirmed visually based on the microscopy images in Figure 6.18(a). The images clearly show that the product crystals are much larger in size compared to the seed crystals. The DSC curves in Figure 6.18(b) confirmed that the seeds and product are the same polymorph. This is to be expected since water is the preferred solvent for Form IV. An inspection of the images to compare visually the product of linear cooling (Figure 6.16(a)) and the product of temperature cycling (Figure 6.18(a)) shows that besides improving the size uniformity, the temperature cycling method also increases the size of the crystals. As can be determined from Figure 6.15(a) and Figure 6.17(a), the average SWMCL at the end of the batch is 220 µm for the linear cooling and 300 µm for the temperature cycling.
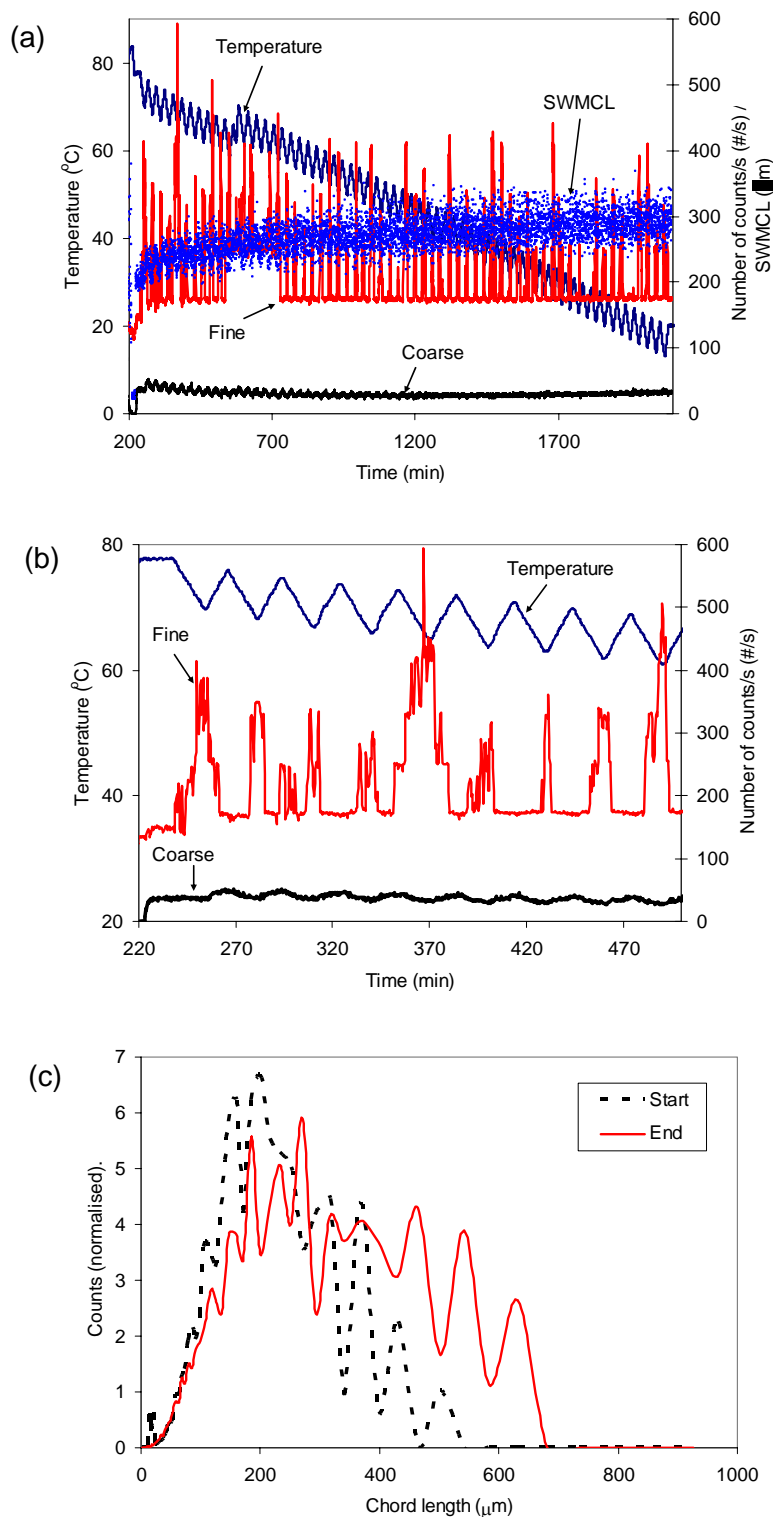
Figure 6.17 Profiles of (a) temperature, fine, coarse and SWMCL; and (b) a zoom out view of a part of the profiles of fine, coarse and temperature; and (c) CLD (normalized to 100) at the start and the end of the seeded cooling crystallisation of Form IV in water with temperature cycling.
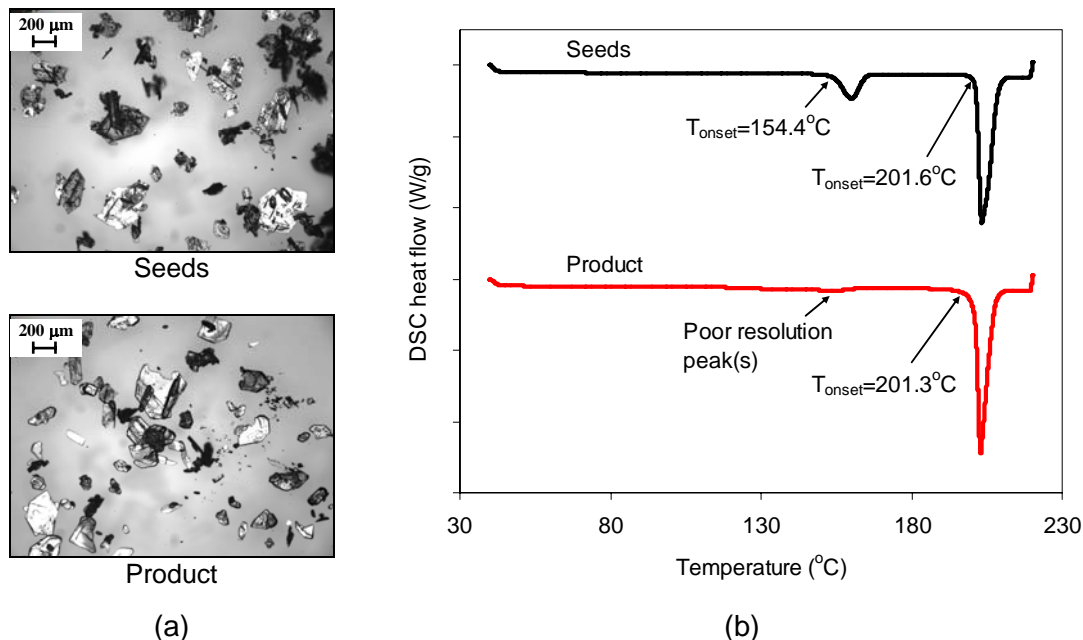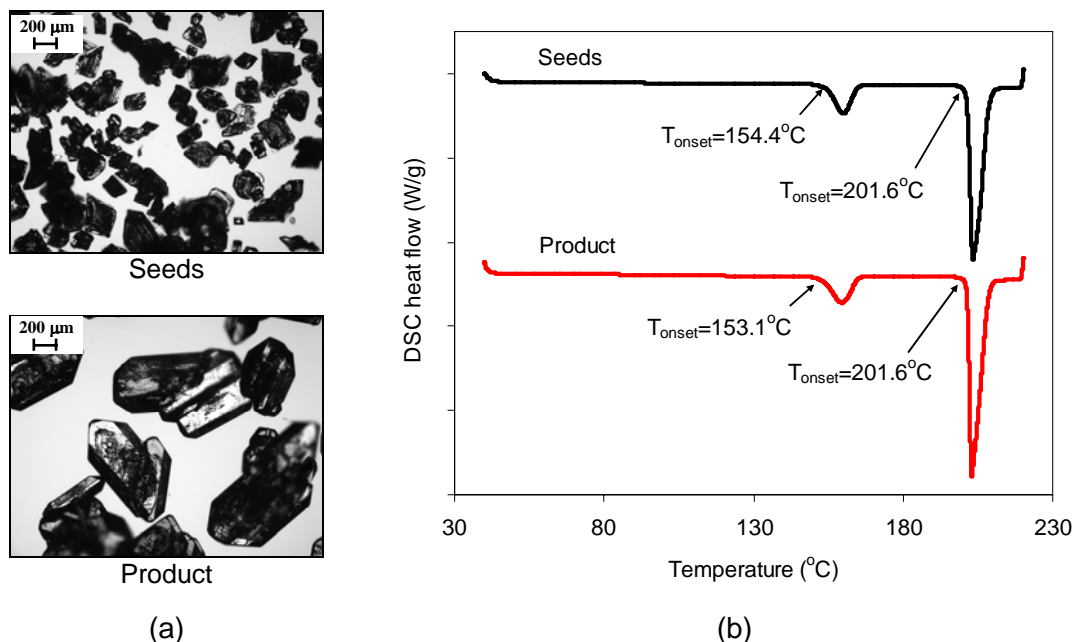
Figure 6.18 (a) Microcopy images and (b) DSC curves of the seeds and product of the seeded cooling crystallisation of Form IV in water with temperature cycling.

Seeding with Form I

Figure 6.19(a) depicts the profiles of temperature, fine, coarse and SWMCL during seeded cooling crystallisation of Form I in water with temperature cycling. It can be seen that the fine and coarse particle counts also show fluctuations throughout the batch time. As Figure 6.19(b) shows, the fine and coarse particles responded to temperature change in reverse to each other. This provides an evidence for the occurrence of Ostwald ripening. Similar to the previous experiment, the amplitude of fluctuations of the coarse is also reduced with time – indicative of a transition between nucleation-dominated to growth-dominated process. Although the evolution of SWMCL implies growth, but as shown by DSC analysis later, the growth took place after the seeds of Form I transformed into Form IV crystals and/or swamped by the nuclei of Form IV. In other words, the growing crystals were Form IV and not Form I. Form IV is the preferred form in water, a solvent which does not promote the formation of Form I. Therefore during the initial part of the batch the Form I seed particles cannot grow, they merely serve as initiator particles for the heterogeneous secondary nucleation of Form IV particles, yielding to a graduate polymorphic transformation of the Form I seed into Form IV. After enough Form IV has formed these particles can grow in water and hence the process becomes gradually growth dominated. This is indicated by the gradually decreasing amplitude of the FBRM
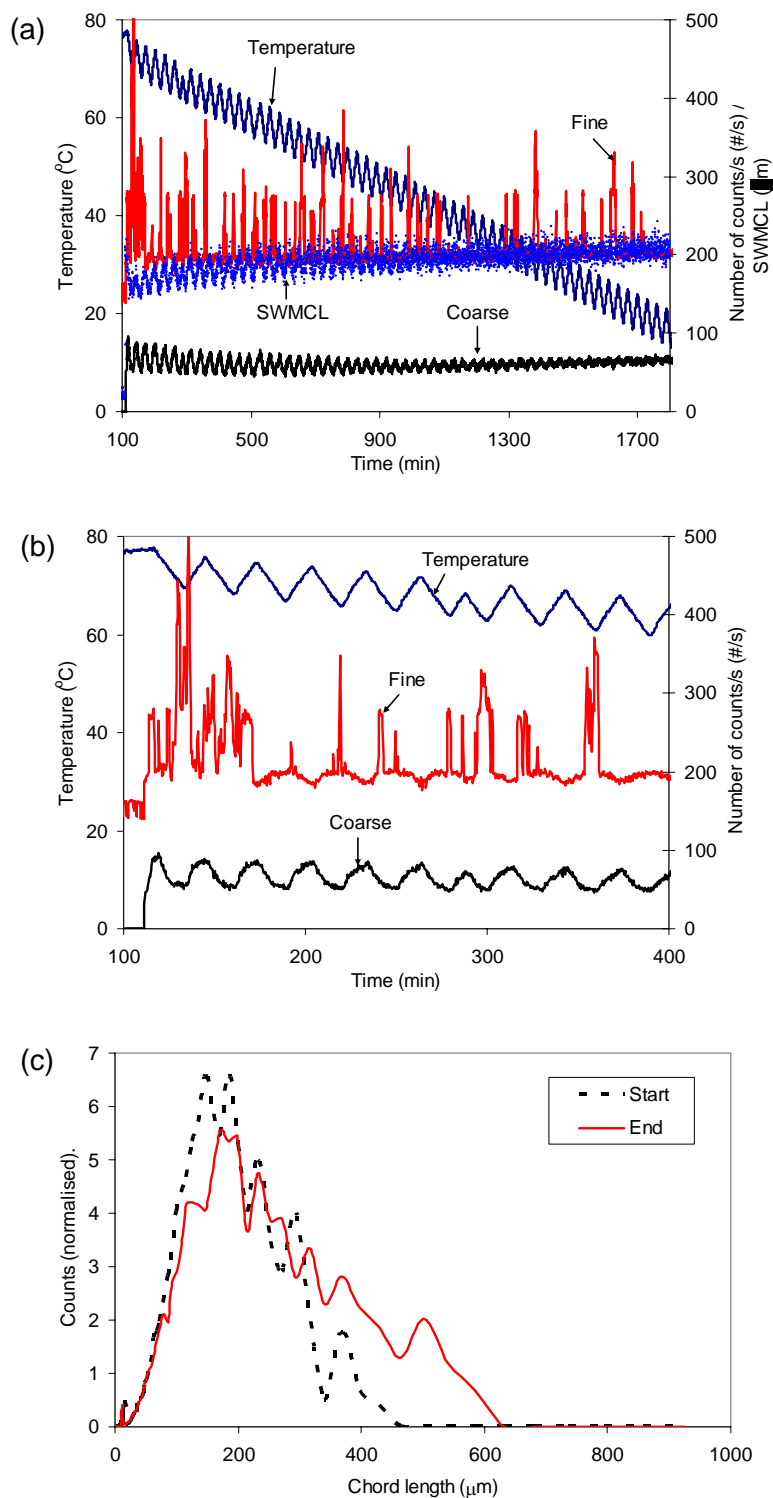
Figure 6.19 Profiles of (a) temperature, fine, coarse and SWMCL; and (b) a zoom out view of a part of the profiles of fine, coarse and temperature; and (c) CLD (normalized to 100) at the start and the end of the seeded cooling crystallisation of Form I in water with temperature cycling.

counts in Figure 6.19(a). The growth of the crystals in the system is also shown in Figure 6.19(c) by the difference between CLD at the start and CLD at the end of the batch.

Microscopy images in Figure 6.20(a) show that during the process, the rod-like Form I seed crystals turned into crystals with a morphology that is typical of Form IV. The change in polymorphic form between the seeds and the product is confirmed by the DSC analysis – the curves are shown in Figure 6.20(b). The seeds produced a DSC curve with a single melting peak at the onset temperature of 201.8°C – a characteristic of Form I crystals , while the product produced a DSC curve with peaks at 154.4°C and 201.7°C – typical DSC peaks for Form IV crystals and a small peak at 120°C – a typical DSC peak due to the formation of hydrate, as mentioned in Chapter 3. Water is also present because larger crystals tend to entrap water (solvent) in their structure and the entrapped water is harder to be removed by a normal drying procedure.
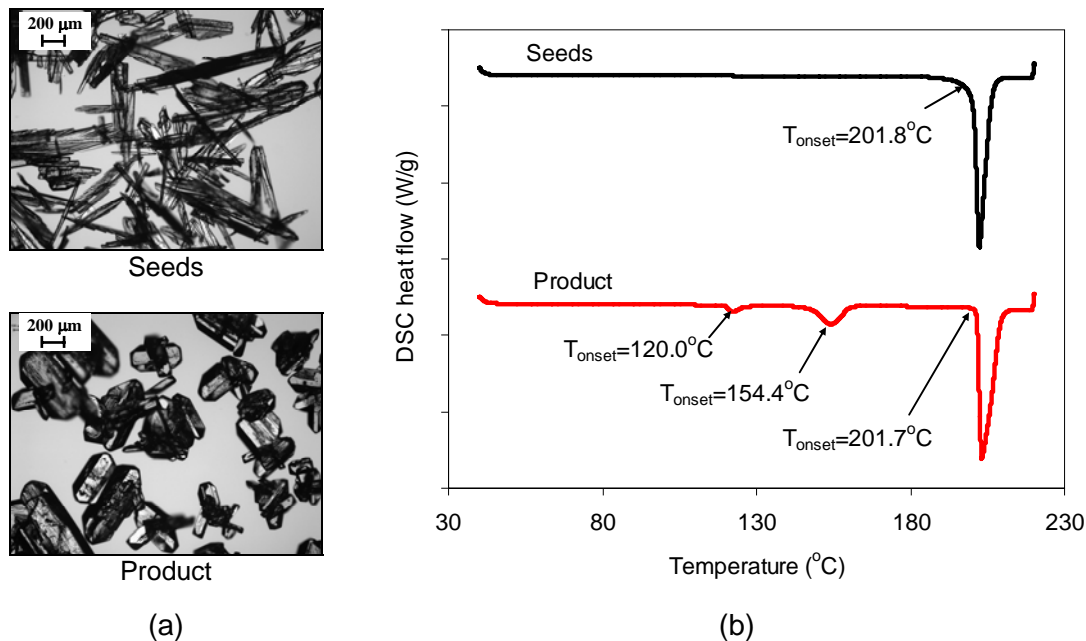
Figure 6.20 (a) Microcopy images and (b) DSC curves of the seeds and product of the seeded cooling crystallisation of Form I in water with temperature cycling.

The seeds of Form I in water transformed into Form IV because Form I is a metastable polymorph in water and water is a preferred solvent for the crystallisation of Form IV. Although Form I is a preferred polymorph to crystallise from n-propanol, the seeds of Form IV did not transform to Form I in n-propanol because Form IV is a more stable polymorph than Form I in the solvent. As shown in this work, Form I seed crystals

grew in n-propanol, but not in water. Form IV seed crystals on the contrary grew in water, but did not grow in n-propanol. Form III seed crystals also did not grow in n-propanol. These results are most likely due to the nature of the sulfathiazole polymorphs that their nucleation and growth are dependent very much on solvent. Table 6.1 summarises the outcomes of all the experiments that have been presented in this chapter.

Table 6.1 Different strategies for seeded cooling crystallisation with temperature cycling approach and theirs outcomes.

Strategy	Polymorphic Transformation?	Growth?	Comment
In n-propanol (a preferred crystallising solvent for Form I)			
Linear cooling:			
- Seeded with Form I	No	Yes	Poor seeds quality propagated to the end product.
Temperature cycling:			
- Seeded with Form I	No	Yes	Poor seeds quality not propagated to the end product.
- Seeded with Form IV	No	No	Form IV unchanged. Form I nucleated. Both Form I and Form IV present in the end product.
- Seeded with Form III	No	No	Same trend as above.
In water (a preferred crystallising solvent for Form IV)			
Linear cooling:			
- Seeded with Form IV	No	Yes	Average SWMCL of the end product is 220 μm.
Temperature cycling:			
- Seeded with Form IV	No	Yes	Average SWMCL of the end product is 300 μm.
- Seeded with Form I	Yes	Yes	Form I transformed into Form IV and grew.

Khoshkhoo and Anwar (1993) have proposed a mechanism to explain the effect of solvent in determining a particular polymorph. It is based on the degree of affinity of

solvent molecules with certain faces of a particular polymorph. The greater the affinity, the stronger the molecules will adsorb onto the faces. This in turns inhibits the deposition of oncoming solute molecules; hence the nucleation/growth of the affected polymorph is inhibited/retarded. For example in this case, the n-propanol molecules have greater affinity with faces of Form IV; so they adsorb strongly onto the faces to inhibit growth, whilst Form I, which is less affected, nucleates and grows. The inability of the seeds of Form IV and Form III to grow in n-propanol may also be due to the effect of impurities. Blagden and co-workers (Blagden et al., 1998a; 1998b) have shown that the presence of ethamidosulfathiazole (one of the by-products of sulfathiazole synthesis) did not disturb the growth of Form I, but inhibited the growth of other forms. However, in our work no impurities in the raw material, seeds and products were detected by high performance liquid chromatography (HPLC) method, providing supportive evidence that the observed effects are due to the solvent-mediated nucleation and growth of the sulfathiazole polymorphs. The HPLC method and its results are briefly presented in Appendix H.

6.4 CONCLUSIONS

Seeded cooling crystallisation with temperature cycling method has been implemented using sulfathiazole in n-propanol and in water as model systems. Results of the experiments showed that the method is capable of correcting the poor quality of the seed crystals to avoid the propagation of the poly-dispersed CSD to the end product. Results also showed the capability of the method to accelerate the growth of the crystals, in comparison with a run using a simple linear temperature profile, by promoting Ostwald ripening. The experiments revealed interesting behaviour of sulfathiazole polymorphs. Form I was found to crystallise and grow from n-propanol regardless of the polymorphic form of seed. Similarly with Form IV in water. These, as well as the inability of the seeds of Form I to grow in water and seeds of Form IV and Form III to grow in n-propanol, show that the growth of the systems is solvent-mediated. The insights into this behaviour of sulfathiazole crystals were captured very well by FBRM. Although the temperature cycling method is conceptually able to control the polymorphic purity of a system; its effect however can be dominated by the effect of solvent, as suggested by the results of the experiments. The study also demonstrated the successful use of ATR-UV spectroscopy for the quantitative monitoring of the solute concentration during the crystallisation process.

CHAPTER 7:
THE EFFECT OF TEMPERATURE CYCLING ON SURFACE FEATURES OF SULFATHIAZOLE CRYSTALS

This chapter presents an investigation of the effects of temperature cycling, performed during seeded cooling crystallisation of sulfathiazole in water, on the surface features of the crystals. The work involves the evaluation of the capability of FBRM as an in situ process analyzer in monitoring and detecting events on the crystal's surface. Ex situ optical microscopy, SEM and AFM were used to examine surface properties of the crystals and provide links to the potential growth mechanism and the FBRM results. Possible explanations for the FBRM results are also put forward and discussed.

7.1 INTRODUCTION

During the implementation of the seeded cooling crystallization with temperature cycling approach presented in Chapter 6, the morphology of sulfathiazole crystals has been indirectly controlled by the alternate heating and cooling procedure. The heating phases are expected to promote dissolution of the unwanted crystal surface features, whereas the cooling phases encourage re-growth. Smoother crystals may have better flowability and friability than rougher crystals; hence controlling the surface properties of the crystalline product may have significant effect on the efficiency of downstream processes and the quality of the final product. The actual sequence of events at a crystal surface, however, may not be as simple as expected. Since the knowledge about the structure of the growing crystal surface at its interface with a supersaturated solution may lead to a better understanding of the growth mechanism (Verma, 1966), therefore, the availability of in-process information that indicates surface events and surface features will be very useful.

There are various types of information about the solid phase during crystallisation that can be obtained from FBRM analysis, as reviewed in Chapter 2, but its practical capability in detecting changes in surface features of crystals with the link to potential growth mechanisms has never been evaluated. However, the effect of surface roughness has been taken into consideration in a method that combined FBRM data and inverse modelling for determining the CSD from the CLD (Hukkanen and Braatz, 2003). The analytical technique most commonly used to study the surface properties

of crystals is microscopy. The technique includes optical microscopy, scanning electron microscopy (SEM) and atomic forced microscopy (AFM). Although optical microscopy is considered as low-tech compared to other techniques, it is still a very useful tool, particularly for a rapid preliminary examination in deciding which other studies or techniques are required. Both SEM and AFM can resolve surface features down to a nanometer scale, but different types of information about the surface features are given since their image formation mechanisms are different. For the SEM, the impingement of an electron beam on the surface of a sample results in the emission of secondary electron, which is detected and its intensity at each data point during the scanning of the electron beam across the surface is used to form a two-dimensional morphological image (Castle and Zhdan, 1997). For the AFM, the detection of surface forces during scanning a sharp tip (probe) on the end of a flexible cantilever across a sample surface while maintaining a small, constant force is used to form a three-dimensional or topographical surface image (Hansma et al., 1989; Drake et al., 1989). Since the SEM images cannot provide the actual positioning of surface features relative to the mean surface level (i.e. height or depth), they may lead to misinterpretation of the data (Castle and Zhdan, 1997). For this reason, SEM analysis is normally complemented with AFM analysis since the latter can provide measurements in three dimensions, including height or depth information.

The aim of the work presented in this chapter is two-fold: (a) to investigate the effect of temperature cycling, implemented during seeded cooling crystallization of sulfathiazole in water, on the surface features of crystals, and (b) to evaluate the capability of FBRM as an *in situ* process analyzer in monitoring surface events and detecting changes in surface features of crystals, which can provide link to potential growth mechanism. The work also involved the use of *ex situ* optical microscopy, SEM and AFM to examine the surface appearance of the crystals at the ends of each heating and cooling phases.

7.2 EXPERIMENTAL METHODS

7.2.1 Materials

Sulfathiazole with a purity of 99% was purchased from Alfa Aesar. The un-sieved raw material was also used as seeds. The ultrapure water was generated from a Milli-Q reversed osmosis unit.

7.2.2 Experimental set-up

The crystallization experiments were conducted using the same experimental set-up as described in Chapter 6, Section 6.2.2.

7.2.3 Seeded cooling crystallization with temperature cycling

The initial solution was prepared to have a concentration corresponding to a saturation temperature at 80°C (i.e. 1.0 g of sulfathiazole per 100 g of water). After it was heated to complete dissolution, the resulting clear solution was cooled to 78°C and equilibrated at this temperature prior to the loading of seeds. The amount of seeds used was about 10% of the amount of solute in the solution. After the seeds were loaded, the systems were subjected to temperature cycling with temperature fluctuations between 6 to 8°C at heating/cooling rates of 0.5°C/min, progressively stepping down towards 20°C. A repeat of the experiment was performed for samples withdrawal at the ends of each heating and cooling phases for microscopy analyses. The samples were vacuum filtered and dried.

7.2.4 Optical microscopy, SEM and AFM

The optical microscopy and SEM systems used in this work were the same as those described in Chapter 3, Section 3.2.4. For the AFM analysis, a small quantity of sample was spread and immobilized onto a double-sided adhesive tape that had been mounted onto metal stubs. Images were taken using a Veeco Explorer operated in contact mode with a silicon nitrite tip of <10 nm radius. A cantilever (Veeco 1950-00 silicon) with a nominal force constant of 0.21 N/m was utilized during imaging.

7.3 RESULTS AND DISCUSSION

7.3.1 Seeded cooling crystallization with temperature cycling

Figure 7.1(a) depicts the evolutions of temperature, FBRM fine and coarse counts during the crystallization run. Similar to the work presented in Chapter 6, in this work fine is defined as crystals with chord lengths of <20 μm, whereas coarse is defined as crystals with chord lengths of >100 μm. The total duration of the experiment was 30 h, during which as can be seen from the figure, the number of fines fluctuated with the change in temperature, due to repeated nucleation and dissolution events. The number of coarse crystals fluctuated in a similar way and as can be seen more clearly from a zoom out view of the initial part of the profiles (from 100 to 400 min) in Figure 7.1(b), the number of fine and coarse responded to temperature change out-of-phase
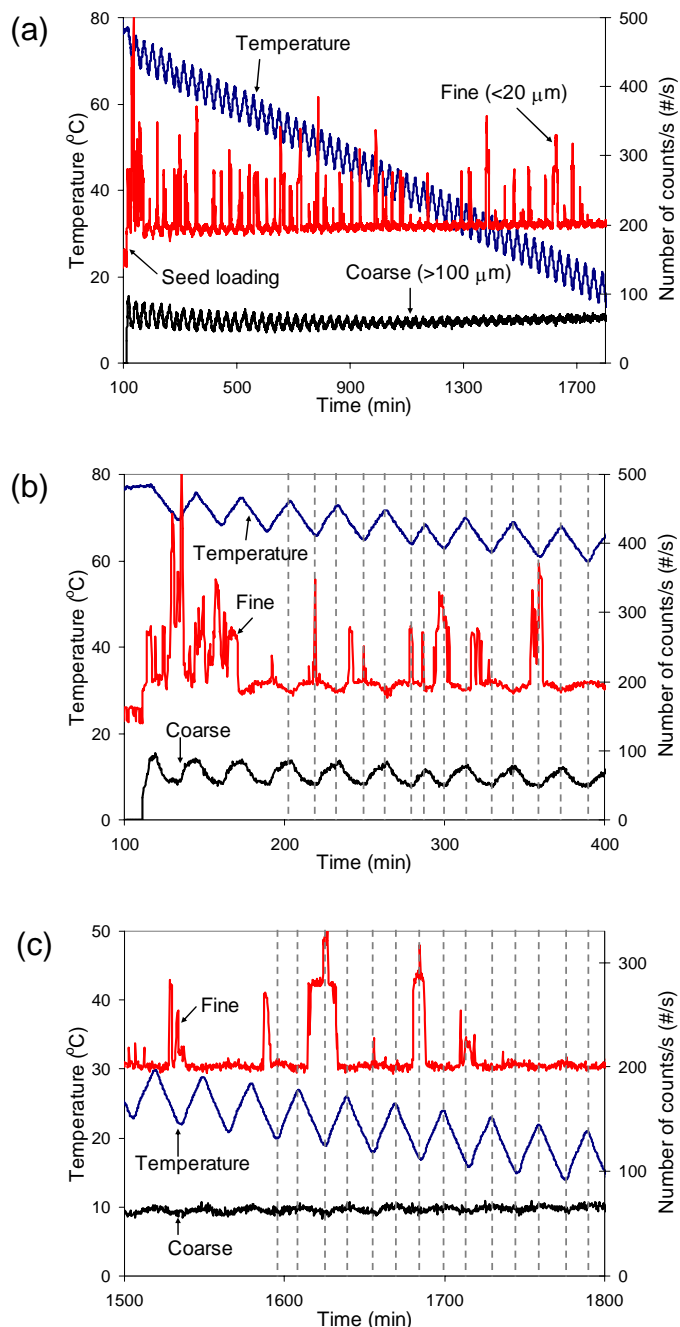
Figure 7.1 Profiles of temperature, FBRM fine and coarse counts/s of (a) overall; (b) zoom-out view of initial part (from 100 to 400 min); and (c) zoom-out view of final part (from 1500 to 1800 min).

with each other (dashed lines were drawn to facilitate the observation): on heating, the number of fine dropped while the number of coarse increased, whereas on cooling, the fine increased while the coarse reduced. Although these responses of fine and coarse to temperature change may in part result from dissolution, re-growth and Ostwald ripening, these processes do not explain the reduction of the coarse counts during

cooling. A zoom out view of the last part of the profiles (from 1500 to 1800 min) in Figure 7.1(c) shows that although the amplitude of the fluctuations of both fine and coarse counts/s has significantly reduced, they are still out-of-phase with each other in response to the temperature change.

7.3.2 Optical microscopy, SEM and AFM images of crystals

Figure 7.2 shows the position of sampling points on the profiles of temperature, FBRM fine and coarse counts/s at the initial phase (Figure 7.2(a)) and at the final phase (Figure 7.2(b)) of the repeated crystallization process. The process was conducted with identical conditions as the experiment shown in Figure 7.1. Some samples were withdrawn during the process. The samples taken at the ends of heating phases are denoted as 'Heat1', 'Heat2', 'Heat3', and 'Heat4', whereas samples taken at the subsequent ends of cooling phases are denoted as 'Cool1', 'Cool2', 'Cool3', and 'Cool4'.
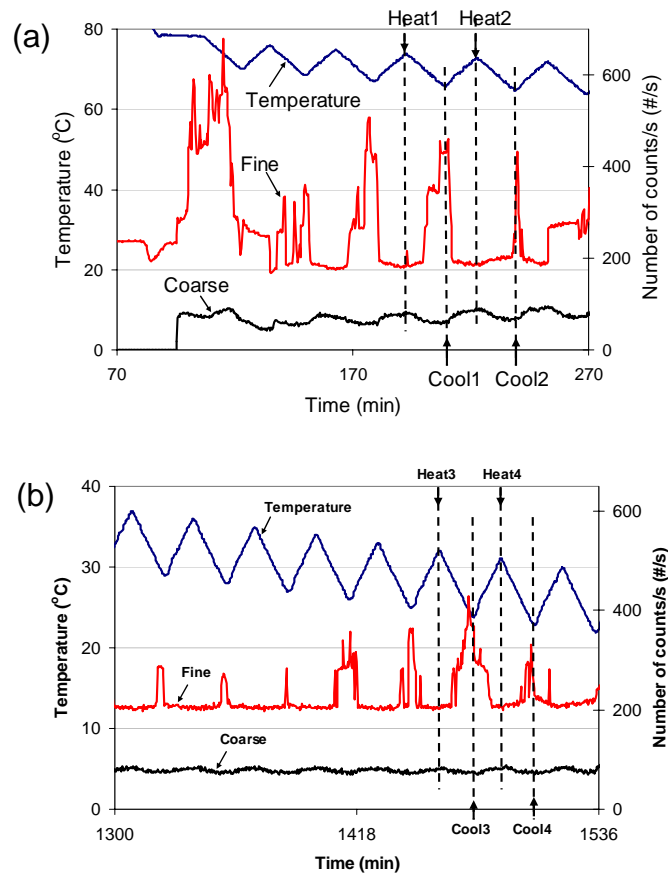
Figure 7.2 Sampling points on the profiles of temperature, FBRM fine and coarse counts/s of a repeated experiment at (a) the initial phase of the batch; and (b) the final phase of the batch.

Figure 7.3 shows optical microscopy and SEM images of Heat1 and Cool1 crystals. It can be observed from Figure 7.3(a) and Figure 7.3(b) that Heat1 crystals have smoother surfaces and blunt edges, whereas Cool1 crystals have rougher surfaces and sharper edges. The SEM images shown in Figure 7.3(c) and Figure 7.3(d), agree well with the optical microscopy images except that some of the Cool1 crystals appear to have steps with edges, while some have large flat areas on their surfaces. These

(a) Heat1 – optical microscopy

(b) Cool1 – optical microscopy

(c) Heat1 - SEM

(d) Cool1 - SEM
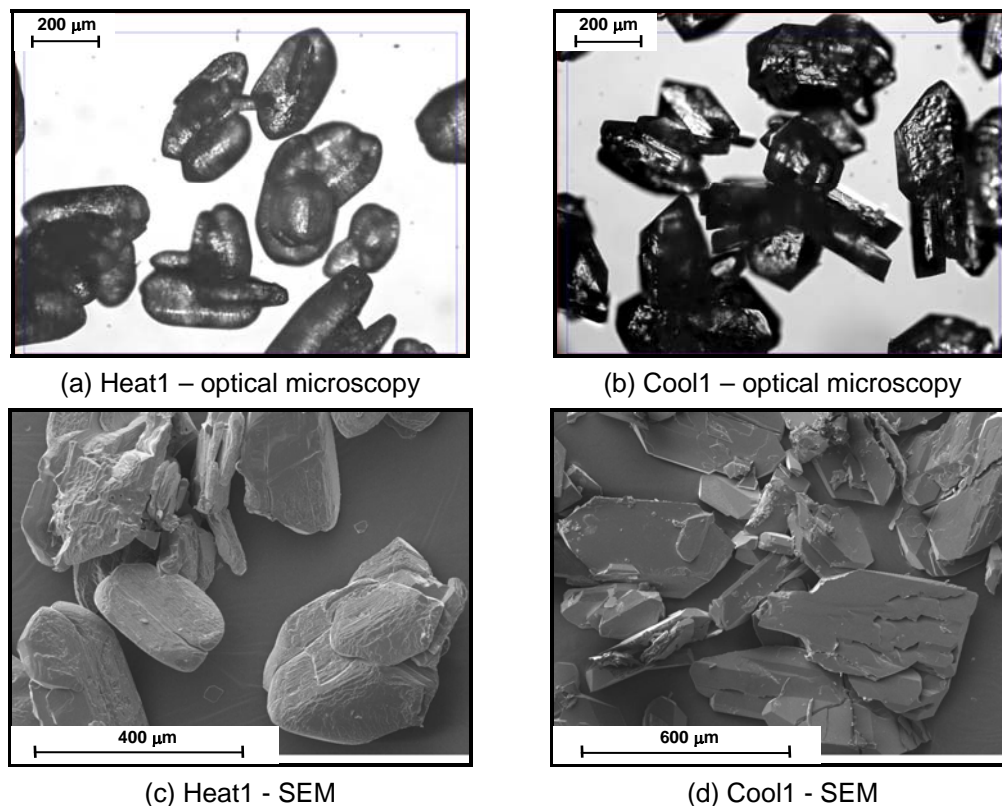
Figure 7.3 Optical microscopy images of (a) Heat1 and (b) Cool1, and SEM images of (c) Heat1 and (d) Cool1 crystals.

results indicate that during the heating phase, some of the growths on the surface of the crystals are dissolved. As can be inferred from the optical microscopy and SEM images of Heat1 crystals, this dissolution process has effectively polished the surface and edges of the crystals. The growths however reappeared during the cooling phase. The removal and reappearance of surface features may affect the measurement of FBRM in such a way that when the FBRM sees a crystal with a smooth surface, it will measure the crystal as a coarse chord; which is a representative of the overall dimension of the crystal. On the other hand, if the FBRM sees a crystal with rough surface and sharp edges, it will measure a few fine chords, representative of the surface features and edges. The effects of the surface properties and the sharper

edges on the FBRM measurement have respectively been noted by Ruf et al. (2000) and Heath et al. (2001). The phenomenon where coarse particles with rough surface features are not recognised as one chord but as multiple fine chords is known as signal splitting (Ruf et al., 2000) or chord splitting (Kail et al., 2008). This process can be hypothetically and schematically described in Figure 7.4. The figure illustrates that in the presence of features on the surface of the crystals, the FBRM light scattering intensity on the surface was distracted or distorted. On the smooth surface of the crystals, the probability for the FBRM light scattering intensity not to be distorted is greater, hence the FBRM is most likely to measure the crystal as one coarse chord.
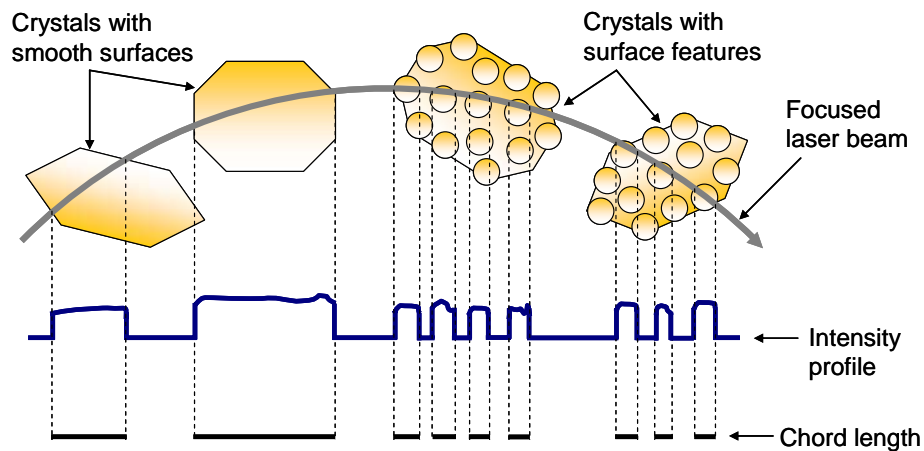
Figure 7.4 A schematic diagram of backscattered light pulses detection and chord length measurement of typical crystals with smooth surfaces and with surface features.
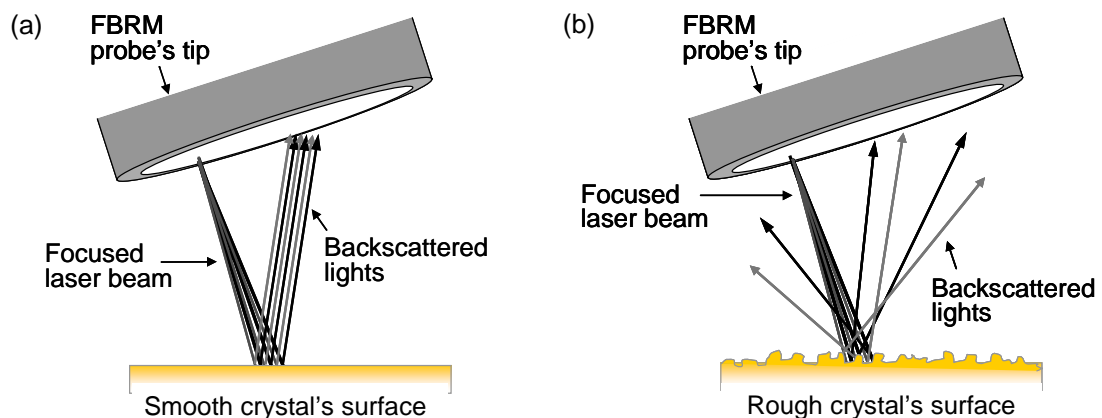
Figure 7.5 Schematic representations of the backscattering of the FBRM laser beam from (a) smooth, and (b) rough crystal's surfaces.

Another phenomenon related to surface properties that may affect the measurement of FBRM is when the laser beam strikes the surface of the crystals in a direction perpendicular to that shown in Figure 7.4. The phenomenon, which is schematically illustrated in Figure 7.5(b), is known as beam spreading (Heath et al., 2002). When the FBRM laser beam strikes the crystal's smooth surface, there is a high probability of the scattered lights to re-enter the FBRM's optical system with sufficiently high intensity to be differentiated from the threshold that determine the baseline for the signal, and therefore be measured. This is illustrated in Figure 7.5(a). However, if the crystal's surface is rough, spreading of the beam away from the FBRM's optical system, as shown in Figure 7.5(b), is very likely. The small fraction of the light scattered back into the optical system produces weak light scattering intensities that the FBRM may consider only as noise. As a result, they are statistically more likely to disappear from the measured data; hence the reduction in coarse counts/s during cooling.
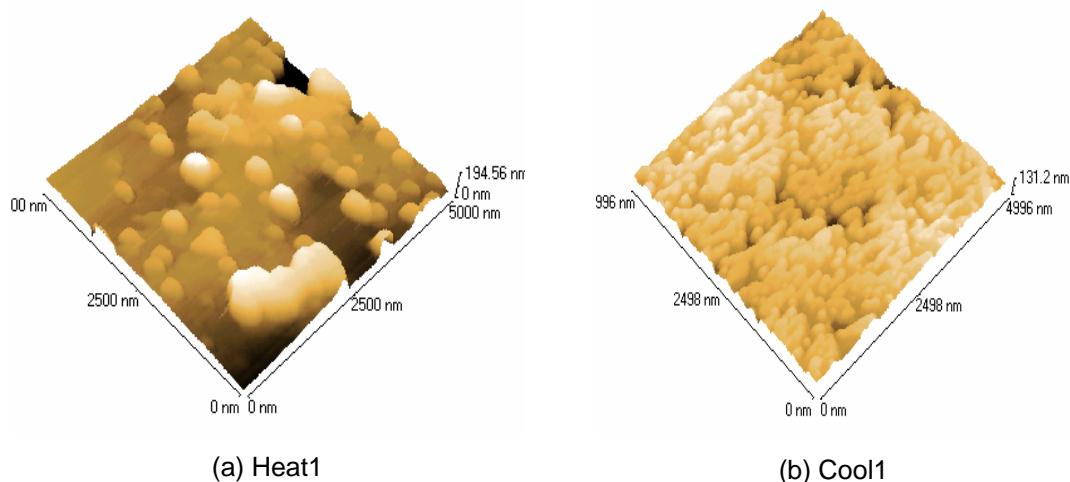
(a) Heat1   (b) Cool1

Figure 7.6 AFM images (5 µm × 5 µm) of (a) Heat1 and (b) Cool1 crystals.

The AFM images of Heat1 and Cool1 crystals with a sample area size of 5 µm × 5 µm are shown in Figure 7.6. It can be seen that the surface of Heat1 crystals consists of nodules of variable sizes with deep valleys. The surface structure of Cool1 crystals, on the other hand, is dominated by tightly packed nodules. These AFM images are consistent with the removal and reappearance of surface features that has been deduced based on the optical microscopy and SEM images. It can be inferred from the images in Figure 7.6 that on heating, the dissolution was proceeded by a pitting and layer-stripping process (Mullin, 2001), which in the end left some sturdy nodules and created valleys on the surface. This prepares the crystal surface with vacancies and kinks. During cooling the supersaturation increases and the growth is facilitated

on the surface features. Based on the image in Figure 7.6(b), the growth of the crystal surface on cooling appears to follow the continuous growth model, which has been briefly described in Chapter 2, section 2.23. The model, also known as the Kossel's model (Mullin, 2001), envisages that loosely adsorbed growth units incorporated into the crystal surface at kinks and the build-up continued until the surface is eventually covered. The loosely adsorbed growth units would be stripped away from the surface during dissolution; hence the crystal surface with the same features as the image in Figure 7.6(a) is expected to reappear at the end of the subsequent heating phase. This observation is also in agreement with the surface-roughening theory (Burton et al., 1951), which suggests that under equilibrium or near-equilibrium growth conditions, surface roughening can take place by the vanishing and rounding of a planar facet. In this case, when the temperature is increased the supersaturation decreases, bringing the system close to equilibrium, which facilitates the roughening mechanism which drives the surface towards a shape with cusp-like surface valleys. The surface roughening phenomenon in organic crystals has been discussed by Bennema (1992) and its application in microelectronics has been intensively studied (Alivisatos, 1998). In a recent study of fat phase crystallisation in milk chocolate, Sonwai and Rousseau (2010) have observed the same phenomenon, which was also promoted by temperature cycling.

The AFM images in Figure 7.6 also reveal that the heights of the crystal's surface features are at the nanometer scale. This information eliminates the signal/chord splitting due to the surface features as one of the possible causes for the FBRM results since as mentioned in Chapter 2, section 2.7.2, the smallest size of chord the FBRM can measure is around 0.5 µm. Thus beam spreading due to the rough surface and signal/chord splitting due to the presence of the sharp edges (which are large enough to be measured by the FBRM as indicated by Figure 7.3(d)) would appear to be causing the fluctuation in the number of coarse.

Figure 7.7 compares the chord length distributions (CLDs) at Heat1 and Cool1. It can be observed that the CLD of Heat1 is relatively narrow with a larger contribution of the coarser chords. Besides having a broader CLD and a larger contribution of the smaller chords, the CLD of Cool1 also has a higher shoulder at the small chord lengths. The trend of these CLDs is consistent with those reported by Pons et al. (2006) in their evaluation study on the effect of faceting on the CLD. They have found that as the

number of facets on a polyhedron increases, the CLD shifts more to the right and the shoulder on the CLD reduces. This is because the increase in the number of facets turns the overall shape of the polyhedron towards a sphere.
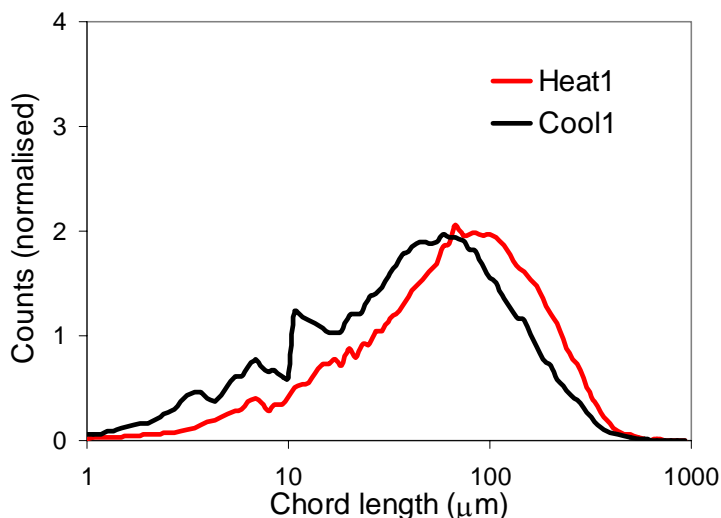
Figure 7.7 A comparison of the unweighted CLDs (normalized to 100) at Heat1 and Cool1.

(a) Heat2 – optical microscopy

(b) Cool2 – optical microscopy

(c) Heat2 - SEM

(d) Cool2 - SEM
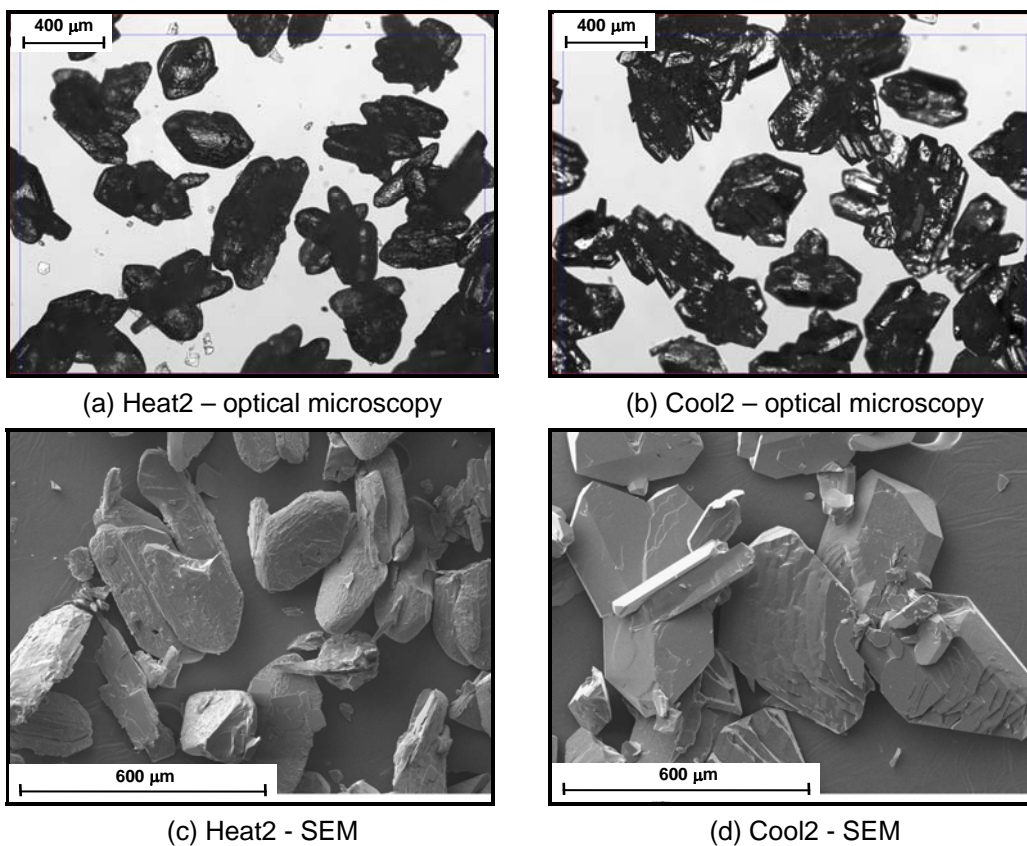
Figure 7.8 Optical microscopy images of (a) Heat2 and (b) Cool2, and SEM images of (c) Heat2 and (d) Cool2 crystals.

Figure 7.8 shows optical microscopy and SEM images of Heat2 and Cool2 crystals. As can be observed from the images, Heat2 and Cool2 crystals exhibit similar properties to Heat1 and Cool1 crystals, respectively. This however should be expected since they are only a temperature cycle away from each other (approximately 30 minutes). The results show the repeatability and consistency of the occurrence of the removal and reappearance of surface features.

(a) Heat3– optical microscopy

(b) Cool3– optical microscopy

(c) Heat3- SEM

(d) Cool3- SEM
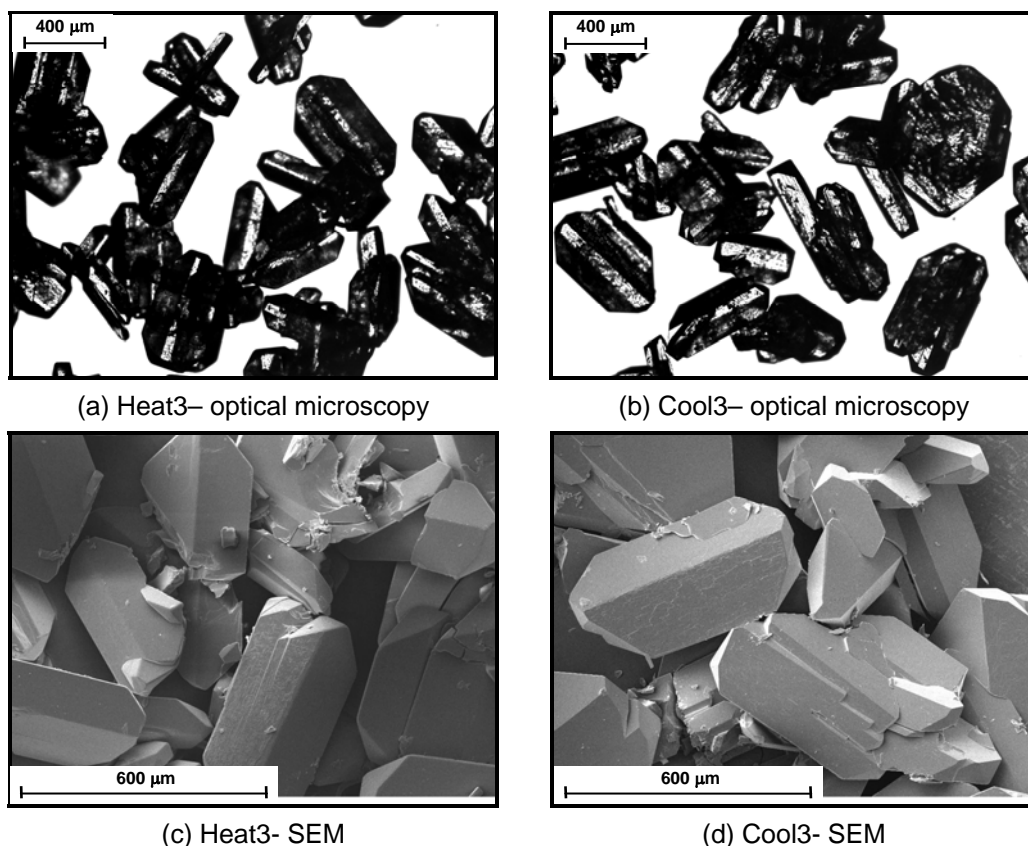
Figure 7.9 Optical microscopy images of (a) Heat3and (b) Cool3 and SEM images of (c) Heat3 and (d) Cool3 crystals.

Optical microscopy and SEM images of Heat3 and Cool3 crystals are presented in Figure 7.9. The crystals were sampled approximately 22 hours after the seed loading and approximately 20 hours after the sampling of Heat2 and Cool2 crystals. For crystals that are suspended in a saturated solution whilst undergoing temperature cycling for 20 to 22 hours, it is expected that they will grow in size. Some increase in average dimension of the crystals can be observed from the optical microscopy images in Figure 7.9(a) and Figure 7.9(b) in comparison to those in Figure 7.8(a) and Figure 7.8(b). In contrast to those of Heat1, Cool1, Heat2 and Cool2 crystals, the optical microscopy and SEM images of Heat3 and Cool3 crystals in Figure 7.9 are

much more similar in their surface appearance. The heating phase did not seem to result in the smoothing or polishing of the surfaces and edges of the crystals and the cooling phase did not appear to cause any growing of surface features. This can be due to the fact that as the process is moving towards lower temperature, the supersaturation keeps reducing until it cannot be consumed in growing surface features anymore. In addition, since the crystals were suspended in the solution for quite a long time, the crystals became aged and hard. As a result, the temperature cycling gave no effect to their surface structure. This may explain the reason why towards the end of the crystallization batch, the amplitude of the fluctuations of both fine and coarse counts/s in response to the temperature change has reduced significantly, as shown in Figure 7.1(c).

(a) Heat4 – optical microscopy   (b) Cool4 – optical microscopy

(c) Heat4 - SEM   (d) Cool4 - SEM
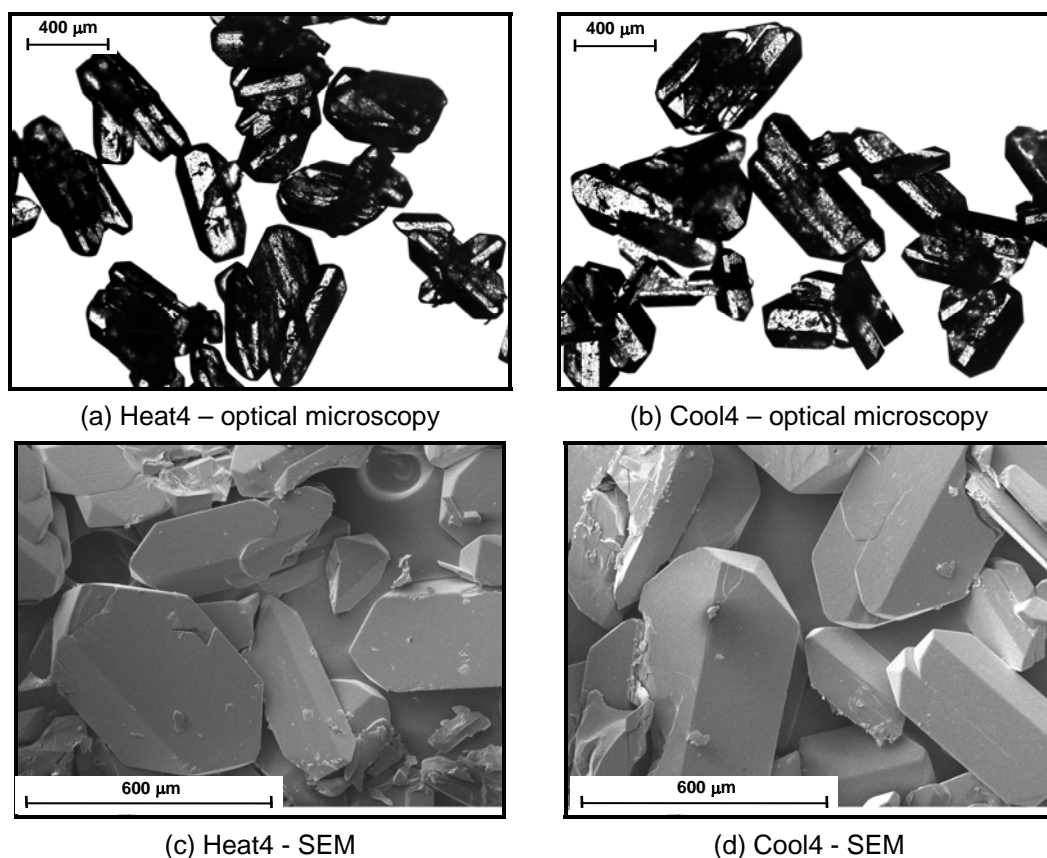
Figure 7.10 Optical microscopy images of (a) Heat4 and (b) Cool4, and SEM images of (c) Heat4 and (d) Cool4 crystals.

Figure 7.10 shows optical microscopy and SEM images of Heat4 and Cool4 crystals. Similar to those of Heat3 and Cool3 crystals, no significant difference in surface appearance can be observed between Heat4 and Cool4 crystals. Based on their SEM images, most crystals have flat surfaces and sharp edges. The AFM images of Heat4

and Cool4 crystals are shown in Figure 7.11. Although the surface of Heat4 crystals seems to be slightly affected by the dissolution process; based on the presence of surface vacancies and kinks that can be observed with a careful examination, the effect however is not as prominent as the one shown by Heat1 crystal in Figure 7.6(a). As mentioned previously, this is probably due to the fact that the maximum temperature during heating phases towards the end of the crystallization run was not high enough to make a great impact to the surface of the already sturdy crystals. No extensive growths are found on the surface of Cool4 crystal, as can be seen in Figure 7.11(b). A possible explanation for this is that the surface nucleation is unlikely to occur at low supersaturation.
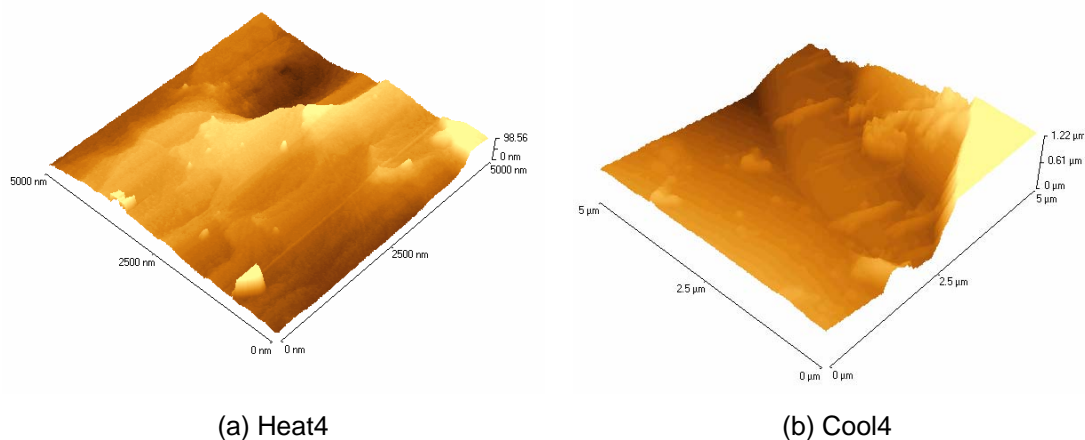
(a) Heat4   (b) Cool4

Figure 7.11 AFM images (5 µm × 5 µm) of (a) Heat4 and (b) Cool4 crystals.
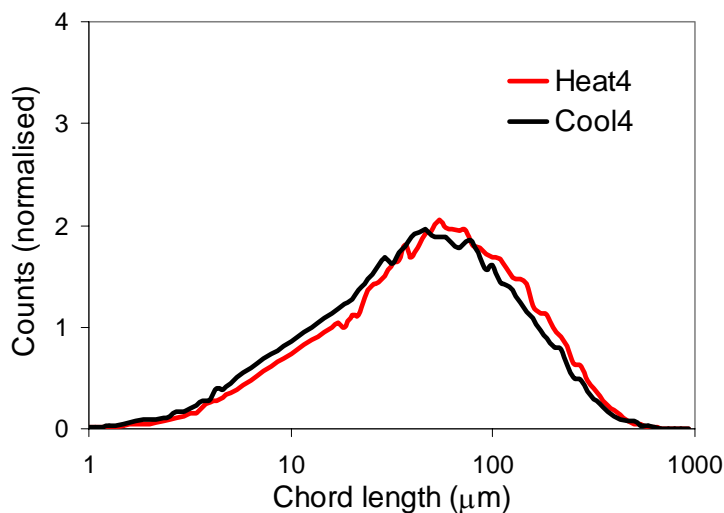
Figure 7.12 A comparison of the unweighted CLDs (normalized to 100) at Heat4 and Cool4. .

Figure 7.12 compares the CLDs at Heat4 and Cool4. It can be seen that although the CLD at point Heat4 is slightly shifted to the right, the difference between them is not as large as the difference between the CLDs at Heat1 and Cool1, shown previously in Figure 7.7. The trend of these CLDs agrees well with the inference made based on the microscopy analyses that Heat4 and Cool4 crystals are very similar in their surface appearance.

Two possible explanations for the out-of-phase profiles of the FBRM's fine and coarse counts/s in response to the temperature change put forward earlier i.e. the signal/chord splitting and the beam spreading, are related to the surface features. There is a possible explanation for the FBRM's result that is independent of the surface features. This explanation is related to the depth of penetration of the FBRM laser beam as a function of crystal size and the number density of crystals. For example, in a suspension of a low concentration of coarse crystals, the laser beam can penetrate far into the medium being measured, which then causes the signal threshold to reduce. This provides a high effective swept volume and allows crystals far away from the focal point, i.e. weaker reflectors, to be measured. The effect of the distance between crystals and the focal point to the FBRM signal is described schematically by Pons et al. (2006) and is shown in Appendix I. If now a high concentration of fine crystals is added to the suspension, the following may occur: (a) due to the volume exclusion effect, the fine crystals tend to be suspended between the probe window and the coarse crystals – this effectively masks the coarse crystals from being in contact with the laser beam. As a result, the FBRM will measure the fine particles rather than the coarse particles; (b) the increase in the solid density will increase the background backscatter level. This in turn causes the signal threshold to increase; which means that it is more difficult to see weakly reflective particles. Since particles that are larger or farther away will be weaker reflectors, it is statistically more likely these will disappear from the measured data; and (c) the increased number of fine crystals will scatter, reflect or absorb the laser light more, which means that the effective penetration depth of the laser is shortened. This consequently will reduce the effective swept volume of the laser, reducing the count rate, especially of the coarse crystals. It is expected that during heating, some of the fine crystals will dissolve and this will expose the coarse crystals to the laser beam; as a result the fine counts/s reduces and the coarse counts/s increases. During cooling, the fine crystals will re-nucleate and subsequently will return to obstruct the coarse crystals from the laser beam; this will

result in an increase in the fine counts/s and a reduction in the coarse counts/s. The phenomenon described above is briefly mentioned by Ruf et al. (2000), in which it was referred to as a masking effect. It is also called a snowstorm effect (Haley, I., personal communication, March 30, 2010) because of its similarity to the visual limitation during a snowstorm when larger objects farther away, which are perfectly visible in clear weather, became difficult to observe or completely invisible due to a dense layer of small snow particles. In the case of very high population of fine particles, they will be very close to each other; hence the difference between the intensity profiles of the backscattered light from the particles in the focal point of the laser beam, or slightly further, will not be significant. This is because in such a case there is a high probability that the laser beam, after passing across one particle, will immediately meet another small particle, which will reflect with minimum intensity, making the differentiation of individual chord lengths difficult. In extreme cases, the continuous reflection with small variations in intensity can be considered by the instrument as noise in an increased signal threshold level and the particles may "disappear" completely from the FBRM measurement. This is similar to the case when very heavy snowfall may appear as a continuous white curtain with indistinguishable snow particles, hindering larger objects farther away. A schematic representation of the snowstorm effect is presented in Figure 7.13.
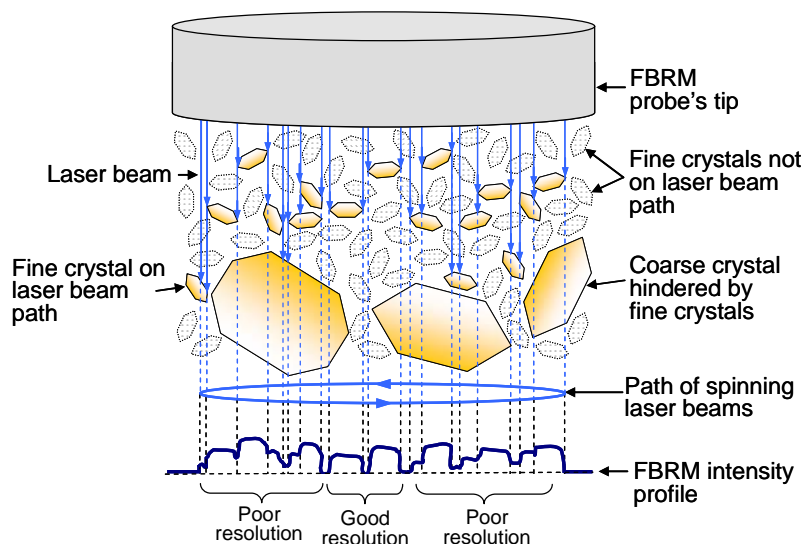
Figure 7.13 A schematic representation of the 'snowstorm' effect.

The snowstorm effect, however, is not the likely cause for the behaviour of the FBRM data produced in this work because of the following reasons: (a) the effect only occurs

when a system has a very high population of very fine crystals compared to the coarse crystals. The count rate of those fine crystals should be in the order of several thousand counts/s (Haley, I., personal communication, March 30, 2010). In this work, the overall count rate of the fine crystals was very low; which was around 200 to 300 count/s (see Figure 7.1). The number is, therefore, insufficient for the snowstorm effect to take place; (b) the fine crystals need to be very small compared to the size of the coarse crystals; their size should be two orders of magnitude smaller than the coarse crystals (Haley, I., personal communication, March 30, 2010). Based on the microscopic images of the crystals (see Figure 7.3, Figure 7.8, Figure 7.9 and Figure 7.10), the identified fine crystals in this work are only a little smaller than the coarse particles. For the snowstorm effect to occur a much greater difference in size is required; and (c) as can be observed from the profiles of the FBRM fine and coarse counts/s shown in Figure 7.1, the number of fine crystals is consistent throughout the experiment; they fluctuated during heating and cooling within the same range. However, the amplitude of the fluctuations in the number of coarse crystals significantly reduced during the experiment. If these fluctuations were caused by the snowstorm effect, they should have been relatively consistent during the entire duration of the experiment, similarly for the consistent fluctuations in the number of fines. The analysis of the potential causes of the observed fluctuations in the FBRM fine and coarse counts indicates that the most likely explanation is based on a combination effect of signal spreading, which is in correlation with changes in surface roughness, and signal/chord splitting, which is in correlation with the formation of sharp edges.

7.4 CONCLUSIONS

The effect of temperature cycling on the surface features of sulfathiazole crystals was investigated using *in situ* FBRM and *ex situ* optical microscopy, SEM and AFM. It was observed that during the initial stage of the crystallization process, during which the average process temperature was higher, the heating phases resulted in crystals with smooth surfaces, while the cooling phases resulted in crystals with features grown on their surfaces. During the final stage of the crystallization process, during which the average process temperature was lower, the effect of both heating phases and cooling phases on the surface appearance of the crystals was not that significant. This is probably because the supersaturation was already depleted and the crystals turned harder. It was also found that the insight into these surface events was detected by

FBRM as a result of a combination of beam spreading caused by changes even at the nanometer scale and signal/chord splitting due to the formation of sharp edges. The study indicates that FBRM may provide useful information related to the potential changes in the surface properties of the crystalline products, which can be used to avoid problems in the downstream processing or in the final product property due to variations in flowability and friability.

CHAPTER 8:
CONCLUSIONS AND FUTURE WORK

This chapter provides an overview of the conclusions that can be drawn from the results of the works presented in this thesis. Some aspects of the works that require further development and improvement, which may form the basis for future investigations, are proposed.

8.1 CONCLUSIONS

The aim of this research project is to develop and apply PAT-based approaches for the monitoring and control of pharmaceutical crystallisation operations to ensure consistent production of the desired quality of APIs for efficient downstream operation and product effectiveness. This aim has been attained through successful achievements of the relevant objectives listed out in Chapter 1 and individually presented in Chapter 2 to Chapter 7. The objectives were to provide a systematic and comprehensive framework for the robust crystallisation operations. The main conclusions of the chapters and thesis are presented below.

In addition to an overview of some aspects of the pharmaceutical crystallisation process as they currently stand, Chapter 2 also presents a comprehensive literature review of the crystallisation and polymorphism of the main model compound, sulfathiazole. This is a part of the objective to gain knowledge and understanding about the formation conditions of the polymorphs, as well as their characteristics, so that these can be accounted for in the crystallisation process design. The work has produced a compilation of literature methods for isolating a particular polymorph and a reconciliation of the various enumerations of the polymorphs that have been in use from 1941 to present.

The crystallisations of sulfathiazole polymorphs using selected literature methods were conducted with their processes monitored and recorded using FBRM and ATR-UV spectroscopy. The availability of the *in situ* process information contributes towards the development of a clear and adequate description of the crystallisation conditions to consistently produce an intended pure sulfathiazole polymorph. Various solid-state characterisation techniques have been utilised to assess the success of these crystallisation processes. With the exception of PXRD, none of the techniques were

able to unambiguously identify the polymorphs. Nonetheless, the combined results of the characterisation studies showed that all of the selected crystallisation methods were able to produce the desired pure polymorphs.

A combined approach of DSC-HSM with image analysis has been introduced and applied in the investigation of sulfathiazole polymorphism. Results showed that the approach is capable of providing a unique insight into the thermal behaviour of the polymorphic system. The capability of image analysis to provide alternative and quantitative ways of presenting the HSM results has also been demonstrated. It translates visual effects, which other characterisation techniques may not be able to provide, into quantitative information. Despite its sensitivity to noise, the light intensity profile obtained from HSM image analysis was found to be capable of describing thermal behaviour of individual crystals and very sensitive to the optical changes happening on the surface of these crystals. The approach contributes to the methods of investigating polymorphism.

The novel DNC approach was introduced and implemented using glycine in water-ethanol mixture as a model system. The approach uses information on nucleation, provided by FBRM, in a feedback control strategy that adapts the process variables, so that the desired quality of product is achieved. In addition, it provides in situ fines removal through the operating policy, rather than having additional equipment and external recycle loops. The approach does not require concentration measurement and has the advantage of being a model-free approach, requiring no information on nucleation or growth kinetics in order to design an operating curve; the system automatically and adaptively detects the boundary of the operating curve. Experimental results demonstrate the benefits of DNC of producing larger crystals with narrower CSD compared to classical operations.

Seeded cooling crystallization with temperature cycling method has been implemented using sulfathiazole in n-propanol and in water as model systems. Results of the experiments showed that the method is capable of accelerating the growth and enhancing the size uniformity of the crystals, in comparison with runs using a simple linear temperature profile, by promoting Ostwald ripening. Although in concept the approach is capable of controlling polymorphic purity of a system, but in practice the effect of solvent-mediated nucleation/growth can be more dominant, as shown by the

results of the experiments. The insights into this behaviour of sulfathiazole crystals were captured very well by FBRM. The study also demonstrated the successful use of a simple non-linear function as a calibration model to relate temperature and absorbance data, obtained using the ATR-UV spectroscopy, to solute concentration during the crystallisation process.

The effect of temperature cycling on the surface features of sulfathiazole crystals was investigated using FBRM and *ex situ* optical microscopy, SEM and AFM. It was observed that during the initial stage of the crystallization process, during which the average process temperature was higher, the heating phases resulted in crystals with smooth surfaces, while the cooling phases resulted in crystals with features grown on their surfaces. These changes on the crystal surface detected by the FBRM as an increase in the number of coarse counts during heating phases and a drop during cooling phases. Laser beam spreading caused by the surface changes and signal/chord splitting due to the formation of sharp edges are offered as an explanation for the FBRM results. The study shows the capability of FBRM to provide useful information with regard to the changes on the surface of the crystalline products. The information can be used to avoid problems in the downstream processing or in the final product property due to variations in flowability and friability, which are related to the crystal surface property.

In general this research project provides a comprehensive framework for the robust crystallisation operations to consistently produce products with the desired quality. This is achieved through the application of PAT, which involves the use of *in situ* analysers for process understanding and process control. The framework is useful in solving some industrially important key challenges in crystallisation, particularly in the control of CSD and polymorphic form. The framework also satisfies the QbD concept, which aspires the incorporation of the process and product knowledge into the process design. Improved control of the pharmaceutical crystallisation processes enhances the production of crystalline APIs, reduces wastage due to failed batches, increases drug product quality, reduces time-to-market and in the end makes new drugs available more quickly and at a lower cost.

8.2 RECOMMENDATIONS FOR FUTURE WORK

The following aspects of the presented works in this thesis could be incorporated in the future works:

a) In the study of sulfathiazole polymorphism, the use of the thermal analysis techniques (DSC, HSM and TG) gave useful results for understanding the polymorphism of the system, but unfortunately they did not unambiguously identify the polymorphs. The use of variable temperature X-ray powder diffractometry (VT-XRPD), a technique where XRD patterns are obtained while the sample is subjected to a controlled temperature change, will be an excellent complement to these thermal analysis techniques. Polymorphic transformation and dehydration events that were inferred from the results of the thermal analysis can be confirmed using VT-XRPD since only diffraction techniques, and in some instances solid-state NMR, can really distinguish unequivocally between the polymorphs.

b) During the implementation of the DNC approach, a suitable automatic control of the solvent/anti-solvent addition or heating and cooling was difficult especially during the initial part of the batch when the first nucleation events were generated. The overshoots and undershoots can be minimized by using an iterative learning control (ILC) approach. The basic principle of ILC is to update the control trajectory for a new batch run using the information from previous batch runs, so that the overall control error would decrease throughout the consecutive batches (Lee and Lee, 2003). The approach would improve performance and would provide increased robustness for industrial implementation.

c) In the implementation of the seeded cooling crystallisation with temperature cycling, the process was driven using a feedback control approach that employs alternating cycles of heating and cooling phases based only on the FBRM readings, so that the number of seed particles is maintained, whilst the dynamic progress of the growth of the seeds in the system is increased. For a more reliable and robust control of polymorphic purity, the utilisation of the supersaturation monitoring and control using the ATR-UV spectroscopy will allow the heating and cooling profiles to be operated and adapted in between the solubility curves of the polymorphs on the phase diagram. This method would lead to a better polymorph control framework.

d) The use of on-line, real-time image analysis of the in-process video microscopy, such as Mettler Toledo's process vision measurement (PVM), could provide an automatic way of detecting changes in surface features and lead to the development of better crystallisation control approaches, which would take additional properties of the product into account in addition to CSD, morphology and polymorphic form.

REFERENCES

Aaltonen, J.; Rantanen, J.; Siiriä, S.; Karjalainen, M.; Jrgensen, A.; Laitinen, N.; Savolainen, M.; Seitavuopio, P.; Louhi-Kultanen, M.; Yliruus, J., (2003), "Polymorph screening using near-infrared spectroscopy", *Anal. Chem.*, 75 (19), pp. 5267 -5273.

Abbas, A.; Nobbs, D.; Romagnoli, J. A., (2002), "Investigation of on-line optical particle characterization in reaction and cooling crystallization systems. Current state of the art", Meas. Sci. Technol., 13, pp. 349–356.

Abu Bakar, M. R.; Nagy, Z. K.; Rielly, C. D. J., (2010), "A combined approach of differential scanning calorimetry and hot-stage microscopy with image analysis in the investigation of sulfathiazole polymorphism", Therm. Anal. Calorim., 99, pp. 609-619.

Abu Bakar, M. R.; Nagy, Z. K.; Saleemi, A. N.; Rielly, C. D., (2009), "The impact of direct nucleation control on crystal size distribution in pharmaceutical crystallization processes", Cryst. Growth Des., 9(3), pp. 1378-1384.

Abu Bakar, M. R.; Nagy, Z. K.; Rielly, C. D., (2009), "Seeded batch cooling crystallization with temperature cycling for the control of size uniformity and polymorphic purity of sulfathiazole crystals", Org. Process Res. Dev., 13, pp. 1343-1356.

Aldridge, S., (2007), "The shape shifter", Chemistry World (www.chemistryworld.org), pp. 64-70.

Ali, H. R. H.; Edwards, h. G. M.; Scowen, I. J., (2009), "Insight into thermally induced solid-state polymorphic transformation of sulfathiazole using simultaneous in situ Raman spectroscopy and differential scanning calorimetry", J. Raman Spectrosc., 40, pp. 887–892.

Alivisatos, A. P., (1996), "Semiconductor clusters, nanocrystals, and quantum dots", Science, 271, pp. 933−937.

Alvarez, A. J.; Singh, A.; Myerson, A. S., (2009), "Polymorph screening: comparing a semi-automated approach with a high throughput method", Cryst. Growth Des., 9 (9), pp. 4181–4188.

Anderson, J.E.; Moore, S.; Tarczynski, F.; Walker, D., (2001), "Determination of the onset of crystallization of N1-2-(thiazolyl)sulfanilamide (sulfathiazole) by UV-Vis and calorimetry using an automated reaction platform; subsequent characterization of polymorphic forms using dispersive Raman spectroscopy", *Spectrochimica Acta Part A*, 57(9), pp.1793-1808.

Anwar, J.; Tarling, S.E.; Barnes, P., (1989), "Polymorphism of sulphathiazole", *J. Pharm. Sci.*, 78 (4), pp. 337-342.

Apperley, D.C., Fletton, R.A., Harris, R.K., Lancaster, R.W., Tavener, S., Threlfall, T.L., Sulfathiazole Polymorphism Studied by Magic-Angle Spinning NMR, *J. Pharm. Sci.*, 1999, 88(12), 1275-1280.

Atkins, P.; de Paula, J., (2005), *Elements of physical chemistry*, 4th ed., Oxford University Press.

Babilev, F. V.; Belskii, V. K.; Simonov, Y. A.; Arzamastev, A. P., (1987), "Polymorphism of Norsulphazol", Khim-Farm. Zh., 21, pp. 1275-1280.

Barrett , P., and Glennon, B. (2002). "Characterizing the Metastable Zone width and solubility curve using Lasentec FBRM and PVM." *Trans IChemE, Part A*, 80, pp. 799-805.

Barrett, P.; Smith, B.; Worlitschek, J.; Bracken, V.; O'Sullivan, B.; O'Grady, D., (2005), "A review of the use of process analytical technology for the understanding and optimization of production batch crystallization processes". *Organic Process Research & Development*, 9, pp. 348-355.

Barth, H. G.; Sun, S. T., (1985), "Particle size analysis", Anal. Chem., 57(5), pp. 151R - 175R.

Barthe, S.; Rousseau, R. W., (2006), "Utilization of focused beam reflectance measurement in the control of crystal size distribution in a batch cooled crystallizer", Chem. Eng. Technol., 29 (2), pp. 207-211.

Beckmann, W., (1999), "Nucleation phenomena during the crystallisation and precipitation of Abecarnil ",J. Cryst. Growth, 198/199, pp.1307-1314.

Beckmann, W., (2000), "Seeding the desired polymorph: background, possibilities, limitations, and case studies", Org. Proc. Res. Dev., 4(5), pp. 372–383.

Beckmann, W.; Otto, W.; Budde, U., (2001), "Crystallisation of the stable polymorph of hydroxytriendione: seeding process and effects of purity", Org. Proc. Res. Dev., 2001, 5 (4), pp. 387-392.

Beckmann, W., (2003), "Crystallization of pharmaceutical compounds - polymorphs, pseudo-polymorphs and particle formation", Eng. Life Sci., 3, pp. 113-120.

Bennema, P., (1994), "Theory of growth and morphology applied to organic crystals; possible applications to protein crystals", J. of Crystal Growth, 122, pp. 110 - 119.

Berglund, K. A., (2002), "Analysis and measurement of crystallization utilizing the population balance", in: *Handbook of industrial crystallization,* Myerson, A. S. (ed.), 2nd ed., Butterworth-Heinemann, pp. 101 – 113.

Bermingham, S. K., (2003), "A design procedure and predictive models for solution crystallisation processes - development and application, Dissertation: Technical University Delft, Delft University Press, Delft.

Bernstein, J., (2002), Polymorphism in molecular crystals, Clarendon Press, Oxford.

Billmeyer Jr., F. W., (1971), Textbook of polymer science, 2nd ed., John Wiley & Sons, New York and London, pp. 173-174.

Billot, P.; Couty, M.; Hosek, P., (2010), "Application of ATR-UV spectroscopy for monitoring the crystallisation of UV absorbing and non-absorbing molecules", Org. Process Res. Dev., 14 (3), pp 511–523

Birch, M.; Fussel, S. J.; Higginson, P. D.; McDowall, N.; Marziano, I., (2005), "Towards a PAT-based strategy for crystallisation development", Org. Pro. Res. Dev., 9, pp. 360-364.

Bingham, A. L., Hughes, D. S., Hursthouse, M. B., Lancaster, R. W., Tavener, S., Threlfall, T. L., (2001), "Over one hundred solvates of sulfathiazole", Chem. Commun., 7, pp. 603-604.

Blagden, N., (2001), "Crystal engineering of polymorph appearance: the case of sulphathiazole", *Powder Technology*, 2001, 121, pp. 46-52.

Blagden, N., Davey, R. J., Lieberman, H. F., Williams, L., Payne, R., Roberts, R., Rowe, R., Docherty, R., (1998a), "Crystal chemistry and solvent effects in polymorphic systems: sulfathiazole", *J. Chem. Soc., Faraday Trans.*, 94(8), pp. 1035-1044.

Blagden, N., Davey, R. J., Rowe, R., Roberts, R., (1998b), "Dissappearing polymorphs and the role of reaction by-products: the case of sulfathiazole", *Int. J. Pharm.*, 172, pp. 169-177.

Boistelle, R.; Astier, J. P., (1988), "Crystallization mechanisms in solution", J. Cryst. Growth, 90, pp. 14-30.

Braatz, R. D.; Hasebe, S., (2001), "Particle Size and Shape Control in Crystallization Processes, *Chemical Process Control - VI*, J. B. Rawlings, B. A. Ogunnaike, and J. W. Eaton, eds., *AIChE Symposium Series*, 97(326).

Braatz, R. D., (2002), "Advanced control of crystallization processes". Annu. Rev. Control, 26 (1), pp. 87-99.

Brittain, H. G., (2006), Methods for the characterization of polymorphs and solvates, in: Polymorphism: in the pharmaceutical industry, Hilfiker, R. (ed.), Wiley-VCH Verlag GmbH & Co., pp. 226 – 271.

Brittain, H.G.; Byrn, S.R. (1999). Structural aspects of polymorphism, in: *Polymorphism in pharmaceutical solids*, Brittain, H.G. (ed.), Marcel Dekker Inc., New York, USA, pp. 73-124.

Brittain, H.G. (1999). "Methods for the characterization of polymorphs and solvates, in: *Polymorphism in pharmaceutical solids*, Brittain, H.G. (ed.), Marcel Dekker Inc., New York, USA, pp. 227-278.

Bugay, D. E., (2001), "Characterization of the solid-state: spectroscopic techniques", Adv. Drug Del. Rev., 48, pp. 43–65.

Burger, A.; Dialer, R. D., (1983), "Neu untersuchungsergebnisse zur polymorphie von sulfathiazole", *Pharm. Acta Helv.*, 1983, 58(3), 72-78.

Burton, W. K.; Cabrera, N.; Frank, F. C., (1951), "The growth of crystals and the equilibrium structure of their surfaces. Philos. Trans. A243, pp. 299-358.

Caillet, A.; Puel, F.; Fevotte, G., (2007), "Quantitative in situ monitoring of citric acid phase transition in water using Raman spectroscopy, In press, Chem. Eng. Process.

Calderon De Anda, J.; Wang, X. Z.; Lai, X.; Roberts, K. J., (2005), "Classifying organic crystals via in-process image analysis and the use of monitoring charts to follow polymorphic and morphological changes", J. Proc. Control, 15, pp. 785–797.

Cardew, P. T.; Davey, R. J., (1985), "The kinetics of solvent-mediated phase transformations". Proc. R. Soc. London, A 398, pp. 415-428.

Carless, J. E.; Foster, A. A., "Accelerated crystal growth of sulfathiazole by temperature cycling", J. Pharm. Pharmacol., 18, pp. 697-708.

Carless, J. E.; Jordan, D., (1974), "The dissolution kinetics of sulfathiazole form I", J. Pharm. Pharmacol., 26, Suppl., 86P-87P.

Carstensen, J. T. Pharmaceutical principles of solid dosage forms. 1993, Technomic Publishing Co., Inc.

Castle, J. E.; Zhdan, P. A. J., (1997), "Characterization of surface topography by SEM and SFM: problems and solutions", Phys. D: Appl. Phys., 30, pp. 722-740.

Chan, F. C.; Anwar, J.; Cernik, R.; Barnes, P.; Wilson, R. M., (1999), "Ab initio structure determination of sulfathiazole polymorph V from synchrotron X-ray powder diffraction data", J Appl Crystallogr., 32, pp. 436-441.

Chen, C.-C.; Song, Y., (2004), "Solubility modeling with a non-random two-liquid segment activity coefficient model", Ind. Eng. Chem. Res., 43, pp. 8354-8362.

Chew, J. W., Black, S. N., Chow, P. S., Tan, R. B. H., (2007a), "Comparison between open-loop temperature control and closed-loop supersaturation control for cooling crystallization of glycine", Ind. Eng. Chem. Res., 46, pp. 830-838.

Chew, J. W.; Chow, P. S.; Tan, R. B. H., (2007b), "Automated in-line technique using FBRM to achieve consistent product quality in cooling crystallization", Cryst. Growth Des. 7(8), pp. 1416-1422.

Choi, Y. J.; Chung, S. T.; Oh, M.; Kim, H. S., (2005), "Investigation of crystallization in a jet Y-mixer by a hybrid computational fluid dynamics and process simulation approach", Cryst. Growth Des., 5, pp. 959-968.

Choong, K. L. & Smith, R., (2004), "Optimization of batch cooling crystallization", Chemical Engineering Science, 59, pp. 313–327.

Clas, S-D., Dalton, C. R.; Hancock, B. C., (1999), "Differential scanning calorimetry: applications in drug development", PSTT, 2, PP. 311–320.

Connolly, M.;Debenedetti, P. G.;Tung, H. H., (1996), "Freeze crystallization of imipenem", J. of Pharm. Sciences, 85, 2, pp.174 - 177.

Costa, C.B.B.; Filho, R.M., (2005), "Evaluation of optimisation techniques and control variable formulations for a batch cooling crystallization process", Chemical Engineering Science, 60, pp. 5312–5322.

Dalton, J. B.; Schmidt, C. L. A., (1933), "The solubilities of certain amino acids in water, the densities of their solutions at twenty-five degrees and the calculated heats of solution and partial molal volumes", Journal of Biological Chemistry, 103, pp. 549-578.

Davey, R. & Garside, J., (2000), *From molecules to crystallizers. An introduction to crystallization.* Oxford University Press.

Desiraju, G. R., (2003), "Crystal and co-crystal", CrystEngComm, 5, pp. 466-467.

Doki, N.; Seki, H.; Takano, K.; Asatani, H.; Yokota, M.; Kubota, N., (2004a), "Process control of seeded batch cooling crystallization of the metastable alpha-form glycine using an in-situ ATR-FTIR spectrometer and an in-situ FBRM particle counter", Cryst. Growth Des., 4 (5), pp. 949-953.

Doki, N.; Yokota, M.; Kido, K.; Sasaki, S.; Kubota, N., (2004b), "Reliable and selective crystallization of the metastable α-form glycine by seeding", Cryst. Growth Des., 4 (1) pp. 103– 107.

Doyle W. M. & Tran, L., (1999), "UV analysis of strongly absorbing chromophores by UV-visible ATR spectroscopy", Spectroscopy, 14(4), pp. 46-54.

Doyle, W. M., (2005), "A beginner's guide to industrial spectroscopic analysis", Technical notes, Axiom Analytical, Inc. website (www.goaxiom.com).

Drake, B.; Prater, C.; Weisenhorn, A.; Gould, S.; Albrecht, T.; Quate, C.; Cannell, D.; Hansma, H.; Hansma, P., (1989), "Imaging crystals, polymers, and processes in water with the atomic force microscope", Science, 243, pp. 1586-1589.

Drebushchak, T. N.; Boldyreva, E. V.; Mikhailenko, M. A., (2008), "Crystal structures of sulfathiazole polymorphs in the temperature range 100-295 K: a comparative analysis", Zhurnal Strukturnoi Khimii, 49, pp. 84-94.

Dunn, M.S.; Ross, F.J., (1935), "Quantitative investigations of amino acids and peptides. IV. The solubilities of the amino acids in water-ethyl alcohol mixtures", *J. Biol. Chem.,* 125(1), pp. 309.

Dunuwila, D.D.; Berglund, K.A., (1997), "ATR FTIR spectroscopy for in situ measurement of supersaturation", J. Cryst. Growth, 179, pp.185–193.

Etter, m. C., (1991), "Hydrogen bonds as design elements in organic chemistry", J. Phys. Chem., 95 (12), pp 4601–4610.

Falcon, J. A.; Berglund, K. A. (2003), "Monitoring of antisolvent addition crystallization with Raman spectroscopy", Cryst. Growth Des., 3 (6), pp. 947-952

Feng, L. L.; Berglund, K. A., (2002), "ATR-FTIR for determining optimal cooling curves for batch crystallization of succinic acid", Cryst. Growth Des., 2 (5), pp. 449-452.

FDA, (2004), "PAT guidance for industry—a framework for innovative pharmaceutical development, manufacturing and quality assurance", http://www.fda.gov/downloads/Drugs/GuidanceComplianceRegulatoryInformation/Guidances/ucm070305.pdf, (Accessed June 28, 2010).

FDA, (2006), "Guidance for industry, Q8 pharmaceutical development", http://www.fda.gov/downloads/RegulatoryInformation/Guidances/ucm128029.pdf, (Accessed June 28, 2010).

Fosbinder, R. J.; Walter, L. A. (1939), "Sulfanilamido derivatives of heterocyclic amines". J. Am. Chem. Soc., 61, pp. 2032-2033.

Frank, T. C.; Downey, J. R.; Gupta, S. K., (1999), "Quickly screen solvents for organic solids", Chem. Eng. Prog., 95 (12), pp. 41-61.

Fredenslund, A.; Gmehling, J.; Rasmussen, P., (1977), Vapor-Liquid Equilibria Using UNIFAC - A Group Contribution Method, Elsevier Scientific, Amsterdam.

Fujiwara, M., Chow, P.S., Ma, D.L. and Braatz, R.D., (2002), "Paracetamol crystallisation using laser backscattering and ATR-FTIR spectroscopy: metastability, agglomeration and control", Cryst. Growth Des., 2(5), pp. 363–370.

Fujiwara, M.; Nagy, Z. K.; Chew, J. W.; Braatz, R. D., (2005), "First principles and direct design approaches for the control of pharmaceutical crystallization". J. Process Control, 15 (5), 493-504.

Garside, J., (1985), "Industrial crystallization from solution", Chemical Eng. Science, 40 (1), pp. 3-26

Gelbrich, T.; Hughes, D. S.; Hursthouse, M. B.; Threlfall, T. L., (2008),"Packing similarity in polymorphs of sulfathiazole", CrystEngComm., 10, pp. 1328 - 1334.

Geppi, M.; Mollica, G.; Borsacchi, Silvia, A.; Carlo, A. V., (2008), "Solid-State NMR Studies of Pharmaceutical Systems", Applied Spectroscopy Reviews, 43: 3, pp. 202-302.

Gmehling, J.; Li, J. D.; Schiller, M., (1993), "A modified UNIFAC model. 2. Present parameter matrix and results for different thermodynamic properties", Ind. Eng. Chem. Res., 32, pp. 178.

Gillon, A. L.; Steele, G.; Nagy, Z. K.; Makwana, N.; Rielly, C. D., (2006), "PAT investigations into the crystallization of caffeine", 13th International Workshop on Industrial Crystallization (BIWIC 2006), Delft, The Netherlands.

Giron, D., (2003), "Monitoring of polymorphism - from detection to quantification", Engineering in Life Sciences, 3 (3), 103-112.

Giron D., (1998), "Contribution of thermal methods and related techniques to the rational development of pharmaceuticals - part 1", PSTT, 1, PP. 191–199.

Giulietti, M., Seckler, M.M., Derenzo, S., Ré, M. I., & Cekinski E., (2001), "Industrial crystallization and precipitation from solutions: state of the technique", Braz. J. Chem. Eng., 18 (4), pp. 423-440.

Gracin, S., Brinck, T., and Rasmuson, A. C., (2002), "Prediction of solubility of solid organic compounds in solvents by UNIFAC", Ind. Eng. Chem. Res. 41, pp. 5114–5124.

Grant, D. J. W., (1999), "Theory and origin of polymorphism", in: *Polymorphism in pharmaceutical solids*, Brittain, H. G. (ed.), Marcel Dekker Inc., New York, pp.1 – 34.

Grove, D. C.; Keenan, G. L. (1941), "The dimorphism of sulfathiazole". J. Am. Chem. Soc., 63, pp. 97-99.

Guillory, J. K., (1967), "Heats of transition of methylprednisolone and sulfathiazole by a differential thermal analysis method.", J. Pharm. Sci., 56, pp. 72-76.
Gutwald, T.; Mersmann, A. Batch cooling crystallization at constant supersaturation: Technique and experimental results. Chem. Eng. Technol. 1990, 13 (1), 229-237.

Hakkinen, A.; Pollanen, K.; Karjalainen, M.; Rantanen, J.; Loui-Kultanen, M.; Nystrom, L., Batch cooling crystallization and pressure filtration of sulfathiazole: the influence of solvent composition, *Biotechnol. Appl. Biochem.*, 2005, 41(1), 17-28.

Hansma, P. K.; Elings, V. B.; Marti, O.; Bracker, C. E., (1989), "Scanning tunneling microscopy and atomic force microscopy: application to biology and technology", Science, 242, pp. 209-216.

Heath, A. R.; Fawell, P. D.; Bahri, P. A.; Swift, J. D., (2002), "Estimating average particle size by focused beam reflectance measurement (FBRM)", Part. Part. Syst. Charact., 19, pp. 84-95.

Hermanto, M.W.; Chiu, M.-S.; Woo, X.Y; Braatz, R.D., (2007), "Robust optimal control of polymorphic transformation in batch crystallization.", AIChE J. 2007, 53, 2643-2650

Higuchi, W. I.; Bernardo, P. D.; Mehta, S. C., (1967), " Polymorphism and drug availability. II. Dissolution rate behavior of the polymorphic forms of sulfathiazole and methylprednisolone.", J. Pharm. Sci., 56, pp. 200-207.

Hilfiker, R.; Blatter, F.; von Raumer, M., Relevance of solid-state properties for pharmaceutical products, in: Polymorphism: in the pharmaceutical industry, Hilfiker, R. (ed.), Wiley-VCH Verlag GmbH & Co., 2006, 1 – 18.

Hixson, A. W.; Knox, K. L. (1951), "Effect of agitation on rate of growth of single crystals", Ind. Eng. Chem. 1951, 43, pp. 2144 - 2151.

Ho, R.; Wilson, D. A.; Heng, J. Y. Y., (2009), "Crystal Habits and the Variation in Surface Energy Heterogeneity", Cryst. Growth Des., 9 (11), pp. 4907–4911.

Hohne, G. W. H.; Hemminger, W. F.; Flammersheim, H. –J., Differential scanning calorimetry, Springer, 2003.

Howard, K. S.; Nagy, Z. K.; Saha, B.; Roberston, A. L.; Steele, G.; Martin, D., (2009), "A process analytical technology based investigation of the polymorphic transformations during the antisolvent crystallization of sodium benzoate from IPA/water mixture ", Cryst. Growth Des., 9, pp. 3964-3975.

Hu, Q.; S. Rohani, S.; Wang, D.X.; Jutan, A., (2005), "Optimal control of a batch cooling seeded crystallizer", Powder Technology, 156, pp.170 – 176.

Hughes, D. S.; Hursthouse, M. B.; Threlfall, T.; Tavener, S., A new polymorph of sulfathiazole, *Acta Cryst. C*, 1999, C55, 1831-1833.

Hukkanen, E. J., Braatz, R. D., (2003), "Measurement of particle size distribution in suspension polymerzation using in situ laser backscattering", Sensors and Actuators B96, pp. 451-459.

Jones, A. G., (2002), *Crystallization Process Systems*, Butterworth-Heinemann.

Jordan, D.; Carless, J. E., (1976), "The crystallization behaviour of sulfathiazole", J. Pharm. Pharmacol., 28, pp. 410-414.

Kahlweit, M., (1975), "Ostwald ripening of precipitates", Adv. Colloid Inter. Sci. 5, pp. 1-35.

Kail, N.; Briesen, H.; Marquardt, W., (2008), "Analysis of FBRM measurements by means of a 3D optical model, Powder Technology, 185, 3, pp. 211-222.

Karjalainen, M., Airaksinen, S., Rantanen, J., Aaltonen, J., Yliruusi, J., (2005), "Characterization of polymorphic solid-state changes using variable temperature X-ray powder diffraction.", J. Pharm.Biomed. Anal., 39, pp. 27-32

Karpinski, P. H., (2006), "Polymorphism of active pharmaceutical ingredients", *Chem. Eng. Technol.*, 29 (2), pp. 233 – 237.

Kee, N. C. S.; Arendt, P. D.; Tan, R. B. H.; Braatz, R. D., (2009a), "Selective crystallization of the metastable anhydrate form in the enantiotropic pseudo-dimorph system of l-phenylalanine using concentration feedback control", Cryst. Growth and Des., 9, pp. 3052–3061.

Kee, N. C. S.; Tan, R. B. H.; Braatz, R. D., (2009b), "Selective crystallization of the metastable α-form of l-glutamic acid using concentration feedback control", Cryst. Growth and Des., 9, pp. 3044–3051.

Khoshkhoo, S. and Anwar, J., (1993), "Crystallization of polymorphs: the effect of solvent", *J. Phys. D Appl. Phys.*, 26, pp. 890-893.

Kim, K-J.; Mersmann, A., (2001), 'Estimation of metastable zone width in different nucleation processes', Chemical Engineering Science, 56, pp. 2315-2324.

Kobayashi, R.; Fujimaki, Y.; Ukita, T.; Hiyama, Y., (2006), "Monitoring of solvent-mediated polymorphic transitions using in situ analysis tools", Org. Proc. Res. Dev., 10, pp. 1219-1226.

Kougoulos, E.; Jones, A.G.; Jennings, K.H.; Wood-Kaczmar, M.W., (2005), "Use of focused beam reflectance measurement (FBRM) and process video imaging (PVI) in a modified mixed suspension mixed product removal (MSMPR) cooling crystallizer", J. of Cryst. Growth, 273 (3-4), pp. 529-534.

Kruger, G. J.; Gafner, G., (1971), "The crystal structure of sulfathiazole II". Acta Crystallogr. B, 27, 326-333.

Kruger, G. J.; Gafner, G., (1972), "The crystal structures of polymorphs I and II of sulphathiazole", Acta Crystallogr. B, 28, pp. 272-283.

Kubota, N.; Doki, N.; Yokota, M.; Sato, A., (2001), "Seeding policy in cooling crystallization", *Powder Tech.,* 121, pp. 31–38.

Kuhnert-Brandstätter, M., Wunsch, S., (1969), Polymorphism and mixed crystal formation in sulfonamides and related compounds. Mikrochim Acta, 6, pp. 1297-1307.

Lagas, M., Lerk, C.F., The polymorphism of sulphathiazole, *Int. J. Pharm.*, 1981, 8, 25-33.

Lee, K. S.; Lee, J. H., (2003), "Iterative learning control-based batch process control technique for integrated control of end product properties and transient profiles of process variables", J. of Process Control, 13, 607-621.

Lever, T., (2007), Optimizing DSC experiments. In: Craig D. Q. M., Reading, M. (eds.), Thermal analysis of pharmaceuticals. Boca Raton, USA: CRC Press; 2007. pp. 24–51.

Lewiner, F.; Fevotte, G.; Klein, J. P.; Puel, F., (2001), "Improving batch cooling seeded crystallization of an organic weed-killer using on-line ATR FTIR measurement of supersaturation". J. Cryst. Growth, 226 (2-3), 348-362.

Lewiner, F.; Fevotte, G.; Klein, J. P.; Puel, F., (2002), "An online strategy to increase the average crystal size during organic batch cooling crystallization", Ind. Eng. Chem. Res., 41, pp. 1321-1328.

Li, M.Z.; Wilkinson, D., (2005), "Determination of non-spherical particle size distribution from chord length measurements. Part 1: Theoretical analysis", Chem Eng Sci, 60(12), pp. 3251–3265.

Lin, S. W.; Ng, K. M. and Wibowo, C. Integrative approach for polymorphic crystallization process synthesis. *Ind. Eng. Chem. Res.*, 46 (2007) 518-529.

Liotta, V.; Sabesan, V., (2004), "Monitoring and feedback control of supersaturation using ATR-FTIR to produce an active pharmaceutical ingredient of a desired crystal size". Org. Process Res. Dev., 8 (3), pp. 488-494.

Liu, X.; Hatziavramidis, D.; Arastoopour, H.; Myerson, A. S., (2006), "CFD simulations for analysis and scale-up of anti-solvent crystallization", AIChE J., 52, 10, pp. 3621-3625.

Loffelmann, M.; Mersmann, A., (2002), 'How to measure supersaturation?', Chemical Engineering Science, 57, pp. 4301-4310.

Lol Mi Lung-Somarriba, B., Moscosa-Santillan, M., Porte, C., Delacroix, A., (2004), "Effect of seeded surface area on crystal size distribution in glycine batch cooling crystallization : a seeding methodology.", J. Cryst. Growth 270 (2004), p. 624.

Lott, W. A.; Bergeim, F. H., (1939), "2-(p-Aminobenzenesulfonamido)-thiazole: a new chemotherapeutic agent", J. Am. Chem. Soc., 61, pp. 3593-3594.

Luner, P. E.; Majuru, S.; Seyer, J. J.; Kemper, M. S., (2000), "Quantifying crystalline form composition in binary powder mixtures using near-infrared reflectance spectroscopy.", Pharm. Dev. Technol., 5, pp. 231-246.

Ma, Z.; Merkus, H. G.; van der Veen, H. G.; Wong, M.; Scarlett, B., (2001), "On-line Measurement of Particle Size and Shape using Laser Diffraction", Part. Part. Syst. Charact., 18, pp. 243–247.

Mangin, D.; Puel, F.; Veesler, S., (2009), "Polymorphism in processes of crystallization in solution: a practical review", Org. Process Res. Dev., 13, pp. 1241–1253.
Marthi, K. A. M.; Pokol, G.; Tomor, K.; Eross-Kiss, K. J., (1992) "DSC studies on the polymorphism and pseudopolymorphism of pharmaceutical substances: A complex system for studying physico-chemical behaviour of binary mixtures", J. Therm. Anal., 38, pp. 1017–1025.

Matthews, H. B.; Rawlings, J.B., (1998), "Batch crystallization of a photochemical modeling, control and filtration", AIChE Journal, 44, pp. 1119–1127.

Maxwell, J. C., (1998), A treatise on electricity and magnetism.Vol.1., 3rd ed., Oxford;New York, Clarendon Press..

Mccrone, W. C., (1965), Polymorphism. In: D. Fox, M. M. Labes, and A. Weissberger (eds.), Physics and Chemistry of the Organic Solid State, Vol. 2, pp. 725-767.

Mersmann, A., (1999), "Crystallization and precipitation", Chemical Engineering and Processing, 38, pp. 345–353.

Mesley, R., (1971), "The polymorphism of sulfathiazole", J. Pharm. Pharmacol., 23, pp. 687-694.

Mesley R. J.; Houghton E. E., (1967), "Infrared identification of pharmaceutically important sulfonamides with particular reference to the occurrence of polymorphism", J. Pharm. Pharmacol. 19 (1967), pp. 295–304.

Mettler Toledo, Lasentec® D600 - with FBRM® Technology, Hardware Manual, 2006.

Miller, S. M.; Rawlings, J. B., (1994), "Model identification and control strategies for batch cooling crystallizers", A.I.Ch.E. Journal, 40, pp. 1312–1327.

Miller, R. P.; Sommer, G. , (1966), ""A hot stage microscope incorporating a differential thermal analysis unit.", J. Sci. Instrum., 43, pp. 293–297.

Milosovich, G. J . (1964), "Determination of solubility of a metastable polymorph. ", Pharm. Sci., 53, pp. 484-487.

Miyazaki, H., (1947), "Polymorphism and melting points of sulfathiazoles". Jpn. J. Pharm. Chem., 19, pp. 133-134.

Modarresi, H.; Conte,E.; Abildskov, J.; Gani, R.; Crafts, P., (2008), "Model-based calculation of solid solubility for solvent selections - a review", Ind. Eng. Chem. Res. 2008, 47, pp. 5234–5242.

Mohameed, H.A.; Abdel-Jabbar, N.; Takrouri, K.; Nasr, A., (2003), "Model-based optimal cooling strategy for batch crystallization processes", Chem. Eng. Res. Des., 81, pp. 578–584.

Morris, K. R., (1999), "Structural aspects of hydrates and sovates", in: *Polymorphism in pharmaceutical solids*, Brittain, H.G. (ed.), Marcel Dekker Inc., New York, USA, pp.125-182.

Mougin, P.; Thomas, A.; Wilkinson, D.; White, G., (2003), "On-line monitoring of a crystallization process", AIChE J., 49 (2), pp. 373-378.

Mougin, P.; Wilkinson, D.; Roberts, K. J., (2002), "In situ measurement of particle size during the crystallization of L-glutamic acid under two polymorphic forms: influence of crystal habit on ultrasonic attenuation measurements," Cryst. Growth Des., 2, pp. 227.

Moustafa, M. A.; Carless, J. E., Application of differential scanning calorimetry to the study of sulfathiazole crystal forms, *J. Pharm. Pharmac.*, 1969, 21, 359-365.

Mullin, J. W., (2001), *Crystallization*, 4th ed., Butterworth and Co (Publishers) Ltd.

Myerson, A. S.; Ginde, R., (2002), "Crystals, crystal growth, and nucleation", in: *Handbook of industrial crystallization*, Myerson, A. S. (ed.), 2nd ed., Butterworth-Heinemann, pp. 33 – 65.

Mullin, J. W.; Gaska, C., (1969), "The growth and dissolution of potassium sulphate crystals in a fluidized bed crystallizer", Can. J. Chem. Engng, 47, pp. 483-489.

Myerson, A. S. (2002), Handbook of Industrial Crystallization;Butterworth-Heinemann Ltd: Oxford.

Nagy, Z. K.; Fujiwara, M.; Braatz, R. D. (2008a), "Modelling and control of combined cooling and antisolvent crystallization processes", J. Process Control, 18, pp. 856–864.

Nagy Z. K.; Fujiwara M.; Woo X., Braatz R., (2008b), "Determination of the kinetic parameters for the crystallization of paracetamol from water using metastable zone width experiments", Ind. Eng. Chem. Res., 47, pp. 1245-1252.

Nagy, Z.K., Gillan, A.L., Steele, G., Makwana, N. and Rielly, C.D., (2007), "Using process analytical technology for in situ monitoring of the polymorphic transformation of organic compounds", Proceedings of the 8th International Symposium on Dynamics and Control of Process Systems (DYCOPS), 3, B. Foss and J. Alvarez, IFAC, Cancum, Mexico, pp. 133-138.

Nagy, Z. K.; Fujiwara, M.; Braatz, R. D., (2006a), "Optimal control of combined cooling and anti-solvent pharmaceutical crystallization", 13th International Workshop on Industrial Crystallization (BIWIC 2006), Delft, The Netherlands.

Nagy, Z. K.; Fujiwara, M.; Braatz, R. D., (2006b), "Recent advances in the modeling and control of cooling and antisolvent crystallization of pharmaceuticals", 8th International IFAC Symposium on Dynamics and Control of Process Systems, Cancun, Mexico, 2, pp. 29-38.

Nagy, Z. K. & Braatz, R.D., (2004a), "Open-loop and closed-loop robust optimal control of batch processes using distributional and worst-case analysis". *J. of Process Control,* 14, pp. 411-422.

Nagy, Z. K.; Chew, J.W.; Fujiwara, M.; Braatz, R.D., (2004b), "Advances in the modeling and control of batch crystallizers". in *Proc. of the 7th IFAC Symp. On Advanced Control of Chemical Processes*, Elsevier Scientific, Oxford, UK, pp. 83-90.

Nagy, Z. K.; Braatz, R.D., (2003), "Robust nonlinear model predictive control of batch processes", AIChE J., 49 (7), pp. 1776-1786.

Nonoyama, N.; Hanaki, K.; Yabuki, Y., (2006), "Constant Supersaturation Control of Antisolvent-Addition Batch Crystallization", Org. Proc. Res. & Dev., 10, pp. 727-732.

Nozaki, Y.; Tanford, C., (1971), "The solubility of amino acids and two glycine peptides in aqueous ethanol and dioxane solutions. Establishment of a hydrophobicity scale", J. Biol. Chem., 246, pp. 2211–2217.

O'Grady, D., Barrett, M., Casey, E.; Glennon, B., (2007), "The effect of mixing on the metastable zone width and nucleation kinetics in the anti-solvent crystallization of benzoic acid. *Trans IChemE*, 85 (A7), pp.945-952.

O'Grady, D.; Glennon, B., (2005), "Use of in-situ instrumentation to characterize anti-solvent addition crystallization". *AIChE Annual Meeting*, Cincinnati, USA.

Ono, T., ter Horst, J.H. and Jansens, P.J., (2004), "Quantitative measurement of the polymorphic transformation of L-glutamic acid using in-situ Raman spectroscopy", Crys. Growth Des., 4(3), pp. 465-469.

O'Sullivan, B.; Barrett, P.; Hsiao, G.; Carr, A.; Glennon, B., (2003), "In situ monitoring of polymorphic transitions", Org. Proc. Res. Dev., 7, pp. 977-982.

O'Sullivan, B. & Glennon, B., (2005), "Application of in situ FBRM and ATR-FTIR to the monitoring of the polymorphic transformation of D-mannitol", Org. Pro. Res. & Dev., 9, pp. 884-889

Parmar, M. M.; Khan, O.; Seton, L.; Ford, J. L., (2007), "Polymorph selection with morphology control using solvents", Crystal Growth & Design, 7 (9), pp 1635–1642.

Parsons, A. R.; Black, S. N.; Colling, R., (2003), "Automated measurement of metastable zones for pharmaceutical compounds", Trans IChemE, 81, A, pp. 700-704.

Patchigolla, K.; Wilkinson, D., (2009), "Crystal shape characterisation of dry samples using microscopic and dynamic image analysis", Particle & Particle Systems Characterization, 26(4), pp. 171 – 178.

Patience, D. B. & Rawlings, J. B., (2001), "Particle-shape monitoring and control in crystallization processes", AIChE J., 47 (9), pp. 2125-2130.

Patience, D. B.; Dell'Orco, P. C.; Rawlings, J.B., (2004), "Optimal operation of a seeded pharmaceutical crystallization with growth-dependent dispersion", Org. Process Res. Dev., 8(4), pp. 609–615.

Paul, E. L.; Tung, H.; Midler, M., (2005), "Organic crystallization processes", Powder Technology, 150 (2), pp. 133-143.

Perry, R.H., Green, D.W., Maloney, J.O., 1984. Perry's Chemical Engineers' Handbook, 6th ed. McGraw-Hill, New York, pp. 3–88.

Pollanen, K. (2006). Monitoring of crystallization processes by using infrared spectroscopy and multivariate methods, Lappeenranta, Finland.

Pollanen, K.; Hakkinen, A.W.; Reinikainen, S.P.; Louhi-Kultanen, A.; Nystrom, L., "A study on batch cooling crystallization of sulphathiazole—process monitoring using ATR-FTIR and product characterization by automated image analysis", Chem. Eng. Res. Des., 2006, 84, pp. 47–59.

Pons, M-N.; Milferstedt, K.; Morgenroth, E., (2006), "Modeling of chord length distributions", Chem. Eng. Sci., 61, pp. 3962-3973.

Puel, F.; Marchal, P.; Klein, J., (1997), "Habit transient analysis in industrial crystallization using two dimensional crystal sizing technique", Chem. Eng. Res. Des. 75, pp. 193-205.

Qu, H., (2007), Towards desired crystalline product properties: in-situ monitoring of batch crystallization, Lappeenranta.

Rastogi, S., Zakrzewski, M., Suryanarayanan, R., (2001), "Investigation of solid-state reactions using variable temperature X-ray powder diffractometry. I. Aspartame hemihydrate", Pharm. Res., 18 (3), pp. 267-273.

Rawlings, J. B., Miller, A. G., and Witkowaski, W. R., (1993), "Model identification and control of solution crystallization processes: A review." *Ind. Eng. Chem. Res*, 32, pp.1275-1296.

Reutzel-Edens, S. M. (2006), "Achieving polymorph selectivity in the crystallization of pharmaceutical solids: Basic considerations and recent advances", Curr. Opin. Drug Discovery Dev., 9, pp. 806-815.

Rodriguez-Hornedo, N., Murphy, D., (1999), "Significance of controlling crystallization mechanisms and kinetics in pharmaceutical systems", J. Pharm. Sci., 88 (7), pp. 651-660.

Rodrıguez-Spong, B.; Price, C. P.; Jayasankara, A.; Matzgerb, A. J.; Rodrı´guez-Hornedoa, N., (2004), "General principles of pharmaceutical solid polymorphism: a supramolecular perspective". Advanced Drug Delivery Reviews 56, 241– 274.

Roelands, C. P. M.; Jiang, S.; Kitamura, M.; ter Horst, J. H.; Kramer, H. J. M.; Jansens, P. J., (2006), "Antisolvent crystallization of the polymorphs of L-histidine as a function of supersaturation ratio and of solvent composition", Cryst. Growth Des., 6 (4), pp. 955-963.

Rogers, R. D., (2003), "Introduction: polymorphism in crystals", Cryst. Growth Des., 3, pp. 867.

Ruf, A.; Worlitschek, J.; Mazzotti, M., (2000), Modelling and experimental analysis of PSD measurements through FBRM. Part. Part. Syst. Charact., 17, pp. 167-179.

Scholl, J.; Bonalumi, D.; Vicum, L.; Mazzotti, M.; Muller, M., (2006), "In situ monitoring and modeling of the solvent-mediated polymorphic transformation of L-glutamic acid". Cryst. Growth Des., 6 (4), 881-891.

Seddon, K. R., (2004), "Pseudopolymorph: a polemic", Cryst. Growth Des., 4, pp. 1087.

Sessiecq, P.; Gruy, F.; Cournil, M., (2000), "Study of ammonium chloride crystallization in a mixed vessel", J. Cryst. Growth, 208, pp. 555-568.

Shaikh, A.A.; Salman, A.D.; Mcnamara, S.; Littlewood, G.; Ramsay, F.; Hounslow, M.J., (2005), "In situ observation of the conversion of sodium carbonate to sodium carbonate monohydrate in aqueous suspension". Ind. Eng. Chem. Res., 44(26), pp. 9921-9930.

Shaktshneider, T. P.; Boldyrev, V. V., (1993), "Phase transformations in sulfathiazole during mechanical activation", Drug Dev. Int. Pharm., 19, pp. 2055-2067.

Shami, E. G., Bernardo, P. D., Rattie, E. S., Ravin, L. J., (1972), "Kinetics of polymorphic transformation of sulfathiazole form I", J. Pharm. Sci., 61(8), pp. 1318-1320.

Shekunov, B. Y.; York, P., (2000), "Crystallization processes in pharmaceutical technology and drug delivery design", J. Crystal Growth, 211, pp. 122-136.

Shenouda, L. S., (1970), "Various species of sulfathiazole form I", J. Pharm. Sci. 59 (1970), pp. 785–787.

Simon, L. L.; Nagy, Z. K.; Hungerbuehler K., (2009), "Comparison of external bulk video imaging with focused beam reflectance measurement and ultra-violet visible spectroscopy for metastable zone identification in food and pharmaceutical crystallization processes", Chemical Engineering Science, 64, pp. 3344-3351.

Sonwai, S. and Rousseau, D., (2010), 'Controlling fat bloom formation in chocolate – Impact of milk fat on microstructure and fat phase crystallisation', Food Chemistry, 119, pp. 286–297.

Stapley, A. G. F.; Himawan, C.; MacNaughtan, W.; Foster, T. J., (2009), "A computational method for extracting crystallization growth and nucleation rate data from hot stage microscope images", Crystal Growth & Design, 9 (12), pp. 5061-5068.

Starbuck, C., Spartalis, A., Wai, L., Wang, J., Fernandez, P., Lindemann, C.M., Zhou, G.X. and Ge, Z.H., (2002), „Process optimisation of a complex pharmaceutical polymorphic system via in situ Raman spectroscopy, Crystal Growth & Design, 2(6), pp. 515–522.

Stephenson, G. A.; Forbes, R. A.; Reutzel-Edens, S. M., (2001), "Characterization of the solid state: quantitative issues", Adv. Drug Del. Rev., 48, pp. 67–90.

Sudo, S.; Sato, R.; Harano, Y; Ogo, Y. Chem. Eng. Jpn. 1991, 24, 237-242.

Tadayyon, A. & Rohani, B. (1998) Determination of Particle Size Distribution by Par-Tec® 100: Modeling and Experimental Results. Part. Part. Syst. Charact. 15, pp. 127-135.

Tai, C. Y.; Wu, J. F.; Rousseau, R. W., (1992), "Interfacial supersaturation, secondary nucleation, and crystal growth,"J. Crystal Growth, 116, pp. 294-306.

Tavare, N.S., (1995), *Industrial Crystallization*, 112–118 (Plenum Press, New York, USA).

Thompson, D.; Kougoulos, E.; Jones, A.; Wood-Kaczmar, M. J., (2005), "Solute concentration measurement of an important organic compound using ATR-UV spectroscopy", J. Cryst. Growth, 276, pp. 230-236.

Threlfall, T. L., (1995), "Analysis of organic polymorphs. A review", *Analyst,* 1995, 120, pp. 2435 – 2460.

Titiz-Sargut, S.; Ulrich, J., (2002), 'Influence of additives on the width of the metastable zone', Crystal Growth & Design, 2, pp. 371-374.

Togkalidou, T.; Fujiwara, M.; Patel, S.; Braatz, R. D., (2001), "Solute concentration prediction using chemometrics and ATR-FTIR spectroscopy", J. Cryst. Growth, 231 (4), pp. 534-543.

Togkalidou, T.; Tung, H. H.; Sun, Y. K.; Andrews, A.; Braatz, R. D., (2002), "Solution concentration prediction for pharmaceutical crystallization processes using robust chemometrics and ATR FTIR spectroscopy". Org. Process Res. Dev., 6 (3), pp. 317-322.

Tóth, J.; Kardos-Fodor, A.; Halász-Péterfi, S., (2005), "The formation of fine particles by salting-out precipitation", Chem. Eng. Processing, 44, pp. 193–200

Vankeirsbilck, T., Vercauteren, A., Baeyens, W., Van der Weken G., Verpoort F., Vergote G., Remon J.P., (2002), "Applications of Raman spectroscopy in pharmaceutical analysis", Trends in Analytical Chemistry, 21 (12), pp. 869-877.

Variankaval, N.; Cote, A. S.; Doherty, M. F., (2008), "From form to function: crystallization of active pharmaceutical ingredients", AIChE J., 54(7), pp. 1682-1688.

Verma, A. R. & Krishna, P. (1966), *Polymorphism and polytypism in crystals*, John Wiley & Sons, Inc.

Vippagunta, S. R.; Brittain, H. G.; Grant, D. J.W., (2001), "Crystalline solids", Advanced Drug Delivery Reviews 48, pp. 3–26.

Vitez, I.M., Newman, A.W., Davidovich, M., Kiesnowski, C., The evolution of hot-stage microscopy to aid solid-state characterizations of pharmaceutical solids, *Thermochimica Acta*, 1998, 324, 187-196.

Vitez, I.M., Newman, A.W., Thermal microscopy, in: Thermal analysis of pharmaceuticals, Craig, D.Q.M. & Reading, M. (ed.), CRC Press, 2007, 221-264.

Wang, F., Wachter, J.A., Antosz, F.J. and Berglund, K.A., (2000), "An investigation of solvent mediated polymorphic transformation of progesterone using in situ Raman spectroscopy", Org. Proc. Res. Dev., 4(5), pp. 391–395.

Wang, X.Z.; De Anda, J.C.; Roberts, K.J.; Li, R.F.; Thomson, G.B.; White, G., (2005), "Advances in on-line monitoring and control of the morphological and polymorphic forms of organic crystals grown from solution", KONA, 23, pp. 69-85.

Wang, X. Z.; Roberts, K. J.; Ma, C., (2008), "Crystal growth measurement using 2D and 3D imaging and the perspectives for shape control", Chem. Eng. Sci., 63, pp.1173–1184.
Warrington, S. B., (2002), Simultaneous thermal analysis techniques. In: Haines, P. J., (ed.), Principles of thermal analysis and calorimetry, Cambridge: The Royal Society of Chemistry; pp. 166–89.

Warstat, A. & Ulrich, J., (2006), "Seeding during batch cooling crystallization – an initial approach to heuristic rules", Chem. Eng. Technol., 29 (2), pp. 187-190.

Wieckhusen, D., (2008), Designing Robust Crystallization Processes for Active Pharmaceutical Ingredients—From Art to Science, in: Process Chemistry in the Pharmaceutical Industry, Vol. 2, Challenges in an Ever Changing Climate, Gadamasetti, K.; Braish, T. (ed.), CRC Press, pp. 295-312.

Witt, W.; Köhler, U.; List, J. (2004), "Direct imaging of very fast particles opens the application of the powerful (dry) dispersion for size and shape characterization", PARTEC, Nürnberg.

Woo, X.Y., Tan, R.B.H., Chow, P.S., Braatz, R.D., (2006), "Simulation of mixing effects in antisolvent crystallisation using a coupled CFD-PDF-PBE Approach". *Crystal Growth & Design,* 6**,** pp. 1291-1303.

Worlitschek, J.; Hocker, T.; Mazzotti, M., (2005), "Restoration of PSD from chord length distribution data using the method of projections onto convex sets", Part. & Part. Systems Charact., 22 (2), pp. 81-98.

Wynn, E.J.W., (2003), "Relationship between particle-size and chord-length distributions in focused beam reflectance measurement: stability of direct inversion and weighting. Powder Technology, 133, 125-133.

Yang, G. (2005). Control and simulation of batch crystallization, Lappeenranta, Finland.

Yang, G.; Kubota, N.; Sha, Z.; Louhi-Kultanen, M.; Wang, J., (2006a), "Crystal shape control by manipulating supersaturation in batch cooling crystallization", *Cryst. Growth Des.,* 6 (12), pp. 2799-2803.

Yang, G.; Louhi-Kultanen, M.; Sha, Z.; Kallas, J., (2006b), "Determination of operating conditions for controlled batch cooling crystallization". *Chemical Engineering and Technology,* 29, pp. 200-205.

Yi, Y. J. & Myerson, A. S., (2006), "Laboratory scale batch crystallization and the role of vessel size", Chem. Eng, Res. Des., 84(A8), pp. 721-728.

Yu, L. X., (2008), "Pharmaceutical quality by design: product and process development, understanding, and control", Pharm. Res., 25, pp. 781-791.

Yu, L., (2007), "Survival of the fittest polymorph: how fast nucleater can lose to fast grower", CrystEngComm, 9, pp. 847–851.

Yu, L.; Reutzel, S. M.; Stephenson, G. A,. (1998), "Physical characterization of polymorphic drugs: an integrated characterization strategy", Pharm Sci Tech Today, 1, pp. 118–127.

Yu, L. X., Lionbergera, R. A., Rawa, A. S., D'Costa, R., Wub, H., and Hussain, A. S. (2003), "Applications of process analytical technology to crystallization processes." Adv. Drug Delivery Rev., 56 (3), pp. 349-369.

Yu, W., Erickson, K., (2008), "Chord length characterization using focused beam reflectance measurement probe - methodologies and pitfalls, Powder Technology, 185, pp. 24-30.

Yu, Z. Q., Tan, R. B. H., Chow, P. S., (2005), "Effects of operating conditions on agglomeration and habit of paracetamol crystals in anti-solvent crystallization", J. Cryst. Gro., 279, pp. 477–488.

Yu, Z. Q.; Chow, P. S.; Tan, R. B. H., (2006a), "Application of attenuated total reflectance-Fourier transform infrared (ATR-FTIR) technique in the monitoring and control of anti-solvent crystallization". Ind. Eng. Chem. Res., 45 (1), 438-444.

Yu, Z.Q.; Chow, P.S.; Tan, R.B.H., (2006b), "Seeding and constant supersaturation control by ATR-FTIR in anti-solvent crystallization", Organic Process Research & Development, 10(4), pp. 717–722.

Yu, Z.Q.; Chew, J. W.; Chow, P.S.; Tan, R.B.H., (2007), "Recent advances in crystallization control: an industrial perspective", Chem. Eng. Res. Des., 85(A7), pp. 893–905.

Zeitler, J. A.; Newnham, D. A.; Taday, P. F.; Threlfall, T. L.; Lancaster, R. W.; Berg, R. W.; Strachan, C. J.; Pepper, M.; Gordon, K. C.; Rades, T., (2006), "Characterization of temperature-induced phase transitions in five polymorphic forms of sulfathiazole by terahertz pulsed spectroscopy and differential scanning calorimetry", J. Pharm. Sci., 95(11), pp. 2486-2498.

Zhang, G. G. Z., Law, D., Schmitt, E. A. & Qiu, Y., (2004), "Phase transformation considerations during process development and manufacture of solid oral dosage forms", Adv. Drug Delivery Rev., 56 (3), pp. 371-390.

Zhang, G.P. & Rohani, S., (2003), "On-line optimal control of a seeded batch cooling crystallizer", Chem Eng Sci, 58(9), pp. 1887–1896.

Zhou, G. X., Fujiwara, M., Woo, X. Y., Rusli, E., Tung, H., Starbuck, C., Davidson, O., Ge, Z., Braatz, R. D., (2006), "Direct design of pharmaceutical antisolvent crystallization through concentration control", Cryst. Growth Design, 6 (4), pp. 892 - 898.

Zhu, Y.; Demilie, P.; Davoine, P.; Delplancke-Ogletree, M., (2004), "Application of density meter in the supersaturation determination of the two-component equilibrium systems", J. Cryst. Growth, 263, pp. 459–465.

APPENDIX A

Crystallographic data for sulfathiazole in Cambridge Structural Database

Table A1 Refcode, cell data and reference for the structures of sulfathiazole polymorphs from the Cambridge Structural Database (retrieved 22 April 2010).

Refcode	Cell data		Reference
Suthaz	<table><tr><td>**Lengths**</td><td colspan="2">**Angles**</td></tr><tr><td>a 8.235</td><td>alpha</td><td>90</td></tr><tr><td>b 8.55</td><td>beta</td><td>93.67</td></tr><tr><td>c 15.558</td><td>gamma</td><td>90</td></tr></table>	System: Monoclinic Space group: P21/c Space group number: 14 R-factor=.038 Z=4 Calculated cell volume=1093.181	Kruger and Gafner, 1971
Suthaz01	<table><tr><td>**Lengths**</td><td colspan="2">**Angles**</td></tr><tr><td>a 10.554</td><td>alpha</td><td>90</td></tr><tr><td>b 13.22</td><td>beta</td><td>108.06</td></tr><tr><td>c 17.05</td><td>gamma</td><td>90</td></tr></table>	System: Monoclinic Space group: P21/c Space group number: 14 R-factor=.069 Z=8 Calculated cell volume=2261.680	Kruger and Gafner, 1972
Suthaz02	<table><tr><td>**Lengths**</td><td colspan="2">**Angles**</td></tr><tr><td>a 17.57</td><td>alpha</td><td>90</td></tr><tr><td>b 8.574</td><td>beta</td><td>112.93</td></tr><tr><td>c 15.583</td><td>gamma</td><td>90</td></tr></table>	System: Monoclinic Space group: P21/c Space group number: 14 R-factor=.063 Z=8 Calculated cell volume=2162.008	Kruger and Gafner, 1972
Suthaz03	<table><tr><td>**Lengths**</td><td colspan="2">**Angles**</td></tr><tr><td>a 8.239</td><td>alpha</td><td>90</td></tr><tr><td>b 15.556</td><td>beta</td><td>90</td></tr><tr><td>c 8.592</td><td>gamma</td><td>86.34</td></tr></table>	System: Monoclinic Space group: P1121/b Space group number: 14 R-factor=.028 Z=4 Calculated cell volume=1098.955	Babilev et al., 1987
Suthaz04	<table><tr><td>**Lengths**</td><td colspan="2">**Angles**</td></tr><tr><td>a 10.867</td><td>alpha</td><td>90</td></tr><tr><td>b 11.456</td><td>beta</td><td>90</td></tr><tr><td>c 8.543</td><td>gamma</td><td>91.87</td></tr></table>	System: Monoclinic Space group: P1121/n Space group number: 14 R-factor=.031 Z=4 Calculated cell volume=1062.972	Babilev et al., 1987
Suthaz05	<table><tr><td>**Lengths**</td><td colspan="2">**Angles**</td></tr><tr><td>a 10.399</td><td>alpha</td><td>90</td></tr><tr><td>b 15.132</td><td>beta</td><td>91.21</td></tr><tr><td>c 14.28</td><td>gamma</td><td>90</td></tr></table>	System: Monoclinic Space group: P21/n Space group number: 14 R-factor=.046 Z=8 Calculated cell volume=2246.566	Hughes et al., 1999

Suthaz06	Lengths		Angles		System: Monoclinic Space group: P21/n Space group number: 14 R-factor=.094 Z=8 Calculated cell volume=2285.129	Chan et al., 1999
	a	14.3296	alpha	90		
	b	15.2733	beta	91.052		
	c	10.4428	gamma	90		

Suthaz07	Lengths		Angles		System: Monoclinic Space group: P21/c Space group number: 14 R-factor=.029 Z=8 Calculated cell volume=2227.375	Drebushchak et al., 2008
	a	10.5006	alpha	90		
	b	12.96	beta	107.653		
	c	17.176	gamma	90		

Suthaz08	Lengths		Angles		System: Monoclinic Space group: P21/c Space group number: 14 R-factor=.061 Z=8 Calculated cell volume=2280.890	Drebushchak et al., 2008
	a	10.534	alpha	90		
	b	13.388	beta	107.943		
	c	17	gamma	90		

Suthaz09	Lengths		Angles		System: Monoclinic Space group: P21/c Space group number: 14 R-factor=.028 Z=4 Calculated cell volume=1076.523	Drebushchak et al., 2008
	a	8.1896	alpha	90		
	b	8.532	beta	94.139		
	c	15.447	gamma	90		

Suthaz10	Lengths		Angles		System: Monoclinic Space group: P21/c Space group number: 14 R-factor=.055 Z=4 Calculated cell volume=1099.488	Drebushchak et al., 2008
	a	8.2394	alpha	90		
	b	8.5952	beta	93.689		
	c	15.5575	gamma	90		

Suthaz11	Lengths		Angles		System: Monoclinic Space group: P21/a Space group number: 14 R-factor=.046 Z=8 Calculated cell volume=2116.277	Drebushchak et al., 2008
	a	15.504	alpha	90		
	b	8.494	beta	112.76		
	c	17.427	gamma	90		

Suthaz12	Lengths		Angles		System: Monoclinic Space group: P21/a Space group number: 14 R-factor=.059 Z=8 Calculated cell volume=2165.108	Drebushchak et al., 2008
	a	15.602	alpha	90		
	b	8.562	beta	112.95		
	c	17.601	gamma	90		

Suthaz13	Lengths		Angles		System: Monoclinic Space group: P21/n Space group number: 14 R-factor=.064 Z=4 Calculated cell volume=1047.441	Drebushchak et al., 2008
	a	10.82	alpha	90		
	b	8.494	beta	91.86		
	c	11.403	gamma	90		

Suthaz14	Lengths		Angles		System: Monoclinic Space group: P21/n Space group number: 14 R-factor=.075 Z=4 Calculated cell volume=1064.955	Drebushchak et al., 2008
	a	10.879	alpha	90		
	b	8.55	beta	91.97		
	c	11.456	gamma	90		

Suthaz15	Lengths		Angles		System: Monoclinic Space group: P21/n Space group number: 14 R-factor=.046 Z=8 Calculated cell volume=2246.566	Gelbrich et al., 2008
	a	10.399	alpha	90		
	b	15.132	beta	91.21		
	c	14.28	gamma	90		

Suthaz16	Lengths		Angles		System: Monoclinic Space group: P21/c Space group number: 14 R-factor=.04 Z=8 Calculated cell volume=2230.814	Gelbrich et al., 2008
	a	10.534	alpha	90		
	b	12.936	beta	107.77		
	c	17.191	gamma	90		

Suthaz17	Lengths		Angles		System: Monoclinic Space group: P21/c Space group number: 14 R-factor=.049 Z=8 Calculated cell volume=2120.004	Gelbrich et al., 2008
	a	17.448	alpha	90		
	b	8.498	beta	112.81		
	c	15.511	gamma	90		

Suthaz18	Lengths		Angles		System: Monoclinic Space group: P21/c Space group number: 14 R-factor=.031 Z=4 Calculated cell volume=1077.203	Gelbrich et al., 2008
	a	8.193	alpha	90		
	b	8.538	beta	94.01		
	c	15.437	gamma	90		

Suthaz19	Lengths		Angles		System: Monoclinic Space group: P21/n Space group number: 14 R-factor=.038 Z=4 Calculated cell volume=1036.507	Gelbrich et al., 2008
	a	10.774	alpha	90		
	b	8.467	beta	91.65		
	c	11.367	gamma	90		

Suthaz20	Lengths		Angles		System: Not given Space group: Space group number: R-factor=0 Z=0 Calculated cell volume=1081.039	Parmar et al., 2007
	a	8.18	alpha	90		
	b	8.56	beta	94.18		
	c	15.48	gamma	90		

Suthaz21	Lengths		Angles		System: Not given Space group: Space group number: R-factor=0 Z=0 Calculated cell volume=2180.375	Parmar et al., 2007
	a	17.4	alpha	90		
	b	8.5	beta	112		
	c	15.9	gamma	90		

Suthaz22	Lengths		Angles		System: Not given Space group: Space group number: R-factor=0 Z=0 Calculated cell volume=1071.104	Parmar et al., 2007
	a	10.9	alpha	90		
	b	8.56	beta	89.6		
	c	11.48	gamma	90		

Suthaz23	Lengths		Angles		System: Not given Space group: Space group number: R-factor=0 Z=0 Calculated cell volume=2280.930	Parmar et al., 2007
	a	10.45	alpha	90		
	b	13.27	beta	107		
	c	17.2	gamma	90		

APPENDIX B

PXRD patterns for sulfathiazole raw material from Sigma

Figure B1 PXRD pattern of sulfathiazole raw material from Sigma in comparison with some major reflections in the reference pattern of Form III (Suthaz12).
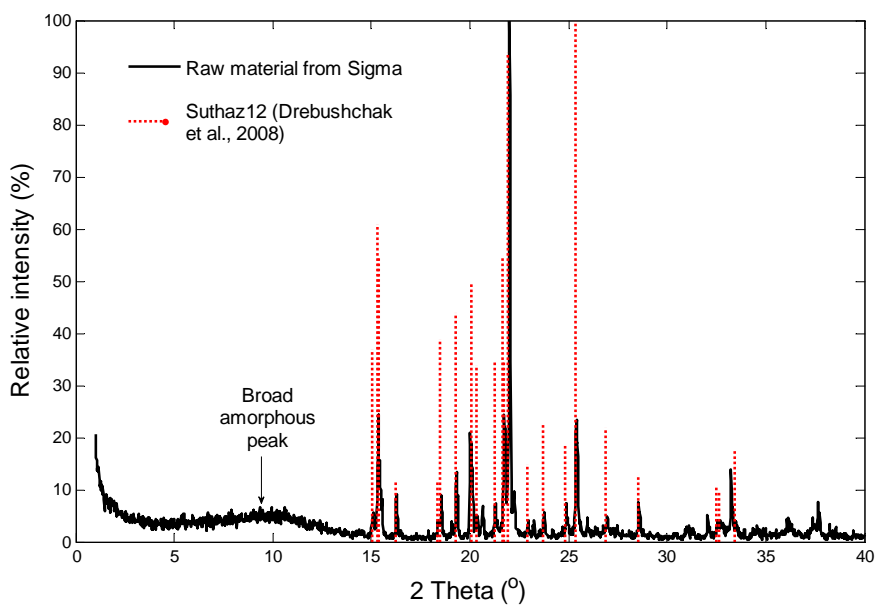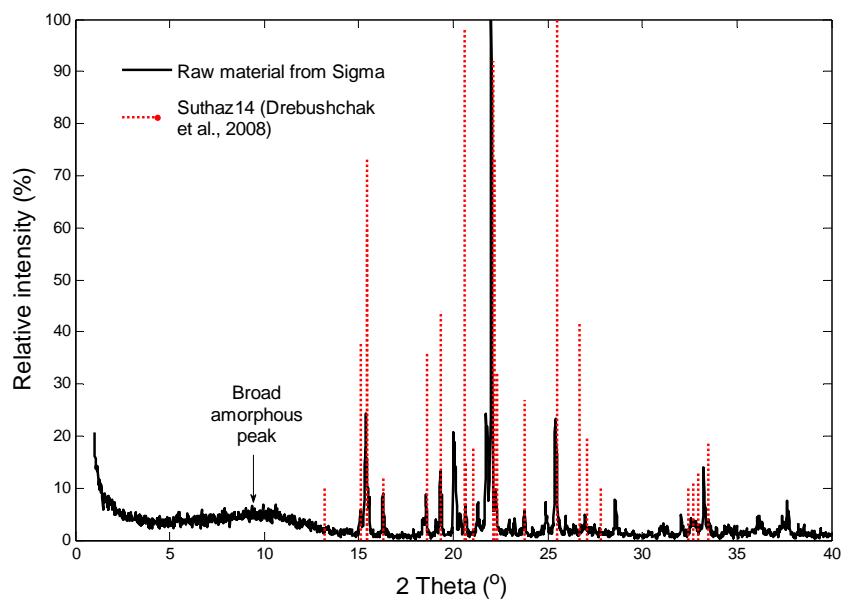

Figure B2 PXRD pattern of sulfathiazole raw material from Sigma in comparison with some major reflections in the reference pattern of Form IV (Suthaz14).

The PXRD patterns for sulfathiazole raw material from Sigma shown in Figure B1 and B2 concur very well with the reference patterns for Form III and Form IV crystals, respectively. The material is therefore expected to contain a mixture of Form III and Form IV. The material is also expected to contain amorphous since broad peaks between 1° to 14° were normally contributed by the material. The atomic/molecular structure of the amorphous material is arranged in a disorderly lattice; hence they diffract X-rays very poorly. The X-ray method allows measurement of the relative amounts of crystalline and amorphous material in a sample based on comparison of the areas under the peaks of the two types of structure. (Billmeyer Jr., 1971).

APPENDIX C

Experimental determination of solubility of a solute in solvent(s)

1. Pour an excess of solute into a solvent (or a known weight ratio of solvents) in a glass tube with cap.
2. If measuring the solubility in a mixture of solvents, repeat procedure 1 with a series of different weight composition ratios of solvents mixture.
3. Label the tubes accordingly for identification.
4. Immerse the tubes in a water bath; securely position them using tube holders on a shaker as shown in a photograph below:
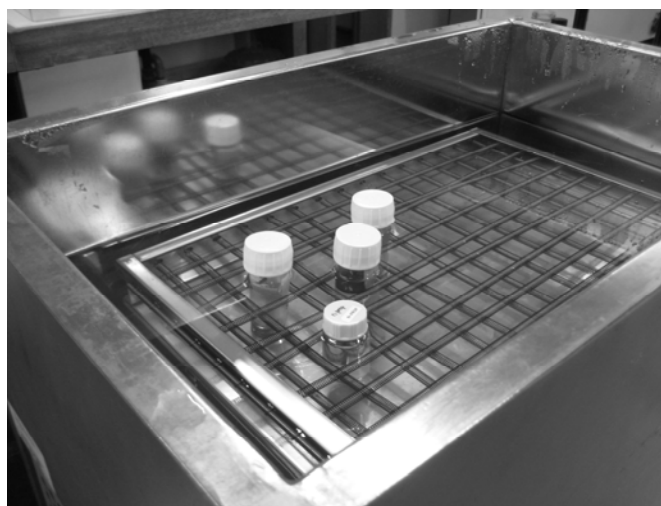

Figure C1 Experimental set-up for solubility experimental determination.

5. Maintain the temperature of the bath at a certain temperature and monitor it using a stainless steel Pt100 thermocouple connected to a digital temperature meter. In order to reduce evaporation and heat transfer, the surface of the water in the bath can be covered with floating plastic balls.
6. Continuously shake the tubes at that temperature for 24 hours.
7. Separate the solution from the solids by filtration through 0.45 μm syringe filters, while the tubes are partially immersed in the bath.
8. Transfer the obtained supernatants into evaporating dishes, which are weighed before the transfer (empty weight, w_0) and weighed again after the transfer (wet weight, w_w).

9. Assay the supernatants on the dishes using a gravimetric analysis method that involves evaporation overnight in a vacuum oven i.e. approximately 12 hours at 35°C initially, and then increase the temperature of the oven to 107°C.

10. Weigh the evaporating dishes then dry, weigh again and dry repeatedly until constant weights are obtained (dry weight, w_d).

11. Solubility, S, of the solute in the solvent or the mixture of solvents at a particular temperature can be calculated as:

$$S = \frac{w_d - w_0}{w_w - w_d} \tag{C1}$$

APPENDIX D

Experimental solubility data for sulfathiazole in *sec*-butanol, acetonitrile, isopropanol and water

Table D1 Experimental solubility data for sulfathiazole in *sec*-butanol.

Temperature (C)	Concentration (g/100g solvent)	Standard deviation
25.00	0.102020	0.007477
29.00	0.136287	0.002994
32.95	0.149390	0.007786
36.00	0.183664	0.000000
40.60	0.208663	0.000000
48.05	0.316656	0.003723

Table D2 Experimental solubility data for sulfathiazole in acetonitrile.

Temperature (C)	Concentration (g/100g solvent)	Standard deviation
25.00	0.822621	0.006360
29.00	0.930510	0.017224
32.95	1.038142	0.000428
36.00	1.271036	0.008397
40.60	1.427831	0.034124
48.05	1.883869	0.050896

Table D3 Experimental solubility data for sulfathiazole in isopropanol.

Temperature (C)	Concentration (g/100g solvent)	Standard deviation
25.00	0.173902	0.006247
29.00	0.213893	0.008348
32.95	0.222182	0.001981
36.00	0.265088	0.007758
40.60	0.310026	0.005588
48.05	0.453860	0.010209

Table D4 Experimental solubility data for sulfathiazole in water.

Temperature (C)	Concentration (g/100g solvent)	Standard deviation
29.00	0.063375	0.002955
32.95	0.080416	0.000000
36.00	0.088225	0.003886
40.60	0.091318	0.000626
50.00	0.147797	0.001903
60.00	0.286173	0.004614
70.00	0.518489	0.073865

APPENDIX E

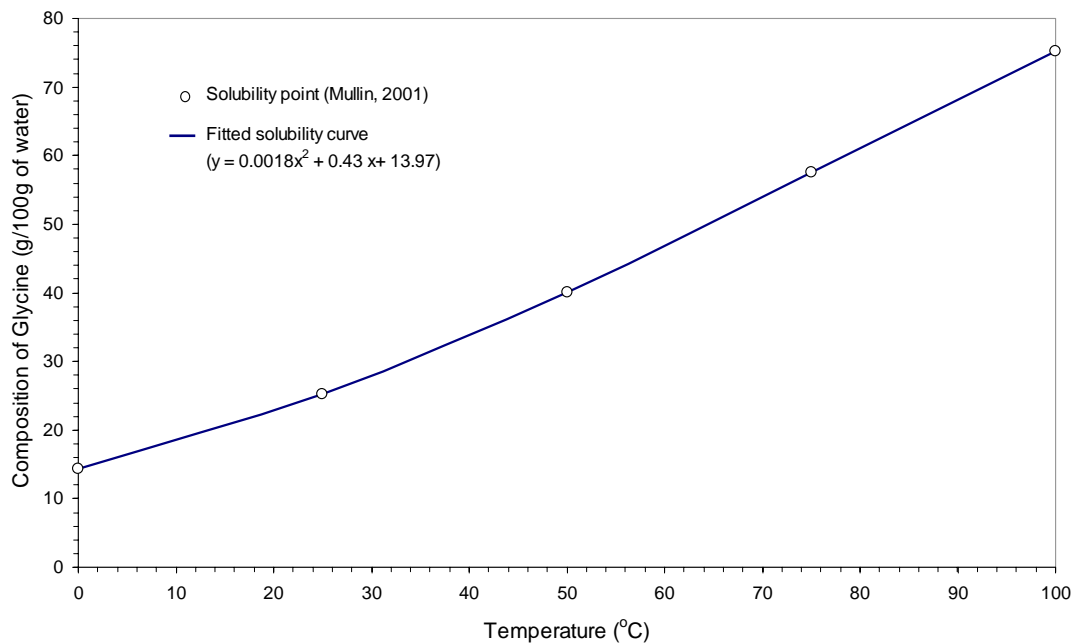## Solubility curve of glycine in water

Figure E1 Solubility curve of glycine in water (Mullin, 2001)

APPENDIX F

Crystallisation control interface used in the DNC experiments
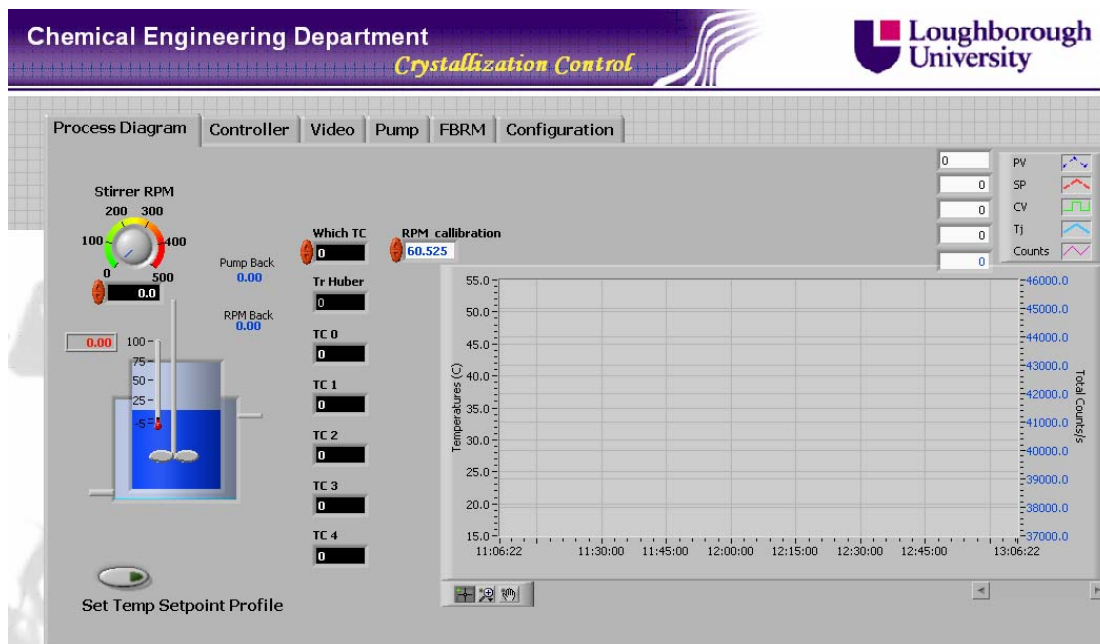

Figure F1 The lay-out of the crystallisation control interface for the process diagram.
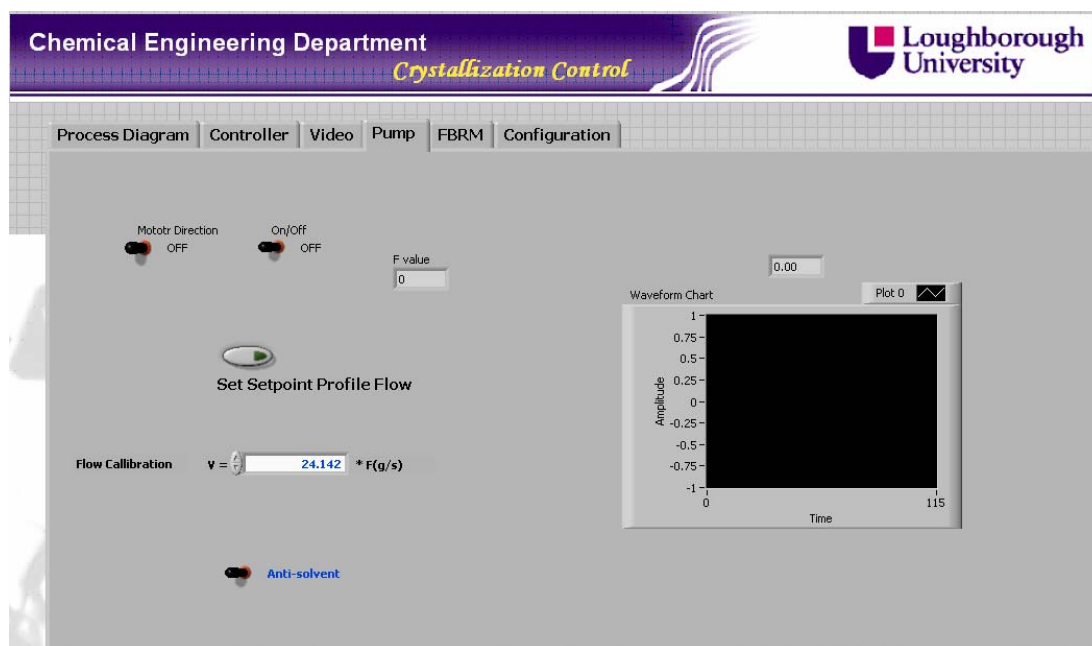

Figure F2 The lay-out of the crystallisation control interface for the pump.

APPENDIX G

Derivation for the calculation of the trajectory solution concentrations due to the dilution as a result of the anti-solvent addition

Let $\quad m_g \;=\;$ amount of glycine (72.3 g);

$\quad\quad m_w \;=\;$ amount of water (300 g);

$\quad\quad m_e \;=\;$ amount of ethanol (variable between 0 to 22000 g);

Water fraction during dilution, $\; x = \dfrac{m_w}{m_w + m_e}$ $\hfill$ (G1)

Concentration of glycine in solvents during dilution, $\; C = \dfrac{m_g}{m_w + m_e}$ $\hfill$ (G2)

Substitute (1) into (2) and rearrange gives

$$C = \left(\frac{m_g}{m_w}\right) x \hfill \text{(G3)}$$

Values of C that correspond to values of x are computed using equations (G1) and (G3).

APPENDIX H

Detection of impurities in sulfathiazole in crystals using HPLC

Sample preparation. About 100 mg of each of samples was weighted and transferred to a clean 100-ml volumetric flask, and a mixture of water (1% acetic acid) - methanol (85:15 v:v) was added to make stock solutions. 1 ml aliquots of the stock solutions were then transferred to 10-ml volumetric flasks and diluted to volume with the water (1% v:v acetic acid)-methanol mixture. About 1.5 ml of the resultant solutions was transferred to vials and the capped vials were positioned on an auto-sampler tray.

HPLC. A HP/Agilent 1100 Series HPLC equipped with a UV detector was used to analyse the eluted compounds in the samples at 254 nm. The analyses were performed on a Gemini C18 column (250 mm x 4.6 mm, 5 µm) using water (1% v/v acetic acid) - methanol (85:15 v:v) as a mobile phase in an isocratic mode at a flow rate of 1 ml/min and a temperature of 35°C. Aliquots of 10 µl from the vials on the auto-sampler tray were injected into the column.

Results.   HPLC chromatograms of raw material and polymorphic forms of sulfathiazole are shown in the figure below.
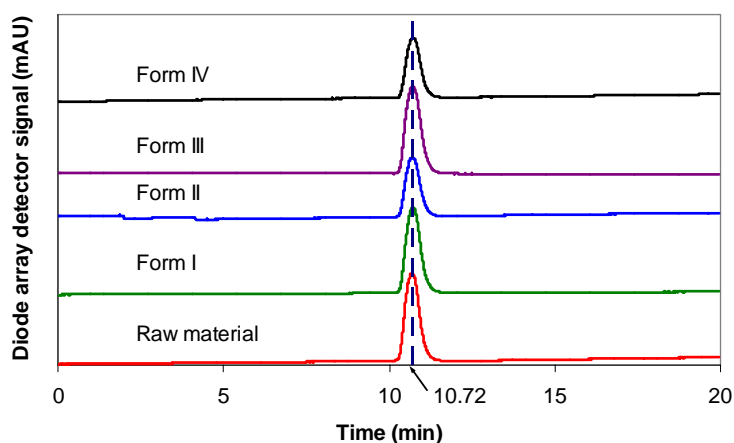

Figure H1 HPLC chromatograms of raw material and polymorphic forms of sulfathiazole.

It can be observed that besides the peak at 10.72 minutes, which are the characteristic peak for sulfathiazole, no other peaks are present. This may imply the absence of impurities in the samples.

APPENDIX I

Effect of the distance between a crystal and the focal point on the FBRM signal.
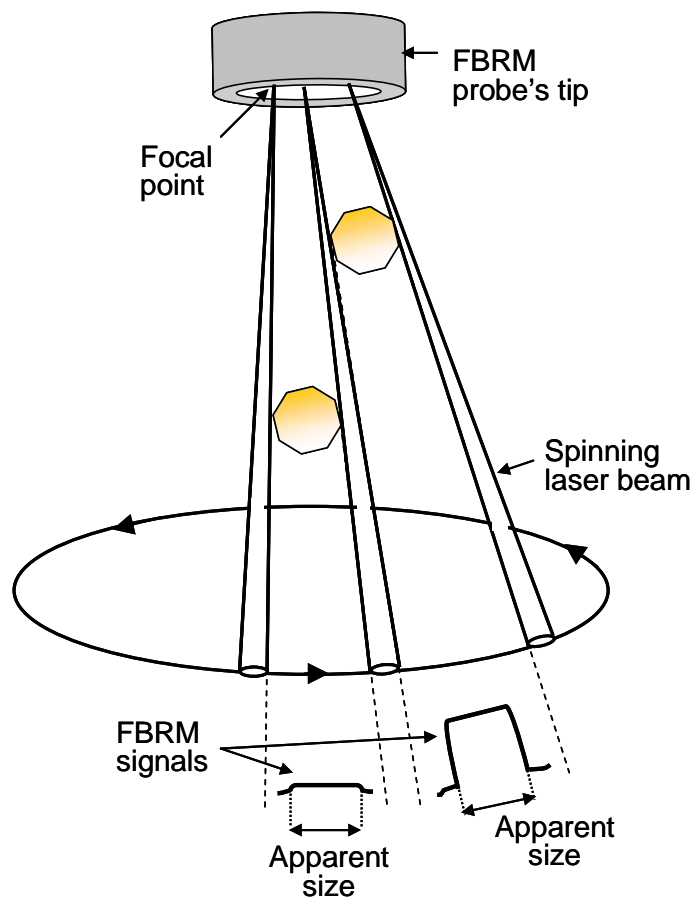

Figure I1 Effect of the distance between a crystal and the focal point on the FBRM signal (modified from Pons et al., 2006).

List of Publications

JOURNAL PAPERS

M. R. Abu Bakar, Z. K. Nagy, A. N. Saleemi, C. D. Rielly, "The impact of direct nucleation control on crystal size distribution in pharmaceutical crystallization processes", Crystal Growth & Design, 2009, 9(3), 1378-1384.

M. R. Abu Bakar, Z. K. Nagy, C. D. Rielly, "Seeded batch cooling crystallization with temperature cycling for the control of size uniformity and polymorphic purity of sulfathiazole crystals", Organic Process Research & Design, 2009, 13, 1343-1356.

M. R. Abu Bakar, Z. K. Nagy, C. D. Rielly, "A combined approach of differential scanning calorimetry and hot-stage microscopy with image analysis in the investigation of sulfathiazole polymorphism", Journal of Thermal Analysis and Calorimetry, 2010, 99, 609-619.

M. R. Abu Bakar, Z. K. Nagy, C. D. Rielly, "Investigation of the effect of temperature cycling on surface features of sulfathiazole crystals during seeded batch cooling crystallization", Crystal Growth & Design, submitted.

M. R. Abu Bakar, Z. K. Nagy, S. E. Dann, C. D. Rielly, "Investigation of the riddle of sulfathiazole polymorphism", Journal of Pharmaceutical Sciences, submitted.

PROCEEDING PAPERS (PEER-REVIEWED)

M. R. Abu Bakar, Z. K. Nagy, C. D. Rielly, "Seeded batch cooling crystallization with temperature cycling for the control of size uniformity and polymorphic purity of sulfathiazole crystals", in Proc. of 16th International Workshop on Industrial Crystallization (BIWIC 2009), Lappeenranta, Finland, September 9-11, 2009.

M. R. Abu Bakar, Z. K. Nagy, C. D. Rielly, "Towards the development of a polymorphic control approach in sulfathiazole crystallization", in Proc. of 15th International Workshop on Industrial Crystallization (BIWIC 2008), Magdeburg, Germany, September 10-12, 2008.

M. R. Abu Bakar, Z. K. Nagy, A. N. Saleemi, C. D. Rielly, "Direct nucleation control of crystal size distribution in pharmaceutical crystallization", in Proc. of 17th International Symposium on Industrial Crystallization (ISIC17), Maastricht, The Netherlands, September 14-17, 2008.

M. R. Abu Bakar, Z. K. Nagy, C. D. Rielly, "Investigation of the polymorphism of sulfathiazole by a combined DSC-HSM approach", in Proc. of 17th International Symposium on Industrial Crystallization (ISIC17), Maastricht, The Netherlands, September 14-17, 2008.

ABSTRACT

M. R. Abu Bakar, Z. K. Nagy, C. D. Rielly, In situ monitoring and control of the polymorph purity of sulfathiazole in batch cooling crystallisation, at the 40th British Association for Crystal Growth (BACG) Annual Conference 2009, Bristol, United Kingdom, September 7-8, 2009.

M. R. Abu Bakar, Z. K. Nagy, C. D. Rielly, A combinational approach of DSC-HSM with image analysis in the study of sulfathiazole polymorphism, at the British Association for Crystal Growth (BACG) Conference 2008, Loughborough, United Kingdom, September 8-9, 2008.

Z. K. Nagy, M. R. Abu Bakar, A. N. Saleemi, C. D. Rielly, Direct nucleation control of crystallization processes using focused beam reflectance measurement, at the British Association for Crystal Growth (BACG) and Irish Association for Crystal Growth (IACG) Conference 2007, Dublin, Ireland, September 3-4, 2007.

PRESENTATIONS

Oral Presentation

M. R. Abu Bakar, Z. K. Nagy, C. D. Rielly, Seeded batch cooling crystallization with temperature cycling for the control of sulfathiazole crystals' properties, at the 40th British Association for Crystal Growth (BACG) Annual Conference 2009, Bristol, United Kingdom, September 7-8, 2009.

Z. K. Nagy, M. R. Abu Bakar, A. N. Saleemi, C. D. Rielly, Direct nucleation control of crystal size distribution in pharmaceutical crystallization, in Proc. of 17th International Symposium on Industrial Crystallization (ISIC17), Maastricht, The Netherlands, September 14-17, 2008.

Z. K. Nagy, M. R. Abu Bakar, A. N. Saleemi, C. D. Rielly, Direct nucleation control of crystallization processes using focused beam reflectance measurement, at the British Association for Crystal Growth (BACG) and Irish Association for Crystal Growth (IACG) Conference 2007, Dublin, Ireland, September 3-4, 2007.

Poster Presentation

M. R. Abu Bakar, Z. K. Nagy, C. D. Rielly, Direct nucleation control of crystal size distribution in pharmaceutical crystallization, selected to present a poster at the SET for BRITAIN Exhibition in the Engineering Section held at the House of Commons on March 9, 2009.

M. R. Abu Bakar, Z. K. Nagy, C. D. Rielly, Getting the Right Crystal, selected to represent the Department of Chemical Engineering at the Graduate School Poster Presentation during the Loughborough University Court Annual Meeting held on February 13, 2009.

M. R. Abu Bakar, Z. K. Nagy, C. D. Rielly, In situ monitoring and control of polymorphic purity in pharmaceutical crystallization, at the Institute of Chemical Engineers United Kingdom (IChemE) global forum, ChemEng08, Birmingham, United Kingdom, October 28-30, 2008.

M. R. Abu Bakar, Z. K. Nagy, C. D. Rielly, Towards the development of a polymorphic control approach in sulfathiazole crystallization, in Proc. of 15th International Workshop on Industrial Crystallization (BIWIC 2008), Magdeburg, Germany, September 10-12, 2008.

M. R. Abu Bakar, Z. K. Nagy, C. D. Rielly, A combinational approach of DSC-HSM with image analysis in the study of sulfathiazole polymorphism, in Proc. of 17th International Symposium on Industrial Crystallization (ISIC17), Maastricht, The Netherlands, September 14-17, 2008.

M. R. Abu Bakar, Z. K. Nagy, C. D. Rielly, A combinational approach of DSC-HSM with image analysis in the study of sulfathiazole polymorphism, at the British Association for Crystal Growth (BACG) Conference 2008, Loughborough, United Kingdom, September 8-9, 2008.

Loughborough Graduate School Poster Competition 2008. Title of poster: "Getting the Right Crystal". The poster won first prize.